THEORETICAL INVESTIGATION OF VOLUTE EFFECT ON LOW-FLOW DYNAMIC STABILITY IN A CENTRIFUGAL PUMP

by

Furio Ciacci

B.S. Aeronautics and Astronautics
Massachusetts Institute of Technology, 1990

SUBMITTED TO THE DEPARTMENT OF AERONAUTICS AND ASTRONAUTICS
IN PARTIAL FULFILLMENT OF THE REQUIREMENTS FOR
THE DEGREE OF

MASTER OF SCIENCE

at the

MASSACHUSETTS INSTITUTE OF TECHNOLOGY
June 1992

Signature of Author _____
Department of Aeronautics and Astronautics
June 1992

Certified by _____
Dr. Jack L. Kerrebrock
R.C. Maclaurin Professor of Aeronautics and Astronautics
Thesis Supervisor

Approved by _____
Professor Harold Y. Wachman
Chairman, Department Graduate Committee

I. ABSTRACT

The present research project sought to eliminate low flow dynamic instability in a family of low specific speed centrifugal pumps. More negative pump characteristic slopes were known to be linked to improved stability, and were sought via appropriate geometry modifications. In the past, the most common solution adopted for improving the pump slope was that of increasing the impeller sweep angle. This resulted in lower head rise at BEP and therefore required pump resizing or a change in design speed.

The effect of a number of geometrical pump parameters on performance was evaluated by means of a volute-impeller interaction code. In particular, larger volutes were found to flatten the pump characteristic by increasing volute mixing losses at the impeller-volute interface at low flow coefficient, and reducing them at high flow coefficients. Following indications that characteristic slope depended on volute tangential speed, a new volute configuration was devised, which obtained most of the flattening through a higher rate of cross-sectional area increase immediately after the tongue. The new pump characteristic was tested via a linear system stability code and predicted to reduce significantly the area of unstable operation.

The new volute design was subsequently implemented on a pump model facility and tested. Experimental results confirmed that the proposed change improved the stability of the system without resulting in significant performance reductions in head rise at design point. The discrepancies between experimental and computational results were analyzed. Conclusions for further design changes and pump volute flow modeling techniques were drawn.

II. ACKNOWLEDGEMENTS

The Author is indebted first and foremost to his supervisor, Professor Jack L. Kerrebrock, for the invaluable guidance and encouragement received through regular and frequent discussion of the subject over more than one year. Professor Kerrebrock's engineering insight, intellectual rigor and enthusiasm are of constant example to his students, and qualities one can only strive for. Professor Belgacem Jaroux and Doctor Andrew Wo must be credited with having introduced and familiarized the Author with a fascinating area of study in his brief period of supervision, and for their continuing support for the remainder of the research time, in spite of the immeasurable distance separating them from the office. The Author owes also much to Mr. Nicolas R. Goulet and Mr. Jeffrey P. Bons in written form, who laid the foundations for the work described here.

Sundstrand, Inc. provided much more than mere funding for the project. In particular, Mr. Paul Westhoff and Mr. Tim Bland's support, direction and criticisms were determinant to its success. Mr. Paul Hermann's and Professor Frank E. Marble's suggestions on a variety of subjects were also of critical importance.

The Author is also profoundly indebted to his office co-workers for their assistance on a myriad of questions, ideas and technical quandaries, as well as their patience in putting up with his less than captivating social habits, particularly in the most stressful periods. In particular, Mr. Scott Sandler deserves the greatest praise, not only for his routinely support and help as research partner, but also for contributing to an office climate which at times was the only reason for showing up in the morning. Similarly, Mr. Martin Graf must be remembered for his invaluable help in reminding the Author that someone more miserable was never far away.

No one can be recognized for ensuring that this work would be carried out by this Author more than his parents, Lucilla and Federico Ciacci, through their constant model, example, support and encouragement in an infinity of different ways and occasions, before and during this experience.

Cambridge, May 7, 1992

III. TABLE OF CONTENTS

IV. LIST OF ILLUSTRATIONS

V. LIST OF TABLES

VI. LIST OF SYMBOLS

a	Speed of sound [m/s]
a	Volute nondimensional area $= \frac{A_i}{\pi D_2 B_2}$
A	Volute or piping cross-section area [m^2]
b	Impeller passage width [m]
B	B parameter: $= \frac{U}{2\ a}(\frac{V}{A_c L_c})^{1/2}$
c	Nondimensional factor
C	Flow velocity [m/s]
d	Radial thickness [m]
D	Diameter [m]
g	Acceleration of gravity
h	Axial height [m]
H	Total head [m]
k	Dynamic head loss factor
L	Length [m]
N	Number of volute elements
N	Pump speed
p	Pressure [N]
Q	Volumetric flow rate [m^3/s]
r	Pump radial coordinate
s	System response parameter
t	Time
U	Impeller tip speed [m/s]
V	Volume [m^3]
Y	Pump area ratio
z	Nondimensional factor
Z	Number of impeller blades
β	Blade trailing edge incidence angle
γ	Bypass exit incidence angle
γ	Fluid specific heat ratio
θ	Pump circumferential angle
η	Efficiency
λ	Friction coefficient $= 0.02 - 0.005\ (1 + \log_{10}(C_i D_h))$
ζ	Volute tongue loss factor
χ	Area ratio $= \frac{D_b b_b}{D_a b_a}$
ρ	Fluid density
σ	Slip factor $= \frac{C_{u\,ac}}{C_{u\,th}}$
φ	Volute local flow coefficient
Φ	Flow coefficient: $= \frac{\dot{m}}{\rho \pi D_2 B_2 U}$
ψ	Volute stream function
Ψ	Head coefficient: $= \frac{\Delta P}{\frac{1}{2}\rho U^2}$
ω	Angular velocity

Subscripts

0	Shutoff
1	Impeller inlet
2	Impeller exit
3	Volute throat

ac	Actual
b	Bypass
BEP	Best Efficiency Point
c	Compressor
cr	Critical
e	Impeller exit
h	Hydraulic
i	Volute cell i
l	Leakage path
lag	Pump response lag
lg	Large plenum
m	Meridional
ov	Overall
P	Pump
PL	Pump leg
pr	Pressure recovery
s	Static
S	Specific
s.b.	Splitter blades
s.f.	Due to skin friction
sm	Small plenum
sm	Static at impeller exit
ss	Steady-state
T	Throttle
th	Theoretical
thr	Pump mean throughflow
TL	Throttle leg
u	Tangential
unst	Unstable oscillations
v	Volute

Abbreviations

ADI	Alternate Direction, Implicit
AM	(Volute) Area Multiplier
BC	Boundary Conditions
BEP	Best Efficiency Point
BHP	Best Head Point
HPU	High Pressure Unit
HSS	High Specific Speed
IC	Initial Conditions
LDV	Laser Doppler Velocimetry
LPU	Low Pressure Unit
LSS	Low Specific Speed
RPM	Revolutions Per Minute
SF	Slip Factor

1.0. INTRODUCTION

1.1.0. Statement of the Problem

The present research project addresses the problem of enabling a family of low specific speed centrifugal pumps designed for aerospace applications to operate stably at flow rates much lower than their best efficiency point. Typically, pressure oscillations appear in these types of pumps at flow rates lower than about 30-50 percent of design. Very large, undamped oscillations often observed in these cases are categorized as 'surge'. Surge propagates to the flow outside the pump and represents a system phenomenon. In addition to loss of performance, it can result in serious damage to the system and the pump itself. A more detailed description of surge in centrifugal compressors is provided, e.g., by Van den Braembussche [18].

Low specific speed pumps are capable of very high performance at relatively reduced sizes, and are therefore attractive for aerospace propulsion applications such as fuel systems. However, most mission requirements include very low output regimes during cruise and approach to landing, which fall well within the typical boundaries of unstable operation. This problem has traditionally been solved by employing multiple pumps or by shunting most of the output around the pump itself. Design trends, however, point to weight reductions for all components, thus making multiple pump configurations less attractive. Simple, direct shunts cannot be employed effectively at certain head and mass flow rate conditions due to rapid heating of the fuel recirculated. The fuel must then be recirculated through the tank, adding to the complexity and bulkiness of the system. This leaves modifying the pump design in order to eliminate the cause of the oscillations as the most attractive option. Changes in design can only come from a better understanding of the flow behavior at low flow rates in the pumps under study. This need was not addressed sufficiently in past research efforts to present a viable and effective design solution.

1.2.0. Research Plan

The efforts described in this thesis cover the theoretical and computational aspects of the third phase of the study of low flow instabilities in a family of centrifugal pumps. The sponsors of the study were interested in extending the range of stable operation for the family without sacrificing pressure rise or compromising on dimensions or weight.

The first phase of the project focused on designing and building an experimental facility for the study of instablity and performance in a centrifugal pump. A computational performance predictor was also developed at this point in time, which formed the foundation for the subsequent study of possible pump design changes. The results of the first phase are summarized in Mr. Nicolas Goulet's Master's thesis [24].

The second phase focused on understanding stability behavior in the pump under study. This was done through flow visualization, pressure and flow measurement techniques. At the same time, a computational algorithm for the prediction of system behavior based on linearized stability theory was developed and successfully compared to the observations. This algorithm was to be utilized later in predicting the effect on stability of changes in performance appropriately generated by design modifications. The results of the second phase are described in Mr. Jeffrey Bons' Master's thesis [26].

The third phase focused on finding a relationship between flow behavior, pump performance and system stability in order to develop a rationale for design improvements. This required the gathering of evidence, which was done both experimentally, by means of Laser Velocimetry measurements and local static pressure measurements, and numerically, by means of the algorithms discussed above. It also included the development of an effective design based on theoretical deductions and computational predictions, which incorporated tradeoffs between the different constraints; its implementation; and successful experimental testing. It is the theoretical and computational aspects of this thrd phase which are the subject of the present thesis. The experimental aspects of the third phase are

presented in Mr. Scott Sandler's 1992 M.S. Thesis. Experimental results were utilized first in order to obtain indication as to the problem areas in the pump and to verify the effectiveness of the computational models employed. They were also necessary in order to assess the effect of the proposed design changes.

The entire study took place at the Gas Turbine Laboratory of the Massachusetts Institute of Technology, under the direct supervision of first Dr. Belgacem Jaroux and, subsequently, Prof. Jack L. Kerrebrock, over the period between Fall 1988 and Spring 1992.

Performance and local pressure and velocity measurements were taken on a pump facility constructed during the previous phases of the project. Both the facility and the experimental apparatus will be described briefly in Chapter 3.0. The original pump, whose characteristics were not disclosed, has been indicated in this study as the High Pressure Unit (HPU). The simple term 'pump' was reserved for the model facility constructed (Low Pressure Unit, or LPU) and studied at the Gas Turbine Laboratory and all data quoted in this document refer to it.

1.3.0. Organization of Thesis

In the present section, the function and importance of each subsequent thesis chapter is outlined.

- Chapter 2.0 provides an overview of the accomplishments of earlier authors in the same field, or of those whose methods and findings are relevant to this investigation. These can be divided into three categories: works on the stability of pumping systems, works on the interaction between impeller and volute in a centrifugal pump and works on the numerical analysis of centrifugal compressor impeller and volute flow.

- Chapter 3.0 summarizes the features of the pump and measurement apparatus that are relevant to the theoretical analysis and to its implementation. The computational and other software tools used are also presented.

- Chapter 4.0 discusses the computational approach to pump performance prediction and the computationally measured effect of some attempted operating parameter changes and more radical design modifications.

- Chapter 5.0 discusses the numerical method used to predict instability based on pump and system performance, and presents the effects on system stability of the proposed changes in the linearized system stability description.

- Chapter 6.0 summarizes the aspects of implementing the proposed changes on the experimental apparatus that are relevant to the theoretical analysis, and outlines the results obtained as compared with those predicted by the models.

- Chapter 7.0 presents the conclusions reached, with respect to improvements to both pump design and theoretical analysis methods. An extension of the new design is proposed and discussed. Two recommendations for better modeling of pump performance and flow behavior are also made and discussed.

2.0. LITERATURE REVIEW

This research project sought to identify modifications to the geometry of a centrifugal pump volute in order to reduce instability at low flow. As a result, it was built upon the foundations laid by past work in two principal areas: the effect of the interaction of volute and impeller geometry on pump performance, as measured by head vs. flow rate and efficiency, and the stability of pumping systems. The assumptions and results of previous works on computational flow description in centrifugal pumps constituted a third subject relevant to the present study. In fact, the predictions of the computational model representing the interaction between volute and impeller did not agree completely with experimental measurements, indicating that some of the assumptions made in developing the model had to be verified and reformulated by means of a two-dimensional representation of the flow in the volute.

The works pertinent to each of these three areas of pump engineering will be presented separately in the following three paragraphs.

2.1.0. The Stability of Pumping Systems

A decrease in the absolute value of the slope of the pump characteristic curve had been predicted by previous research to result in greater stability at the flow rates involved. It was observed to do so in the present study. The effect of pump geometry on the slope of the characteristic are discussed in the following section.

In 1980, Greitzer [16] analyzed the stability of a 'Basic Pumping System' consisting of an active element (pump), a resistive element (throttle), inertial elements (piping) and compliant elements (plenums) that are capable of storing energy through compression. If we characterize the oscillatory response of the system as e^{st}, then the exponent s must satisfy the equation

$$s^2 + s\left[\left(\frac{1}{B\,\frac{\partial\Psi_T}{\partial\Phi}}\right) - B\left(\frac{\partial\Psi_P}{\partial\Phi}\right)\right] + \left[1 - \frac{\left(\frac{\partial\Psi_P}{\partial\Phi}\right)}{\left(\frac{\partial\Psi_T}{\partial\Phi}\right)}\right] = 0 \qquad (2.1.1)$$

from which it follows that the dynamic stability of this system depends on the interrelationship of three factors: the slopes of the pump and throttle characteristics and the parameter B, defined as

$$B = \frac{U}{2a}\left(\frac{V}{A_c L_c}\right)^{1/2} \qquad (2.1.2)$$

where U is the rotor speed, a is the speed of sound, V is the size of the plenum volume, A_c is the compressor flow-through area and L_c is the effective length of the compressor duct. B represents the ratio of inertia to compliance in the system. In addition, dynamic instability can physically occur only at operating points where the characteristic of the pump is positively sloped, causing mass and pressure oscillations to be in phase and the net energy input to the fluid to be positive [Fig.2.1.1].

The present pump rig is, in essence, a development of the 'Basic Pumping System' concept. In 1989, Goulet [24] applied the above analysis to the present rig by means of a linear computational model. In 1990, Bons [26] expanded the model to account for a lag in the response of the pump, which effectively increases stability, and variability of the pump wheel speed, which increases the effective inertia of the system and increases stability as well.

2.2.0 Interaction Between Impeller and Volute

The importance of matching between impeller and volute geometry has been recognized by authors in pump design since the nineteen thirties. Usually, the shape of the impeller and volute are chosen in order to obtain the desired head and flow rate at design conditions. For a pump of the kind analyzed in this study, in

proximity of the best efficiency point, the volute and impeller characteristics, i.e. the relationships between head rise and flow rate in both these two pump elements, in their simplest forms are:

$$H/\eta = H_0 - const_1\ Q \qquad \text{(impeller)} \tag{2.2.1.a}$$

$$H = Q/const_2 \qquad \text{(volute)} \tag{2.2.1.b}$$

In 1947, Anderson [2] suggested that the impeller head could be broken down into head due to impact and head due to centrifugal pressures. By analyzing the impeller velocity diagrams pertaining to the impact component, he concluded that the area of the volute throat determined the point of best hydraulic efficiency of the pump. Head predictions based on this theory displayed very good agreement with measurements [2] [6]. The head at BEP was related to the parameter

$$Y = 0.95\ \pi\ D_2\ b_2\ \sin\beta\ A^{-1}, \tag{2.2.2}$$

defined as the area ratio of the pump. In 1963, Worster, in analyzing pumps with free-vortex volute designs [7], pointed out that the nondimensional flow rate and head rise coordinates of the intersection point between the volute and impeller characteristics

$$\phi = \frac{H_0}{\dfrac{2\ A^{1/2}/D_2}{\ln(1 + 2\ A^{1/2}/D_2)} + \dfrac{A}{\pi\ D_2\ b_2\ \tan\beta}} \tag{2.2.3.a}$$

$$\Psi = \frac{H_0}{1 + \dfrac{\ln(1 + 2\ A^{1/2}/D_2)}{2\ A^{1/2}/D_2}\ \dfrac{A}{\pi\ D_2\ b_2\ \tan\beta}} \tag{2.2.3.b}$$

which determine the BEP location in the absence of losses, depended on the parameter $\pi\ D_2\ b_2\ \tan\beta\ A^{-1}$, which is almost the same as Anderson's area ratio, and

on the ratio of the impeller outlet swirl velocity to the mean velocity in the volute throat, which for a volute with rectangular cross-section and radial thickness B has the form

$$\frac{2\ A^{1/2}/D_2}{\ln(1 + 2\ A^{1/2}/D_2)} \qquad (2.2.4)$$

As will be mentioned in Section 4.4.0, one of the factors recognized by the present study to affect the performance of the pump near and above design flow was the difference between the tangential velocity at the impeller exit and the tangential velocity in the volute throat for certain ranges of θ. In addition, Worster suggested that the most important factor in determining the pump's specific speed is the ratio of the square root of the volute throat area to the impeller diameter. Thus, a pump with a larger throat area would have a higher specific speed.

Worster also analyzed variations in pump performance resulting from changes in a number of geometrical parameters. In particular, the change in the operating point head coefficient resulting from varying the number of blades by $\pm$25% was found to be minimal. This resulted from the fact that the number of blades affects the Busemann coefficient H_0, i.e. the shutoff head coefficient. In the present study, it was found that altering the slip factor by the same amount across the flow coefficient range resulted in a vertical shift of the volute local pressure profiles [Fig.2.2.1], the pump pressure characteristic [Fig.2.2.2.i] and efficiency variation with flow rate [Fig.2.2.2.ii]. Since the ideal impeller slip factor is directly related to the impeller blade exit angle, these findings can be considered to be consistent.

Stepanoff [6] had predicted significant variations in design head and flow coefficient to result from changes in impeller exit passage width [Fig.2.2.3]. Similarly, a significant change in characteristic shape was observed in the present pump when the impeller exit passage width parameter was corrected from 0.0127m to 0.0150m in the impeller-volute interaction code [Figs.2.2.4].

Worster derived the characteristic curves of a family of pumps obtained by varying only volute throat areas. The shifting volute characteristic results in flatter overall curves and larger BEP flow coefficient [Fig.2.2.5]. Finally, the characteristic curve of a pump fitted with an Archimedean spiral volute was measured and compared to that of the same pump fitted with a free vortex design volute and three different tongue designs [Fig.2.2.6], showing in particular a noticeable decrease in the slope of the characteristic curve. Measurements of volute static pressure showed somewhat higher but not substantially different circumferential pressure variations for the Archimedean spiral volute compared to the free vortex spiral design [Figs.2.2.7]. Volute cross-sectional area rather than the impeller's exit area was found by Worster to affect the BEP for low specific speed pumps, such as the one presently studied. In fact, a flatter characteristic and a much less significant outward shift of the BEP flow coefficient, with η_{BEP} roughly constant, were also observed in the modified volute proposed for the present pump presented in Section 4.5.0, which has in common with Worster's Archimedean volute a rectangular cross-section and a rapid throat area expansion downstream of the inlet. Finally, the shape of the tongue was found experimentally to result in a horizontal shift of the efficiency curve, suggesting that it may be possible to offset the effects of a different volute area profile on BEP by modifying the tongue. In general, Worster found wide volutes to have 'both constructional and hydraulic advantages'. In spite of this, most of the past design and research efforts to improve performance have been directed at the impeller.

In 1980, Anderson [11] related the area ratio to the matching between impeller exit and volute velocity. This suggested that improvements to the characteristic slope could be produced by acting on the volute and impeller exit dimensions. However, the impeller exit passage width cannot be varied along the circumference, and the large head loss predicted in [11] [Fig.2.2.3] may therefore not be avoidable. By contrast, the substantial slope variation in [7] was achieved at the expense of a small BEP shift, resulting in limited head loss and no significant efficiency penalty [Fig.2.2.6]. The observation was made that, in practice, specific speed and area ratio were not strictly related and at any given specific speed, pumps with varying area ratios could and had been made to date.

Schweiger [13] suggested that inaccurate theoretical prediction of pump behavior at very low flow rates may be caused by swirl developing at the impeller inlet and discharge. Experimentally, he found that extending the impeller blades into the suction pipe increased H_0 and the stability of the pump characteristic. Weissgerber and Carter [14] compared performance predictions obtained with a computational loss analysis procedure to measured values for six pumps with varying geometries. They observed that the predicted performance values were substantially lower than those measured at flow rates below 50% of design. Similarly, the present computational prediction loses effectiveness at flow rates below 30% of design. The comparison of experimentally derived and computationally predicted volute pressure profiles for the present pump at low flow coefficients indicated that the failure of the model to predict the strong tongue effect on the flow, which appeared in the form of steep tangential pressure gradients just before the pump exit [Figs.2.3.1], was one of the possible explanations for this discrepancy. Another contributor was the inaccuracy in estimating the slip factor at low flow coefficient. Weissgerber and Carter attributed the discrepancy of design point to two phenomena: flow separation from the blade suction surface and recirculation between the separated region and the outward jet flow near the blade trailing edges. In the model, these two effects would be lumped into a corrected impeller exit velocity component ratio and slip factor.

In 1986, Lorett and Gopalakrishnan [21] developed an analytical procedure describing the effect of volute-impeller interaction on the volute flow at circumferential steps around the impeller discharge. Contrary to previous models, the impeller flow was assumed unsteady and dependent on the flow velocity in the volute throat, which varies along the circumference, thus including the effect of reverse flow and improving performance prediction at low flow performance. This required a step by step calculation of the flow conditions in the volute throat and impeller channel in discrete segments of the circumference, through a marching solution of discretized continuity and momentum equations. This procedure is at the basis of the computational code developed by Goulet in 1989 [24] for the present project. Details of the model and the code are presented in Chapter 4.0 and Appendix A.

2.3.0. Computational Flow Analysis in Centrifugal Compressors and Pumps

The computational model adopted for predicting overall pump performance proceeds by determining flow rate and head coefficients at discrete locations around the volute. The predicted values for flow and head coefficient at these locations showed some discrepancy with those obtained by Laser Velocimetry [Figs.2.3.1], suggesting that some of the assumptions incorporated in the model be reconsidered. In particular, the assumptions of impeller slip factor independent of the volute angle and of zero-thickness volute were reevaluated. The assumptions incorporated in the model are discussed further under Section 3.2.0.

2.3.1. The Assumption of Constant Slip Factor

In pump literature, the impeller slip factor is generally regarded as function of the geometrical characteristics of the pump. A number of correlations on the blade passage angle and impeller blade trailing edge angle, proposed by various authors, were gathered and compared with experimental data by Wiesner in 1967 [8]. Possibly the simplest and most common of them is due to Busemann:

$$\sigma = 1 - \frac{(\sin\beta)^{1/2}}{Z^{0.7}} \tag{2.3.1}$$

Eck's correlation accounts for the comparative length of the blade passage:

$$\frac{C_{u\,ac}}{C_{u\,th}} = \frac{1}{1 + \dfrac{2\cos(\pi/2 - \beta)}{Z\,(1 - D_1/D_2)}} \tag{2.3.2}$$

The above correlations and others due to Stodola, Stanitz, etc., predict slip factor quite well near design conditions, but become significantly less effective at low or high values. In 1967, Sakai and others [9] applied potential flow theory to the

impeller channel and corrected the boundary conditions by adopting an outer boundary radius larger than R_2 and dependent on the number of blades. Their flow rate dependent slip factor correlated better with their experimental measurements than the predictions by the above formulas. However, predictions could not be obtained below 0.7 of design flow rate due to strong three-dimensional effects in the volute channel. In 1974, Whitfield [10] analyzed the interaction between jet and wake flows in separated impellers, characterized by two different slip factors, and obtained a correlation between flow rate and overall slip factor that improved the agreement with experimental results. In 1980, Salemi and Di Matteo [12] analytically derived slip factor correction terms to account for impeller wall friction forces and blockage due to low energy flow accumulation on the blade suction surface. The resulting slip factor expression took into account fluid properties and flow rate in addition to pump geometry and showed good correlation with experimental values, particularly at flow rates near 40% of design. There have been no attempts to date to predict slip factor variations with volute angle in pumps with asymmetric casing geometry, even though an analysis of Miner's theoretical and experimental velocity measurements on one such pump [23] [25] [27] revealed that slip factor values varied significantly with θ [Fig.2.3.2] The variations appeared to be more significant away from the design operating point, partly explaining the reduced realism of a constant slip factor approximation at low flow rates. Miner adopted a two-dimensional potential flow model to the impeller and volute domain and successfully compared its findings to laser velocimetry measurements at four discrete 'windows' around the volute. The circumferential variations increased with distance from the operating point, in agreement with the intuitive reasoning that circumferentially varying flow conditions at off-design operation must influence flow behavior at the impeller exit and the slip factor. A clear case of this principle is flow reversal. The prediction of slip factor variation with θ and its incorporation in the present study are discussed in Section 4.1.0.

2.3.2 The Assumption of Zero-Thickness Volute and Instant Mixing

Laser velocimetry measurements at grid points covering most of the volute cross-section in proximity of the tongue indicated that C_{u3} varies substantially with radius in the volute [29]. These variations are associated with mixing times of the order of one half impeller rotation for the impeller and volute flow. This pointed out the need for a computational performance predictor to account for radial effects in the volute and their dependence on the design of the casing. The shape of a recommended two-dimensional algorithm is discussed in detail under Section 7.3.2.

A large body of literature is available on the subject of two-dimensional flow analysis in compressors and pumps. In 1944, Emmons applied the relaxation method to the numerical solution of compressible flow problems in two dimensions [1]. His indications were followed by Stanitz, who applied the technique to the solution of the irrotationality condition in the blade passage and corresponding volute segment for conical mixed-flow compressors in 1948 [3], and for centrifugal straight-bladed compressors in 1949 [4]. Stanitz reproduced the strong flow deceleration along the outer portion of the blade suction surface [Fig.2.3.3] and related it to frequently observed separation phenomena. Indications were also given for problems involving incompressible flow, and a coordinate transformation reducing the actual real domain to a rectangle [Fig.2.3.4] was recommended when using differently shaped blades such as logarithmic spirals. These indications were followed in theoretical attempts made on the present pump to estimate the value of slip factor from flow behavior near the blade in the impeller's rotating reference frame. More recently, Miner [23] [25] applied two-dimensional, potential flow analysis to the impeller and volute of a centrifugal pump and obtained excellent agreement with laser velocimetry measurements at various radial stations in the impeller.

3.0 RESEARCH FACILITIES

The present chapter reviews the aspects of the design, operation and instrumentation of the research facilities that are relevant to the theoretical investigation that is the subject of this thesis. Details of the computational procedures and copies of the software used are provided in the appropriate chapters and appendices.

3.1.0. The Experimental Apparatus

A pump loop was the experimental facility used in providing input to the theoretical models and in verifying their predictions. The relevant characteristics of this apparatus will be briefly presented in this section. The reader interested in a more detailed description is invited to consult Mr. Bons's or Mr. Goulet's thesis [26] [24].

3.1.1. Purpose

The experimental facility was designed for the purpose of testing a scale-up model of the centrifugal pump of interest. The scaling included the change from fuel to water as the working fluid. The test section was therefore represented by the pump and diffuser [Fig.3.1.1]. These elements were constructed of transparent and machinable plexiglass in order to allow for visual inspection, laser velocimetry measurements and the installation of pressure tappings.

Since measuring and understanding the mechanism of low-flow dynamic instability in the pump was of primary interest to the project, and the linear stability theory of Section 2.1.0 [16] was to be applied and verified against the actual behavior of this experimental facility, the pump loop was designed as a 'basic pumping system', characterized by a certain amount of inertia and compliance [Fig.3.1.2]. The inertia of the piping was determined by the linear dimensions and cross-sectional area

distributions of the pump and throttle legs. The compliance of an actual system was simulated by including two large tanks, one in the pump leg and one in the throttle leg, where energy could be stored through compression of air bags of controlled volume [Fig.3.1.3]. This simulated the effect of such phenomena as elasticity in the fuel system walls and in the fuel itself. Each air bag volume setting would yield a different B parameter for the system and a different stability response along the operating line.

The pump speed, another element found by Bons to be important in predicting system stability at a particular point, could be varied continuously by means of an electric motor directly connected to the shaft, and a throttle was included to adjust the flow rate through the system to any desired value. The throttle consisted of two servo-actuated valves in parallel with automated positioning to values prescribed by a voltage signal. All the components of the loop could be accessed and replaced easily, thus allowing for testing of redesigned components or changes in the loop setup. A transfer system was built to store the entire water content of the loop during frequent modifications.

3.1.2. Features

Since the pump model was scaled upwards from the original to allow for local investigation of pressure and velocity distributions, its operating quantities had to be sized in order to maintain a comparable specific speed. Design point quantities are listed in Table 3.1.1 on the following page (in part from [26]).

The volute thickness in the original design was 0.867 in. just after the tongue and increased more or less linearly up to 4.167 in. at 16.3° upstream of the tongue. After this point, the outer volute wall departed tangentially to form a rectangular cross-section inlet to a transition segment [Fig.4.4.4]. The cross-section at the transition outlet was circular and had an area approximately 1.72 times as large as that at its inlet. The circumferential profile of the volute radial thickness was an essential factor in the prediction and improvement of pump performance near shutoff. In the original design, as it was previously stated, the volute radial

thickness increased linearly with θ between 0.867 in. and 4.167 in.; in the new design proposed in order to increase stability the volute radial thickness increased along two successive parabolic arcs between the same two end values [Fig.4.5.2].

Table 3.1.1. Pump Features and Operating Parameters

Pump wheel speed	ω_P	~420 rpm
Impeller tip velocity	U	~13.31 m/s
Pump specific speed	N_S	~600
Impeller suction pipe diameter	D_1	0.201 m (7.93 in)
Impeller diameter	D_2	0.610 m (24.0 in)
Impeller discharge width	b_2	0.0150 m (0.590 in)
Impeller discharge blade angle	β_2	34°
Total number of blades	Z	8
Number of splitter blades	$Z_{s.b.}$	4

In the model pump, the volute was machined from of a single piece of plexiglass, the volute backplate, which in the finally assembly was enclosed by and bolted to a concentric cylindrical piece, the volute seal, inside which the transition element was placed [Figs.3.1.1 and 6.1.1]. The purpose of the transition element was that of changing the pump exit cross-section from rectangular to circular. The diffuser section was bolted to the external volute casing, at the exit of the transition element. This allowed easy access of instrumentation to the diffuser and transition. It would also allow easier implementation of the recommendations made in Section 7.3.2, which included the removal of the diffuser and its replacement with a straight pipe. The diameter of the discharge pipe was 8 inches.

The configuration described above was critical in approaching the problem of modifying the volute shape without violating the constraints of the assembly. More details on the solutions adopted appear in Chapter 6.0.

3.1.3. Instrumentation

Flow velocity measurements in the impeller were conducted using a Lexel Model 95 argon-ion laser [Fig.3.1.4]. Two beams, green and blue, were used to obtain velocity measurements along two directions normal to each other. The setup allowed the measurement of tangential and radial flow velocities along rectangular grids of 21 evenly spaced locations inside the volute cross-section [Fig.3.1.5]. The grids were located at regular angle intervals immediately upstream and downstream of the volute tongue [Fig.3.1.6]. Due to the opacity of the impeller shroud surface and the presence of steps on the upper volute wall in proximity of the impeller exit, velocity measurements at radial locations closer to the impeller exit boundary than 1/8 of the volute radial thickness, as well as at volute angles less than 60° downstream of the tongue, were not attempted. In order to supply information to the two-dimensional volute flow model proposed and discussed in Section 7.3.2, an additional laser velocimetry series of measurements across the operating flow coefficient range would have to be conducted at the volute-transition boundary, between 9° and 15° downstream of the tongue and on its outer side. Measurements at all the points on the cross-sectional grid were obtained by acting on the control volume through a Model 9430 Position Controller connected to a Model 9400 Mirror Mount Traverse System which enabled the control volume to move in three spatial dimensions. The sequential scanning of control volumes in the cross-sectional grid was software controlled and programmed on the computer through a RS-232 interface.

The flow rate through the pump was monitored by means of a Yokogawa ADMAG Series AM220 magnetic flow meter positioned in the pump discharge leg of the piping system. The flow rate in the leakage path was measured with an Omega FPM5300 turbine flow meter.

Steady-state static pressure measurements during the preliminary phase of the project were conducted using water manometers connected to pressure tappings positioned at regular intervals in the volute centerline and along the axial planes of the suction pipe, transition and diffuser elements [Fig.3.1.7]. After the installation of the modified volute, Validyne P305 differential pressure transducers replaced

the water manometers, which were employed to measure the water pressure characteristics in the two plenums. The transducers were connected to a Model DSS-48C7/Mk4 Double Scanivalve System, which could scan up to 8 ports/second.

The impeller wheel speed was measured by means of a Lebow 1604 Rotary Transformer. Shaft torque data were obtained through a Lebow 1604 Torque Sensor. Both instruments were connected to the data acquisition system through a Lebow 7540 Strain Gage Indicator.

For more details on the istrumentation, the reader is advised to consult Mr. Scott Sandler's Master's Degree thesis [29].

3.1.4. Data Acquisition

All the instruments used, except for the manometers, were connected to an IBM PC. Signals from the Laser Velocimeter were processed by a TSI model 1990C Counter-Type Signal Processor. The TSI Data Analysis Software provides laser velocimetry data reduction on the PC. A Scanivalve Digital Interface Unit performed all the required analog-to-digital conversions for the pressure transducer data. The Data Translation DT2810 board performed all the required analog-to-digital conversions for the flow rate, wheel speed and torque signals. Final data reduction and presentation was done on a Macintosh SE.

3.2.0. The Computational Apparatus

All the software customized to this research was written in FORTRAN. It was developed, tested and applied on the VAX network of the Gas Turbine Laboratory. Versions of the software were developed for use on the project's own Macintosh SE. Some software elements were developed independently on the MIT Project Athena VAX and IBM network. Listings of some versions of the programs used appear in the appendices to this document. Additional software for the data acquisition system was either developed in Basic or prepackaged.

Kaleidagraph™ 2.0 and Excel™ 2.2 were employed on the Macintosh for the analysis and representation of both computational and experimental data. This document was produced using Macintosh Microsoft Word™ 4.0 for the written sections and Kaleidagraph™ 2.0 for the graphs.

4.0 PREDICTION OF GEOMETRY EFFECTS ON CHARACTERISTIC

Improving low-flow stability in the pump system through a change in its characteristic required an understanding of the relationship between the pump's geometry parameters and the slope of the pressure curve at each operating point by means of a computational model.

4.1.0. Computational Modeling of Pump Performance

In a pump of the type considered, the pressure field in the volute depends on the flow velocity distribution along the impeller exit channel, which in turn depends on the exit pressure profile and is therefore unsteady whenever the rotating impeller encounters a circumferentially varying pressure field in the volute. Modeling the mutual influences of impeller and volute is critical to accurate performance prediction at all off-design flow coefficients and for all non free-vortex volute designs, where the impeller exit pressure profile varies with volute angle. It was therefore required of the present study. The need to incorporate the volute-impeller interaction assumption into a reasonable prediction of radial thrust and efficiency among other performance measurements led Lorett and Gopalakrishnan in 1986 to develop the interaction model described in [21], of which the model used in the present study is a second-generation derivative. Section 4.1.1 is devoted to a succint description of Lorett and Gopalakrishnan's interaction model.

4.1.1. The Impeller-Volute Interaction Model

Prior to 1986, radial thrust and performance prediction models incorporated the assumption of steady flow in the impeller channels, which was unrealistic at off-design conditions. Lorett and Gopalakrishnan determined the pressure and exit velocity distributions by dividing the volute channel and its impeller exit boundary in a number N of discrete steps and solving discretized forms of the continuity, momentum and Euler equations at each step. The solution required assuming

initial static pressure, tangential velocity and impeller exit meridional velocity conditions at the volute inlet, then relaxing the velocity values found at the end of the volute march in order to satisfy the energy equation at the boundary between element N and element 1:

$$C_0^2 = C_N^2 + 2g\,(H_{sN} - H_{s0})(1-\zeta)\,, \tag{4.1.1}$$

where ζ is a loss coefficient connected with the presence of the volute tongue, and periodicity conditions for tangential velocity at the volute inlet:

$$C_N = C_0 \tag{4.1.2}$$

As the model marches along the volute, the flow entering the volute from the impeller exit boundary of element i [Fig.4.1.1] is

$$\Delta Q_i = C_{m2i}\,\frac{\pi\, D_2\, b_2}{N\, Z}\,, \tag{4.1.3}$$

While continuity provides the volute tangential velocity at the exit of the element i:

$$C_{i+1} = \frac{Q_i + \Delta Q_i}{A_{i+1}} \tag{4.1.4}$$

The static pressure at the inlet to the following element i+1 is obtained from the momentum equation

$$H_{s,i+1} = H_{si} + \frac{2}{g}\,\frac{[Q_iC_i + \Delta Q_iC_i - Q_{i+1}C_{i+1}]}{(A_i + A_{i+1})} - \Delta H_{s.f.,i} \tag{4.1.5}$$

Where the losses due to skin friction in the volute element i are represented by the term

$$\Delta H_{s.f.,i} = \lambda \frac{\Delta L}{D_h} \frac{C_1^2}{2g},$$

(4.1.6)

which includes the effect of volute cross-section geometry and flow velocity. Finally, the exit velocity at the impeller exit in the following element is predicted applying the Euler equation to the impeller channel when discharging into element i+1:

$$C_{m,i+1} = C_{mi} + \frac{2g \sin^2\beta}{D_2 - D_1} \Delta t \, (H_s - H_{sm})_{i+1},$$

(4.1.7)

where Δt represents the time interval required by an impeller angular location to move from volute element i to element i+1:

$$\Delta t = \frac{60}{RPM \, N \, Z}$$

(4.1.8)

Lorett and Gopalakrishnan recognized that some assumptions incorporated in the model were likely to result in prediction errors. In particular, they pointed to the problems generated by: (1) neglecting the contribution by C_{m2} to volute flow energy as compared to C_2, which should not be very significant at very low specific speeds; (2) neglecting the upstream effect of the volute tongue, which is compensated by adopting the energy equation as a closure condition; and (3) assuming attached flow along the tongue walls. This last assumption was proven to be realistic in the pump considered in this study, where no separation in the volute channel was observed. In spite of the errors induced by the above simplifications, volute static pressure and radial thrust predictions agreed with the experimental findings of other authors [Fig.4.1.2]. Different assumptions for the Goulet model, and their likely impact on performance prediction, are discussed in the following section.

4.1.2. The Goulet Version of the Model

The volute-impeller interaction model version developed initially for the present project incorporated all the features of the original model, plus a leakage path from the impeller shroud to the pump inlet. The volute was divided into 100 circumferential elements. The following assumptions were restated and applied:

1) No blade-to-blade variations in the impeller flow (actuator disk);
2) Negligible radial variations in volute pressure and velocity (infinitely thin volute);
3) Complete mixing of impeller and volute flow momentum within each cell;
4) Leakage flow rate parbolic with respect to volute static pressure:

$$C_{ml} = U\left(\frac{\Psi}{k}\right)^{1/2} ; \qquad (4.1.9)$$

5) Same swirl at leakage path inlet and volute: $C_{ul} = C$;
6) No inlet swirl;
7) Constant slip factor σ, the ratio between impeller exit real and ideal relative tangential velocity.

Of these, assumptions (2), (3) and (7) were subsequently discussed and revised. The details of these discussions appear in this chapter and Section 7.3.2.

The iteration progressed from the volute inlet to its exit and recirculation path as in the original model. Initially, the conditions specified at the volute inlet were:

1) The pressure coefficient Ψ_0;
2) The volute tangential velocity C_0;
3) The impeller exit velocity C_{m20}.

The latter two, however, became relaxed as part of the convergence conditions described in the previous section. The final set of predicted results, therefore, included C_0 and C_{m20} as determined for a specified volute inlet pressure coefficient, impeller exit slip factor and pump geometry. Because of the behavior of the impeller characteristic, however [Fig.4.1.3], for flow coefficients lower than BEP there were two possible operating points corresponding to the same Ψ_0, so care had

to be taken in selecting the appropriate C_0 and C_{m20} guesses, and in mapping the results.

The presence of leakage led to modified continuity and momentum equations [Fig.4.1.1] across volute element i:

$$\varphi_{i+1} = \varphi_i + \frac{C_{m2i}}{N\,U} - \frac{C_{lmi}}{N\,U}\chi_l \tag{4.1.10}$$

$$\Psi_{i+1} = \Psi_i - \Delta\Psi_{s.f.} + \frac{4}{a_i + a_{i+1}}\left(\varphi_i \frac{C_i}{U} - \varphi_{i+1}\frac{C_i}{U} + \frac{C_{m2i}\,C_{u2i}}{N\,U^2} - \frac{C_{lmi}\,C_i}{N\,U^2} \right) \tag{4.1.11}$$

The second closure condition was given by the conservation of total pressure across the tongue:

$$C_0 = U\left(\frac{C_n}{U^2} + (Y_{smi} - Y_{si})\,(1 - \zeta) \right)^{1/2} \tag{4.1.12}$$

where the effect of losses has been lumped into the tongue loss factor ζ.

The results obtained from the iteration included a number of overall pump operating parameters:

1) Overall flow coefficient;
2) Overall pump head coefficient;
3) Overall hydraulic efficiency;
4) Flow angle of attack on volute tongue.

4.1.3. Upgrades and Modifications to the Model

The first test of the model in the form described in the previous section was conducted by comparing the predicted volute static pressure profile distributions with pressure data obtained by connecting manometers to pressure taps along the

centerline of the pump volute. The results of this comparison at four different operating points are displayed in [Figs.2.3.1]. It became evident that the ability of the model to predict local pressure behavior was adequate at flow coefficients near design, but declined sharply for lower operating points. Overall pump characteristic prediction was also less effective at low flow coefficents [Fig.4.1.4]. In particular, the sharp pressure increase in proximity of the volute tongue observed experimentally was not predicted. This phenomenon was attributed to sharp flow deflections due to the presence of the tongue, and the resulting marked shifts of the stagnation streamline and location of the stagnation point on the tongue at low flow coefficients [Fig.4.1.5], which could not be picked up by a one-dimensional, radially-constant-property model. The inability to predict the near-tongue head rise was connected to the overall pressure coefficient underprediction. This was improved in part by correcting the model to reproduce the steep area increase at the end of the volute resulting from the tangential departure of the outer wall 16.3° before the cutwater.

Sandler's Laser velocimetry measurements in the volute cross-section showed large radial variations in tangential flow speed from the inner to the outer boundary. These, in combination with the large average circumferential velocity, indicated the presence of strong radial pressure gradients, which would be responsible for inaccuracies in the predicted profile. Namely, at every cell location the 'average' cell static pressure, calculated from the equation of momentum in the volute, was significantly different from that at the impeller exit. This affected the velocity distribution in the impeller channel and at the volute-impeller interface. The model was adjusted to account for this phenomenon, assuming of a linear radial distribution of tangential speed. The results obtained by incorporating this behavior were significantly different from those obtained with the original assumption; the correspondence with the experimental results, however, was significantly worse [Fig.4.1.6]. This indicated that radial variations had to be accounted for in order to improve local prediction, but assumptions as to their quantitative significance had to be derived either experimentally or with the help of a two-dimensional code. The experimentally derived characteristic, however, could be obtained from the result of the prediction that incorporated a linear radial pressure profile, by adjusting it to account for appropriate slip factor variations

with flow coefficient [Figs.7.3.4 and 7.3.5]. More on two-dimensional radial velocity and pressure distributions appears in Section 7.3.2 of this thesis, while the combination of linear radial volute pressure profile and variable slip factor is discussed in Section 7.3.3.

The assumption of constant slip factor σ around the circumference and at all flow coefficients was thought to be partly responsible for inaccuracies in the local and overall performance predictions respectively. The code was therefore modified in order to account for varying σ along the Ψ vs. Φ characteristic. This required modifying the theory of the code in order to adopt the definition of slip factor as the ratio of the actual to ideal absolute impeller discharge tangential velocities,

$$\sigma = \frac{C_{u2\,ac}}{C_{u2\,th}} \tag{4.1.13}$$

in order to compare the resulting distribution with those of other authors [9] [12]. However, the problem was that, while σ depended on Φ, the value of Φ was determined for given volute inlet pressure coefficient $\Psi(0)^*$ and σ values. This would have required changing the algorithm and adding another layer of iteration. Moreover, the σ would have had to be adjusted according to a purely empirical relationship derived for a different pump. It was therefore decided to obtain an indication of the importance of σ behavior with Φ by means of an inverse method. A slip factor distribution accompanying flow rate was obtained by adjusting the σ input continuously, in order for the computationally predicted local characteristic slope to converge to the experimentally determined characteristic slope at all flow coefficients [Fig.4.1.7]. The σ distribution found by means of this inverse method was consistent with the observations of the other authors to which it was compared, indicating that the dependence of slip factor on flow rate was responsible for some of the inaccuracies in the overall prediction. The overall head values measured experimentally, however, were too high to be matched by appropriate slip factor choice with flow coefficient. Also, overall SF level appeared similar enough to match the angle dependence patterns measured by Sandler and Miner [Fig.4.1.8]. However, the presence of other effects prevented a more

quantitative determination of this dependence. Insufficient velocity data at volute area locations made it impossible to derive a relationship between local values of flow coefficient and other quantities, in particular the angular derivative of the volute static pressure coefficient [Figs.4.1.9].

Modified versions of the code were also produced to include and model the effect of a proposed bypass system between the pump exit channel and volute locations. The distribution of the bypass and its cross-sectional area could be specified by the user of the program, as could the exit angle in the bypass duct. The flow in the bypass was assumed to be direct and driven by the pressure between the exit channel and each of the volute locations specified. More on the intent of the bypass system and its effect on performance is included under Section 4.3.0.

In different versions of the software, the model was modified to include variations in a number of geometrical pump parameters such as impeller ideal discharge angle, number of blades and the mobility of the flow in the leakage path. A variable area multiplier (AM) for the volute cross-section, which could be visualized as the ratio between the exit area of the new volute under consideration and that of the original volute, was introduced in order to obtain quick estimates of solution sensitivity to volute size. The sensitivity of the solution to frictional losses in the volute, expressed by means of a variable numerical coefficient for the term in the momentum equation, was included. Due to the spiral shape of the volute, the shape of volute cells spaced at regular angle intervals varies from very elongated at the volute inlet to very short near the exit. The possible effect of this distortion on the results was investigated by introducing a variable number of volute cells in the computation. The effects of all these changes on the characteristic slope were determined and evaluated. The results for these analyses were included under Section 4.2.0.

4.1.4. Recommendations for Future Upgrades

Understanding the behavior of slip factor around the impeller exit in a centrifugal pump with a volute is a problem in itself. This problem has not been addressed directly in the literature, although a strong variation in slip factor with angle, particularly at off-design conditions, can be inferred from the data presented by Miner [25]. In particular, a relationship should be obtained between the circumferential behavior of σ and that of other quantities, such as the pressure coefficient and the local impeller exit flow coefficient. At this time, there appear to be two ways to accomplish this:

1) A theoretical or numerical study of the flow in the impeller channel accounting for flow conditions in the volute and the possibility of separation along the suction side of the impeller blade. In this approach, an inviscid, potential flow model in the impeller's reference frame would be used to determine the velocity and pressure field acting on the boundary layer. It would be possible to adopt a computer-based, faster version of the procedure described By Stanitz [4] and mentioned in Section 2.3.2, in order to solve for the flow in the blade passage and at its exit. The comparative length and difficulty of this approach discouraged the focusing of this project toward its discussion and away from the goal of overall system stability.

2) Experimental measurements of impeller exit tangential velocity, radial and tangential pressure and velocity profiles in the volute at all angles and over the whole pump operating range. A correlation between pressure profiles and measured slip factor values was attempted for the pressure and velocity data available [Figs.4.1.9]. Comparisons were made difficult by the limited number of angles and flow coefficients for which measurements were available.

Even though the correlation between theory and experiment in his research was excellent, Miner's velocity data locations were also too sparse to allow a meaningful analysis, and did not include pressure measurements.

The inclusion of a slip factor variable with flow coefficient in the code should also be considered. The main problem is that the input to the code is the volute inlet pressure coefficient, to which corresponds an overall flow coefficient which

depends on the slip factor, as well as other quantities such as pump design, wheel speed, etc.. The overall flow coefficient would then be used to determine the correct value of slip factor. This results in the need for an iterative process which would multiply several times the computation time currently required. The modification to the code should therefore be designed to minimize the increase in computation time. It seems that more success in matching prediction to observed results through slip factor adjustment might be achieved by incorporating this behavior in the code already modified to account for radial variations. More on the results of this technique appears in Section 7.3.3.

The two-dimensional code described in Section 7.3.2 could be considered an extension of the interactive model, since it would provide a more accurate estimate of the exit static pressure driving the impeller flow.

4.2.0. Sensitivity of Prediction to Pump Geometrical Parameters

The volute characteristic curve obtained computationally for flow coefficient values below 0.1, which was close to the BEP, is shown in Figs.4.2.1, 4.2.2 and 4.2.3. At flow coefficient values below the BHP at 0.06, the slope of the volute characteristic became positive, and remained so until shutoff. The value of this slope was somewhat higher than measured by Goulet [24], but it remained close to his computational estimate in spite of the larger impeller discharge area [Fig.2.2.4.i]. The ratio of the flow coefficient recirculated into the volute to that entering the diffuser was largely the same for flow coefficients between 0.008 and 0.1 [Fig.4.2.4]. The aim of the efforts described in this section was to lower the curve slope for Φ_{ov} below 0.06 through appropriate modifications of the pump design and working parameters. Several hypotheses were formulated and tested in the attempt.

In summary, the predicted effect of modifying each of the following pump design characteristics was modeled and analyzed:

1. The leakage path. This was done by assigning different values to the parabolic leakage factor k specified in Goulet's version and by comparing the results of the code in the full leakage and no leakage option.

2. The impact of frictional losses in the volute. This was accomplished by attaching a user-specified sensitivity factor to the frictional loss term in the discretized momentum equation included in the model.

3. Impeller exit blade angle. This was done by assigning a lower value to the exit angle parameter β_2 specified in Goulet's version of the model.

4. The volute cross-sectional area. This was done by including as user-specified input a multiplier of the original area.

5. The number of blades and volute cells. This was done by including the number of blades and volute cells in the range of input values.

6. The position of the tongue relative to the impeller exit boundary. This was done by modifying the volute inlet cross-sectional area and, accordingly, the subsequent area distribution in the model.

4.2.1. Hypotheses

The pressure rise between volute elements was predicted through the discretized momentum equation at each cell i, corrected for leakage effects and skin friction:

$$\Psi_{i+1} = \Psi_i - \Delta\Psi_{s.f.\,i} + \frac{4}{a_i + a_{i+1}} \left(\varphi_i \frac{C_i}{U} - \varphi_{i+1} \frac{C_i}{U} + \frac{C_{m2i}\, C_{u2i}}{N\, U^2} - \frac{C_{lmi}\, C_i}{N\, U^2} \right) \tag{4.2.1}$$

It was believed that varying some of the quantities involved in the relationship would increase the influence of negatively sloping terms at low Φ_{ov}, or could otherwise affect differently the pressure buildup around the circumference at

different flow rates. Therefore, characteristic curves for varying quantities involved in the momentum equation were derived, including in particular the impeller exit blade angle β_2. A sensitivity factor was also attached to the friction loss term $\Delta\Psi_{s.f.}$ in order to determine its influence on the results. The effect of a volute configuration without a leakage path and the two associated momentum equation components was compared to the original one.

Leakage flow momentum loss is also included in the momentum equation. In the assumption of parabolic leakage flow rate, the meridional speed is related to pressure differential at the ends of the path by:

$$C_{lm} = U\,(\Delta\Psi/k)^{1/2} \qquad (4.2.2)$$

The effect of varied mobility of the leakage path flow was investigated by varying the value of the leakage flow factor k and by eliminating leakage altogether.

In pump design situations, it is common to increase the back-sweep of the impeller blades in order to obtain a more negatively-sloped overall characteristic. In the present case, that would require a lower setting for β_2.

It was also believed that momentum addition by the impeller to the flow already in the volute might become too small as Φ_{ov} decreased. Consequently, a variable area multiplier was introduced to evaluate the effect of smaller volute cross-sectional areas on overall performance.

It was then argued that loss of momentum influx to the volute might be related to backflow in the impeller. In order to make the impeller less sensitive to backpressure, configurations with higher solidity were attempted. The presence of backflow as evidenced by the behavior of the impeller exit radial velocity component was also investigated, both computationally and experimentally. Different distances between tongue and impeller exit were tried, which corresponded to varying the radial thickness of the recirculation volute path.

Finally, it was argued that computational results may be affected by the mesh choice made. As it was pointed out in the previous section, the original 100-cell arrangement, cells immediately upstream of the tongue were small in cross-section and very long, while those immediately downstream of it were very thin and wide.

4.2.2. Testing

The predicted slope at low flow rates was slightly higher for a configuration without leakage path [Fig.4.2.5]. As can be seen from the volute element momentum equation, the significance of the leakage momentum increased with flow rate. Its removal caused therefore larger pressure recovery across the element at higher flow rates. This indicated that acting on the shape and size of the leakage path would not result in stability gains without power losses.

Increasing frictional losses improved the pressure curve slope. Unfortunately, these losses were largely proportional to the square of the normalized volute tangential speed, since at every volute cell i

$$\Psi_{s.f.i} = \lambda(C_i) \frac{\Delta L_i}{D_{h\,i}} \frac{C_{i2}}{U} \tag{4.2.3}$$

and therefore increased with flow rate and resulted in the behavior shown in Fig.4.2.6. Even though heavier losses could be accomplished through a different cross-section shape and material finishing, they would have yielded lower BEP and design head rises and were not therefore considered a viable solution.

Characteristic points were obtained for impeller speed as low as 8 m/s, and impeller blade exit angle β_2 lowered to 0.300 rad (17.2 deg.). Although the new parameter β_2 resulted in a lower slope for the characteristic at low flow, the pressure rise at BEP was naturally affected by the decrease in exit speed [Figs.4.2.7]. Compensating for the design head loss would have required increasing the impeller wheel speed Increasing the exit back-sweep of the impeller blades is

often done in order to obtain a negative characteristic, however it must be compensated by an increase inperipheral speed, which is not always desirable. The model predicted the effect shown in Fig.4.2.8 for the original volute and Fig.4.4.8 for the modified volute: the speed at the impeller exit was somewhat lower, compared to that in the volute, than in the original design. The difference increased with flow rate due to the direction of the exiting flow relative to the impeller. This fact resulted in a lower head recovery than in the original case. This effect was superposed to the usual others described and caused the behavior seen in Figs.4.2.7.

Characteristic points for volute area multipliers between 0.6 and 1.1 were derived [Figs.4.2.1, 4.2.2 and 4.2.3]. A smaller area had the effect of producing a substantial acceleration in the flow, that was then found to be linked to the higher slopes observed. Details are provided in the following section.

The number of volute cells was varied between 33 and 500. The 33 cell arrangement guaranteed the least cell deformation throughout the volute. It was found that adopting new mesh selections with different numbers of cells did not alter the pump characteristic prediction [Fig.4.2.9].

4.2.3. Comments

The rise in pressure was decomposed into a part dependent on the ratio between flow coefficient and impeller blade exit angle, which is negligible at low Φ_{ov}, and a part dependent on the ratio between volute tangential speed and impeller tip speed:

$$\Psi_t = \sigma - \left(\frac{\Phi}{\tan\beta_e}\right)^2 + \left(\frac{C}{U}\right)^2 \qquad (4.2.4)$$

The dependence of the last term on Φ in first approximation can be estimated:

$$\frac{C}{U}(\Phi) \sim \frac{\Phi}{A},$$

(4.2.5)

where A represents the cross-sectional area in the volute. The possible characteristic curves in this approximation can be represented as a family defined by several parameters: the slip factor σ, the impeller exit blade angle β_e, and the inverse of the volute cross-secional area A. It is then evident that varying input parameters will have the effect of shifting the characteristic from one curve of a family dependent on the tangential velocity C parameter to another. The attempt to reduce the curve slope by decreasing the volute cross-sectional area resulted in somewhat higher C values at every flow coefficient and steeper characteristics. On the contrary, increasing the back-sweep of the impeller blades implied having a smaller β_e and, consequently, a larger influence of the inverse parabolic component. This supported the argument that some improvement might result from adopting a higher volute area immediately after the tongue, in order to slow down the volute flow, while maintaining the same area at the exit. Doing so would in practice allow the use of two different values of A depending on the operating point. At low flow, most of the acceleration along the circumference due to mass conservation with Φ takes place in the volute, and a larger cross-sectional area in the early volute would result in a slower increase of C with Φ. Since at high flow coefficient a greater increase in flow velocity takes place at the flow turning into the passage on the outer side of the tongue, if the exit area is not varied, the relationship between C and Φ would not be affected as significantly as in the the low-flow case by a larger cross-sectional area in the early volute. However, it was apparent that a tradeoff had to be established between low-flow stability, overall BHP pressure rise and other considerations in selecting the design of the pump.

EFFECT OF PROPOSED PUMP MODIFICATIONS

4.3.0. Effect of a Tongue Bypass Device

4.3.1. Hypothesis

Two of the recognized factors affecting overall pump performance were the asymmetry induced in the flowfield by the presence of the tongue and the drop in momentum at low overall flow rates. A bypass system, which connected the diffuser transition passage to the volute cells [Fig.4.3.1], was devised. This system had the advantages of increasing momentum at selected points in the volute and being able to be switched on and off. In its simplest form, it was pressure-driven, thus having the disadvantage of decreasing influence on volute momentum with flow coefficient. However, it was still thought to contribute toward a reduction of the asimmetry of the volute area profile.

4.3.2. Implementation

The flow through the bypass was considered pressure-driven and parabolically related to the pressure drop across it. The bypass flow speed was then given by

$$C_b = U\,(\Delta\Psi/k)^{1/2}, \tag{4.3.1}$$

analogously to the flow in the impeller leakage path. Assuming no resistance to the flow, the coefficient k was considered unity. The total flow through the bypass depended on the cross-sectional area, which had to be selected. Injecting the bypass flow into the volute had two consequences: increasing the amount of flow through an additional term in the continuity equation, and increasing the pressure coefficient through an additional term in the momentum equation. The latter effect was expected to be much lower, especially at low Φ_{ov}, since bypass speed scaled with pressure drop as indicated above. The condition that flow might travel from the diffuser to the volute only, and not vice versa, was posed. This was expected to improve performance at high flow coefficients.

The original bypass configuration had a single channel between the diffuser transition and the volute section immediately after the tongue. This was later expanded into channels connecting the diffuser transition with points in the volute between 4° and 179°, spaced every 7°. This increased the bypass flow fraction substantially without increasing cross-sectional areas. Flow coefficient profiles with and without bypass at the same inlet pressure coefficient input value $\Psi^*(0)$ are compared in [Fig.4.3.2].

4.3.3. Results

The code was modified in order to model the effect of bypasses of the types described, and calculations were performed at various flow coefficients as well as various bypass areas A_b, bypass exit angles γ_e and blockage factors k_b without significant differences in performance. The effect of a bypass system, with linearly increasing area over the whole circumference and a total area approximately 6 times as large as that of the previously tested configuration, was noticeable but marginal [Fig.4.3.3]. The effect of changing the bypass exit angle was insignificant [Fig.4.3.4].

It appeared that no noticeable benefit to low-flow performance resulted from employing a bypass; it became possible, however, to model low flow performance with very large volute cross-sectional areas, which were associated with very small characteristic slopes and led to the new volute area design proposed. Results indicated that a much flatter pump characteristic, with a comparable BEP head coefficient rise could be obtained for a multiple of current volute area AM of 2.2 [Fig.4.3.5]. Divergence problems were observed for solutions tried on non-bypass configurations at AMs comparably high. For the area increase proposed in the new volute design, however, divergence of the solution did not occur and the bypass was not adopted in predicting its performance.

4.4.0. Effects of Larger Volute Cross-Sections

A larger volute cross-sectional area was expected to result in lower volute tangential speeds. Higher volute speeds were associated with higher overall flow rates, while the impeller exit tangential velocity decreased due to the exit blade orientation and was less sensitive to flow variations, as long as the wheel speed was not varied. It was therefore predicted [Figs.4.4.1 and 4.4.2], and confirmed by experimental observation, that exit velocities substantially lower than volute speeds were associated with high flow coefficients in the original volute design. Such differences were expected to translate into mixing losses directly related to operating flow rate. In addition, the static pressure of the exit flow was predicted to decrease as the component was accelerated by the oncoming flow.

At the same time, a larger volute design, incorporating both a steeper area profile just downstream of the tongue and a larger exit area was predicted to yield tangential impeller exit velocities consistently higher than those in the volute [Fig.4.4.3]. The volute cross-section could be increased proportionally in order to minimize mixing losses at higher flow coefficients. This was offered as an explanation for the higher head coefficients predicted at high flows and the lower ones at BHP. A flatter characteristic was predicted, consistently with the fact that the variance of the impact of mixing losses with flow coefficient was reduced. This meant that the flatter shape of the predicted characteristics was also consistent with the smaller range of volute speeds over the entire range of flow coefficients expected with a larger cross-section. This led to the proposed volute configuration denoted as 10/1991 [Fig.4.4.4]. This geometry yielded the characteristic change of Fig.4.4.5.

With this, however, several questions arose. First, the onset of instability moved from Φ=0.06 upwards, thus reducing the margin at the operating point. Given the gain in head coefficient, however, it appeared that the operating point might also be moved to the right as well, without affecting performance. In fact, the BEP itself was expected to shift upwards, thus affecting the pump's specific speed and size and making the benefits of the projected change debatable. Second, the realism of the model was expected to decrease as the area of the volute increased. Adopting

larger areas might have required introducing radial variation of volute quantities and the effect of different cross-sectional shapes. Third, it was unclear how such an increase could be reproduced in the experimental setup without substantial modifications to the existing structure.

4.5.0. Volute with High Initial Slope

In response to the three concerns above, it was fortunately found that expanding the volute area in its first portion had an effect on velocity distribution and overall performance similar to that obtained with the 10/1991 volute design, even though the area at the exit of the volute did not increase [Figs.4.4.6 and 4.5.1]. An overall characteristic curve, predicted for an area profile which increased up to about half of the final area increase at about 50°, is compared to that given by the original and 10/1991 designs in Figs.4.5.2 and 4.4.4. In all cases, the predicted operating point pressure coefficients were noticeably higher than in the base case, indicating that considerably flatter characteristics could be obtained without modifying the existing structure.

The steeply diverging volute walls required, however, posed the question of losses due to separation. If the volute cross-section could be treated as a normal diverging passage, there was little doubt that massive separation would occur, and nullify the effect of the sudden area increase. Due to the presence of radial velocity components from the impeller exit and strong vorticity in the cross-sectional plane, however, the realism of the simple diverging passage assumption was greatly reduced. In both proposed new geometries, the predicted pressure gradients along the volute circumference, which could be associated with separation, were not substantially different from those measured in the old volute design, for which no separation was observed [Figs.4.5.3 and 4.4.7]. In the modified pump, a strong circumferential vortex shed from the tongue along the volute wall, which would have effectively prevented any boundary layer separation from occurring, was later observed.

It was decided to first examine the possibilities offered by a change in the distribution of volute cross-sectional area without changing the exit area and,

consequently, without changing the BEP, BHP and specific speed of the pump. For this purpose, the prediction code was modified to observe the effect of varying area profiles on the predicted characteristic, while maintaining the exit area at the tongue unchanged. The polar coordinates of a breakpoint in the volute area profile were used as parameters in the search [Fig.4.5.4, 4.5.5 and 4.5.6]. The effect of a number of break points of 2 or larger was investigated and found to be insignificant. An effective tradeoff between performance improvement, model realism and design practicality was reached with the configuration summarized in Table 4.5.1 on the following page [Fig.4.5.2].

The above points were connected by means of two second-order curve fits, such that (1) the slopes of both curves at the break points were the same, and (2) the slope of the latter curve at the beginning of the straight volute wall section was zero. This led to the following radial area distribution:

$$A(N) = 0.00138 + \begin{cases} \backslash A(-2.627\ 10^{-5}\ N^2 + 5.255\ 10^{-4}\ N & 0 \le N \le \\ 10,-3.552\ 10^{-7}\ N^2 + 6.821\ 10^{-5}\ N + 1.981\ 10^{-3} & 10 \le N \le 95) \end{cases} \quad (4.5.1)$$

which was implemented on the pump with the approach described under Chapter 6.0.

Table 4.5.1. Volute Parameters in Proposed Design

	Angle [°]	Cell Nr.	Area [m^2]
Immediately after tongue	0	0	0.00138*
Profile break point	10	36	0.00401
Start of straight volute wall	344	95	0.00663*
Immediately before tongue	360	100	0.00771*†
Pump exit at tongue	360	(100)	0.00548

* Same as in old design.

† Based on distance between volute wall and impeller tip; includes areas on both sides of the tongue

5.0 PREDICTION OF CHARACTERISTIC EFFECT ON STABILITY

The prediction of instability for the pump in its original and modified configurations, and connected to the experimental loop apparatus, was based on the Greitzer stability theory. As described in Section 2.1.0, the behavior of mass flow and pressure perturbations in a pumping system composed of a compressor, a throttle and other devices whose inertia and compliance can be estimated depends on three factors: the local pump pressure characteristic slope, the local throttle characteristic slope and the ratio of the system's inertia and compliance, or B parameter. Thus stability is generally dependent on the operating point of the system considered. However, a positive slope is required of the pump characteristics, as was pointed out in the previous chapters.

5.1.0. The Determination of System Stability

In the present experimental setup, the compliance of the system was controlled by varying the volume of air-filled air bags within the two plenum vessels. Once the volume was fixed, the pump was started and the behavior of perturbations was observed throughout the pump's operating range. The behavior of the pump was represented in terms of a critical flow coefficient Φ_{tr}, where the onset of instability occurred, whose value depended on the setting on the plenum volume and, consequently, on the B parameter. It is then proper to say that

$$\Phi_{tr,} = \Phi_{tr}(B) \tag{5.1.1}$$

In the linear analysis procedure, Φ_{tr} was defined as the flow coefficient value at which the eigenvalues of the system of four equations derived by Bons:

Momentum conservation in the piping ducts:

$$\frac{d\dot{m}_P}{dt} = \frac{A_P}{L_P}(p_{lg} - p_{sm} - \Delta p_P - \Delta p_{PL}) \tag{5.1.2.a}$$

$$\frac{d\dot{m}_T}{dt} = \frac{A_T}{L_T}(p_{sm} - p_{lg} - \Delta p_T - \Delta p_{TL}) \tag{5.1.2.b}$$

Mass conservation in isentropically compressible plenums:

$$\frac{dP_{sm}}{dt} = \frac{\gamma P_{sm}}{\rho V_{sm}}(\dot{m}_P - \dot{m}_T) \tag{5.1.2.c}$$

$$\frac{dP_{lg}}{dt} = \frac{\gamma P_{lg}}{\rho V_{lg}}(\dot{m}_T - \dot{m}_P) \tag{5.1.2.d}$$

have zero real part. In the approximation of this linearization, instability is identified by a positive real part for the eigenvalue, while the imaginary coefficient represents the frequency of the unstable oscillations ω_{unst}. This can be shown to be connected to the value of the B parameter [26]:

$$B = \frac{U}{2\,\omega_{unst}\,L_{PL}} \tag{5.1.3}$$

Since the boundary between stability and instability is not sharp under real-life conditions, a semi-arbitrary criterion had to be established to identify the onset of instability in experimental observations. Φ_{tr}, was therefore defined as the flow coefficient value at which the RMS amplitude of the pressure oscillations grew to 3% of the design pressure rise. This criterion was applied by Bons and adopted for the sake of consistency in the work done by Sandler.

Both experimental observations and linear predictions showed the following two facts [Fig.5.1.1]:

1) As the throttle flow coefficient was reduced, a first stability-instability transition was encountered for certain plenum volume settings corresponding to B parameter values above a certain critical threshold B_{cr}. B_{cr} was seen to depend on a number of operating conditions, as described below.
2) As the throttle flow coefficient was reduced further, a second transition, from unstable operation to stable operation, was encountered at very low flow coefficients. The origin of this second transition was less clear than that of the first. The best curve fits of experimental characteristic data, which were used for the computational predictions as well, appeared to be fifth-order polynomials. These curves displayed substantial flattening in proximity of shutoff. Since the margin of uncertainty in steady-state measurements made at extremely low flow coefficients was severely increased by ample pressure oscillations, it remained unclear how real the effect was, considering also that predictions obtained using third- and even second-order fits displayed a similar phenomenon.

The stability observations for the original pump design were conducted first by Bons [26], who obtained satisfactory agreement between the predictions of the linear theory and his experiments. Sandler's M.S. thesis [29] contains more detail on the procedures followed in the measurements done in this stage of the project, which was centered on the behavior of perturbations in the pump with a modified volute.

The presence of the pump in the system had several effects. First, the wheel speed fluctuated in response to mass and pressure variations, storing energy and adding to the inertia of the system. This was more significant at higher speeds and resulted in somewhat better stability. This could be seen in three ways: (1) comparing the predicted instability boundary of a pump with fixed wheel speed and that of a pump with variable wheel speed [Fig.5.1.2]; (2) comparing the predicted stability boundaries of pump operation at different wheel speeds [Fig.5.1.3]; and (3) comparing the measured stability boundaries of pump operation at different wheel speeds [Fig.5.1.4]. The third set of observations had been collected by Bons and corroborated the trends shown by the other two. An element of difference was that actual stability performance at different speed was

affected not only by different B parameter corrections, but also by changing characteristic shapes [Fig.5.1.5].

Second, due to the non-negligible linear dimensions of the compressor, a lag in the response of the pump to changing conditions contributed to a delay in the onset of instability. This lag time was defined by Bons as:

$$\tau = \frac{L_{thr}}{\Phi\ U} z_{lag} \tag{5.1.4}$$

Where z_{lag} was a factor to be determined by the fit between predicted and experimental data. Bons estimated z_{lag} to be approximately 0.03. The effect of a lag in the predicted response of the pump, and therefore its stability, for z_{lag} values between 0.01 and 0.15 can be observed in Fig.5.1.6.

Third, the presence of the pump during operation affected the pressure in the plenums, thereby reducing or increasing the effective volume of the air bags and slightly varying B across the operating range. Even more significant than the dependence on flow coefficient was the effect of a new pump configuration, observed when the new volute was installed. This resulted in a different relationship between the system characteristics and the B parameter for the new pump, about which more is said in Chapter 6.0.

5.2.0. The Linear Stability Code

The code took as main input the following values: pump volute design, pump speedline, volume setting of the pump and throttle plenums. The value of the lag factor and the shutoff plenum pressures could be changed. It proceeded to examine discrete operating points, corresponding to flow coefficients regularly spaced every 0.001 between 0.001 and 0.07. For each of these operating points, the local speedline slope for the appropriate design was determined from relationships established as curve fits to either experimental or computational data.

It was also necessary to use curve fit relationships for the variation of impeller tip speed with flow coefficient. The dependence of impeller tip speed on flow rate was determined experimentally for each speedline considered. The throttle slope was then estimated at the chosen operating point by subtracting the pressure loss in the pump and throttle legs from the pump pressure rise. The actual plenum volumes were corrected for the effect of pressure increments due to pump operation. For every flow coefficient analyzed, the output would list the real and imaginary part of the system eigenvalues and the B parameter corresponding to that frequency of unstable oscillations. Please refer to Appendix B for details of the code and the output.

5.3.0. Results

The predicted effect of the characteristic derived through the volute-impeller interaction code for the new pump volute design was determined by introducing the predicted characteristics for 100%, 80% and 60% of design speed, the speedlines for which the wheel speed and plenum pressure dependence on the flow rate had been already determined by Bons. For comparison, the effects of the predicted characteristics for a pump fitted with the old volute configuration at 100%, 80% and 60% of design speed were introduced. Using the same experimentally derived relationships between system parameters and B isolated the effect of the steady-state characteristic slope. The predictions of the effect of the 10/1991 volute configuration, with its much larger exit area and considerably flatter characteristics, were also included for reference.

Third-order curve fits were adopted for the positively-sloped portion of the characteristic, reflecting the smoothness of its shape as predicted by the interaction code. By comparison, fifth-order fits were adopted in the prediction of stability for the experimentally derived characteristics of Chapter 6.0, reflecting the roughness and kinks in real-life pump behavior.

The results were shown in the form of stability maps, where the proper system condition could be identified for each flow coefficient and B parameter value

[Figs.5.3.1]. The points on each curve were the critical instability inception flow coefficients for that configuration and B. In the regions to the right of the curves, the eigenvalues of the linearized system of Section 5.1.0 were positive, whereas they were negative in the rest of the map.

Two important effects were predicted as a consequence of the characteristic slope change caused by the modifications to the volute: a shift to the right of the threshold B value and a smaller unstable flow range at each B higher than the threshold value. This indicated a larger range of possible stable operation for the pump and the system relative to the original volute design. The results confirmed the expected benefits resulting from a pump with lower tangential speed in the volute and suggested the convenience of implementing the proposed design on the pump test apparatus. It was clear that this analysis simply confirmed that a flatter characteristic, such as that predicted for the proposed volute design, would yield a larger range of stable operation. The predicted effect of the proposed geometrical changes on the characteristic had still to be verified experimentally as described in the following chapter.

6.0. NEW VOLUTE TESTING

6.1.0 Implementation of New Design

Keeping the transition inlet cross-sectional area and shape fixed avoided a number of technical difficulties connected with the three-dimensional layout of the volute backplate, transition and seal pieces. Some difficulties, however, remained. As can be seen from Fig.6.1.1, the volute backplate and seal were bolted together through the same circular steel ring along their respective outer and inner edges. The length of the bolts was close to the uncarved thickness of the backplate. Expanding the volute radial thickness in proximity of the transition would have therefore interfered with this configuration and required drilling new holes. In addition, it would have been necessary to redesign and rebuild the transition piece.

Changing the volute area distribution between the same end values limited the scope of the hardware modifications to the volute backplate. The original volute radial profile was carved on the inside of the backplate, so that additional plexiglass had to be carved out in order to achieve the new profile desired. Since the original pressure tappings were located along the radial centerline of the previous volute, additional holes had to be drilled to house tappings along the new centerline [Fig.6.1.2]. The pump was then cleaned, reassembled and readied by Sandler for the measurements.

6.2.0 Testing Procedure

Overall pressure measurements were then conducted by Sandler on the pump, now fitted with the volute modified according to specifications, at 23, 50 and 80 percent of its design speed. Overall pressure measurements were defined as the differences between the pressure measured at the last diffuser location and the suction pipe location. Individual component performance was also estimated in terms of the pressure rise difference between the ends of each component, as described in Section 6.3.2.

simply reflects the previous findings [Fig.6.3.2]. Data for other speedlines, however, suggest that the new pump design interacts with the system so as to yield a slightly different B parameter corresponding to a system configuration [Figs.6.3.3 and 6.3.4], as described below. Since Bons's 80% speedline characteristic equation appeared inconsistent with Sandler's values, Figs.6.3.3 and 6.3.4 were included only with the intent of showing the difference between predictions based on system parameters and B.

The new design resulted in a significantly smaller instability region [Fig.6.3.1] as predicted by the linear stability code. In particular, the lowest B value for which instability can occur shifted upward from about 0.260 to about 0.285 and the higher critical flow coefficient shifted downward by about 0.007 above B=0.285. In addition, the lower Φ_{cr} shifted inward by about 0.003 and the area of the instability region between B=0.260 and 0.500 decreased by more than 30% overall. These results were in agreement with the predictions obtained using model-derived overall pump characteristics.

The speed characteristic of the pump, which described the variation in impeller wheel speed with flow rate, was a important factor in the determination of the B parameter, particularly at low speedlines. The plenum pressure characteristics exhibited similar variations for the original and the modified pump. Pressure variations with the pump on, however, were consistently different across the whole operating range. Specifically, the pressure rise in the small volume was larger, and that in the large volute was smaller. The consequent reduction in compliance for the small plenum resulted in lower B parameters for the new volute pump at the same loop settings as in the stability prediction, and was expected to have the same effect on experimental measurements with the plenums at least partially filled.

If one effect of the new pump design was that of lowering the B parameter for the systems in which it is inserted, then there appeared to be an additional independent benefit from adopting it. Since fuel systems are not defined in terms of a B parameter but, similarly to the one considered in this study, in terms of geometrical and material properties, applying a modified pump would improve the response not only of the pump, but of the system as well. In order to establish

The speed characteristic, i.e. the wheel speed variation with flow rate, and the pressure differences from pump off conditions for both plenums were also recorded at that time. These additional data were used in predicting the dependence of the critical flow coefficient on B through the linearized stability theory, applied to experimentally derived data instead of predictions [Figs.6.3.1, 6.3.2, 6.3.3 and 6.3.4].

Subsequently, the behavior of the system was studied by Sandler across the operating flow coefficient range of the pump. This was done by setting the air plenums on a certain volume, and moving the throttle from design point down to near shutoff. The amplitude of the pressure oscillations was recorded, and whenever their RMS amplitude reached 3% of the design head rise value, surge was detected, and the amplitude and frequency of the oscillations, as well as the average flow rate were recorded and the B parameter estimated. This allowed for the production of stability maps analogous to those presented in Chapter 5.0.

6.3.0. Results

6.3.1. Overall Performance

The predicted trend towards flatter characteristics with increasing volute cross-sectional areas was confirmed by the experimental measurements [Figs.6.3.5]. In terms of absolute results, as in the case of the old volute, the experiment showed characteristic flatter curves than predicted.

The 50 percent speedline was the only one for which a direct stability comparison with experimental results was possible. Pressure and speed characteristics for the original volute were available. The plenum pressure characteristics, however, were not, and the same characteristics were used in the new and the old case. While this has no effect on the mapping of the critical flow coefficients versus system B parameters [Fig.6.3.1], a comparison between the two designs on the effect of plenum air volumes is impossible at 50% and the mapping versus V_{sm} values

this, however, the effect of the new pump on all the actual systems involved should have been tested; moreover, pursuing this consideration would have been required a study of the possible benefits to stability deriving from redesigning the fuel system in order to obtain a lower B parameter, which was outside the scope of the present work. These were the reasons why this aspect of the change in performance was not discussed further. It was however believed to represent an important area of investigation.

6.3.2 Individual Component Performance

The contributions of the various flow segments in the pump were estimated separately by obtaining the difference between pressure transducer measurements at the end and beginning of each segment [Fig.3.1.7]. The parts studied were:

Impeller:	Normalized pressure value at V1
Volute:	Normalized pressure difference V7-V1
Tongue:	Normalized pressure difference TR1-V7
Diffuser:	Normalized pressure difference YSEX-TR1

Several differences in the contributions of individual pump parts appeared between the new volute pump and the old one [Figs.6.3.6, 6.3.7 and 6.3.8]. In particular, the contribution of the tongue region appeared to be less sensitive to operating point and displayed much smaller slopes in the low-flow region [Figs.6.3.9 and 6.3.10].

In addition, it appeared that the diffuser was in both cases, and particularly for the modified pump, the largest contributor to the positive slope of the characteristic at low flow coefficient. This suggested that better stability behavior may be obtained by eliminating the diffuser and increasing the volute exit area to coincide with the diffuser area, or at least accomplishing part of the diffusion within the volute. The advantage resides in the fact that while the head rise in the diffuser varied with the square of the tangential flow velocity at the pump exit, the volute performance would be more constant since, due to flow recirculation, the volute flow velocity

resulted less dependedent on flow coefficient. The discussion of this solution appears in Section 7.3.1.

6.3.3 Volute Pressure Profiles

The observed volute static pressure variations were compared to the predictions for the new volute near BEP [Fig.6.3.11]. The large gradient immediately after the cutwater due to the rapid area expansion was effectively reproduced in the computation. After the slope break point, the pressure increase continued at a slower pace. In proximity of the tongue, the pressure trend reversed, possibly due to accelerating flow in the nearly constant-area volute channel with additional flow being injected by the impeller. There was a noticeable increase in static pressure values in the last 15-20° before the exit tongue plane, which was related to a combination of the effect of the diverging passage in the last 16° of the volute, where the volute wall departed tangentially from its profile, and that of some flow being turned away from the exit channel and slowed down at its inlet (this operating flow coefficient is somewhat below the tongue design value).

The noticeable pressure decrease in the last fourth of the volute indicated that the volute profile could be better optimized in order to avoid losing some of the benefits of the steep area increase and obtain an even flatter pressure characteristic curve.

6.3.4 Time Resolved Measurements

The critical pressure coefficients derived experimentally by Sandler on the new volute design were compared to those measured by Bons on the original design [Fig.6.3.12]. The area of instability appeared to have been significantly reduced, with the greatest benefit taking place between B=0.3 and 0.5. The fact that B_{cr} seemed lower for the new design was considered to be caused by lack of measurements in lower B ranges by Bons at this speedline. Similar maps taken by Bons at different speeds show the region of surge extending below B=0.25 [26]. If

that was the case, B_{cr} for the old design at 80% of design speed would correspond to a Φ_{cr} around 0.02. It appeared that the expectations set by the pump performance predictions were met and exceeded.

7.0 CONCLUSIONS

The results of this work proved that pump system stability gains which would have required compromising with performance requirements or operating limits (such as pump speed) if addressed more traditionally, were achieved by an innovative volute design. This has more general implications on the design of a new pump that incorporates these findings and additional modifications along trends pointed out in this study and discussed in this section.

7.1.0. Conclusions about Pump Stability and Pump Design

Current design resources exist to address virtually every aspect of pump performance. On the other hand, every design choice results in enhancing some performance parameters while sacrificing others. Choices in such cases are therefore made on the basis of the application of the design rather than on general pump theory guidelines, within the constraint imposed by the physics of the flow. One example is the obvious restriction that the BEP head H_{BEP} of a stable pump must be lower than its shutoff head H_0. The best performance by a stable pump can therefore be obtained by designing it so as to obtain as flat an overall characteristic as possible. Negative-sloped characteristics do not represent a stability advantage per se, and do not maximize the performance that can be obtained. It appears therefore that the changes suggested and tested result in significant stability improvements at the limited performance cost of 1 to 2 percent less BEP head. If the design point flow rate, as in this case, is higher than that at BEP, there seems to be a performance advantage in the form of additional design head rise that could be traded for a more negative characteristic.

In general, finding design changes that do not compromise on some parameters or require variable geometry with flow rate depend on the knowledge of the changes in flow behavior through the operating range of the pump. One example of this principle is the rationale for the elimination of the diffuser described in Section 7.3.1: the pressure rise in a diffuser located at the exit of the compressor is higher

at larger flow rates because most of the flow acceleration takes place at the flow turning in proximity of the tongue [Fig.4.1.5]. As the flow rate decreases, due to the flow turning, the tangential velocity in the volute becomes higher than that at the pump exit, so that greater head can be obtained by diffusing the flow inside the volute. Adopting a larger exit area throughout the volute and at the exit, therefore, results in a flatter diffusion characteristic across the operating range. Performance predictions for this design are shown in Section 7.3.1.

7.2.0. Discrepancies among Results

7.2.1. Compressor Characteristic Estimate

Even though the values predicted by the interactive code did not match those measured experimentally, trends resulting from design changes were successfully reproduced. This indicated that some mechanisms included in the model and on which the changes were based, such as the mixing between the impeller and volute jets, were significant in determining performance in the actual pump. Two sources of discrepancy that were discussed but not corrected in the model, the slip factor variation with flow rate and the nonuniformity of the radial speed profile, showed potential for interesting predictability improvements, as discussed in Section 7.3.3.

7.2.2. Compressor Stability Determination

It is clear that feeding a simplified, linearized theory of stability with somewhat uncertain local compressor characteristic slopes derived from curve fits of experimental operating points, which themselves carried some uncertainty, had to result in predictions with a significant degree of approximation. Additionally, the criterion adopted to establish instability in under experimental conditions was not consistent with that of the predictions. The present criterion, by which pressure oscillations of RMS amplitude equal or greater than 3% of the BEP steady-state value were categorized as 'surge', was adopted in order to perform a meaningful

comparison of the data obtained for the modified volute to those obtained for the original. Within this context, the trends predicted were confirmed by the measurements taken. In particular, there is a discrepancy of about 2% between the predicted and measured threshold value of B, B_{crit}. The discrepancy between the values of the flow coefficient at which instability is first encountered, corresponding to B_{crit}, is much larger. The uncertainty in the prediction of the local characteristic slope, more than the model, particularly at low flow coefficients, may be responsible for a significant part of this discrepancy.

7.3.0. Recommendations for Further Work

7.3.1. On A Larger Volute, Diffuserless Configuration

The contributions of individual compressor components to the overall characteristic in both the old and new volute design were presented and discussed in Section 6.3.2. From the measurements taken, it appeared that the diffuser was the largest contributor to the positive slope of the characteristic. Its contribution derives from the recovery property of the diffuser pipe. In general, the pressure recovery across a pipe diffuser for an incompressible liquid is given by:

$$\Delta p = c_{pr} \rho C_{inlet}^{2} \tag{7.3.1}$$

which, in the present case, can be written as

$$c_{pr} = \frac{1}{2} \Delta\Psi \frac{U^2}{C_{inlet}^2} \tag{7.3.2}$$

Where the coefficient c_{pr}, defined as the diffuser pressure recovery factor, is function of diffuser geometry parameters, throat Mach and Reynolds numbers and

throat blockage. A discussion of diffuser preformance is given, for example, in [19]. The discussion of the variation of c_{pr} for the present pump diffuser was done by Goulet in [24]. Since the pressure recovery is proportional to the square of the inlet velocity and the variation of c_{pr} is approximately negative linear with Φ, the diffuser head coefficient rise contribution slope at constant wheel speed is positive, as proven by the observations [Figs.6.3.9 and 6.3.10].

While eliminating a diffuser from the original or modified consideration would result in a more stable characteristic, it would likely compromise the head rise at BEP flows and higher [Fig.7.3.1]. It is possible, however, to increase the area of the pump exit cross-section and accomplish the diffusion, at least in part, inside the volute. This would have a dual effect:

1) the volute represents a longer, more slender diffuser with less blockage. This would result in a higher c_{pr} and more effective diffusion.

2) at low flow coefficient, the tangential velocity of the flow recirculating in the volute becomes higher than that at the pump exit plane. Therefore, a higher head rise at low flow coefficients can be obtained by diffusing the flow in the volute. As the flow rate increases, the amount of flow turning into the exit passage, and the consequent acceleration, increases. This acceleration takes place at the pump exit, so that some of it can only be recovered by an external diffuser. The comparative performance of the volute-diffuser with respect to an external diffuser, therefore, is worse at high flow rates. This condition can be improved, however, by adopting a larger pump exit cross-sectional area. The design head coefficient loss predicted was only 3% for a pump with volute design analogous to the modified one and an exit area equal to that at the original transition outlet, still considerably lower than that at the diffuser exit [Fig.7.3.2]. The predicted stability benefits, which can be inferred by the characteristic slope, were favorable and much more significant [Fig.7.3.3]. The 'original' configuration used for comparison was the modified pump version which had already shown a substantial stability improvement over the 'real' original configuration.

The actual performance benefits and tradeoffs resulting from the adption of a similar configuration seemed worth investigatng by implementing it on the existing Gas Turbine Lab pump testing facility or a similar one.

7.3.2. On a Two-Dimensional Volute Flow Model

Before the modified volute was tested, it was highly uncertain whether the geometry trends predicted by the model would be reproduced on the real pump. This was motivated by the significant discrepancies that were observed between predicted and measured local and overall pressure values. At about the same time, large radial variations in radial and tangential velocity in the volute were measured by laser velocimetry [29]. The introduction of a radial pressure gradient in the volute, based on a linear volute velocity distribution, did not improve the predictive capabilities of the model [Fig.4.1.6], although it was later discovered that the pump characteristic predicted by this version of the model could be adjusted to that measured experimentally by varying the slip factor throughout the operating range. By contrast, due to large differences in value, appropriate slip factor variations with flow rate could only approximate the slope of the measured characteristic. Since slip factor values would have had to exceed 1 over the whole flow coefficient range, it was clear that slip factor alone was unable to explain the discrepancies between overall performance measurements and predictions in the radially constant volute velocity approximation.

The fact that introducing radial variation of volute velocity per se did not improve the model prediction suggested that the distribution of velocity may be different from linear. Laser velocimetry measurements obtained at grids were not conclusive, since the profiles obtained changed substantially depending on throttle flow rate, radial and axial location (height of the measurement). At the same time, only a small number of grids were obtained in two short sections of the volute [Fig.3.1.6], making it impossible to detect any trend along the volute, similarly to what had happened with the slip factor. It was therefore thought that a two-dimensional volute flow model would help determine the correct profiles at each angular location and flow rate. Such a model, connected with the original interactive procedure would provide a corrected estimate of the pump performance.

Several clues pointed to possible characteristics for the model. First, Miner [23] had indicated that the inviscid, potential and two-dimensional flow assumption

allowed simple and realistic velocity predictions that were confirmed by laser velocimetry data. Second, it was indeed possible to attach the interactive model to the volute model. In this configuration, the interactive model would provide the velocity distributions $C_{m2}(\theta)$ and $C_{u2}(\theta)$ at the impeller exit boundary which would allow the development of the solution in the interior of the volute domain. In turn, the solution obtained in the volute would provide the velocity and pressure profiles necessary in order to estimate more realistic static pressure values at the impeller exit and revise the interactive determination of the impeller exit velocity field. The convergence of these two algorithms to sufficiently stable velocity profiles would indicate the presence of a solution, from which local and overall pressure values could be derived.

Several questions were also formulated. First, the laser velocimetry measurements detected significant axial variations in the radial velocity profiles. This tri-dimensionality was largely due to the presence of the relatively narrow impeller exit jet close to the centerline of the much higher volute passage, combined with the two narrow leakage passages at the top and bottom of it. This interaction had an effect in the form of two vortices that occupied the upper and lower portions of the volute cross-section. It is therefore unclear whether sufficient accuracy could be obtained by modeling only two-dimensional effects. Second, an understanding of the flow behavior at the pump exit boundary, over the whole pump operating flow coefficient range, is necessary to the correct implementation of the solution of this elliptical problem. This would require either conducting a series of LDV measurements at the transition inlet or experimenting with different velocity profiles until a correspondence with the performance measurements is found. Third, the computational time of the two iterations coupled together was estimated to be of the order of several hours, compared with the time required, on the order of one minute, by the interactive procedure. This suggested that solutions should be developed in order to increase the speed of the computation or to improve predictive capabilities by incorporating relevant flow properties within the framework of the original interactive code. This constitutes the subject of Section 7.3.3.

7.3.3. On Radial Pressure Corrections Combined with Slip Factor Flow Coefficient Variations

It was observed that it was possible to match the measured pump characteristic with the predicted one by correcting the volute head coefficient with a radial variation term and introducing a variation in impeller slip factor with flow rate. The variation required could not be determined a priori, but could be derived from the local shift required by the matching of the two curves. The slip factor variation adopted to match the predicted characteristic slope in the constant volute velocity approximation with that measured [Fig.4.1.7] was found to be consistent with the behavior determined by other authors researching this subject [9] [10] [12].

The validity of the slip factor approach and its general applicability to different designs had to be tested. This was done by comparing the slip factor distributions with overall flow coefficient that were required by the matching for both the original and modified volute designs [Fig.7.3.4 and 7.3.5]. It was unclear which operating parameter was most closely related to slip factor.

Since the model accepted as input the head coefficient at the volute inlet, the slip factor corresponding to each operating point and configuration had to be determined iteratively: once the operating point corresponding to that pressure input value was determined, the slip factor was adjusted according to the dependency relation used, and the iteration series was repeated until convergence. This requires a change in the model which should result in computations 10 to 100 times longer, depending on the accuracy sought. Most importantly, a sound dependency relation between slip factor and some operating variable, such as the overall flow coefficient or the impeller exit local flow coefficient, is necessary. The latter variable choice, however, would require the introduction of a slip factor variable with angle and the discussion of its implications with respect to local pressure and volute velocity predictions.

VII. REFERENCES

[1] H.W. Emmons, *The Numerical Solution of Compressible Fluid Flow Problems*, NACA TN 932, May 1944.

[2] H.H. Anderson, *Centrifugal Pumps - An Alternative Theory*, Proceedings of the Institution of Mechanical Engineers, vol. 157, 1947.

[3] J.D. Stanitz, *Two-Dimensional Compressible Flow in Conical Mixed-Flow Compressors*, NACA TN 1744, Nov. 1948.

[4] J.D. Stanitz, G. O. Ellis, *Two-Dimensional Compressible Flow in Centrifugal Compressors with Straight Blades*, NACA TN 1932, Aug. 1949.

[5] H.H. Anderson, *Modern Developments in the Use of Large Single-Entry Centrifugal Pumps*, Proceedings of the Institution of Mechanical Engineers, vol. 169, 1955.

[6] A.J. Stepanoff, *Centrifugal and Axial Flow Pumps*, Wiley, 1957.

[7] R.C. Worster, *The Flow in Volutes and Its Effects on Centrifugal Pump Performance*, Proceedings of the Institution of Mechanical Engineers, vol. 177 No. 31, 1963.

[8] F.J. Wiesner, *A Review of Slip Factor for Centrifugal Impellers*, ASME Journal of Engineering for Power, October 1967, p. 558.

[9] T. Sakai et al., *On the Slip Factor of Centrifugal and Mixed-Flow Impellers*, Transactions of the ASME, 67-WA/GT-10, 1967.

[10] A. Whitfield, *Slip Factor of a Centrifugal Compressor and Its Variation with Flow Rate*, Proceedings of the Institution of Mechanical Engineers, vol. 188 32/74, 1974.

[11] H.H. Anderson, *Prediction of Head, Quantity and Efficiency in Pumps - the Area Ratio Principle*, Proceedings of the 25th Annual International Gas Turbine Conference, New Orleans, LA, Mar. 1980.

[12] C. Salemi, V. Di Matteo, *Slip Factor Calculation in Centrifugal Pumps by Means of Evaluation of Wall Boundary Layer*, Proceedings of the 25th Annual International Gas Turbine Conference, New Orleans, LA, Mar. 1980.

[13] F. Schweiger, *Some Effects on the Design of Centrifugal Pumps*, Proceedings of the 25th Annual International Gas Turbine Conference, New Orleans, LA, Mar. 1980.

[14] C. Weissgerber, A.F. Carter, *Comparisons of Hydraulic Performance Predictions and Test Data for a Range of Pumps*, Proceedings of the 25th Annual International Gas Turbine Conference, New Orleans, LA, Mar. 1980.

[15] S. Yedidiah, *Centrifugal Pump Problems - Causes and Cures*, Petroleum Publishing Co., 1980

[16] E.M. Greitzer, *The Stability of Pumping Systems: The 1980 Freeman Scholar Lecture*, ASME Journal of Fluids Engineering, vol. 103, Jun. 1980.

[17] W.A. Connor, *Design and Off-Design Performance Prediction of High Pressure Ratio Centrifugal Compressors*, Von Karman Institute Lecture Series 1984-07, May 1984.

[18] R.A. Van den Braembussche, *Surge and Stall in Centrifugal Compressors*, Von Karman Institute Lecture Series 1984-07, May 1984.

[19] D.G. Wilson, *The Design of High-Efficiency Turbomachines and Gas Turbines*, MIT Press, 1984.

[20] V.S. Lobanoff, R.R. Ross, *Centrifugal Pumps - Design and Application*, Gulf Publishing Company, 1985

[21] J.A. Lorett, S. Gopalakrishnan, *Interaction Between Impeller and Volute of Pumps at Off-Design Conditions*, ASME Journal of Fluids Engineering, vol. 108/13, Mar. 1986.

[22] T.M. Sideris, R.A. Van den Braembussche, *Flow in Volutes and the Influence on the Flow in Centrifugal Compressors*, Von Karman Institute Lecture Series 1987-01, Jan. 1987.

[23] S.M. Miner, *Potential Flow Analysis of a Centrifugal Pump: Comparison of Finite Element Calculation and Laser Velocimeter Measurement*, PhD Thesis, Department of Mechanical Engineering, University of Virginia, Jan. 1988.

[24] N.R. Goulet, *An Experimental Facility for the Study of Unsteady Flow in Turbopumps*, MS Thesis, Department of Aeronautics and Astronautics, Massachusetts Institute of Technology, May 1989.

[25] S.M. Miner, R.J. Beaudolin, R.D. Flack, *Laser Velocimeter Measurements in a Centrifugal Flow Pump*, ASME Journal of Turbomachinery, vol. 111/205, Jul. 1989.

[26] J.P. Bons, *Instabilities and Unsteady Flows in Centrifugal Pumps*, MS Thesis, Department of Aeronautics and Astronautics, Massachusetts Institute of Technology, May 1990.

[27] S.M. Miner, R.D. Flack, P.E. Allaire, *Two Dimensional Flow Analysis of a Laboratory Centrifugal Pump*, ASME Paper 50-GT-90, 1990.

[28] B. Neumann, *The Interaction between Geometry and Performance of a Centrifugal Pump*, Mechanical Engineering Publications Ltd., London, 1991

[29] S.B. Sandler, *Turbopump Stability and Unsteady Flow*, MS Thesis, Department of Aeronautics and Astronautics, Massachusetts Institute of Technology, May 1992.

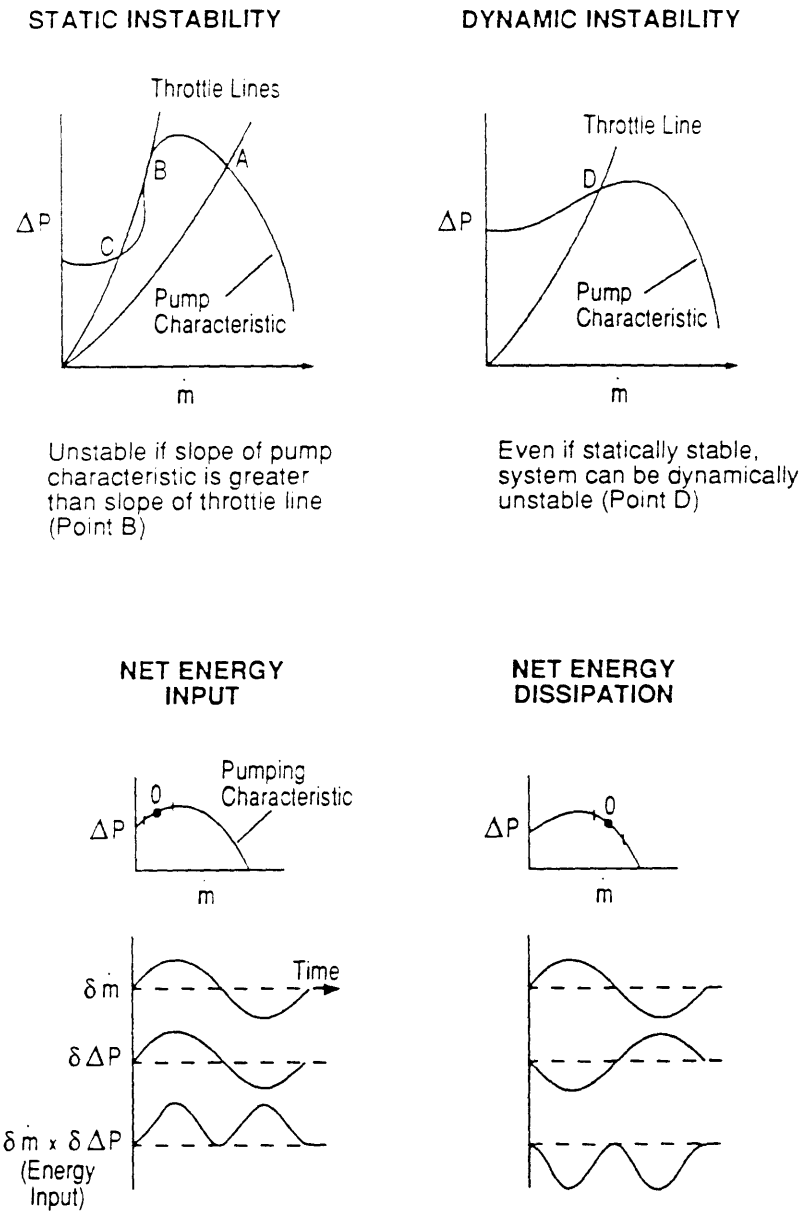

Fig.2.1.1 Relationship between Pump Characteristic Slope and Instability Potential

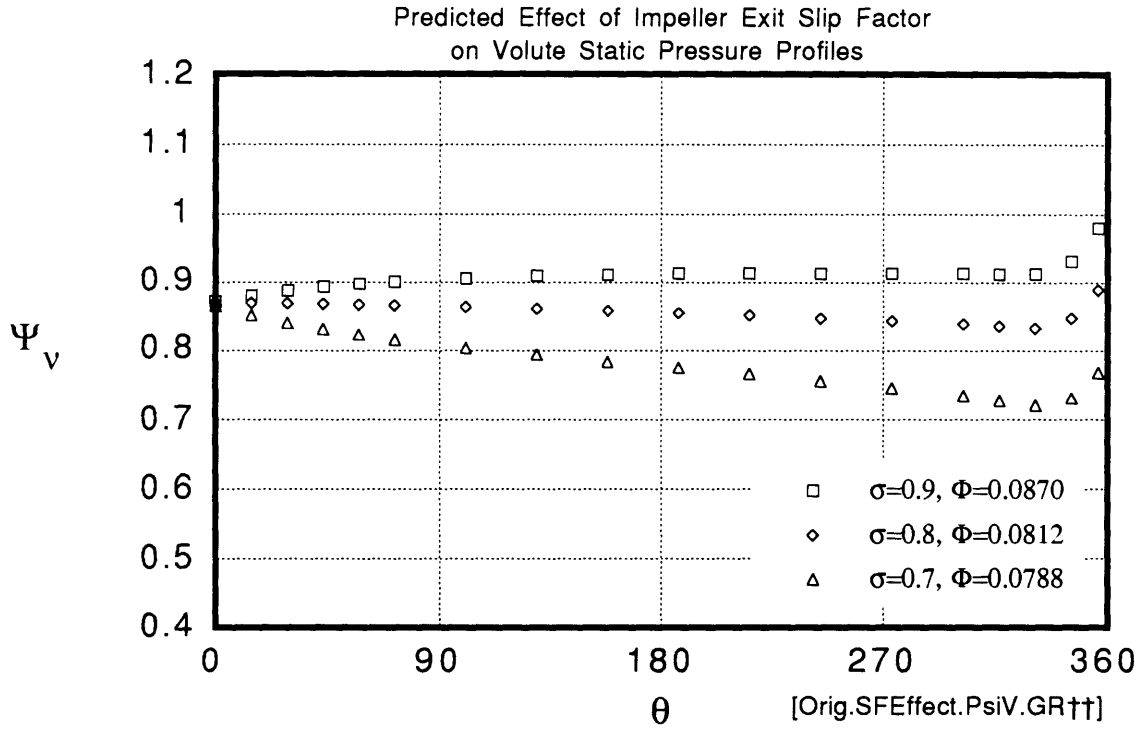
Predicted Effect of Impeller Exit Slip Factor
on Volute Static Pressure Profiles
1.2
1.1
1
0.9
0.8
0.7
0.6
0.5
0.4
Ψν
0
90
180
270
360
θ
σ=0.9, Φ=0.0870
σ=0.8, Φ=0.0812
σ=0.7, Φ=0.0788
[Orig.SFEffect.PsiV.GR††]

Fig.2.2.1

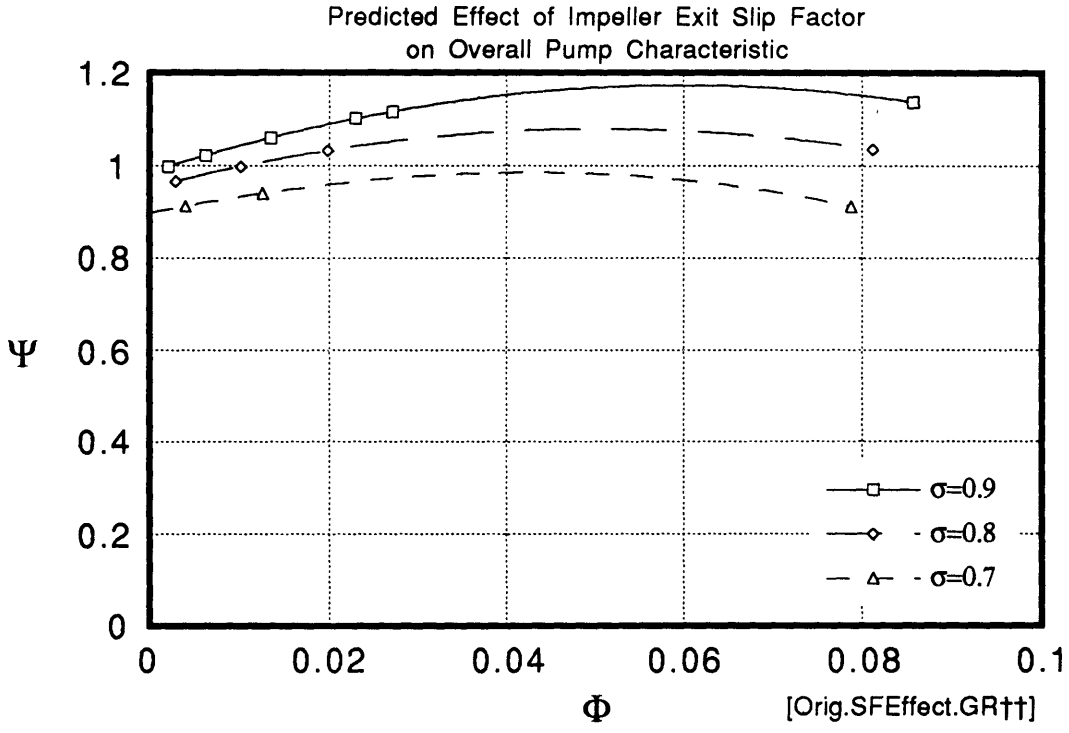
Predicted Effect of Impeller Exit Slip Factor
on Overall Pump Characteristic
1.2
1
0.8
Ψ 0.6
0.4
0.2
0
0
0.02
0.04
0.06
0.08
0.1
Φ
[Orig.SFEffect.GR††]
σ=0.9
σ=0.8
σ=0.7

Fig.2.2.2.i

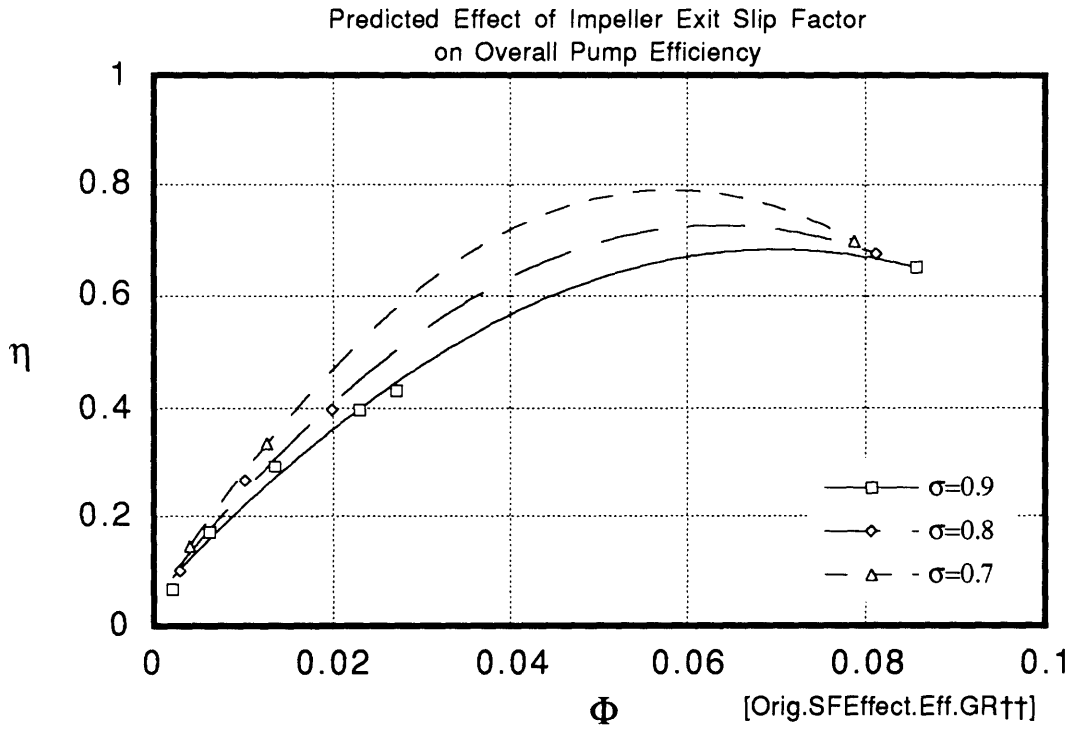
Predicted Effect of Impeller Exit Slip Factor
on Overall Pump Efficiency
1
0.8
0.6
0.4
0.2
0
η
0
0.02
0.04
0.06
0.08
0.1
Φ
[Orig.SFEffect.Eff.GR††]
σ=0.9
- σ=0.8
- σ=0.7

Fig.2.2.2.ii

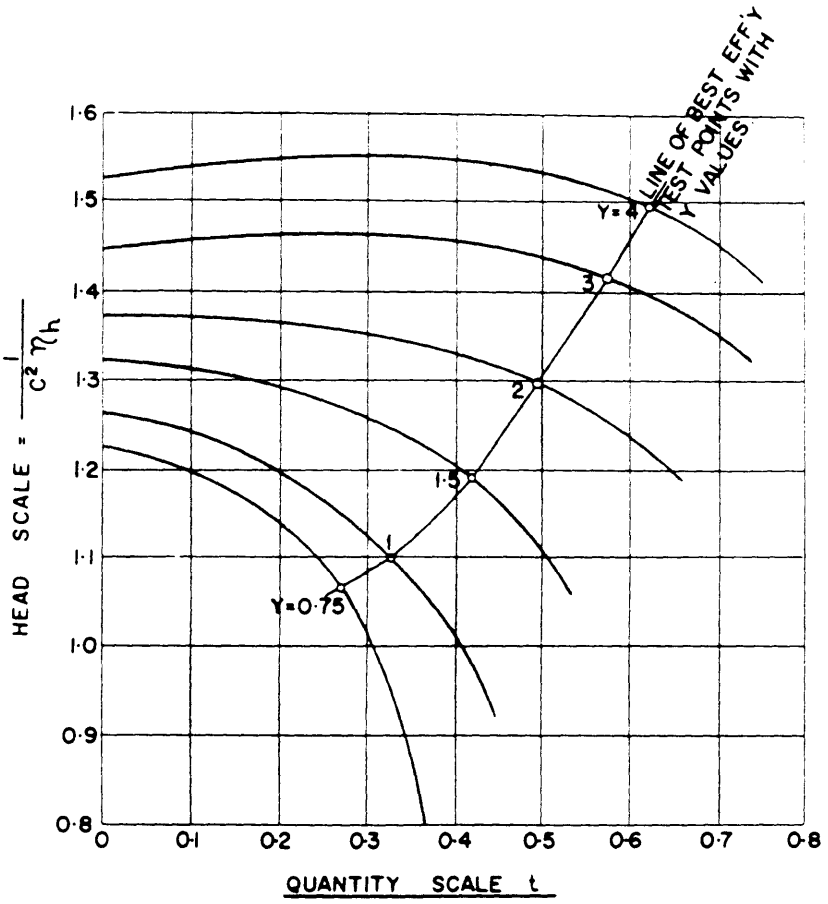

Fig.2.2.3

Effect of Impeller Exit Passage Width on BEP Operating Parameters (from Anderson)

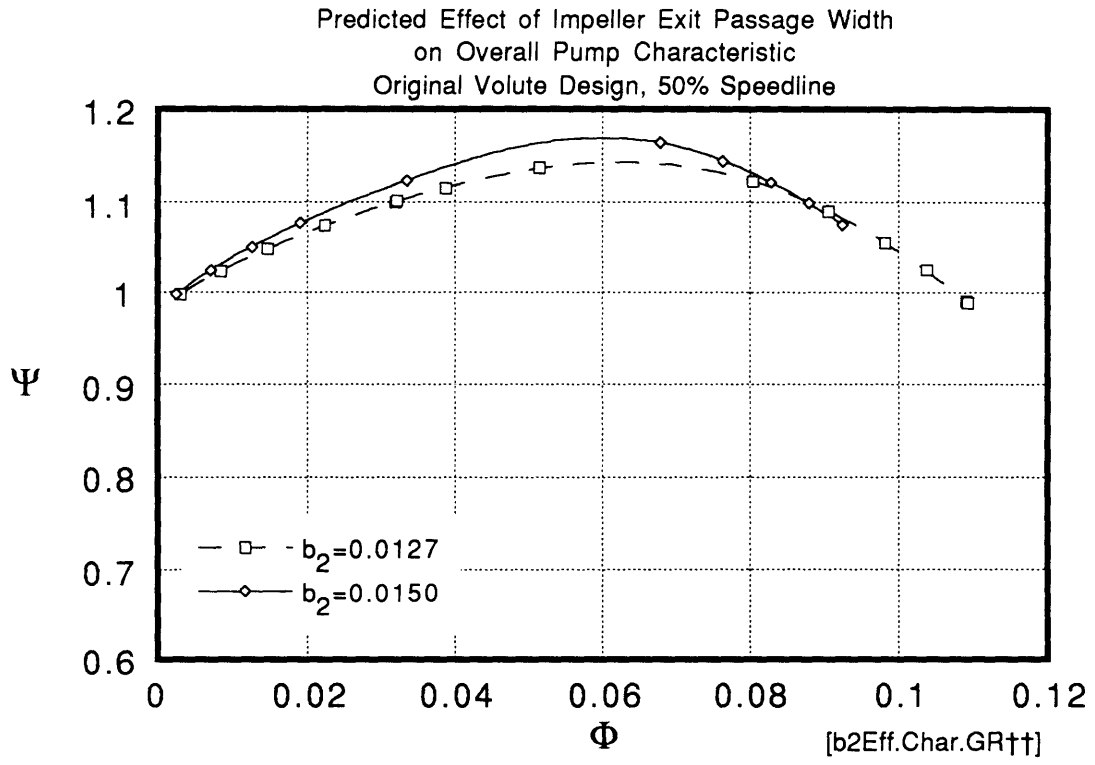
Predicted Effect of Impeller Exit Passage Width
on Overall Pump Characteristic
Original Volute Design, 50% Speedline
1.2
1.1
1
0.9
0.8
0.7
0.6
Ψ
0
0.02
0.04
0.06
0.08
0.1
0.12
Φ
b2=0.0127
b2=0.0150
[b2Eff.Char.GR††]

Fig.2.2.4.i

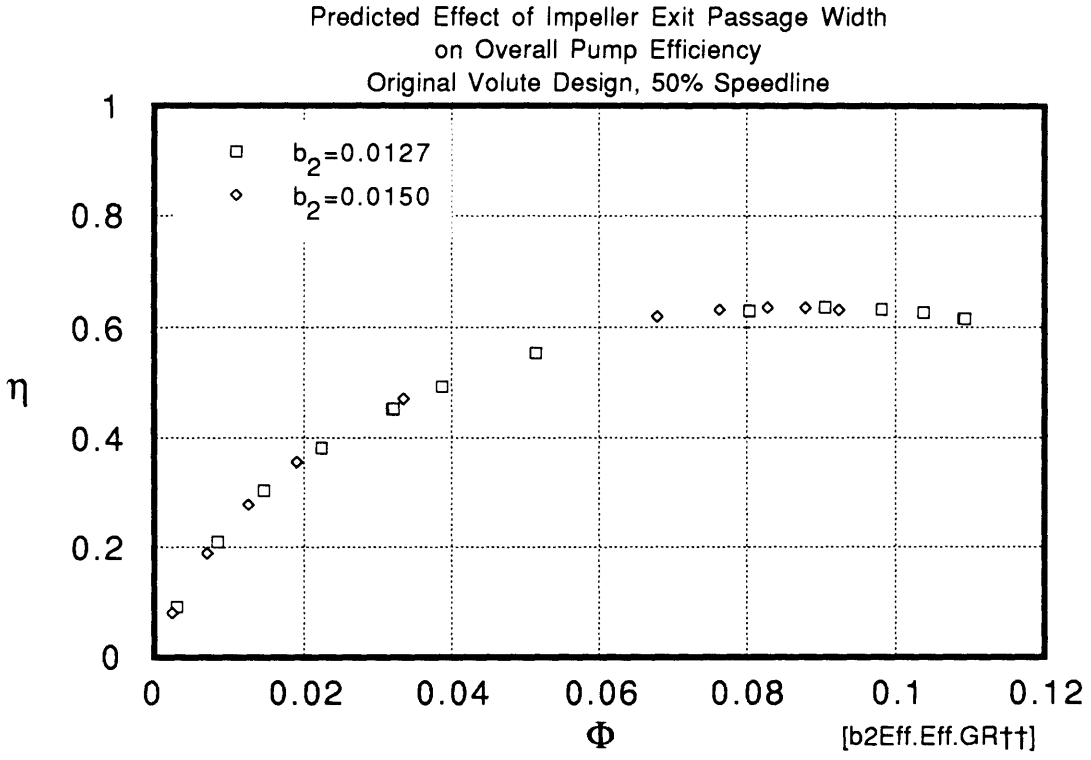
Predicted Effect of Impeller Exit Passage Width
on Overall Pump Efficiency
Original Volute Design, 50% Speedline
b2=0.0127
b2=0.0150
η
Φ
[b2Eff.Eff.GR†††]
1
0.8
0.6
0.4
0.2
0
0
0.02
0.04
0.06
0.08
0.1
0.12

Fig.2.2.4.ii

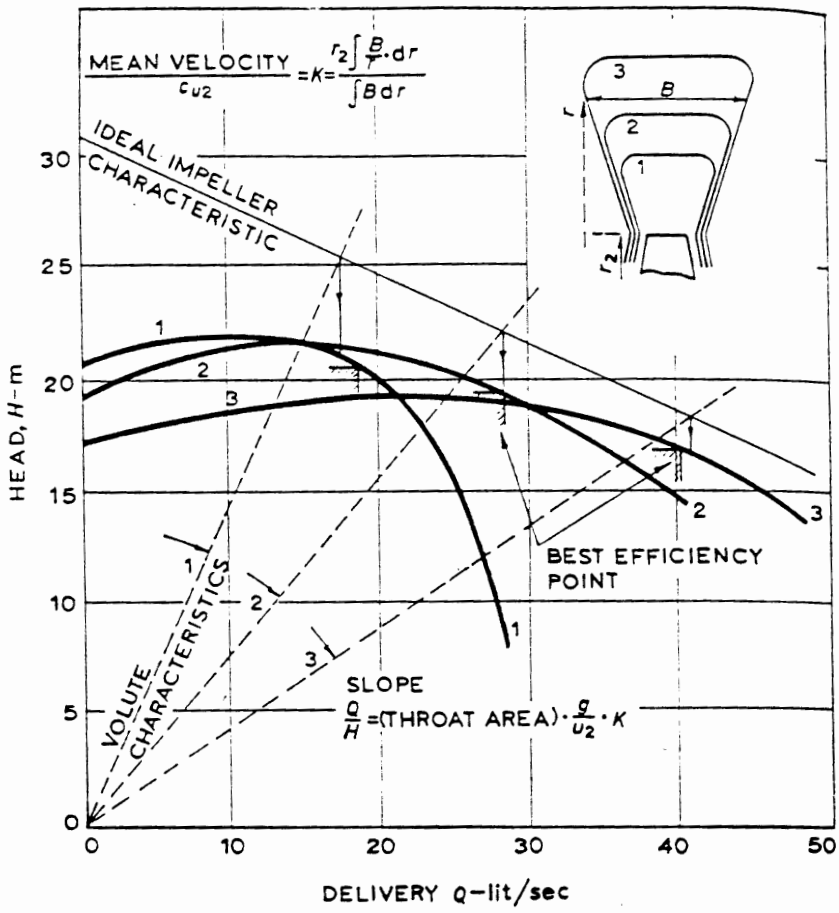

Fig.2.2.5

Effect of Volute Cross-Section Areas on Characteristic Shape and BEP (from Worster)

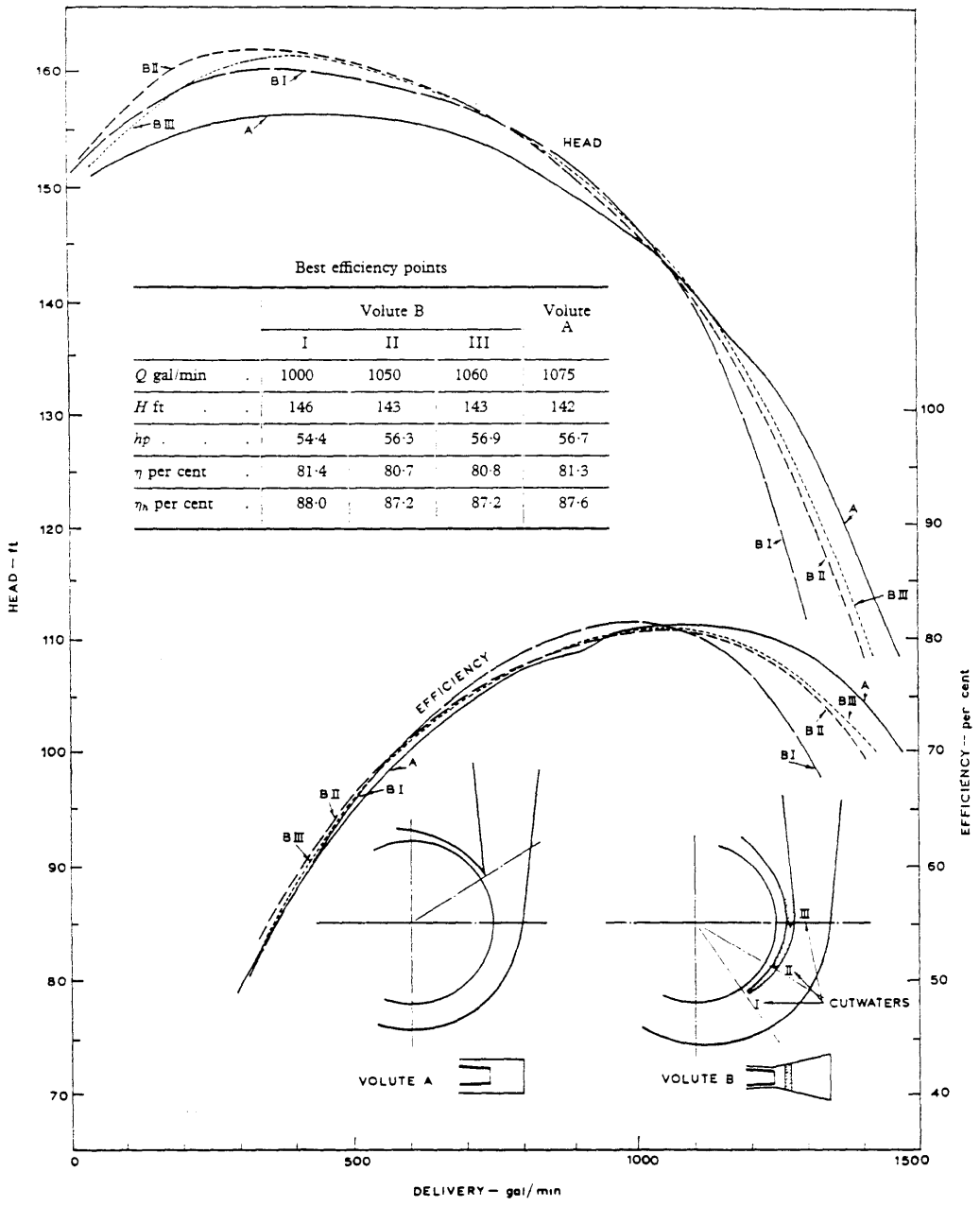

Best efficiency points

	Volute B			Volute A
	I	II	III	
Q gal/min	1000	1050	1060	1075
H ft	146	143	143	142
hp	54·4	56·3	56·9	56·7
η per cent	81·4	80·7	80·8	81·3
η_h per cent	88·0	87·2	87·2	87·6

Fig.2.2.6

Effect of Varying Tongue Designs and Volute Archimedean Spiral Area Profile

(from Worster)

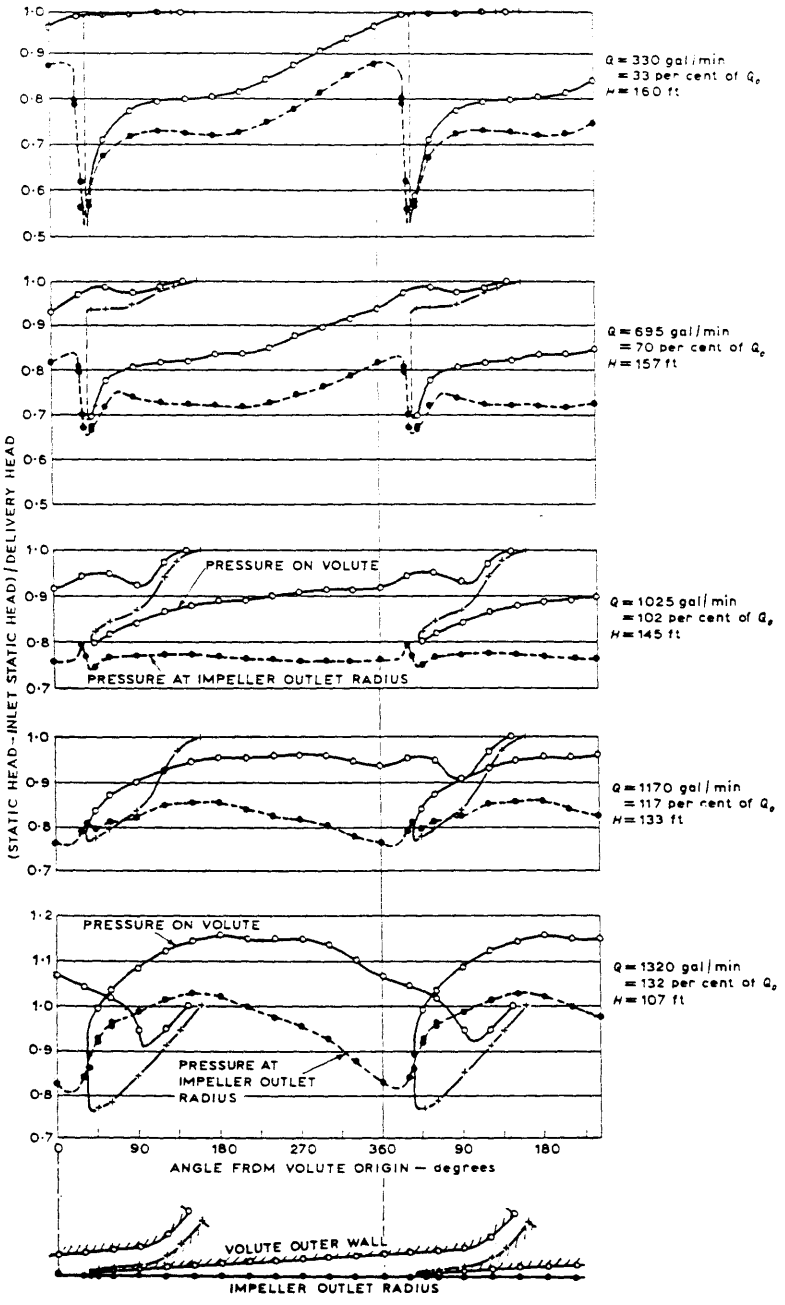

Fig.2.2.7.ii

Volute Static Pressure Measurements for Free Vortex Area Profile (from Worster)

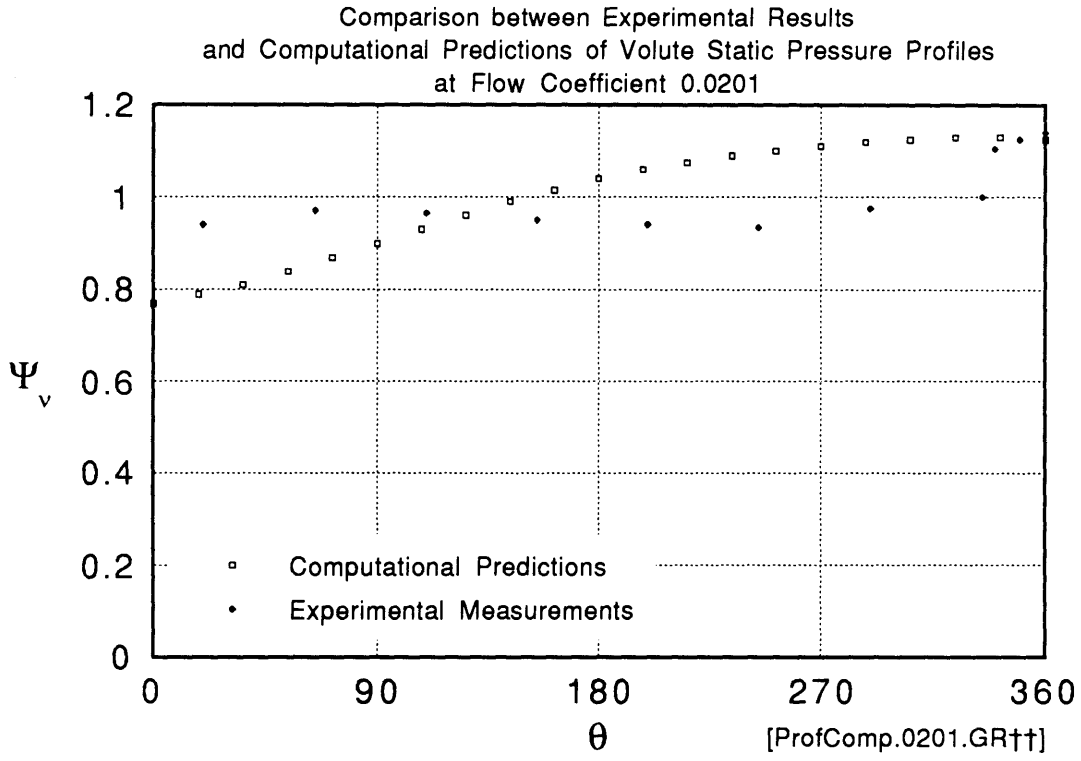
Comparison between Experimental Results
and Computational Predictions of Volute Static Pressure Profiles
at Flow Coefficient 0.0201
1.2
1
0.8
0.6
0.4
0.2
0
Ψν
Computational Predictions
Experimental Measurements
0
90
180
270
360
θ
[ProfComp.0201.GR††]

Fig.2.3.1.i

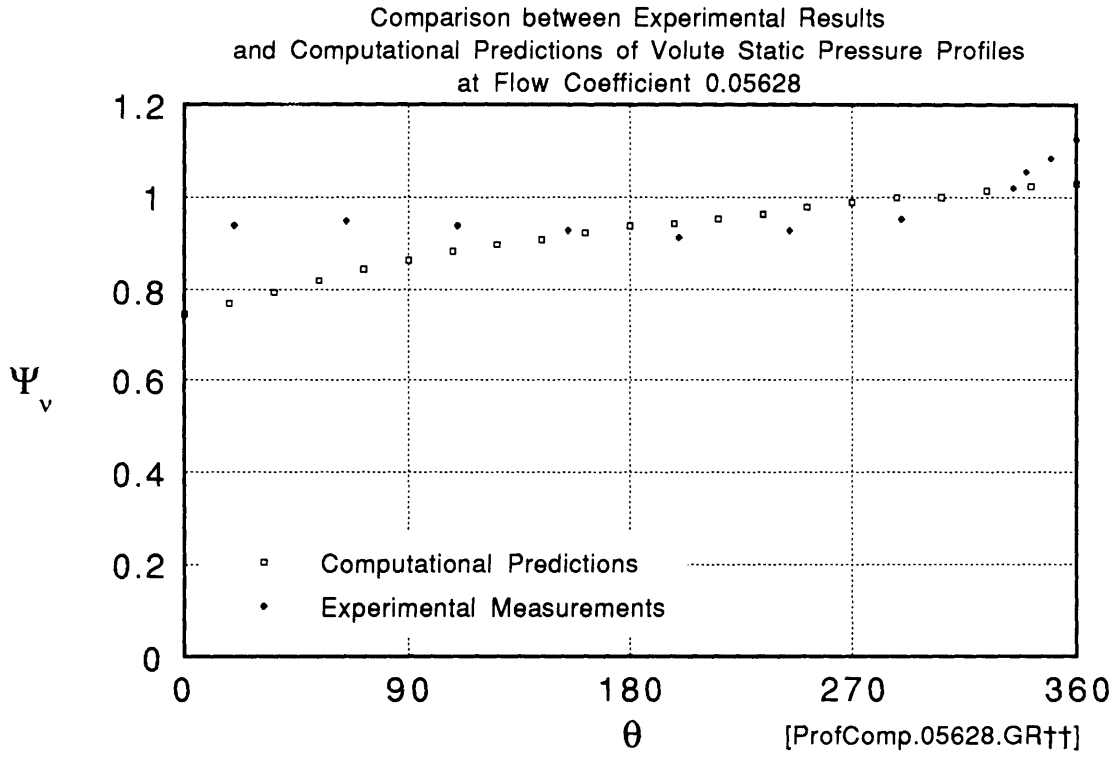
Comparison between Experimental Results
and Computational Predictions of Volute Static Pressure Profiles
at Flow Coefficient 0.05628
1.2
1
0.8
0.6
0.4
0.2
0
Ψν
0
90
180
270
360
θ
Computational Predictions
Experimental Measurements
[ProfComp.05628.GR††]

Fig.2.3.1.ii

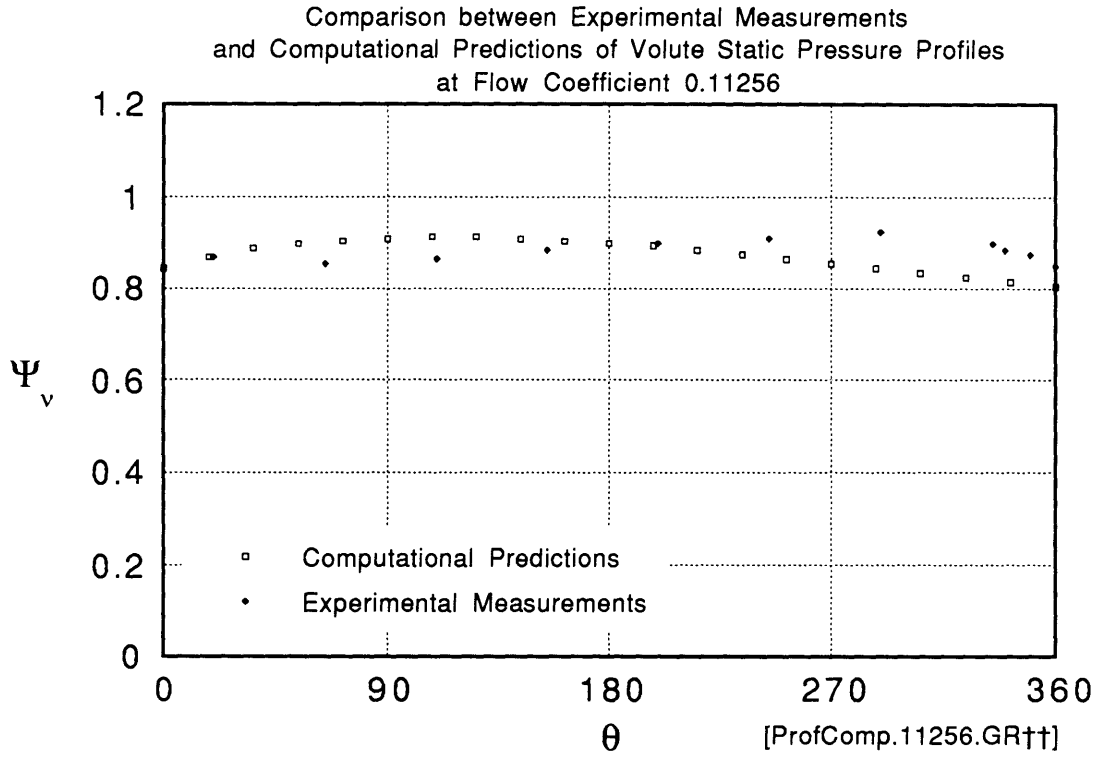
Comparison between Experimental Measurements
and Computational Predictions of Volute Static Pressure Profiles
at Flow Coefficient 0.11256
1.2
1
0.8
0.6
0.4
0.2
0
Ψν
Computational Predictions
Experimental Measurements
0
90
180
270
360
θ
[ProfComp.11256.GR††]

Fig.2.3.1.iii

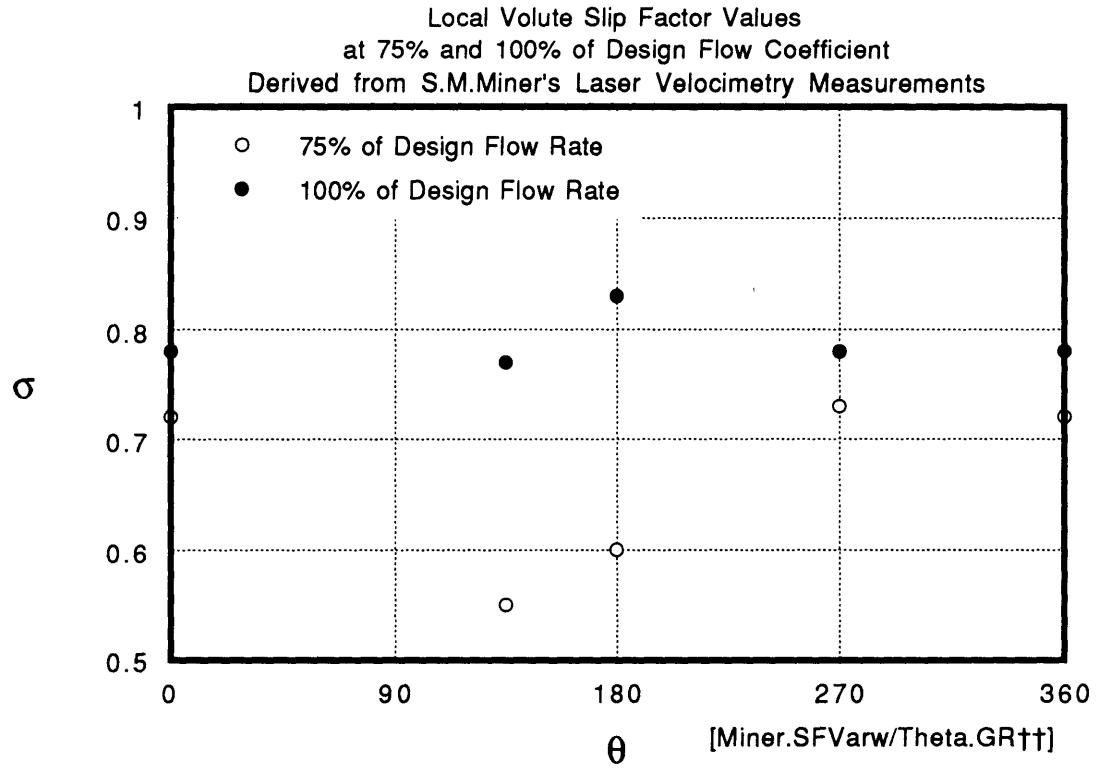
Local Volute Slip Factor Values
at 75% and 100% of Design Flow Coefficient
Derived from S.M.Miner's Laser Velocimetry Measurements
75% of Design Flow Rate
100% of Design Flow Rate
σ
1
0.9
0.8
0.7
0.6
0.5
0
90
180
270
360
θ
[Miner.SFVarw/Theta.GR††]

Fig.2.3.2

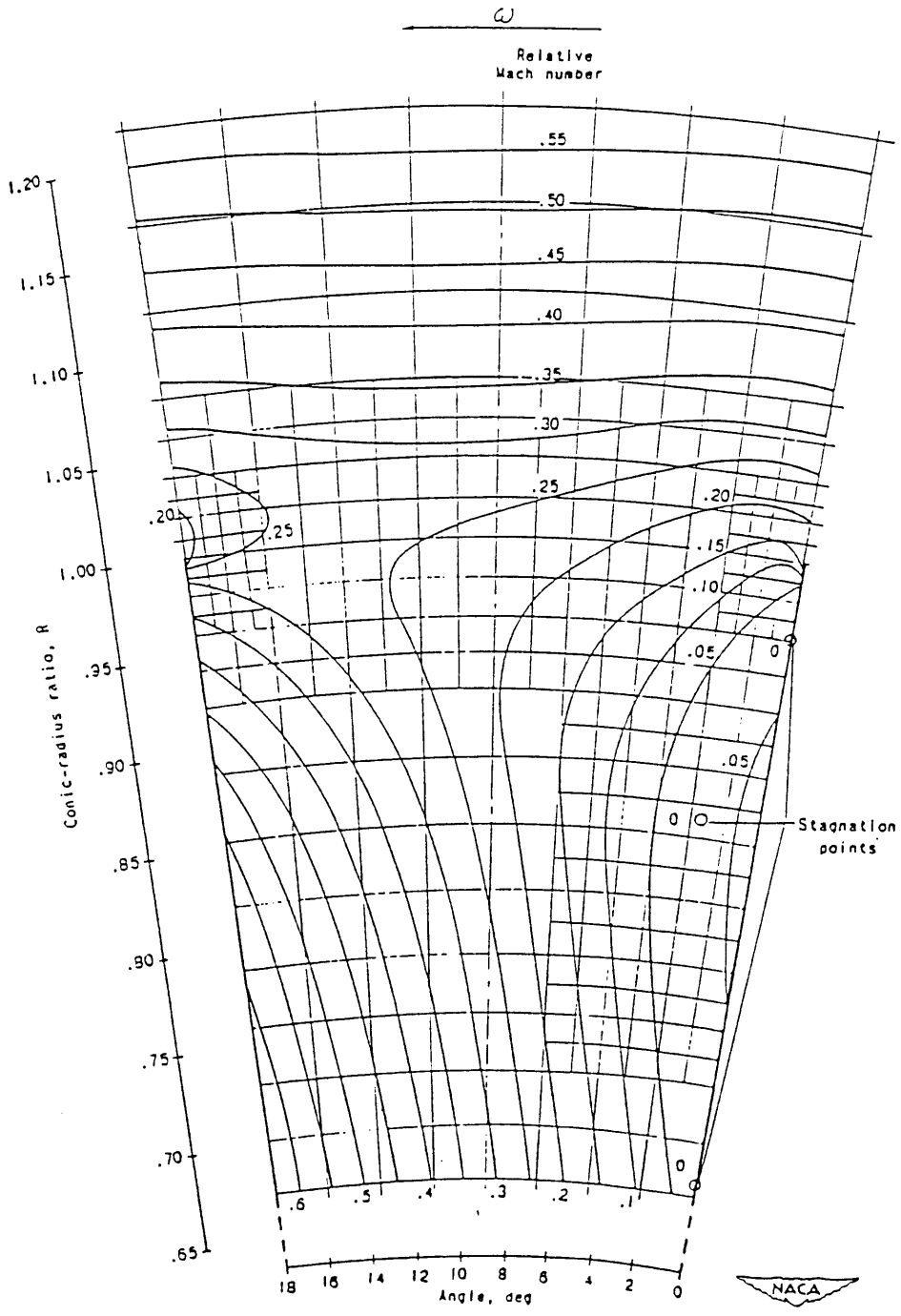

Fig.2.3.3 Mach Number Field inside Impeller Straight Blade Passage and Diffuser Section
(from Stanitz)

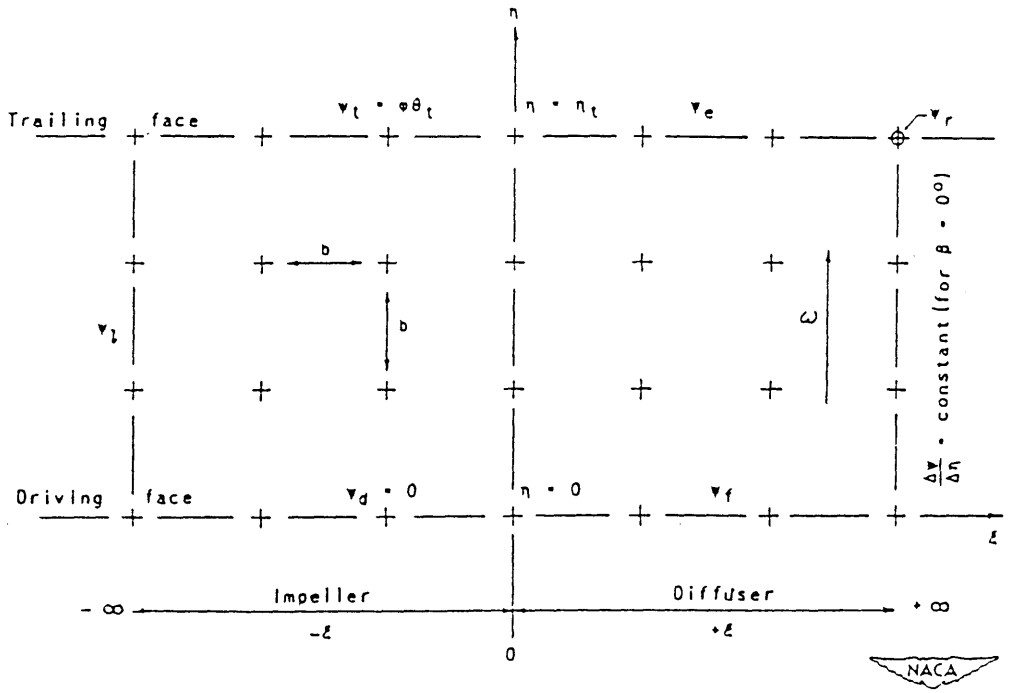

Fig.2.3.4 Transformed Computational Domain Rectangle (from Stanitz)

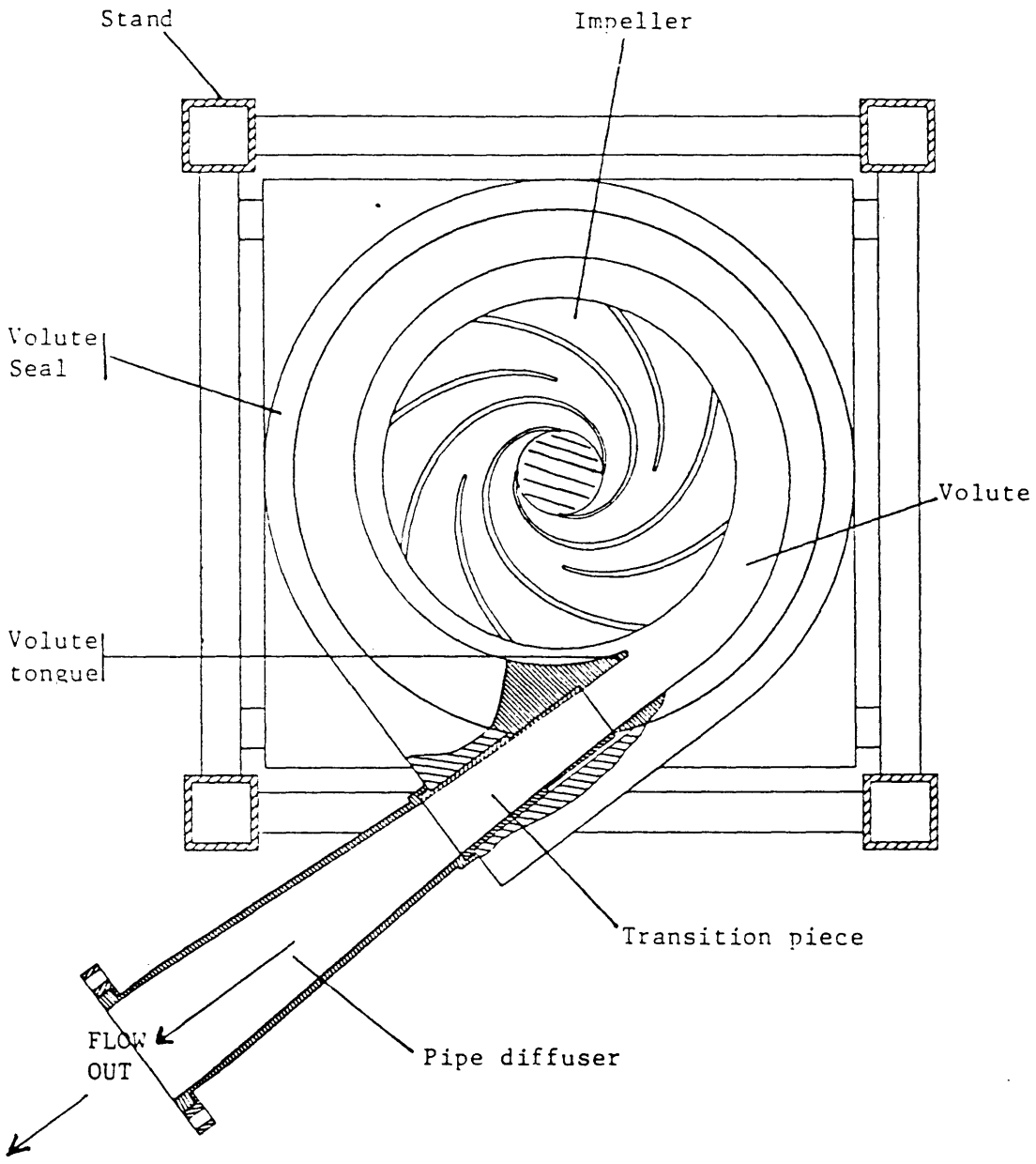

Fig.3.1.1

Top View of Test Section Assembly and Component Identification (from Goulet)

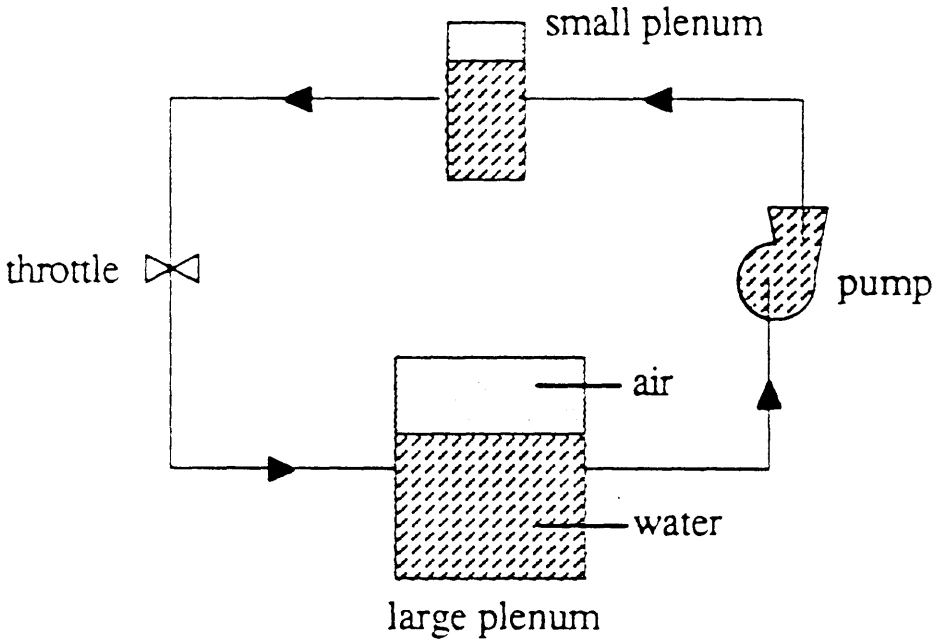

Fig.3.1.2 Schematic of the Closed Loop Pumping System (from Goulet)

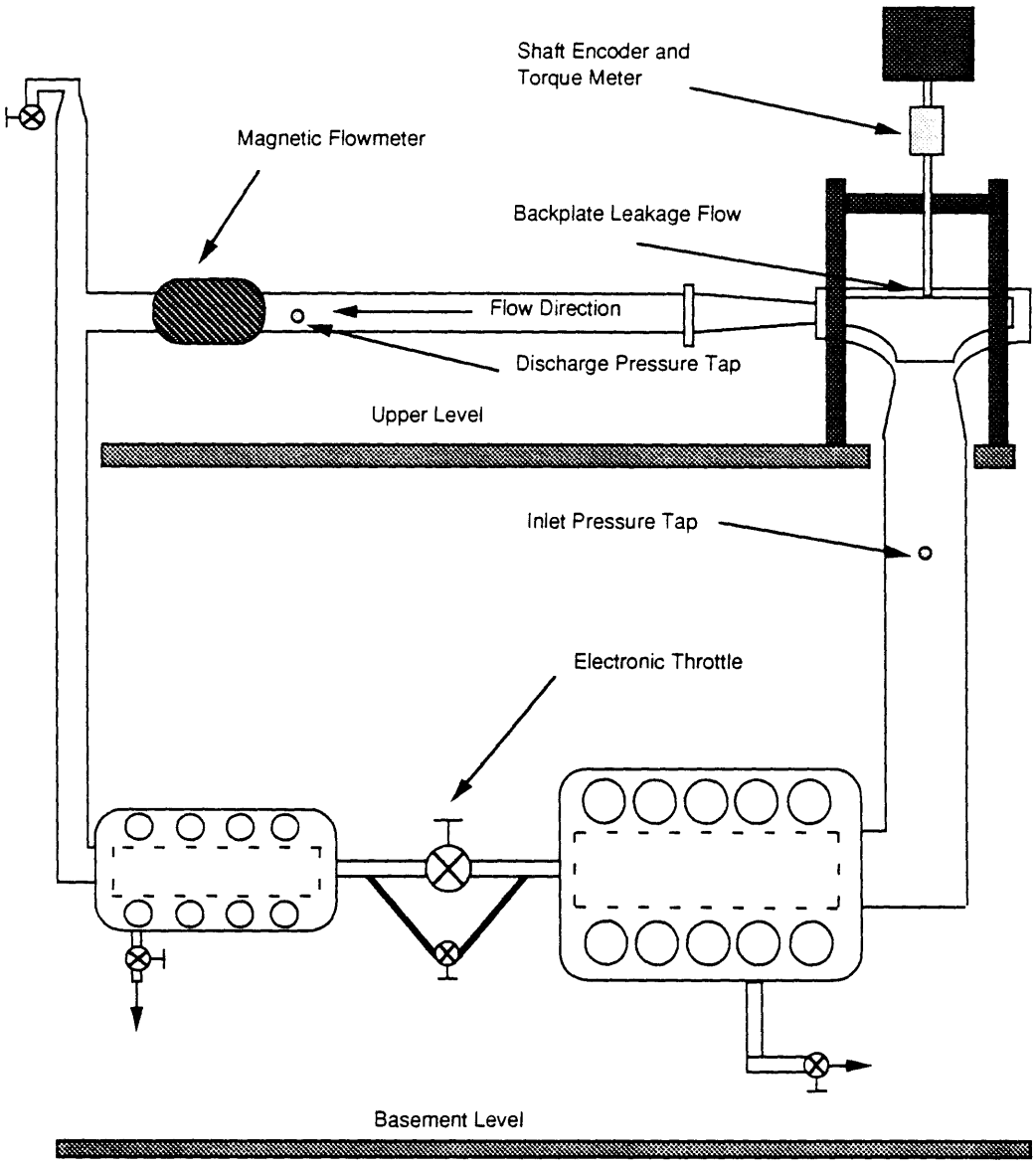

Fig.3.1.3 Pumping System and Instrumentation Layout (from Sandler)

Laser Velocimeter Optics Arrangement

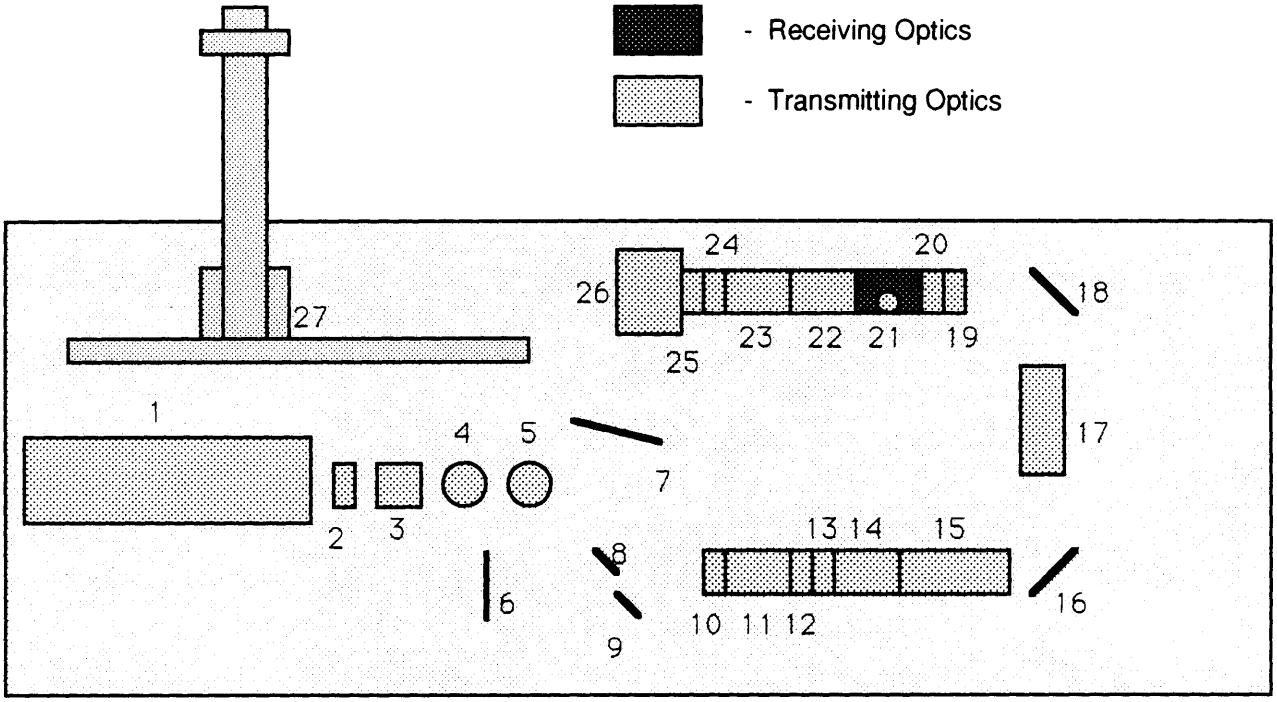

List of Components:

1. Lexal Laser
2. Polarization Rotator
3. Beam Collimator
4. Attenuator
5. Dispersion Prism
6. Mirror
7. Mirror
8. Mirror
9. Mirror
10. Blue Beam Polarization Rotator
11. Beam Splitter
12. Beam Displacer
13. Green Beam Polarization Rotator
14. Beamsplitter
15. Bragg Cell
16. Mirror
17. Bragg Cell
18. Mirror
19. Beam Steering Module
20. Beam Steering Module
21. Receiving Optics Assembly
22. Field Stop
23. Beam Stop
24. Beam Spacer (22mm to 9mm)
25. Beam Spacer
26. Beam Expander
27. XYZ Traverse

Fig.3.1.4

Laser Velocimetry Radial Cross-Section Grid
Shape and Dimensions

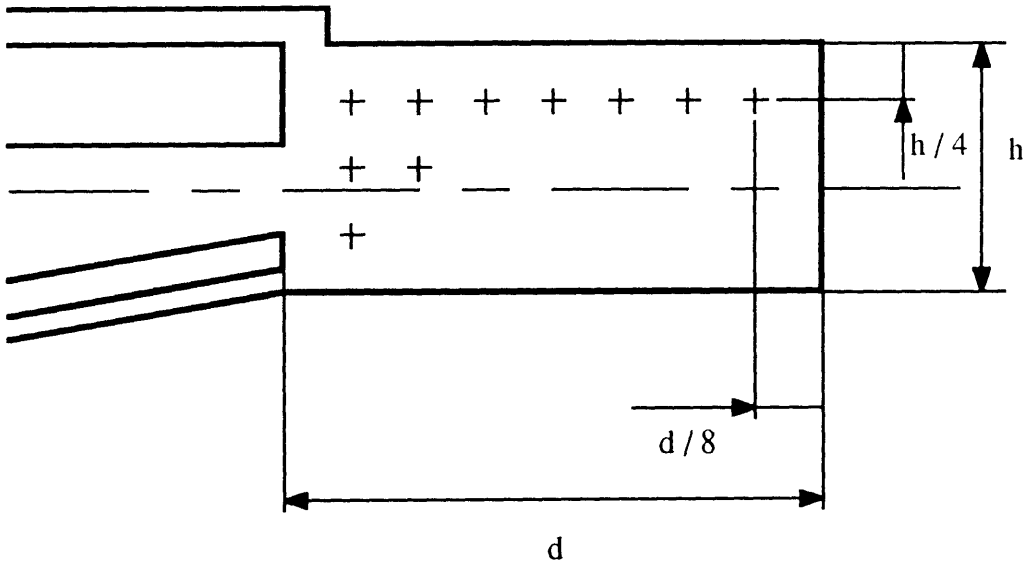

Fig.3.1.5 Laser Velocimetry Radial Cross-Section Grid Shape and Dimensions

Volute Locations of LDV Grids

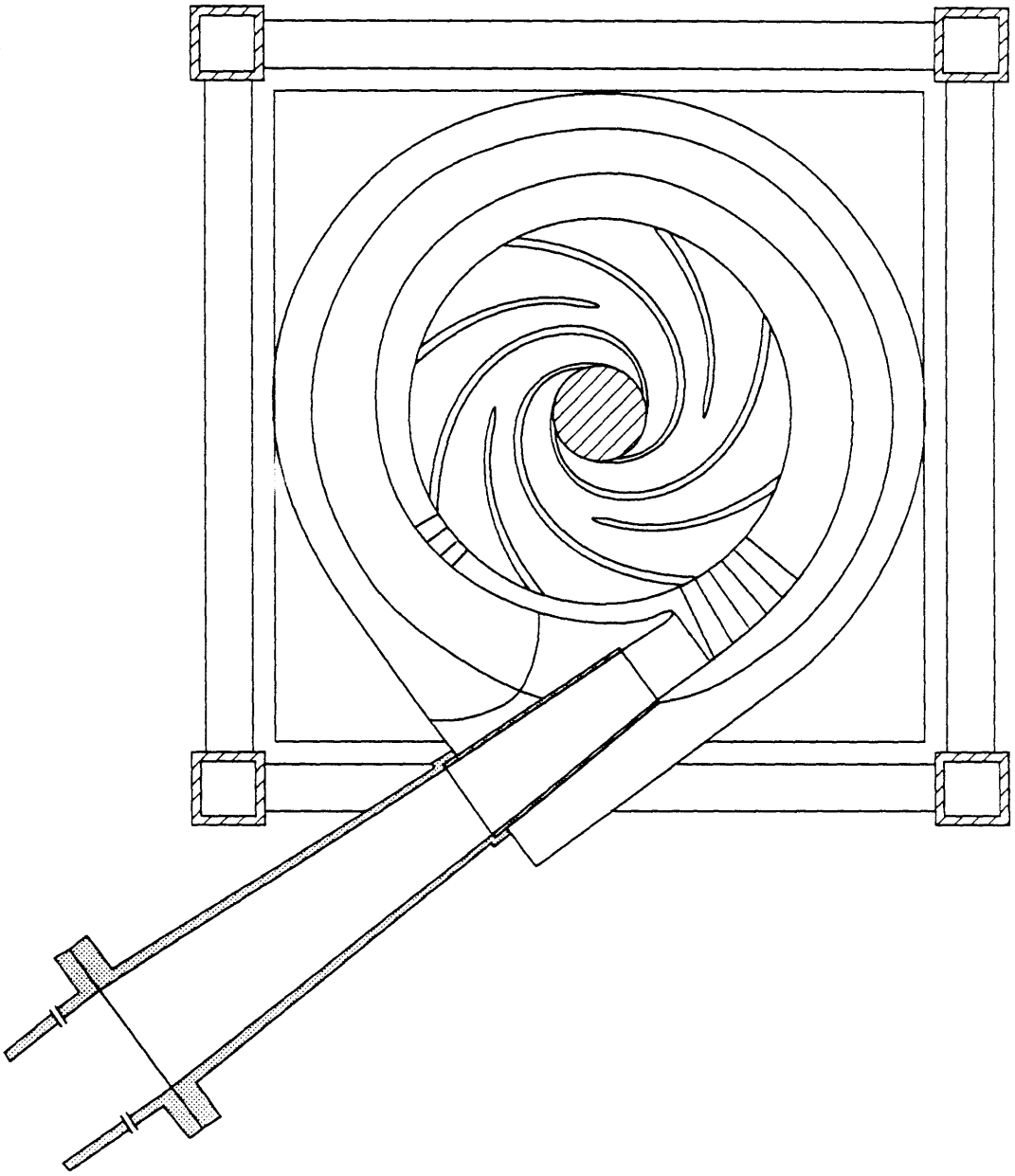

Fig.3.1.6 Angular Locations of Laser Velocimetry Grids

Original Volute Pressure Tap Locations

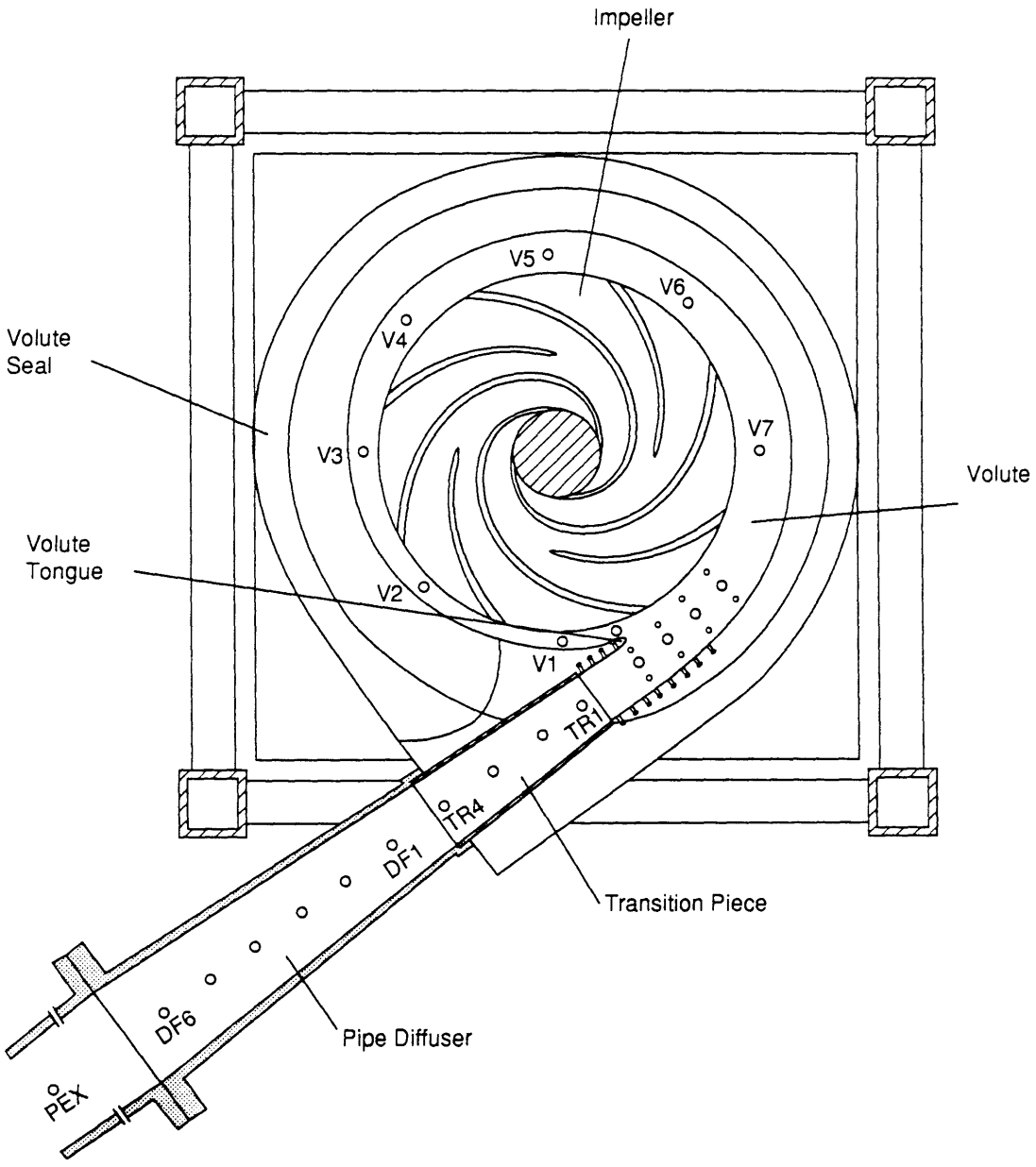

Fig.3.1.7

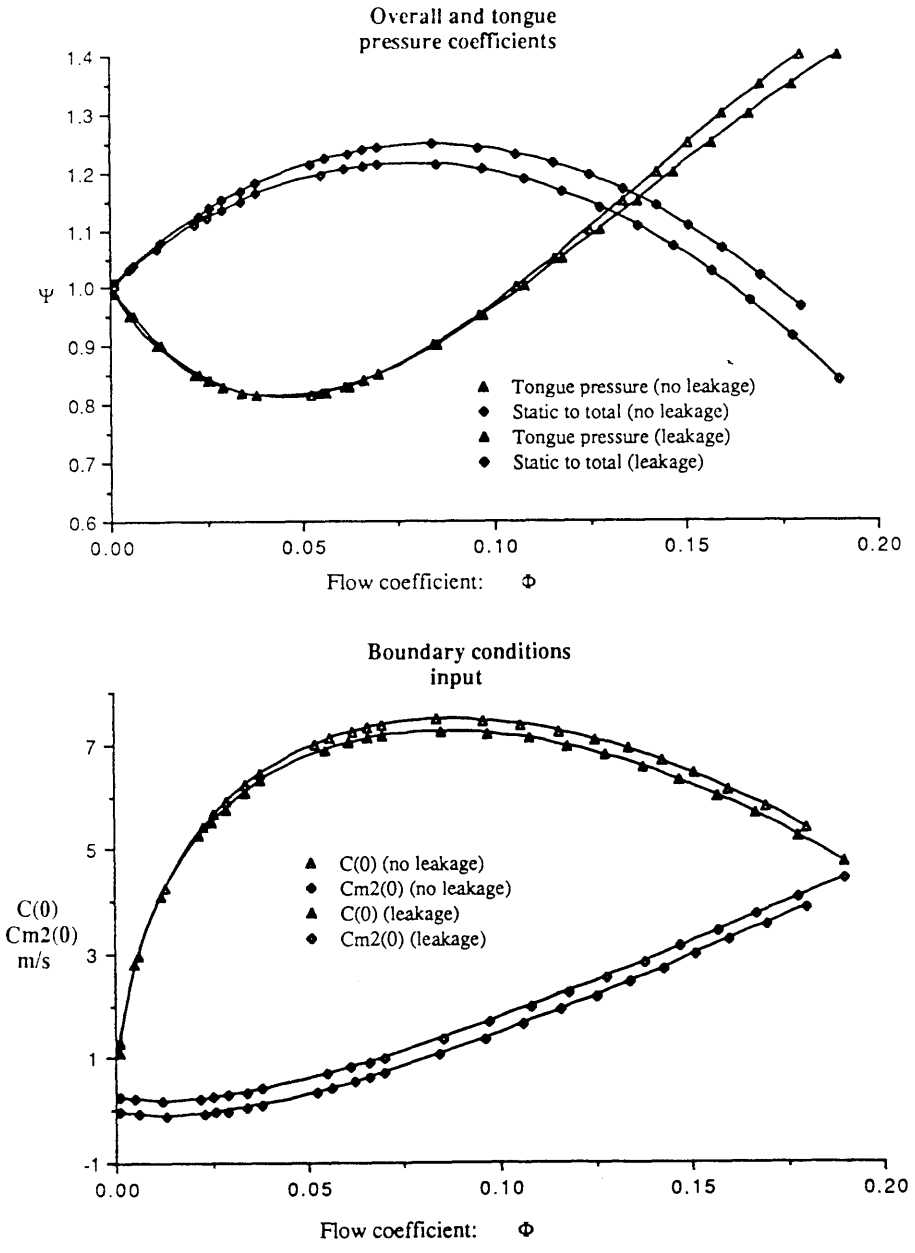

Fig.4.1.1

Flow Coefficient Dependence of Interac tive Model Input Quantities for Original Volute Design
(from Goulet)

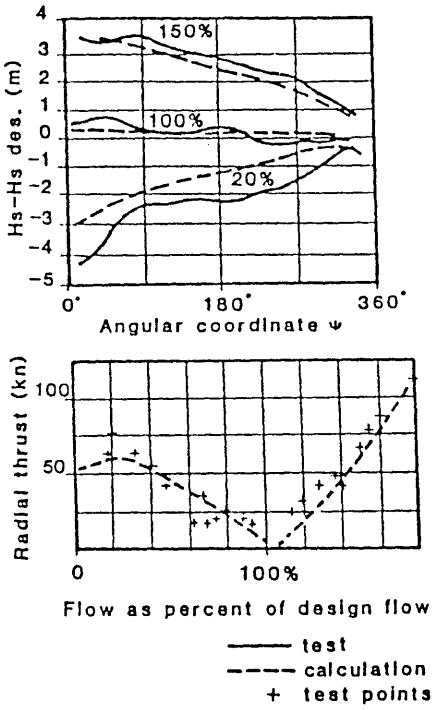

Fig.4.1.2 Comparison between Predicted and Measured Volute Pressure and Radial Thrust Values
(from Lorett and Gopalakrishnan)

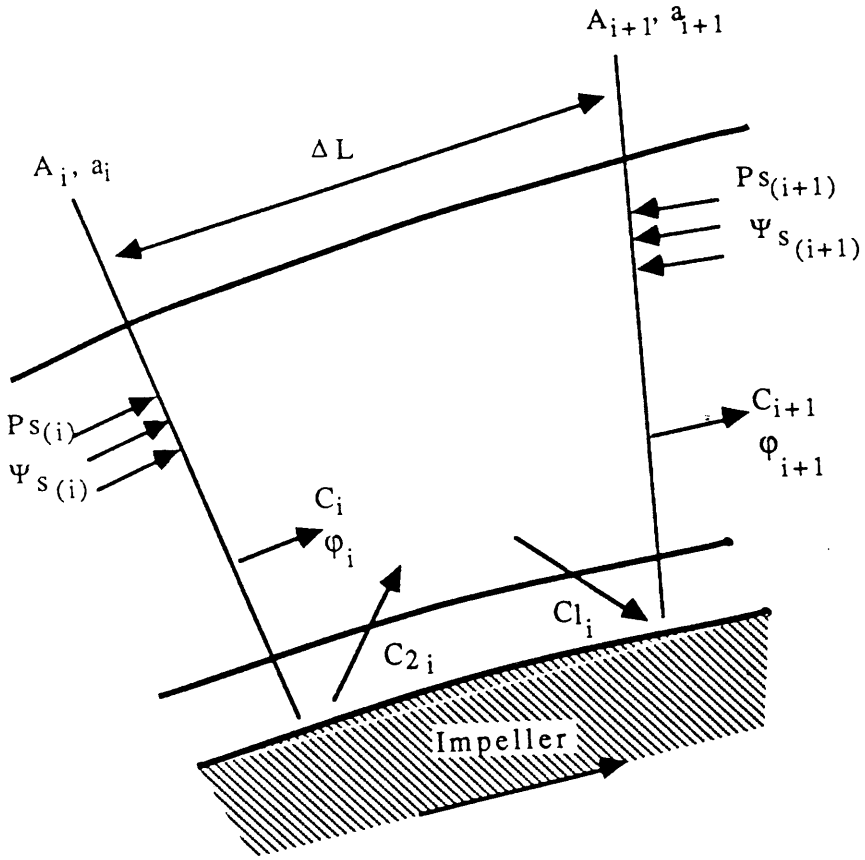

Fig.4.1.3

Mass and Momentum Addition across Volute Cell (from Goulet)

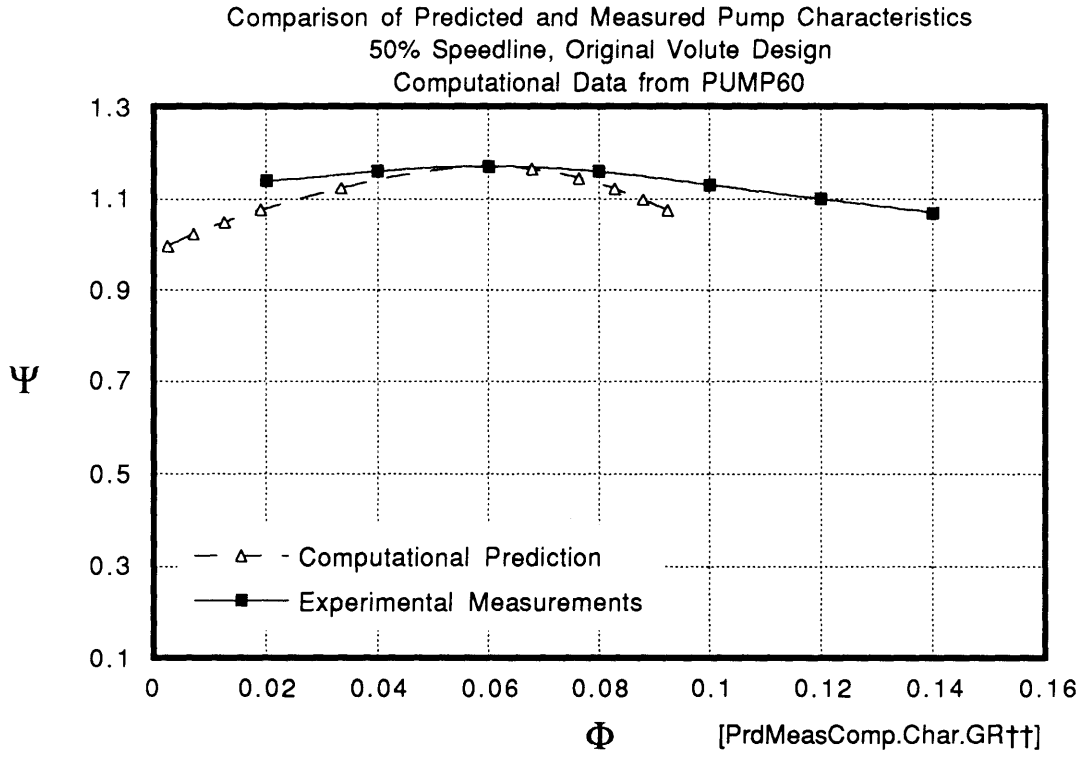
Comparison of Predicted and Measured Pump Characteristics
50% Speedline, Original Volute Design
Computational Data from PUMP60
1.3
1.1
0.9
0.7
0.5
0.3
0.1
Ψ
0
0.02
0.04
0.06
0.08
0.1
0.12
0.14
0.16
Φ
[PrdMeasComp.Char.GR††]
Computational Prediction
Experimental Measurements

Fig.4.1.4

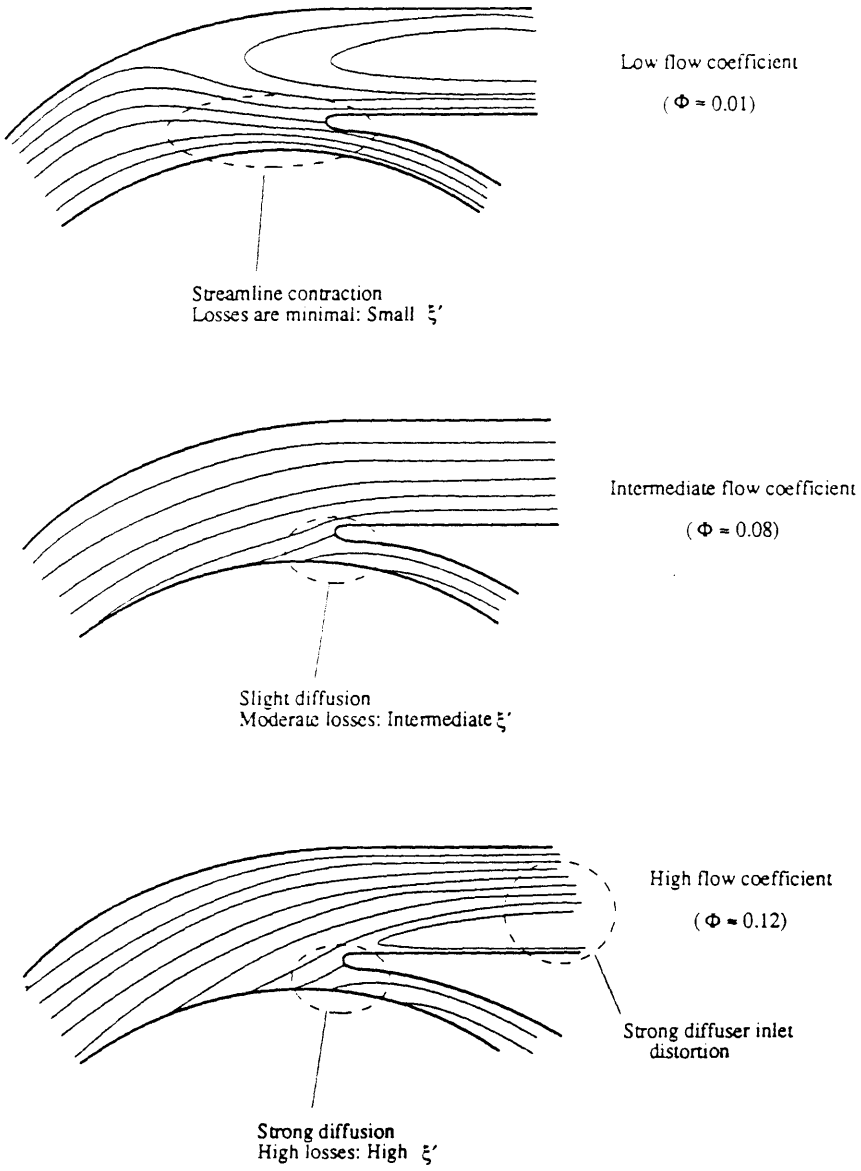

Fig.4.1.5

Observed Flow Behavior in Proximity of the Tongue for Various Flow Coefficients

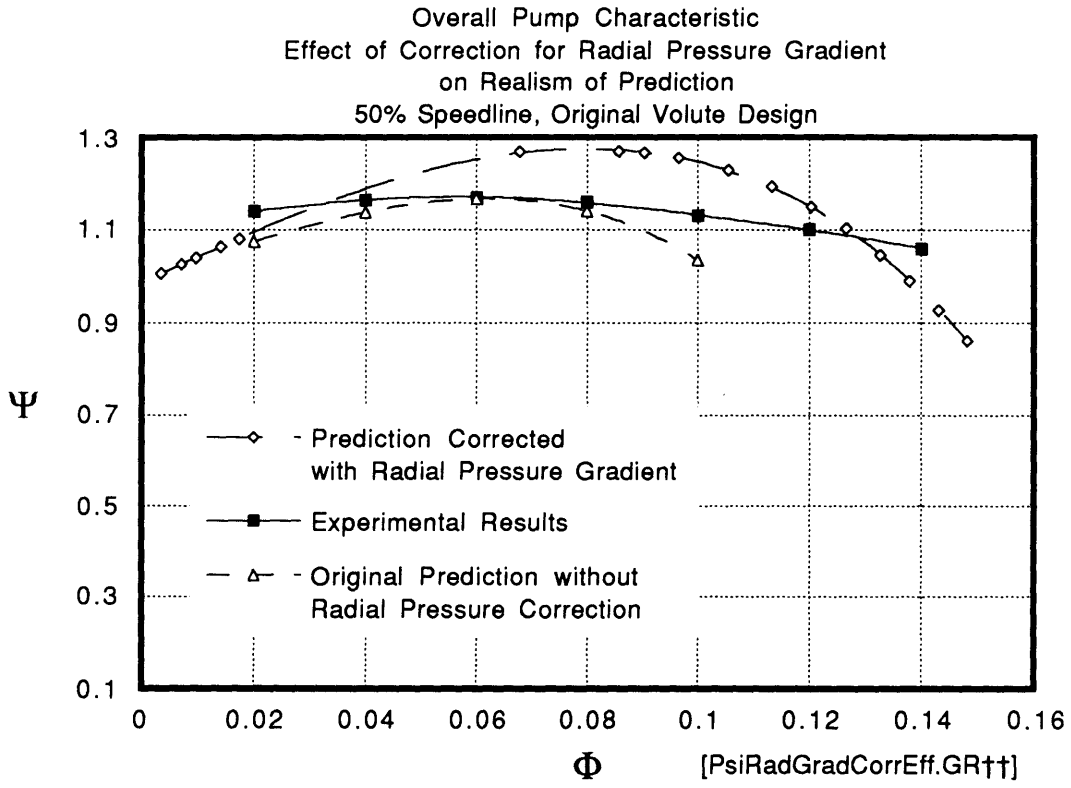
Overall Pump Characteristic
Effect of Correction for Radial Pressure Gradient
on Realism of Prediction
50% Speedline, Original Volute Design
Ψ
1.3
1.1
0.9
0.7
0.5
0.3
0.1
0
0.02
0.04
0.06
0.08
0.1
0.12
0.14
0.16
Φ
[PsiRadGradCorrEff.GR††]
- Prediction Corrected with Radial Pressure Gradient
Experimental Results
- Original Prediction without Radial Pressure Correction

Fig.4.1.6

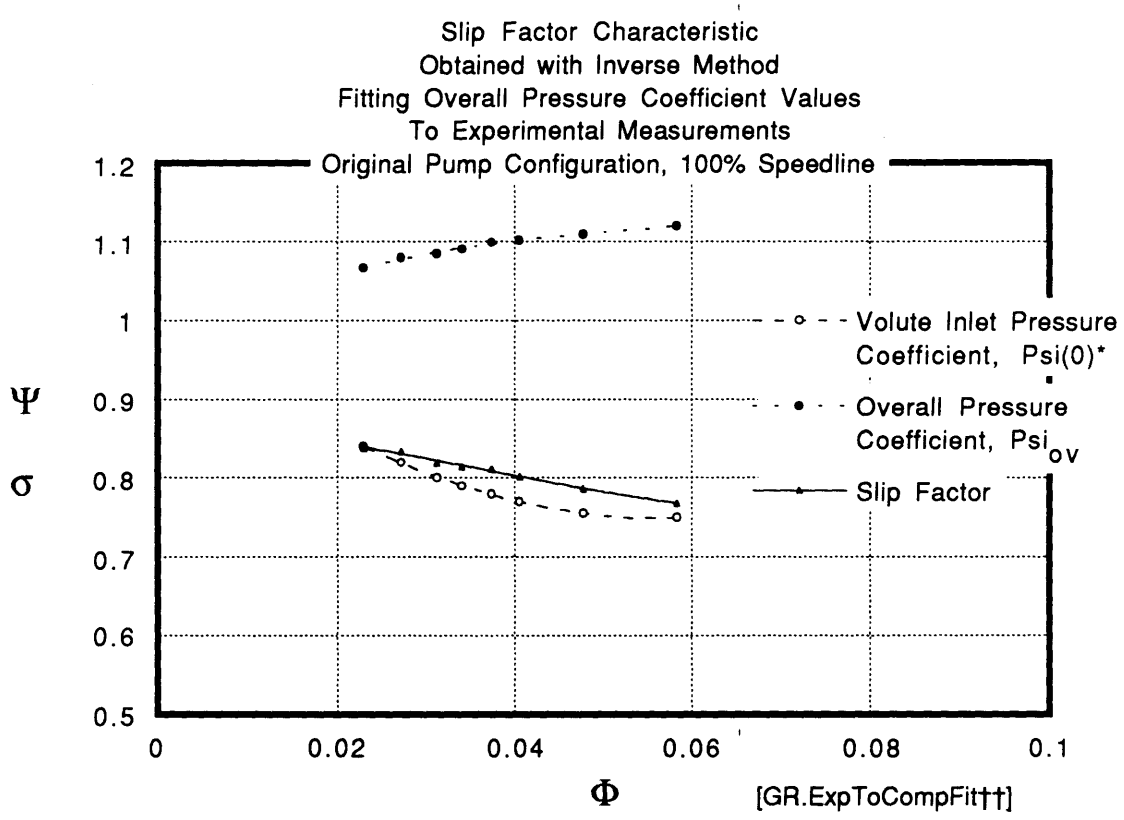

Fig.4.1.7 Slip Factor Characteristic Obtained With Inverse Method - Fitting Overall Pressure Coefficient Values to Experimental Measurements

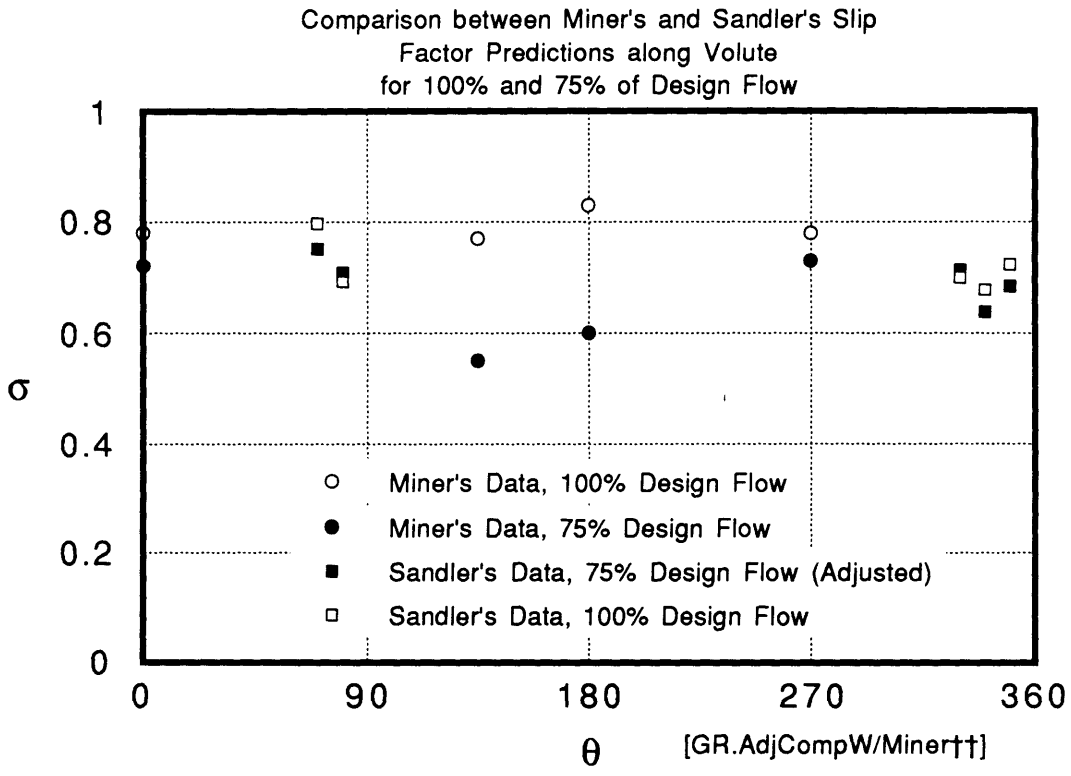
Comparison between Miner's and Sandler's Slip
Factor Predictions along Volute
for 100% and 75% of Design Flow
1
0.8
0.6
0.4
0.2
0
σ
0
90
180
270
360
θ
[GR.AdjCompW/Miner††]
Miner's Data, 100% Design Flow
Miner's Data, 75% Design Flow
Sandler's Data, 75% Design Flow (Adjusted)
Sandler's Data, 100% Design Flow

Fig.4.1.8

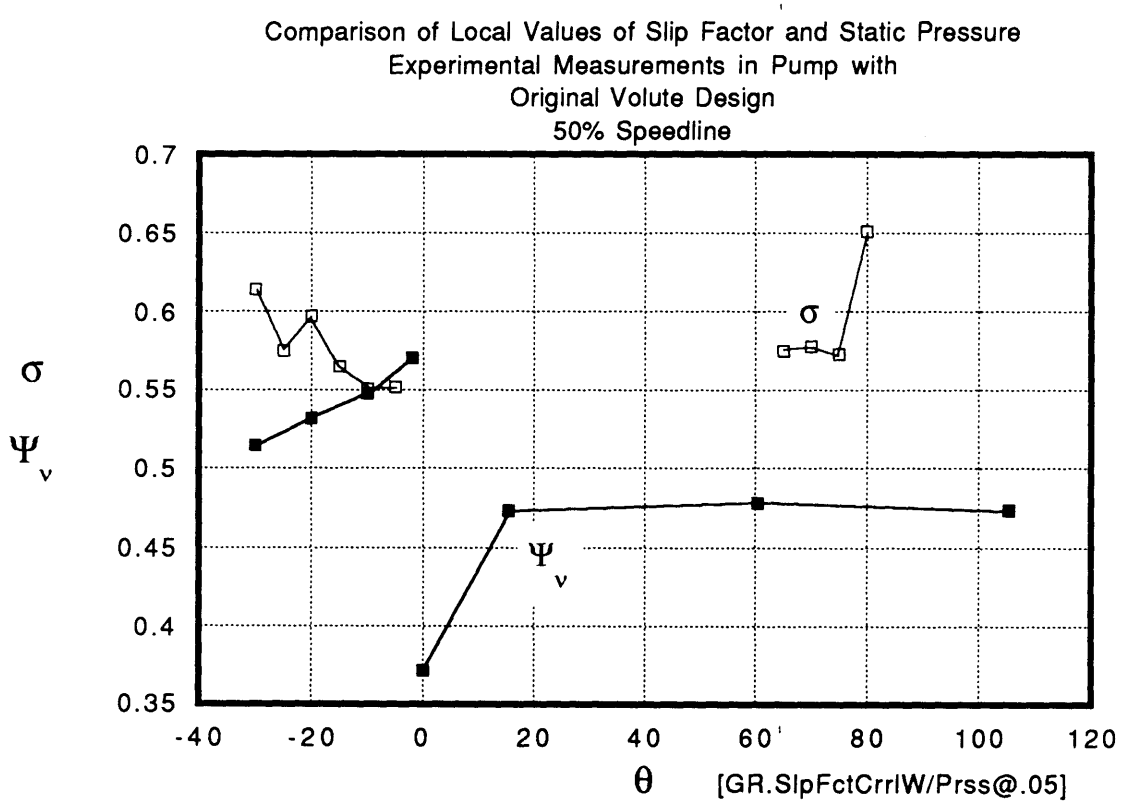
Comparison of Local Values of Slip Factor and Static Pressure
Experimental Measurements in Pump with
Original Volute Design
50% Speedline
0.7
0.65
0.6
0.55
0.5
0.45
0.4
0.35
σ
Ψν
-40
-20
0
20
40
60
80
100
120
θ
[GR.SlpFctCrrlW/Prss@.05]

Fig.4.1.9.i

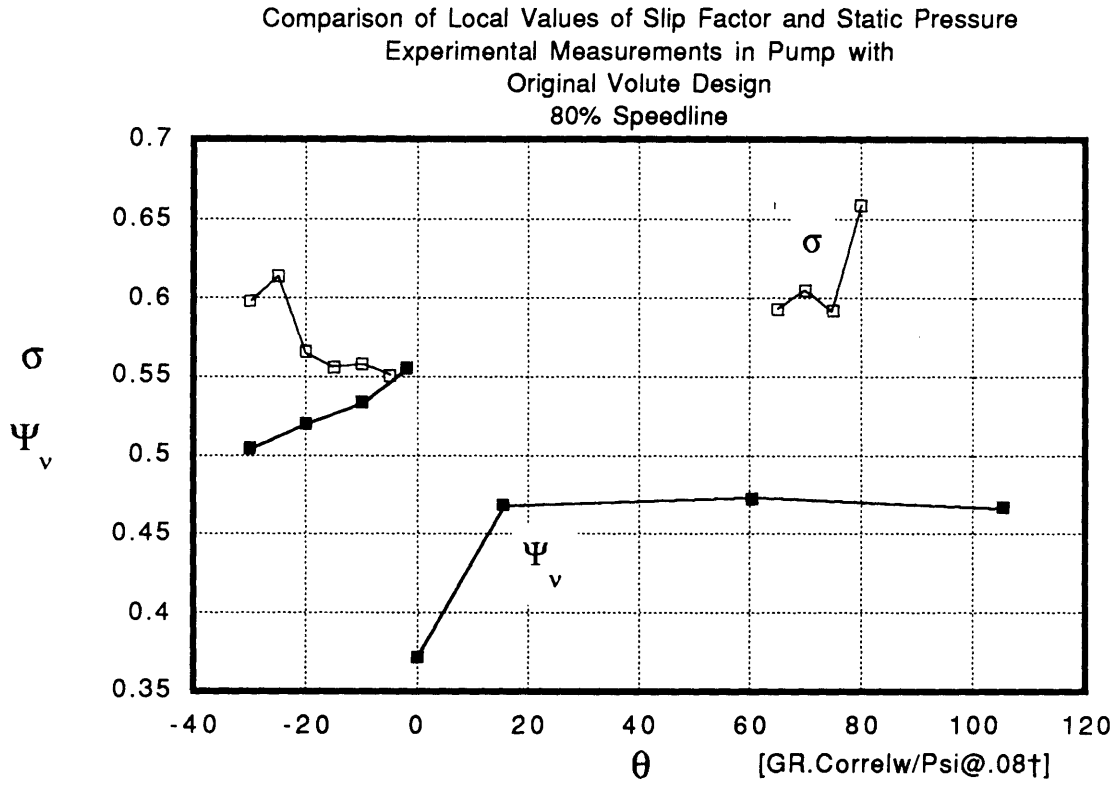
Comparison of Local Values of Slip Factor and Static Pressure
Experimental Measurements in Pump with
Original Volute Design
80% Speedline
0.7
0.65
0.6
0.55
0.5
0.45
0.4
0.35
σ
Ψν
-40
-20
0
20
40
60
80
100
120
θ
[GR.Correlw/Psi@.08†]

Fig.4.1.9.ii

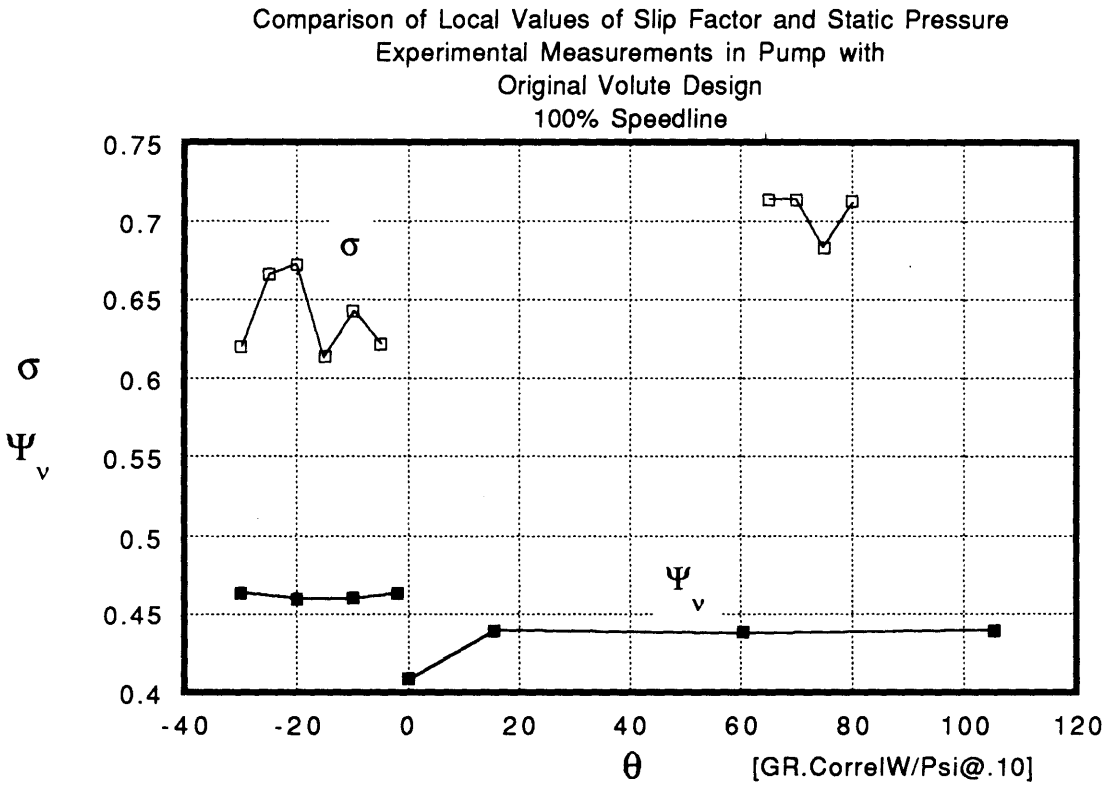
Comparison of Local Values of Slip Factor and Static Pressure
Experimental Measurements in Pump with
Original Volute Design
100% Speedline
0.75
0.7
0.65
0.6
0.55
0.5
0.45
0.4
σ
Ψν
σ
Ψν
-40
-20
0
20
40
60
80
100
120
θ
[GR.CorrelW/Psi@.10]

Fig.4.1.9.iii

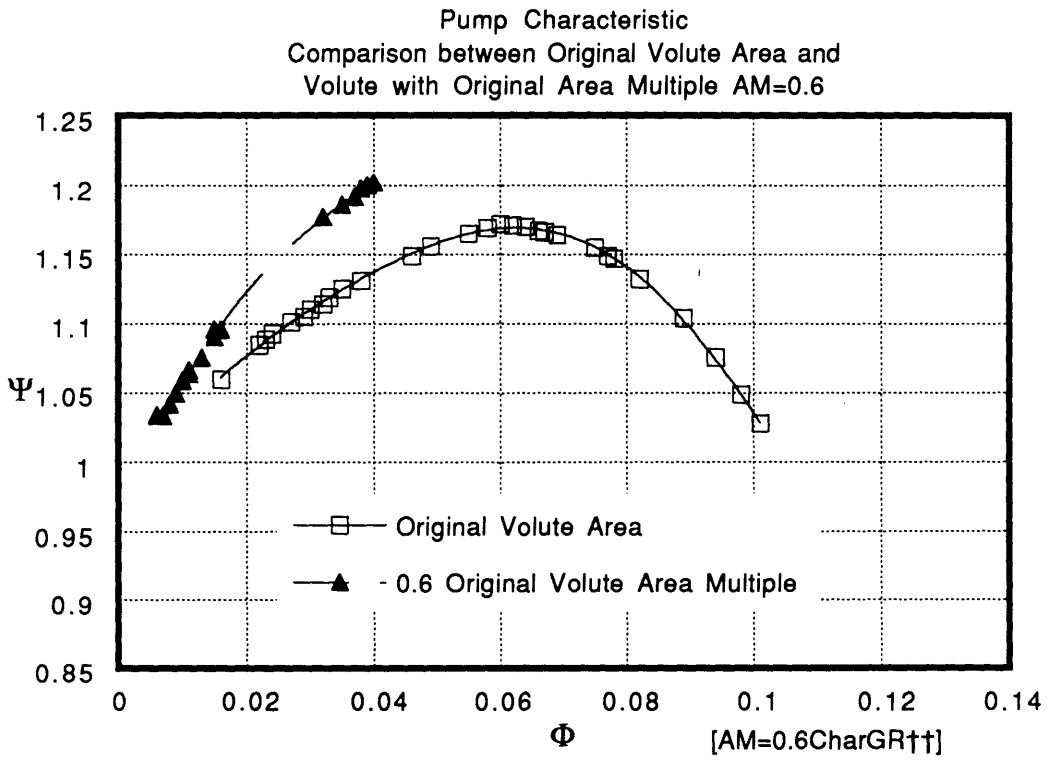
Pump Characteristic
Comparison between Original Volute Area and
Volute with Original Area Multiple AM=0.6
1.25
1.2
1.15
1.1
Ψ1.05
1
0.95
0.9
0.85
0
0.02
0.04
0.06
0.08
0.1
0.12
0.14
Φ
[AM=0.6CharGR††]
Original Volute Area
0.6 Original Volute Area Multiple

Fig.4.2.1

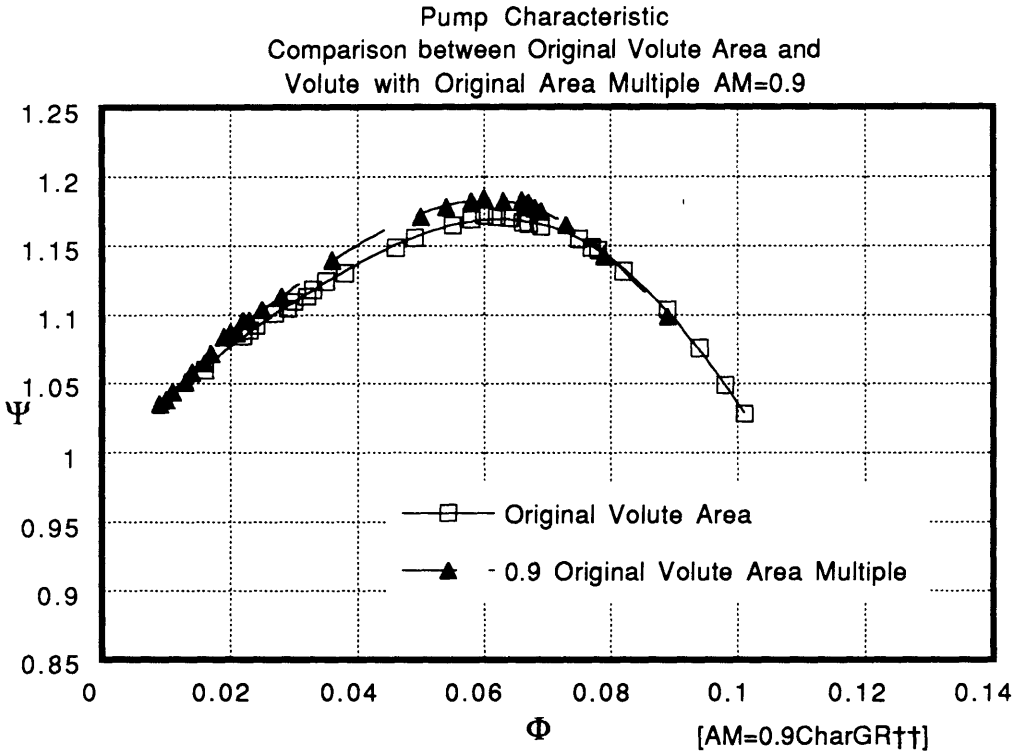
Pump Characteristic
Comparison between Original Volute Area and
Volute with Original Area Multiple AM=0.9
1.25
1.2
1.15
1.1
1.05
1
0.95
0.9
0.85
Ψ
0
0.02
0.04
0.06
0.08
0.1
0.12
0.14
Φ
[AM=0.9CharGR††]
Original Volute Area
0.9 Original Volute Area Multiple

Fig.4.2.2

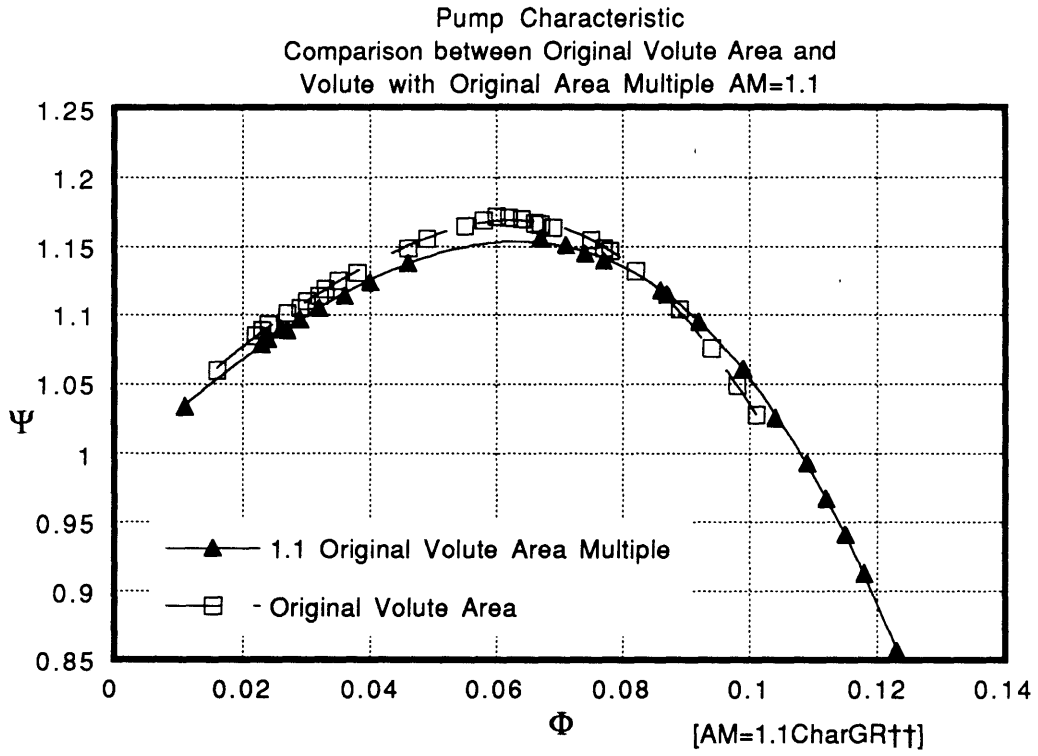
Pump Characteristic
Comparison between Original Volute Area and
Volute with Original Area Multiple AM=1.1
1.25
1.2
1.15
1.1
1.05
Ψ
1
0.95
0.9
0.85
0
0.02
0.04
0.06
0.08
0.1
0.12
0.14
Φ
1.1 Original Volute Area Multiple
- Original Volute Area
[AM=1.1CharGR††]

Fig.4.2.3

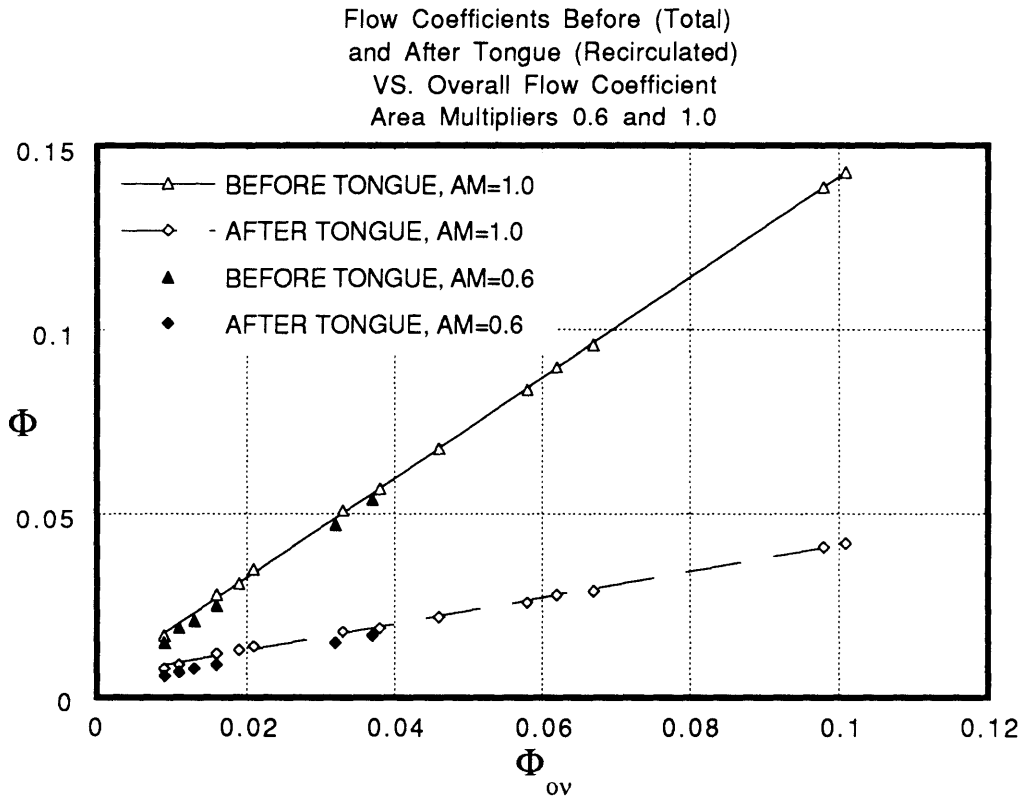
Flow Coefficients Before (Total)
and After Tongue (Recirculated)
VS. Overall Flow Coefficient
Area Multipliers 0.6 and 1.0
BEFORE TONGUE, AM=1.0
AFTER TONGUE, AM=1.0
BEFORE TONGUE, AM=0.6
AFTER TONGUE, AM=0.6
0.15
0.1
0.05
0
Φ
0
0.02
0.04
0.06
0.08
0.1
0.12
Φ ov

Fig.4.2.4

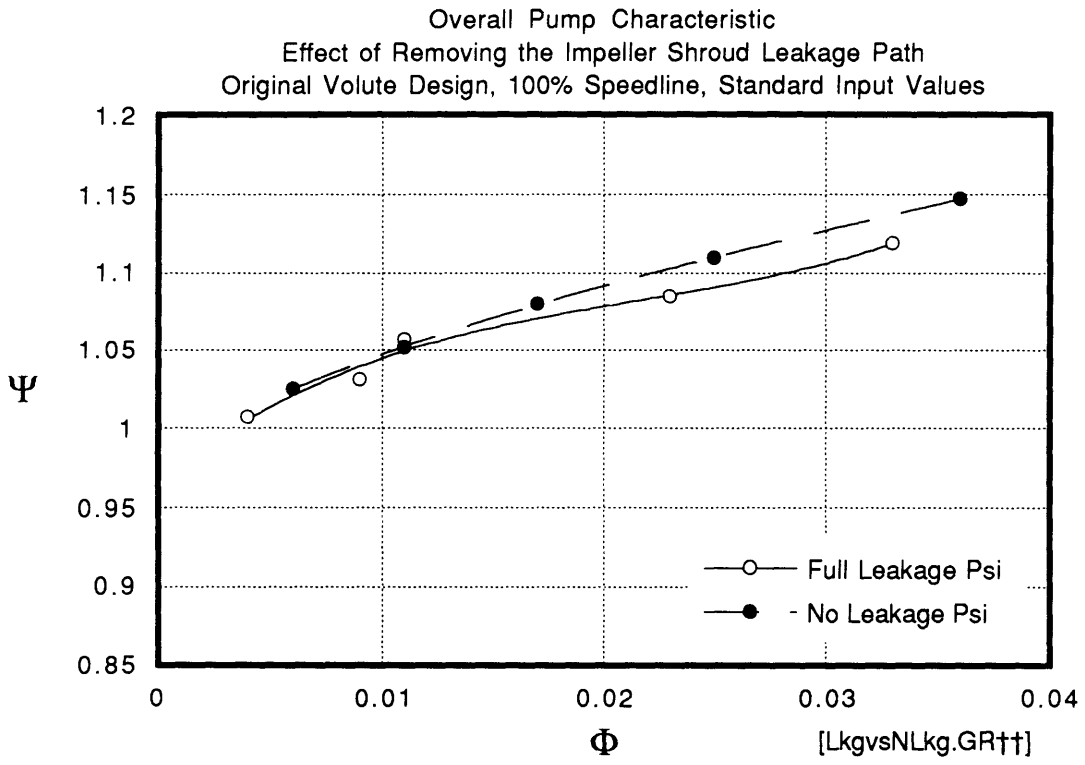
Overall Pump Characteristic
Effect of Removing the Impeller Shroud Leakage Path
Original Volute Design, 100% Speedline, Standard Input Values
1.2
1.15
1.1
1.05
1
0.95
0.9
0.85
Ψ
0
0.01
0.02
0.03
0.04
Φ
[LkgvsNLkg.GR††]
Full Leakage Psi
No Leakage Psi

Fig.4.2.5

There is no text material missing here.
Pages have been incorrectly numbered.

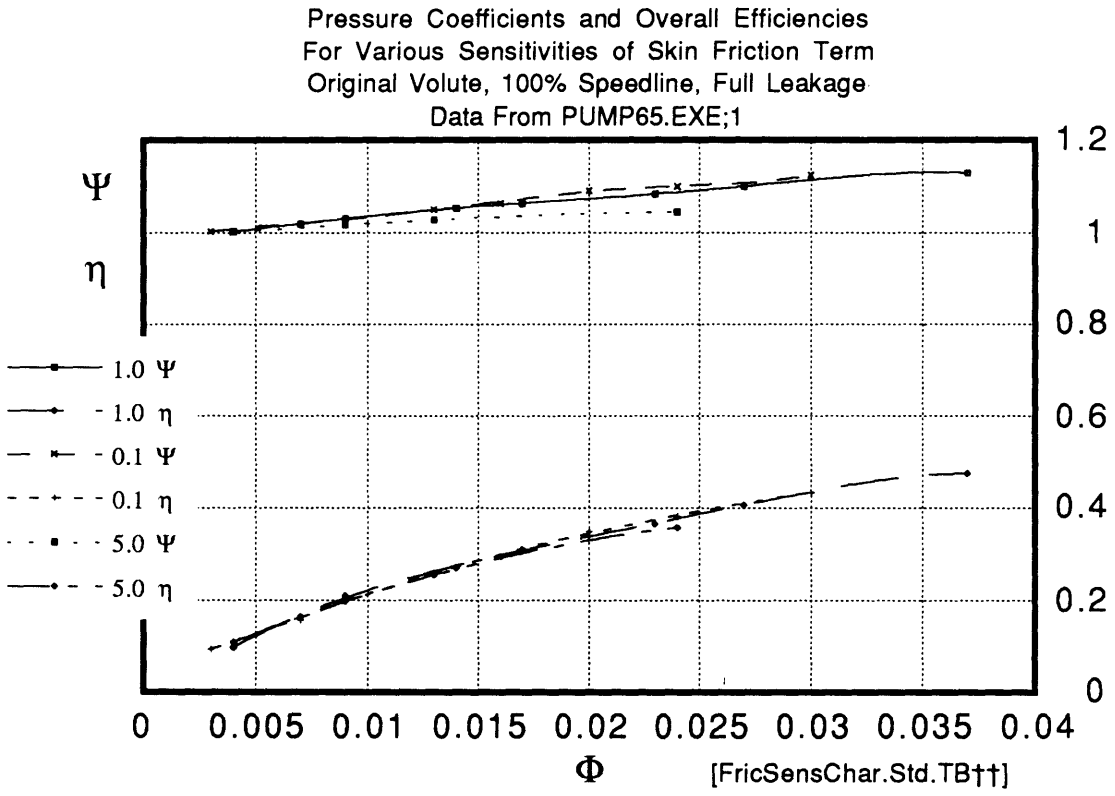
Pressure Coefficients and Overall Efficiencies
For Various Sensitivities of Skin Friction Term
Original Volute, 100% Speedline, Full Leakage
Data From PUMP65.EXE;1
Ψ
η
1.0 Ψ
1.0 η
0.1 Ψ
0.1 η
5.0 Ψ
5.0 η
1.2
1
0.8
0.6
0.4
0.2
0
0 0.005 0.01 0.015 0.02 0.025 0.03 0.035 0.04
Φ
[FricSensChar.Std.TB††]

Fig.4.2.6

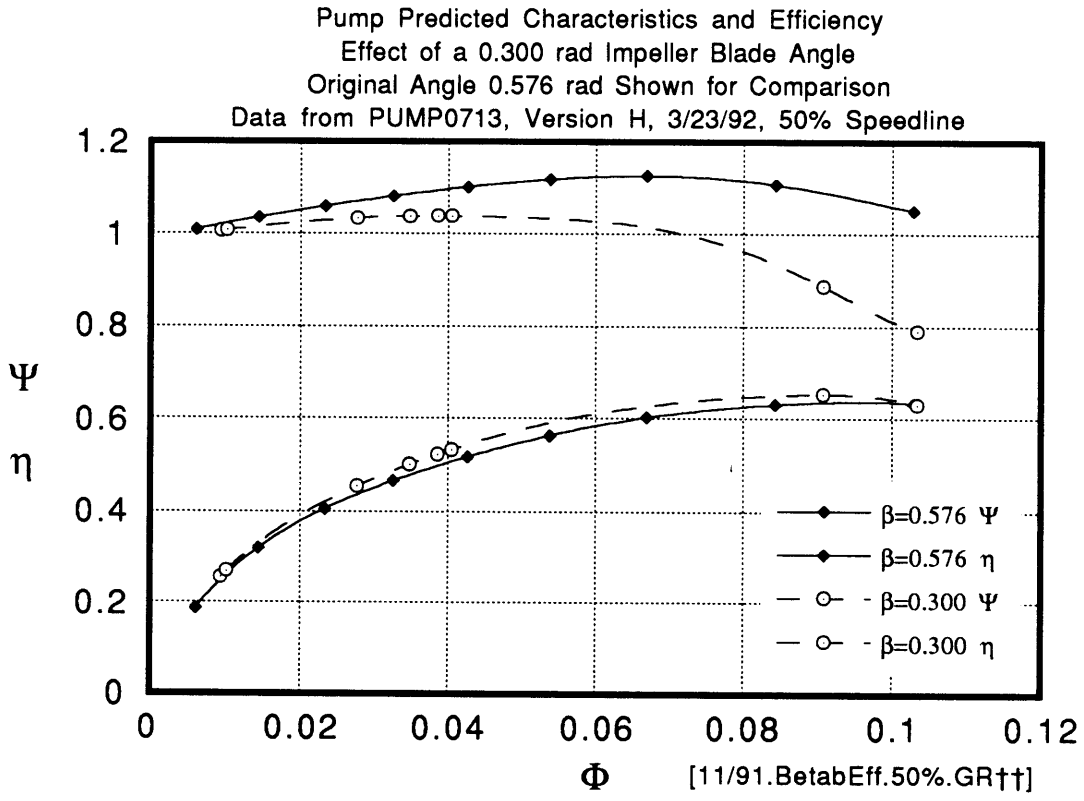
Pump Predicted Characteristics and Efficiency
Effect of a 0.300 rad Impeller Blade Angle
Original Angle 0.576 rad Shown for Comparison
Data from PUMP0713, Version H, 3/23/92, 50% Speedline
1.2
1
0.8
Ψ
0.6
η
0.4
0.2
0
0
0.02
0.04
0.06
0.08
0.1
0.12
Φ
[11/91.BetabEff.50%.GR††]
β=0.576 Ψ
β=0.576 η
β=0.300 Ψ
β=0.300 η

Fig.4.2.7.i

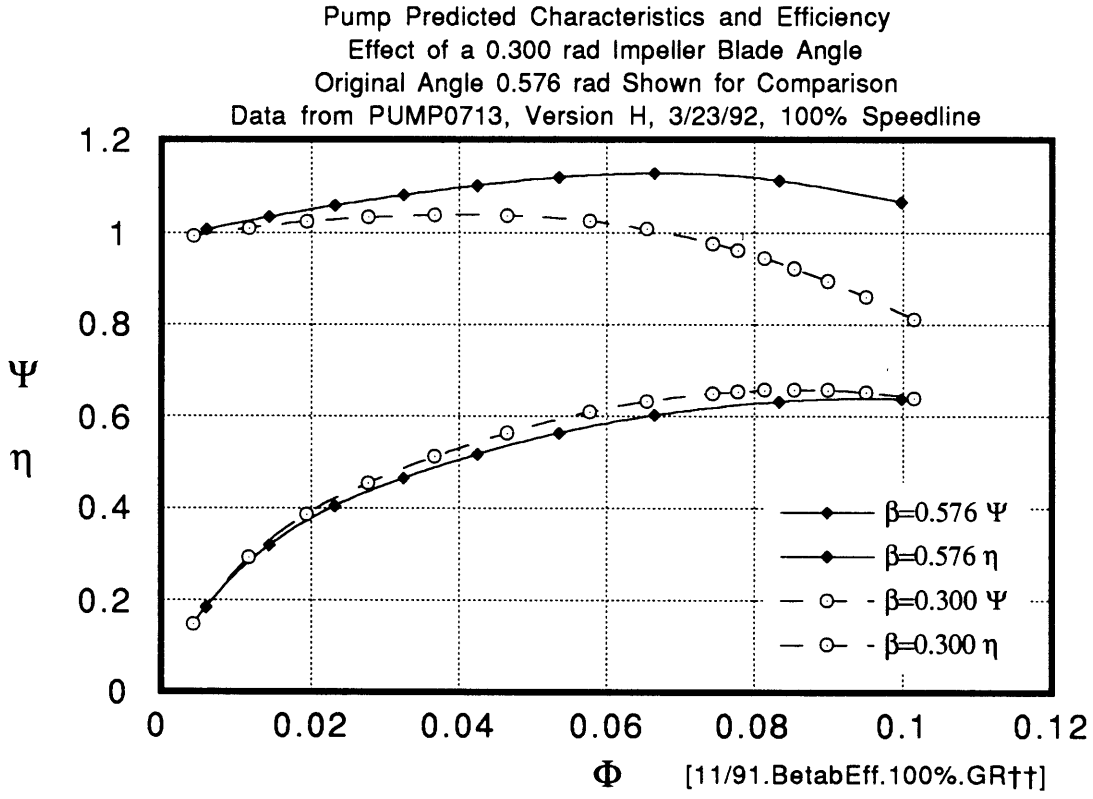
Pump Predicted Characteristics and Efficiency
Effect of a 0.300 rad Impeller Blade Angle
Original Angle 0.576 rad Shown for Comparison
Data from PUMP0713, Version H, 3/23/92, 100% Speedline
1.2
1
0.8
0.6
0.4
0.2
0
Ψ
η
0
0.02
0.04
0.06
0.08
0.1
0.12
Φ
[11/91.BetabEff.100%.GR††]
β=0.576 Ψ
β=0.576 η
β=0.300 Ψ
β=0.300 η

Fig.4.2.7.ii

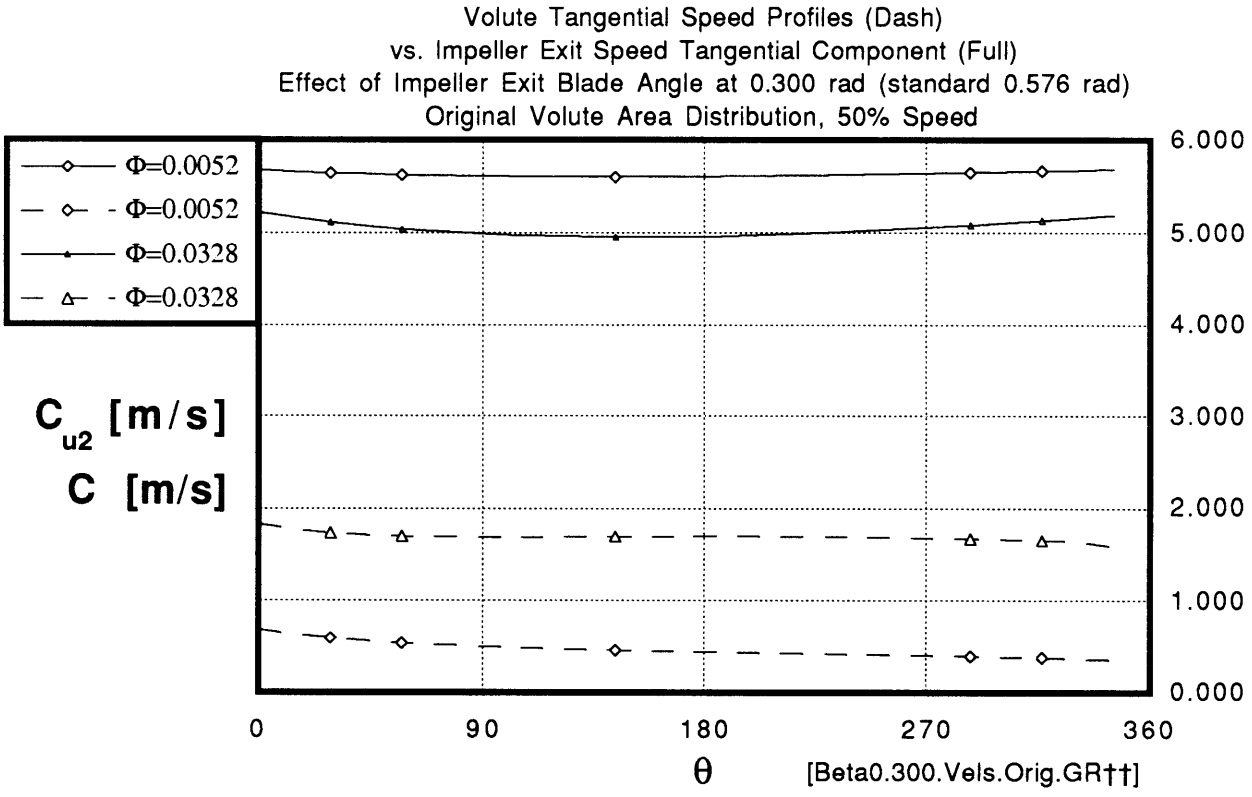
Volute Tangential Speed Profiles (Dash)
vs. Impeller Exit Speed Tangential Component (Full)
Effect of Impeller Exit Blade Angle at 0.300 rad (standard 0.576 rad)
Original Volute Area Distribution, 50% Speed
Φ=0.0052
- Φ=0.0052
Φ=0.0328
- Φ=0.0328
C u2 [m/s]
C [m/s]
6.000
5.000
4.000
3.000
2.000
1.000
0.000
0
90
180
270
360
θ
[Beta0.300.Vels.Orig.GR††]

Fig.4.2.8

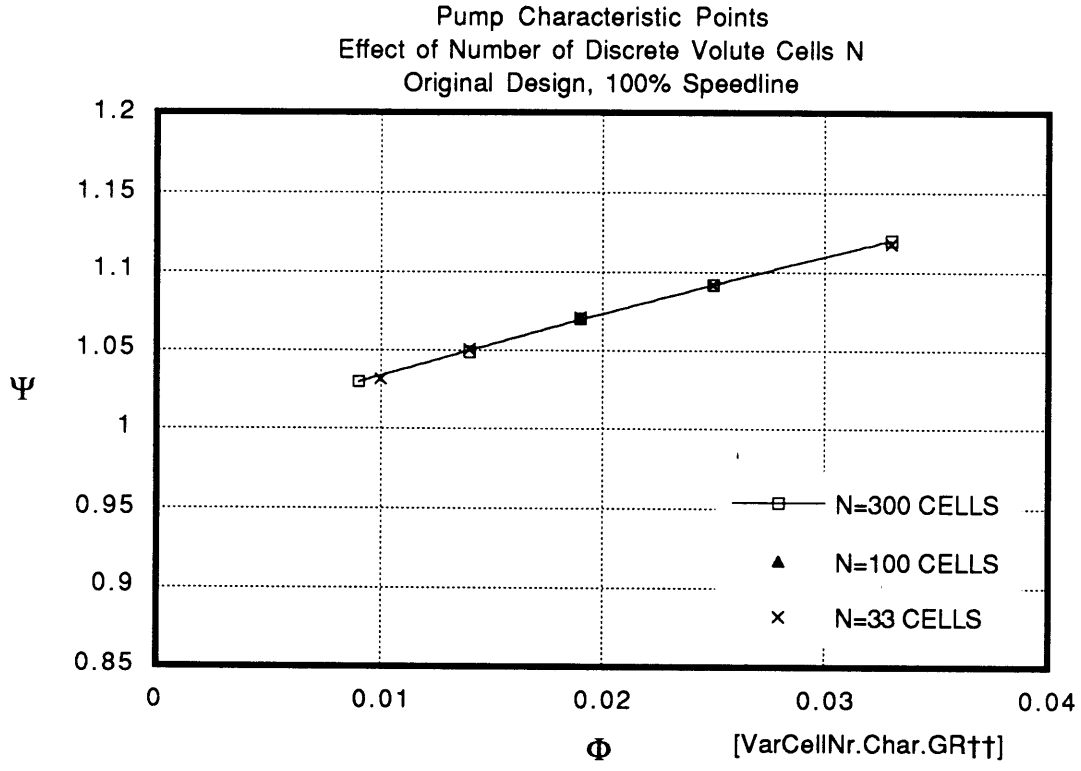
Pump Characteristic Points
Effect of Number of Discrete Volute Cells N
Original Design, 100% Speedline
1.2
1.15
1.1
1.05
1
0.95
0.9
0.85
Ψ
0
0.01
0.02
0.03
0.04
Φ
[VarCellNr.Char.GR†††]
N=300 CELLS
N=100 CELLS
N=33 CELLS

Fig.4.2.9

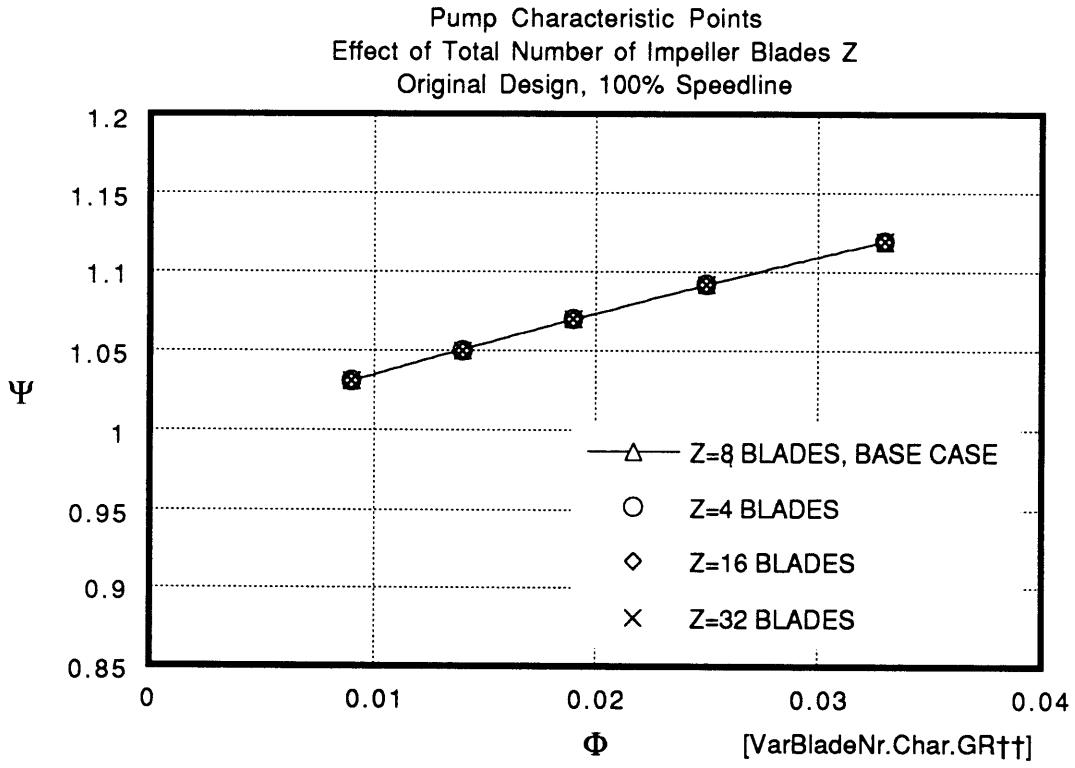
Pump Characteristic Points
Effect of Total Number of Impeller Blades Z
Original Design, 100% Speedline
1.2
1.15
1.1
1.05
1
0.95
0.9
0.85
Ψ
0
0.01
0.02
0.03
0.04
Φ
[VarBladeNr.Char.GR††]
Z=8 BLADES, BASE CASE
Z=4 BLADES
Z=16 BLADES
Z=32 BLADES

Fig.4.2.10

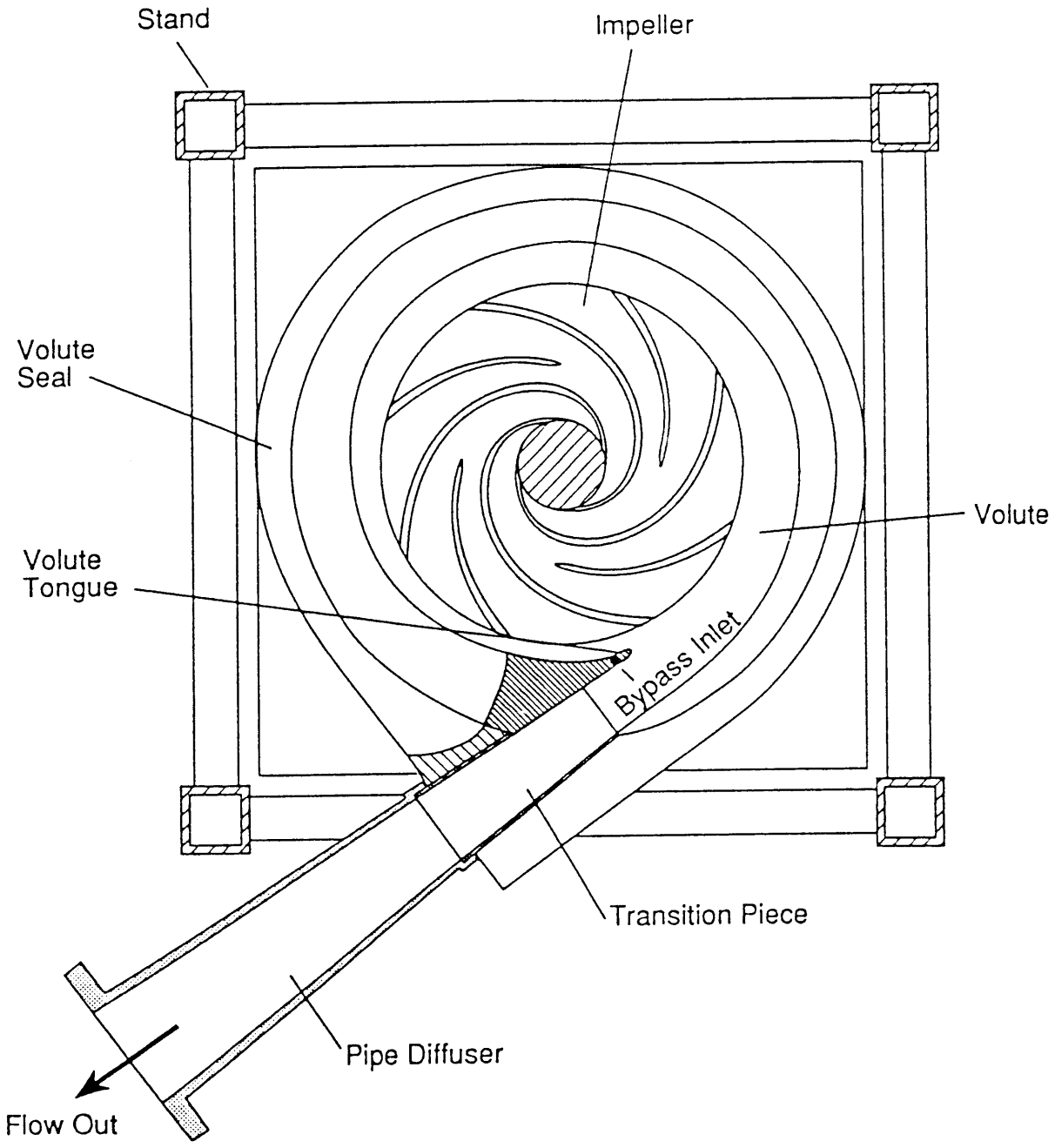

Fig.4.3.1 Location of Tongue Bypass Device

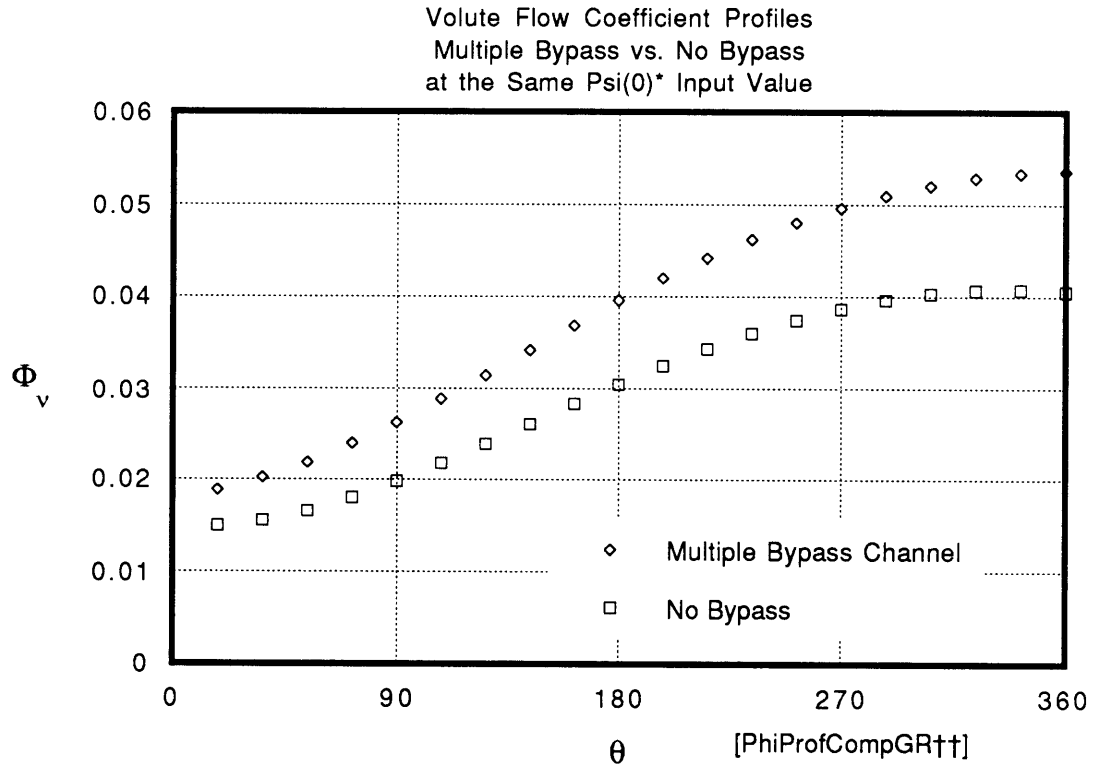
Volute Flow Coefficient Profiles
Multiple Bypass vs. No Bypass
at the Same Psi(0)* Input Value
0.06
0.05
0.04
0.03
0.02
0.01
0
Φν
0
90
180
270
360
θ
[PhiProfCompGR†††]
Multiple Bypass Channel
No Bypass

Fig.4.3.2

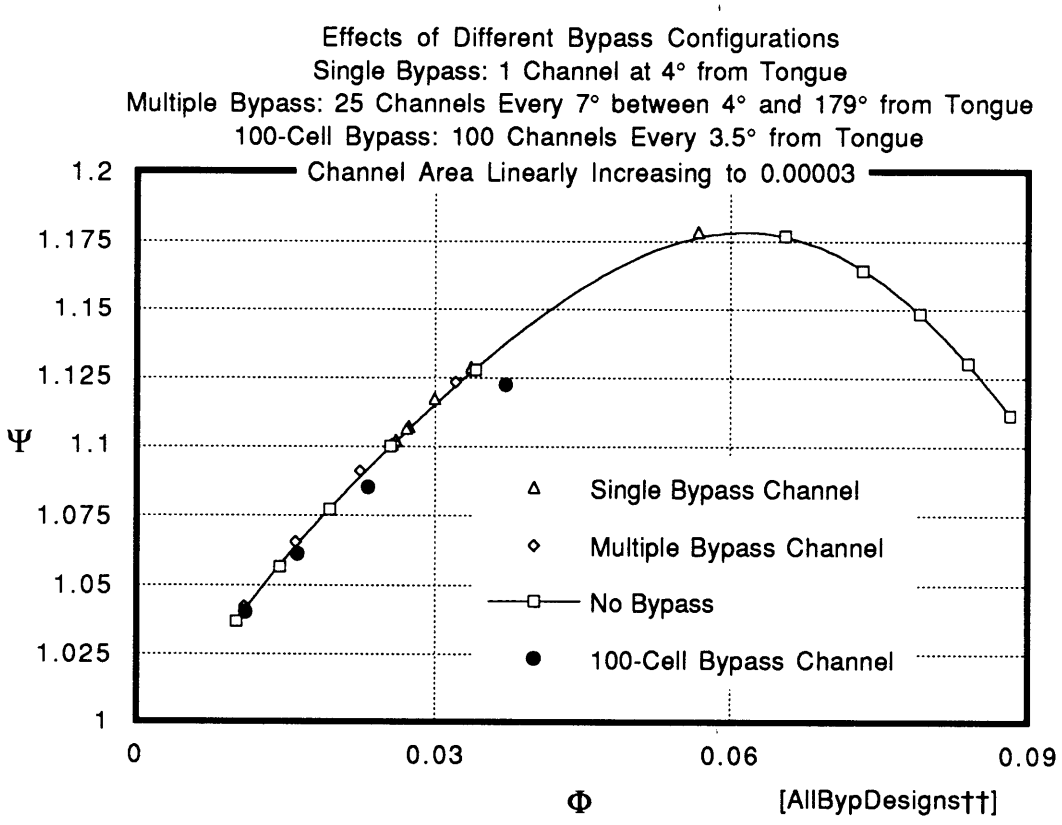
Effects of Different Bypass Configurations
Single Bypass: 1 Channel at 4° from Tongue
Multiple Bypass: 25 Channels Every 7° between 4° and 179° from Tongue
100-Cell Bypass: 100 Channels Every 3.5° from Tongue
Channel Area Linearly Increasing to 0.00003
1.2
1.175
1.15
1.125
Ψ 1.1
1.075
1.05
1.025
1
0
0.03
0.06
0.09
Φ
[AllBypDesignstt]
Single Bypass Channel
Multiple Bypass Channel
No Bypass
100-Cell Bypass Channel

Fig.4.3.3

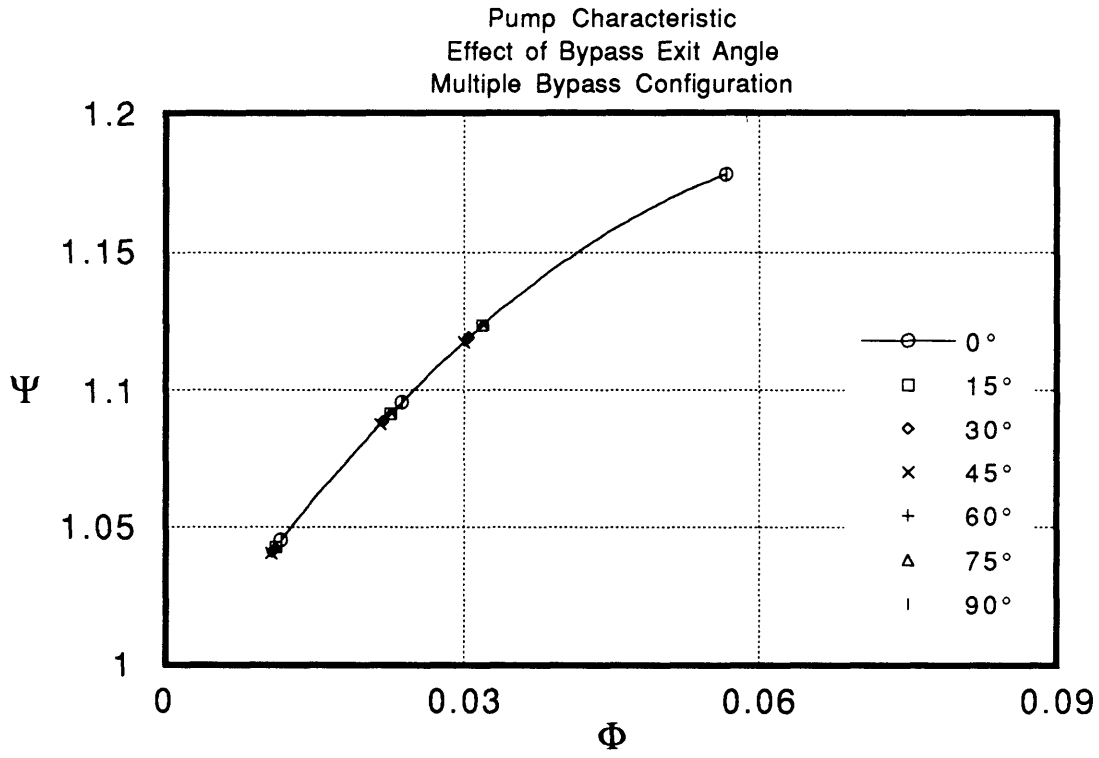
Pump Characteristic
Effect of Bypass Exit Angle
Multiple Bypass Configuration
1.2
1.15
1.1
1.05
1
Ψ
0
0.03
0.06
0.09
Φ
0°
15°
30°
45°
60°
75°
90°

Fig.4.3.4

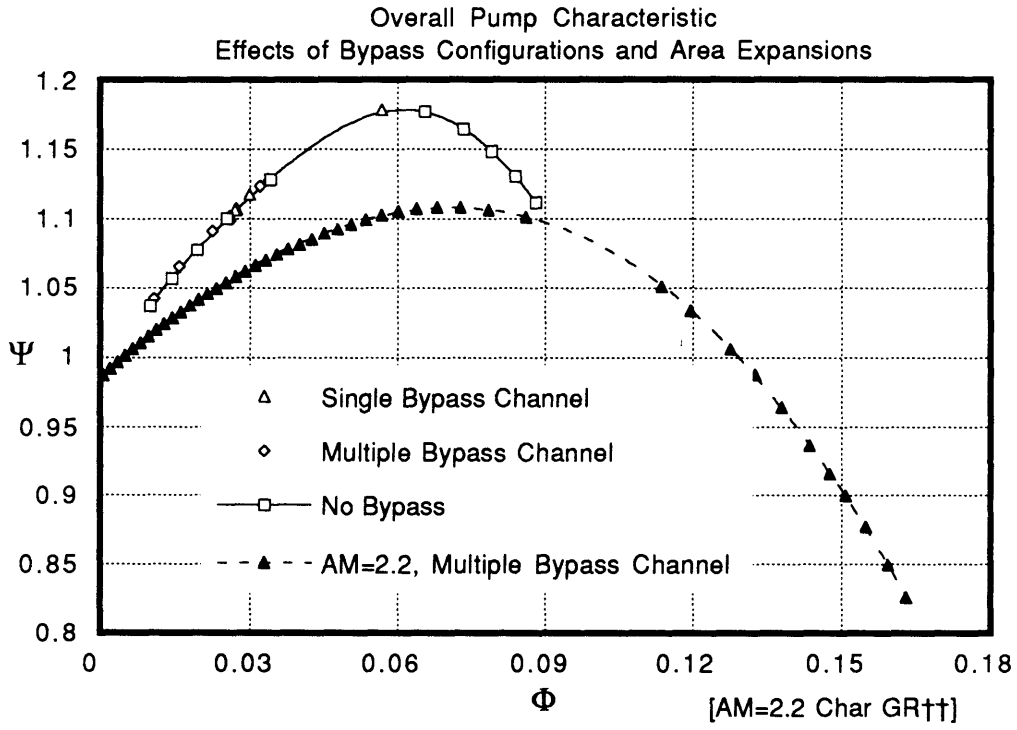
Overall Pump Characteristic
Effects of Bypass Configurations and Area Expansions
1.2
1.15
1.1
1.05
Ψ 1
0.95
0.9
0.85
0.8
0
0.03
0.06
0.09
0.12
0.15
0.18
Φ
[AM=2.2 Char GR††]
Single Bypass Channel
Multiple Bypass Channel
No Bypass
AM=2.2, Multiple Bypass Channel

Fig.4.3.5

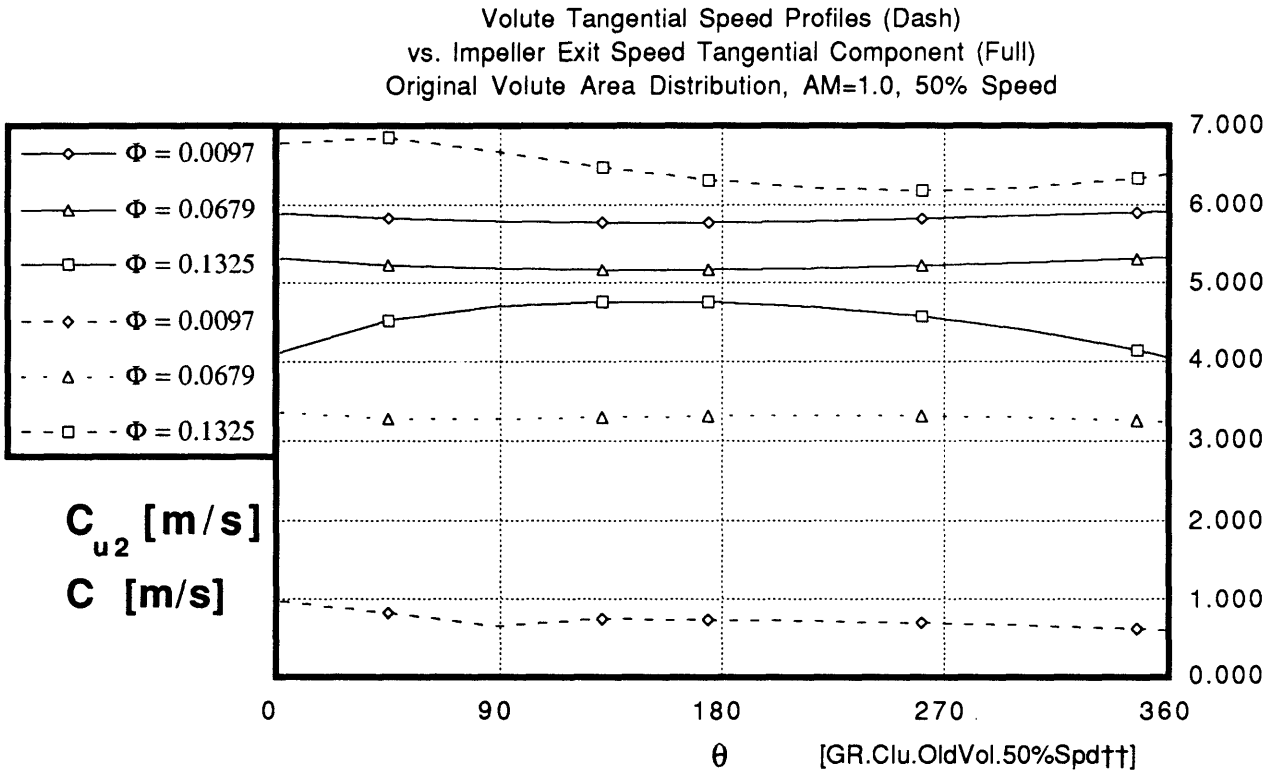
Volute Tangential Speed Profiles (Dash)
vs. Impeller Exit Speed Tangential Component (Full)
Original Volute Area Distribution, AM=1.0, 50% Speed
Φ = 0.0097
Φ = 0.0679
Φ = 0.1325
Φ = 0.0097
Φ = 0.0679
Φ = 0.1325
C u2 [m/s]
C [m/s]
7.000
6.000
5.000
4.000
3.000
2.000
1.000
0.000
0
90
180
270
360
θ
[GR.Clu.OldVol.50%Spd††]

Fig.4.4.1

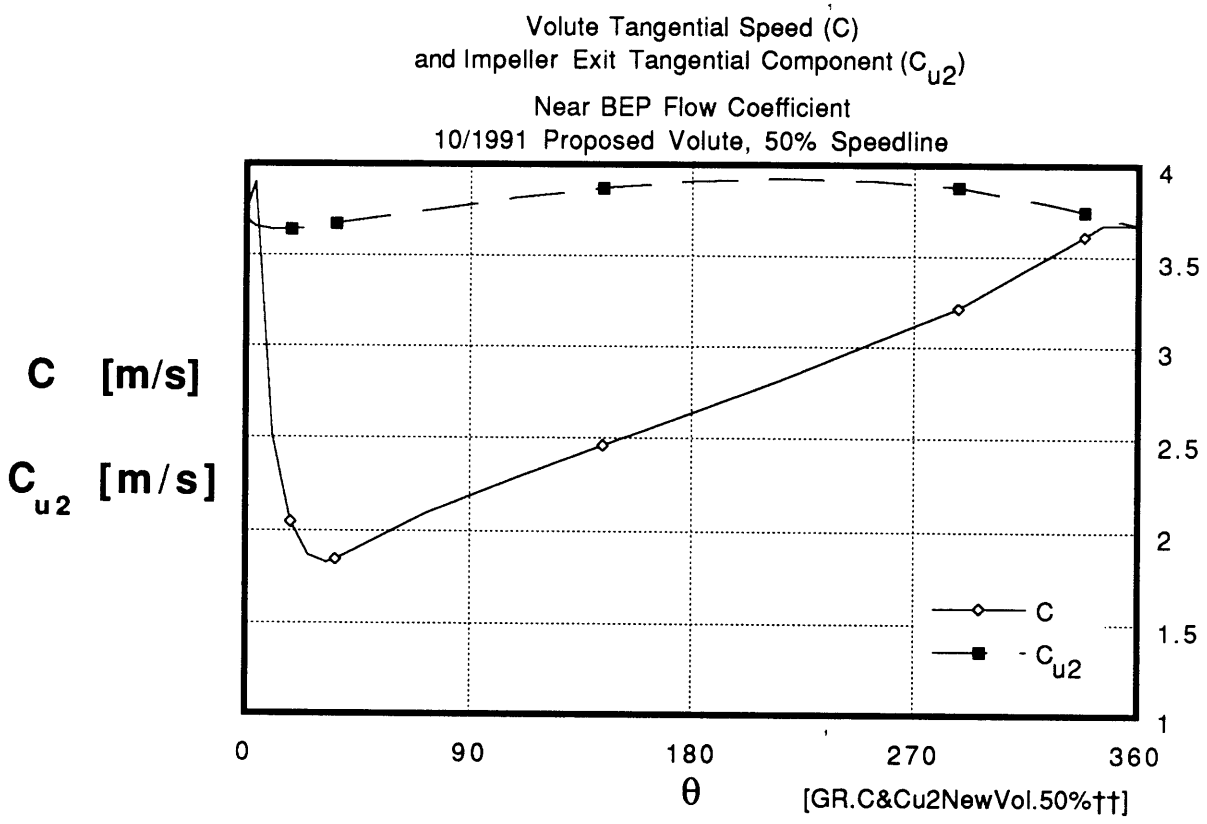
Volute Tangential Speed (C)
and Impeller Exit Tangential Component (C_{u2})
Near BEP Flow Coefficient
10/1991 Proposed Volute, 50% Speedline
C [m/s]
C_{u2} [m/s]
4
3.5
3
2.5
2
1.5
1
C
- C_{u2}
0
90
180
270
360
θ
[GR.C&Cu2NewVol.50%††]

Fig.4.4.2

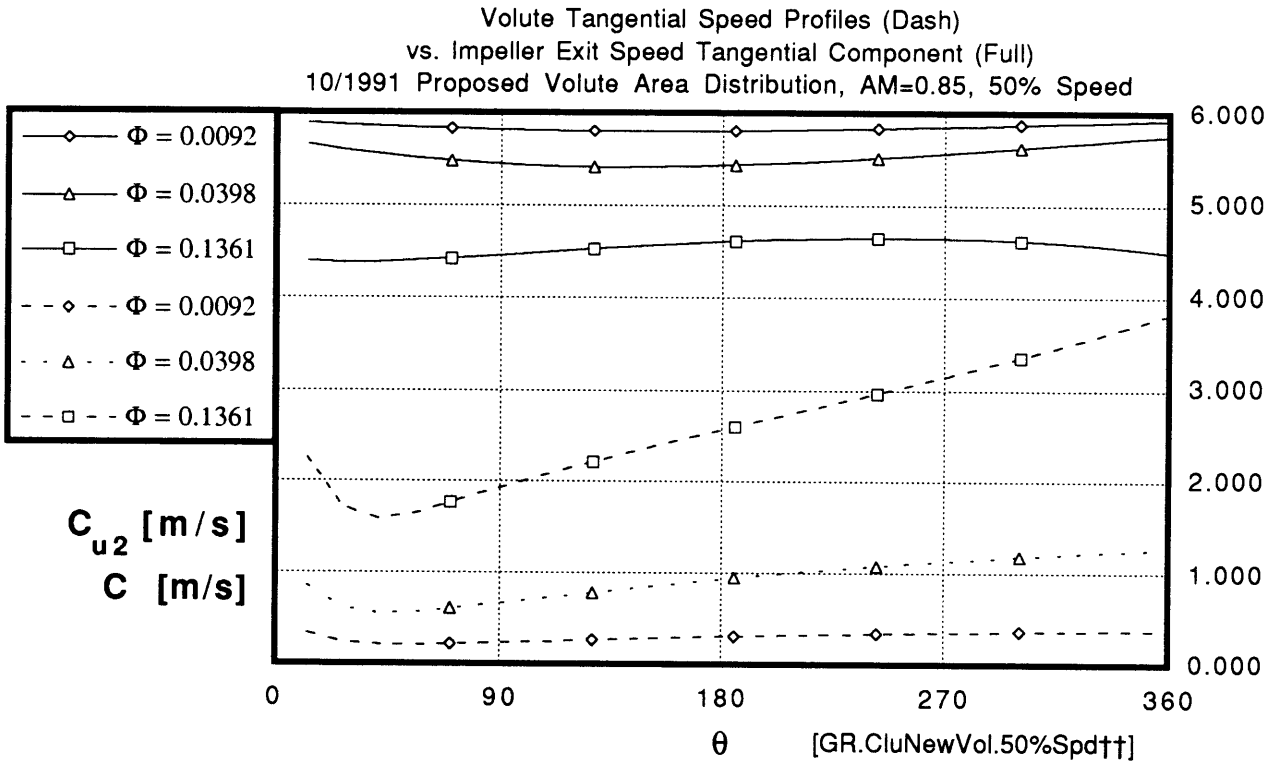
Volute Tangential Speed Profiles (Dash)
vs. Impeller Exit Speed Tangential Component (Full)
10/1991 Proposed Volute Area Distribution, AM=0.85, 50% Speed
Φ = 0.0092
Φ = 0.0398
Φ = 0.1361
Φ = 0.0092
Φ = 0.0398
Φ = 0.1361
C u2 [m/s]
C [m/s]
6.000
5.000
4.000
3.000
2.000
1.000
0.000
0
90
180
270
360
θ
[GR.CluNewVol.50%Spd††]

Fig.4.4.3

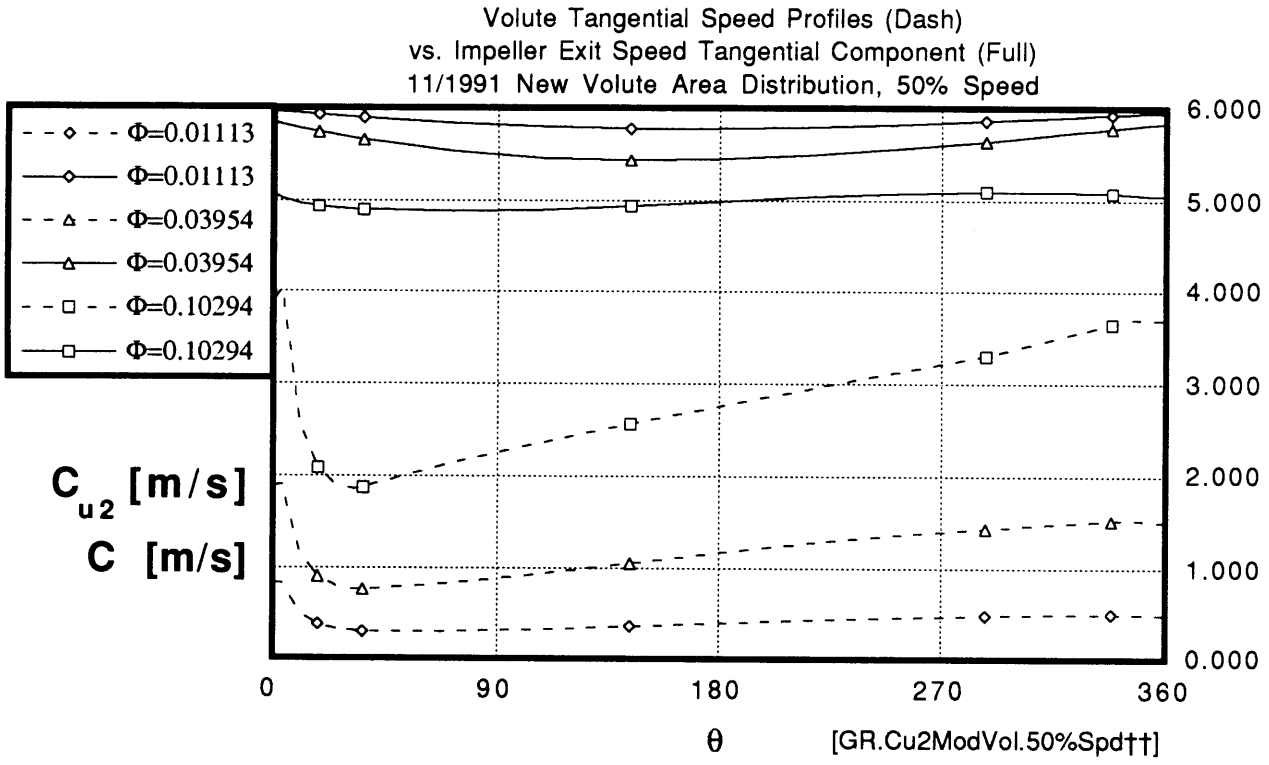
Volute Tangential Speed Profiles (Dash)
vs. Impeller Exit Speed Tangential Component (Full)
11/1991 New Volute Area Distribution, 50% Speed
Φ=0.01113
Φ=0.01113
Φ=0.03954
Φ=0.03954
Φ=0.10294
Φ=0.10294
C u2 [m/s]
C [m/s]
6.000
5.000
4.000
3.000
2.000
1.000
0.000
0
90
180
270
360
θ
[GR.Cu2ModVol.50%Spd††]

Fig.4.4.4

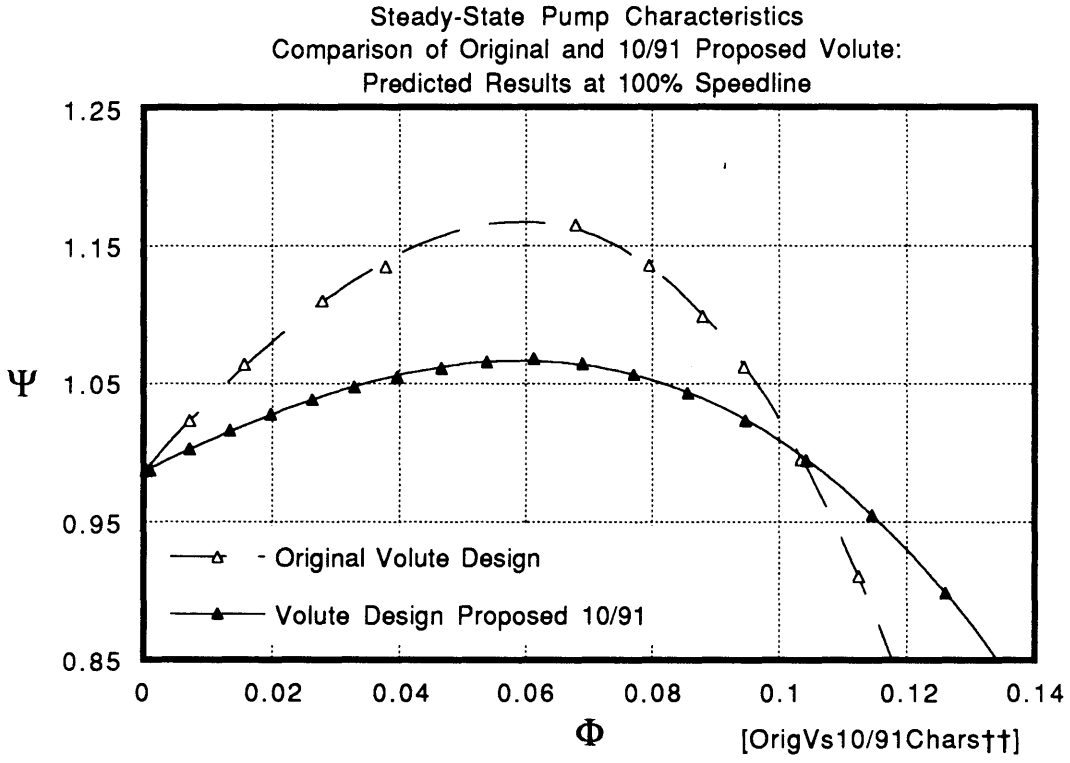
Steady-State Pump Characteristics
Comparison of Original and 10/91 Proposed Volute:
Predicted Results at 100% Speedline
1.25
1.15
1.05
0.95
0.85
Ψ
0
0.02
0.04
0.06
0.08
0.1
0.12
0.14
Φ
- Original Volute Design
Volute Design Proposed 10/91
[OrigVs10/91Chars††]

Fig.4.4.5

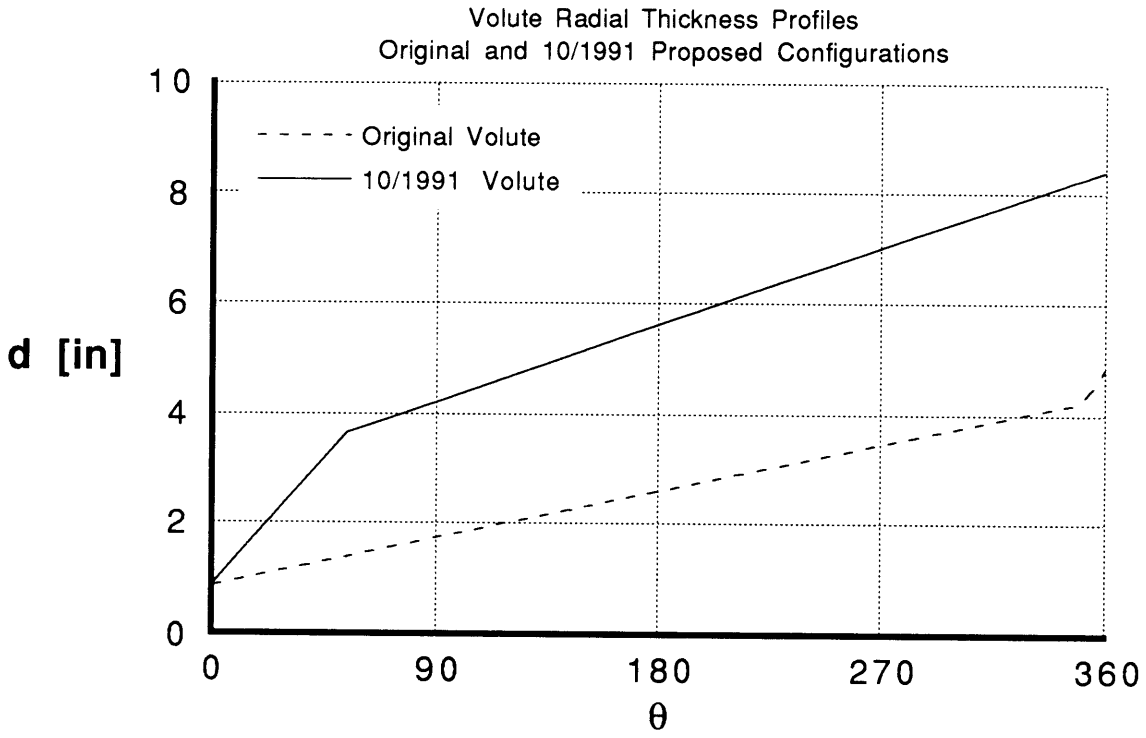
Volute Radial Thickness Profiles
Original and 10/1991 Proposed Configurations
Original Volute
10/1991 Volute
d [in]
10
8
6
4
2
0
0
90
180
270
360
θ

Fig.4.4.6

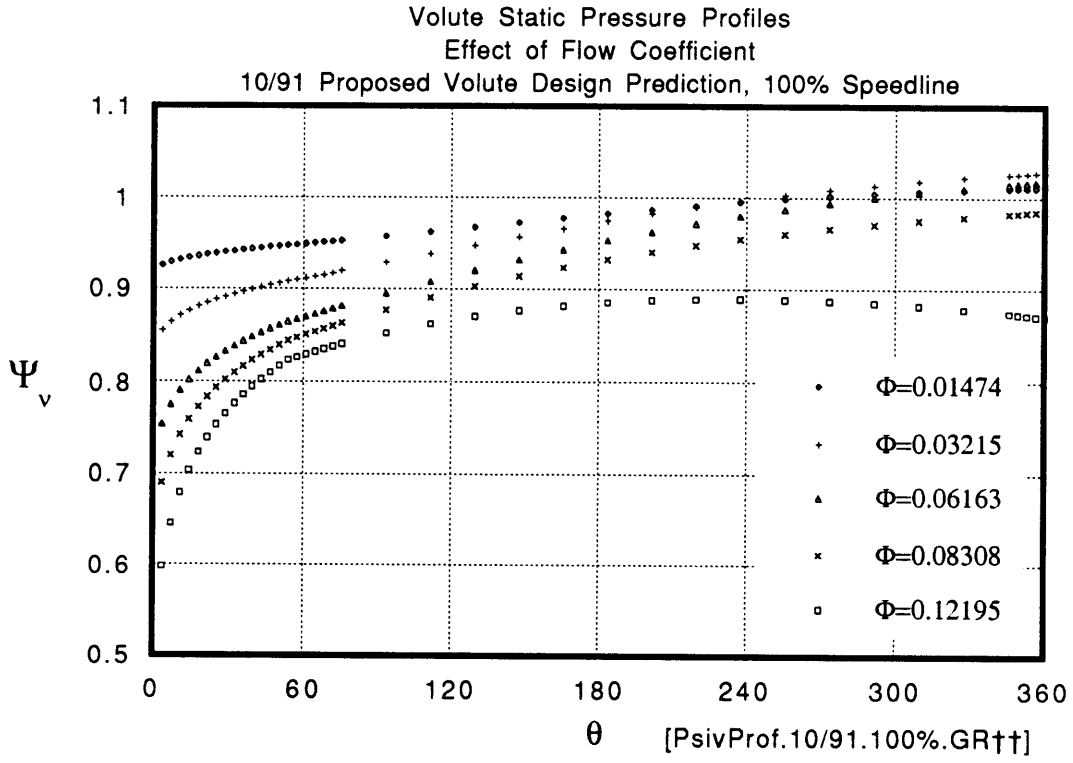
Volute Static Pressure Profiles
Effect of Flow Coefficient
10/91 Proposed Volute Design Prediction, 100% Speedline
1.1
1
0.9
0.8
0.7
0.6
0.5
Ψv
0
60
120
180
240
300
360
θ
[PsivProf.10/91.100%.GR††]
Φ=0.01474
Φ=0.03215
Φ=0.06163
Φ=0.08308
Φ=0.12195

Fig.4.4.7

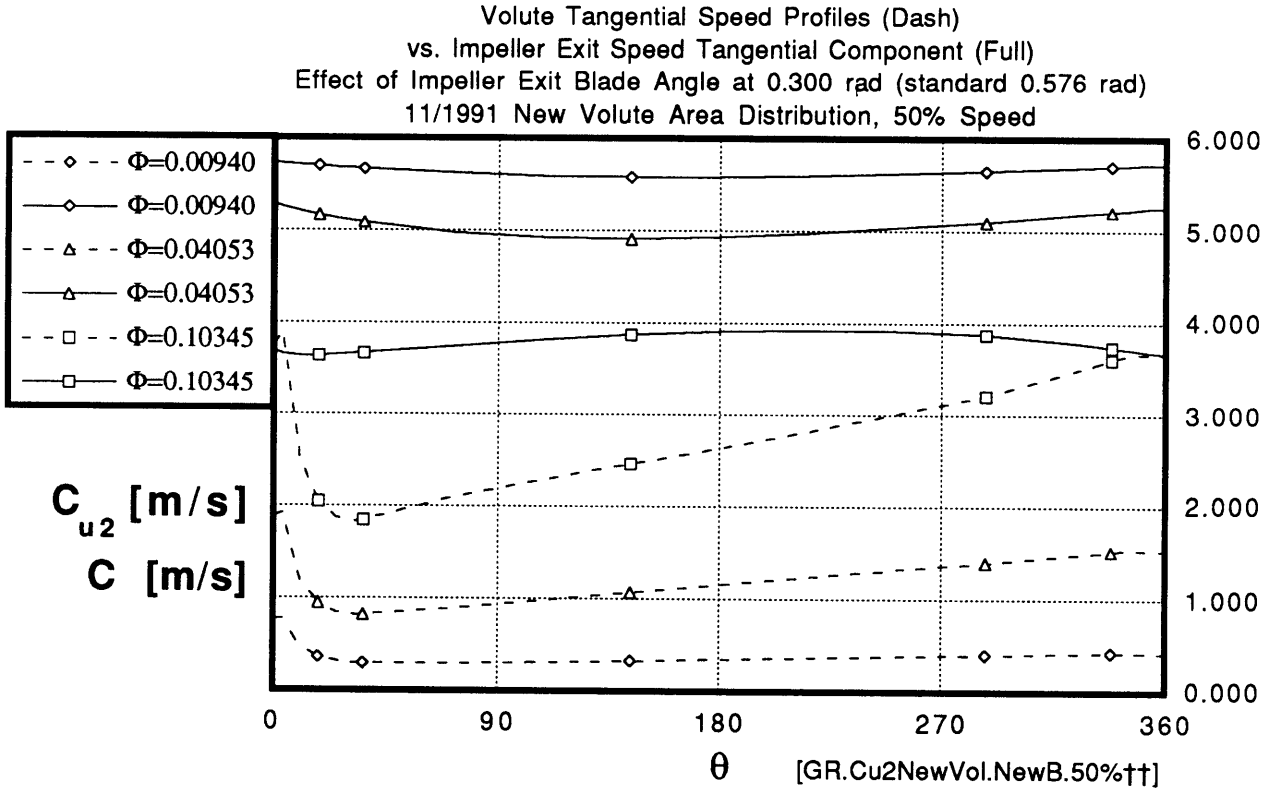
Volute Tangential Speed Profiles (Dash)
vs. Impeller Exit Speed Tangential Component (Full)
Effect of Impeller Exit Blade Angle at 0.300 rad (standard 0.576 rad)
11/1991 New Volute Area Distribution, 50% Speed
Φ=0.00940
Φ=0.00940
Φ=0.04053
Φ=0.04053
Φ=0.10345
Φ=0.10345
C u2 [m/s]
C [m/s]
6.000
5.000
4.000
3.000
2.000
1.000
0.000
0
90
180
270
360
θ
[GR.Cu2NewVol.NewB.50%††]

Fig.4.4.8

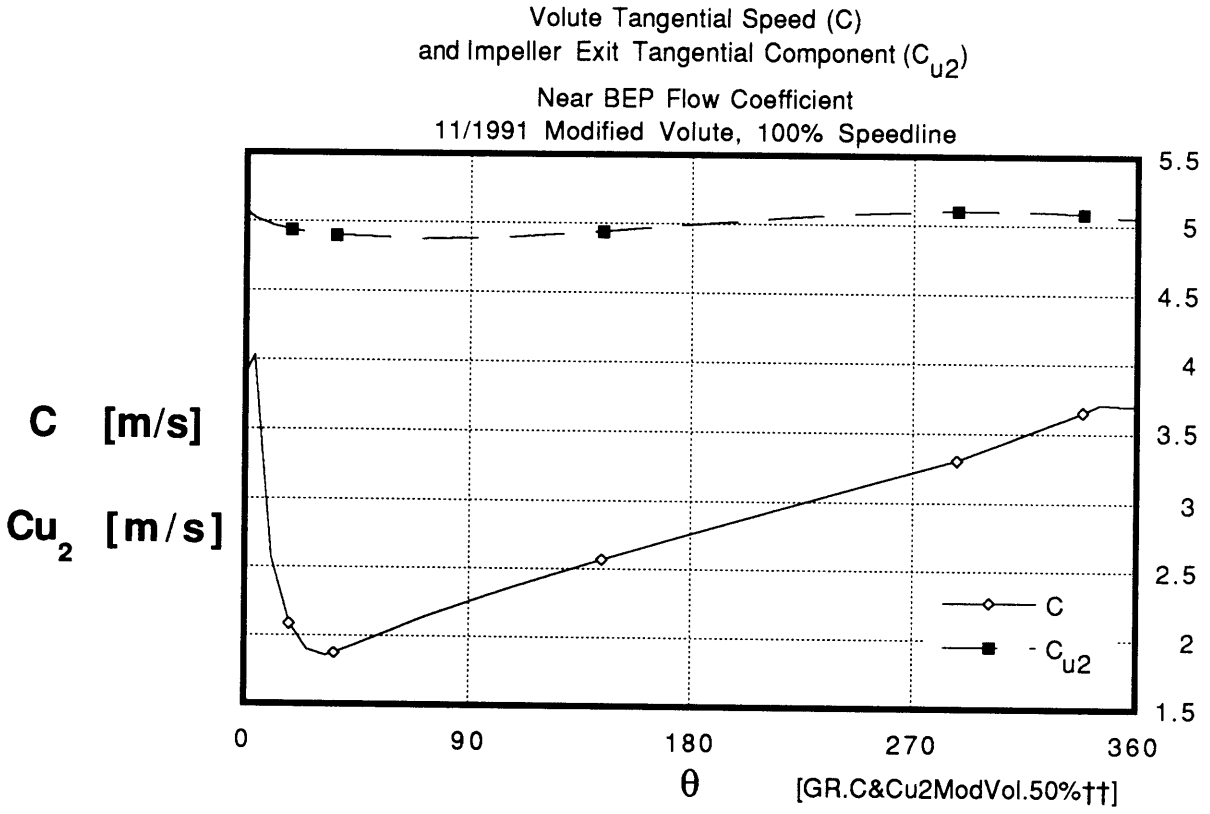
Volute Tangential Speed (C)
and Impeller Exit Tangential Component (C_{u2})
Near BEP Flow Coefficient
11/1991 Modified Volute, 100% Speedline
C [m/s]
Cu_2 [m/s]
5.5
5
4.5
4
3.5
3
2.5
2
1.5
C
- C_{u2}
0
90
180
270
360
θ
[GR.C&Cu2ModVol.50%††]

Fig.4.5.1

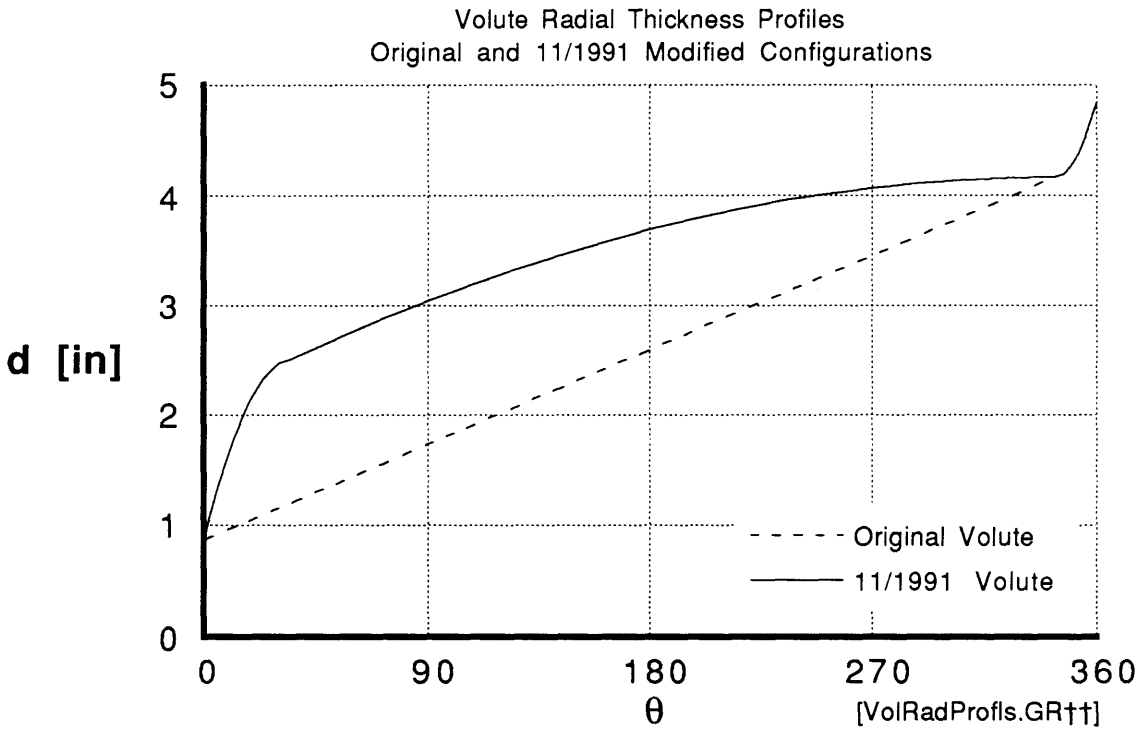
Volute Radial Thickness Profiles
Original and 11/1991 Modified Configurations
d [in]
5
4
3
2
1
0
0
90
180
270
360
θ
[VolRadProfls.GR††]
Original Volute
11/1991 Volute

Fig.4.5.2

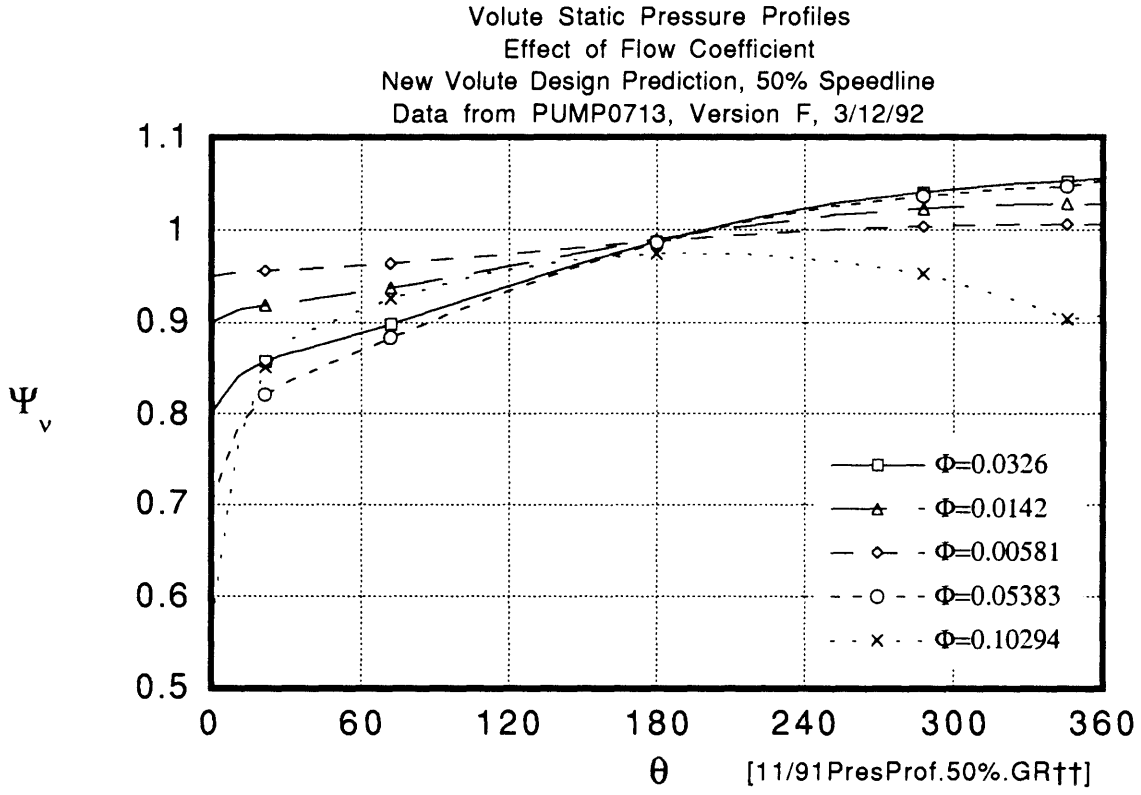
Volute Static Pressure Profiles
Effect of Flow Coefficient
New Volute Design Prediction, 50% Speedline
Data from PUMP0713, Version F, 3/12/92
1.1
1
0.9
0.8
0.7
0.6
0.5
Ψν
0
60
120
180
240
300
360
θ
[11/91PresProf.50%.GR††]
Φ=0.0326
Φ=0.0142
Φ=0.00581
Φ=0.05383
Φ=0.10294

Fig.4.5.3

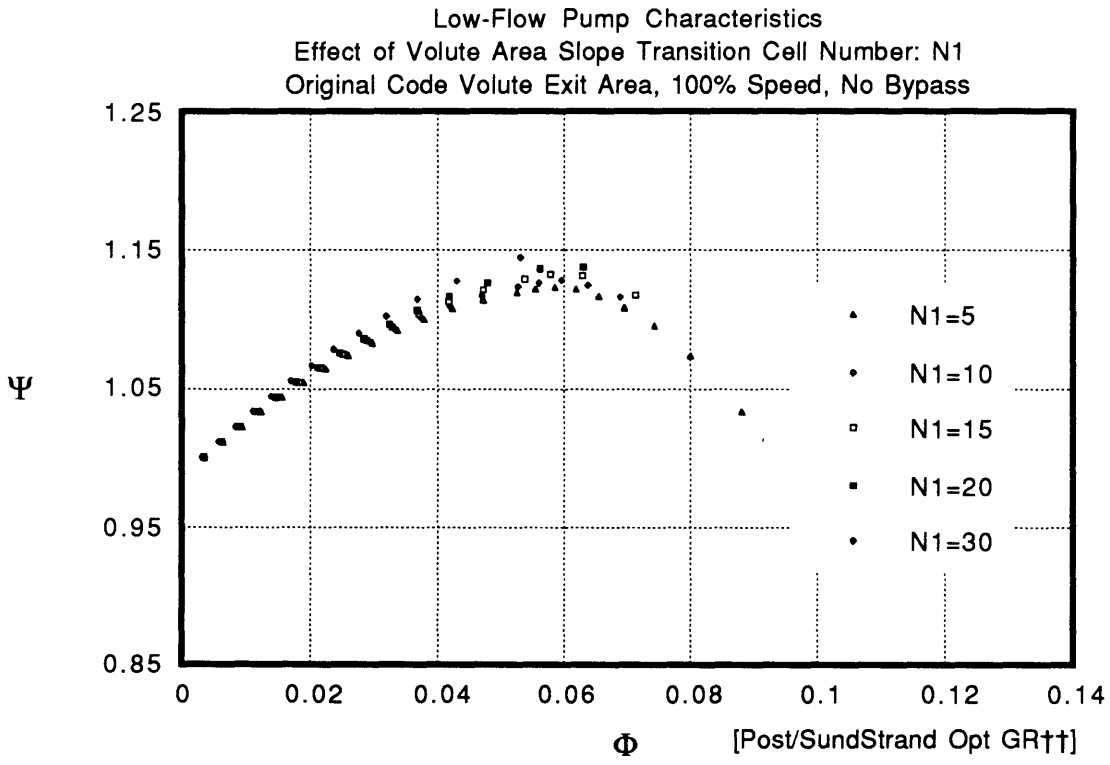
Low-Flow Pump Characteristics
Effect of Volute Area Slope Transition Cell Number: N1
Original Code Volute Exit Area, 100% Speed, No Bypass
1.25
1.15
1.05
0.95
0.85
Ψ
0
0.02
0.04
0.06
0.08
0.1
0.12
0.14
Φ
[Post/SundStrand Opt GR††]
N1=5
N1=10
N1=15
N1=20
N1=30

Fig.4.5.4

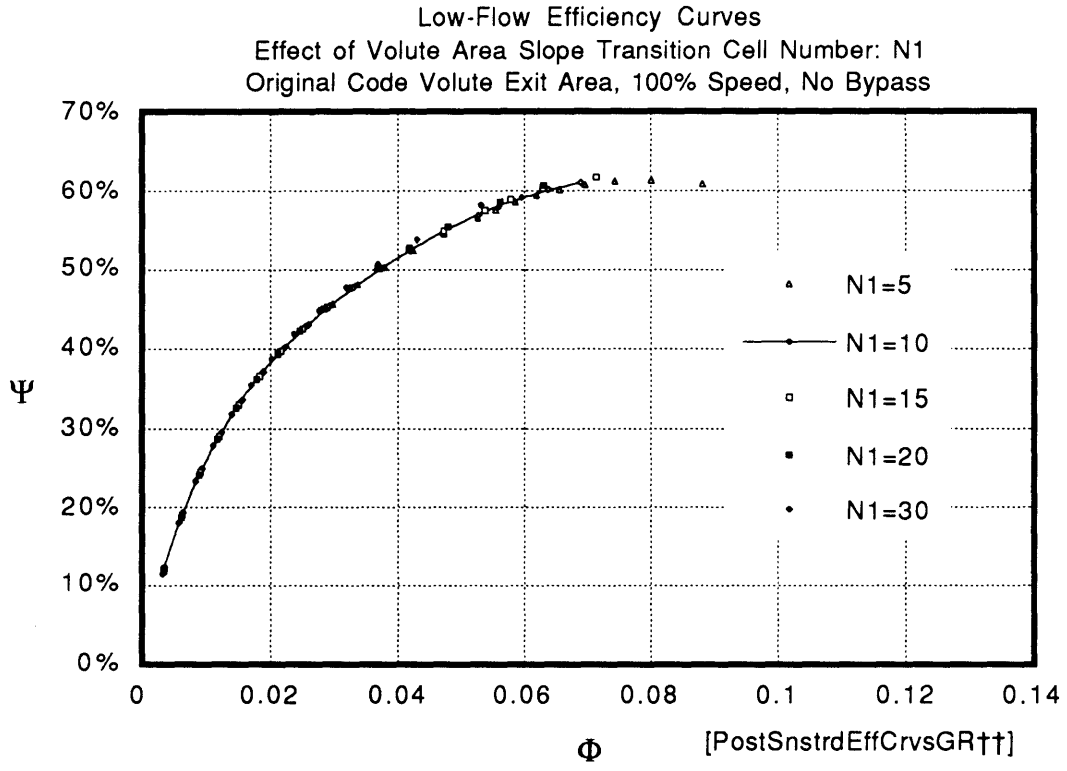
Low-Flow Efficiency Curves
Effect of Volute Area Slope Transition Cell Number: N1
Original Code Volute Exit Area, 100% Speed, No Bypass
70%
60%
50%
40%
30%
20%
10%
0%
Ψ
0
0.02
0.04
0.06
0.08
0.1
0.12
0.14
Φ
[PostSnstrdEffCrvsGR††]
N1=5
N1=10
N1=15
N1=20
N1=30

Fig.4.5.5

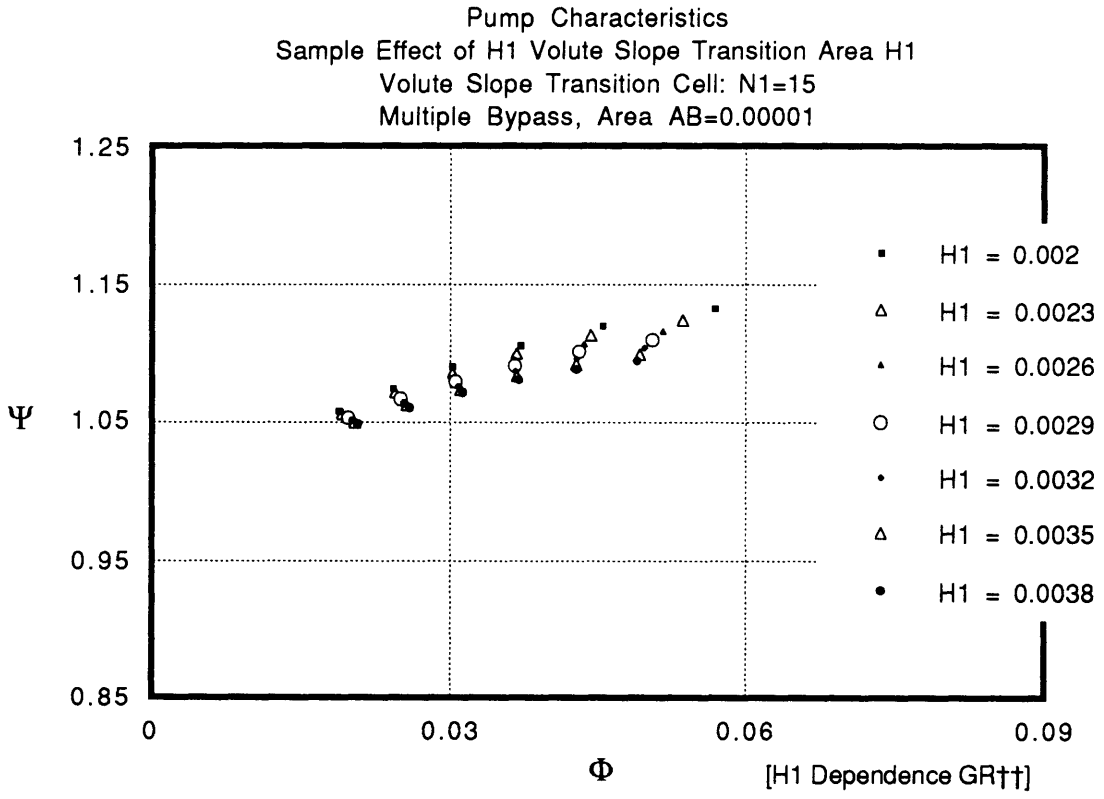
Pump Characteristics
Sample Effect of H1 Volute Slope Transition Area H1
Volute Slope Transition Cell: N1=15
Multiple Bypass, Area AB=0.00001
1.25
1.15
1.05
0.95
0.85
Ψ
0
0.03
0.06
0.09
Φ
[H1 Dependence GR†††]
H1 = 0.002
H1 = 0.0023
H1 = 0.0026
H1 = 0.0029
H1 = 0.0032
H1 = 0.0035
H1 = 0.0038

Fig.4.5.6

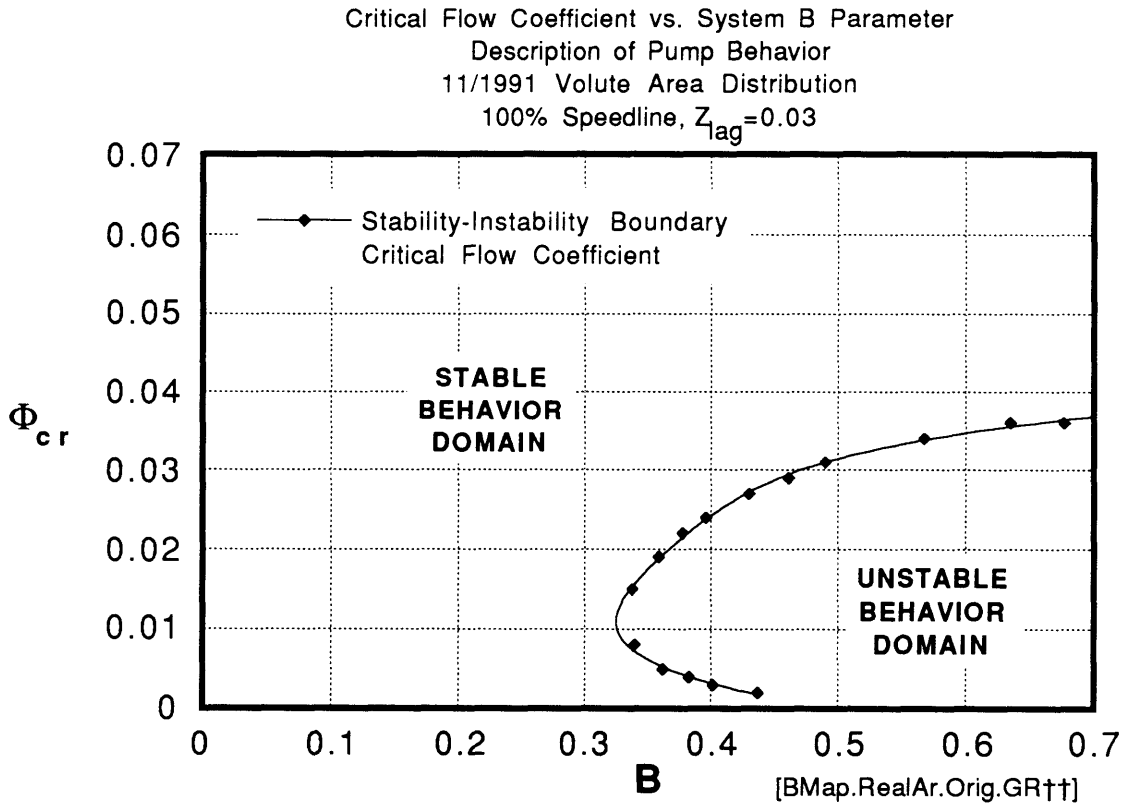
Critical Flow Coefficient vs. System B Parameter
Description of Pump Behavior
11/1991 Volute Area Distribution
100% Speedline, Z_{lag}=0.03
Stability-Instability Boundary
Critical Flow Coefficient
STABLE BEHAVIOR DOMAIN
UNSTABLE BEHAVIOR DOMAIN
Φ_{cr}
0.07
0.06
0.05
0.04
0.03
0.02
0.01
0
0
0.1
0.2
0.3
0.4
0.5
0.6
0.7
B
[BMap.RealAr.Orig.GR††]

Fig.5.1.1

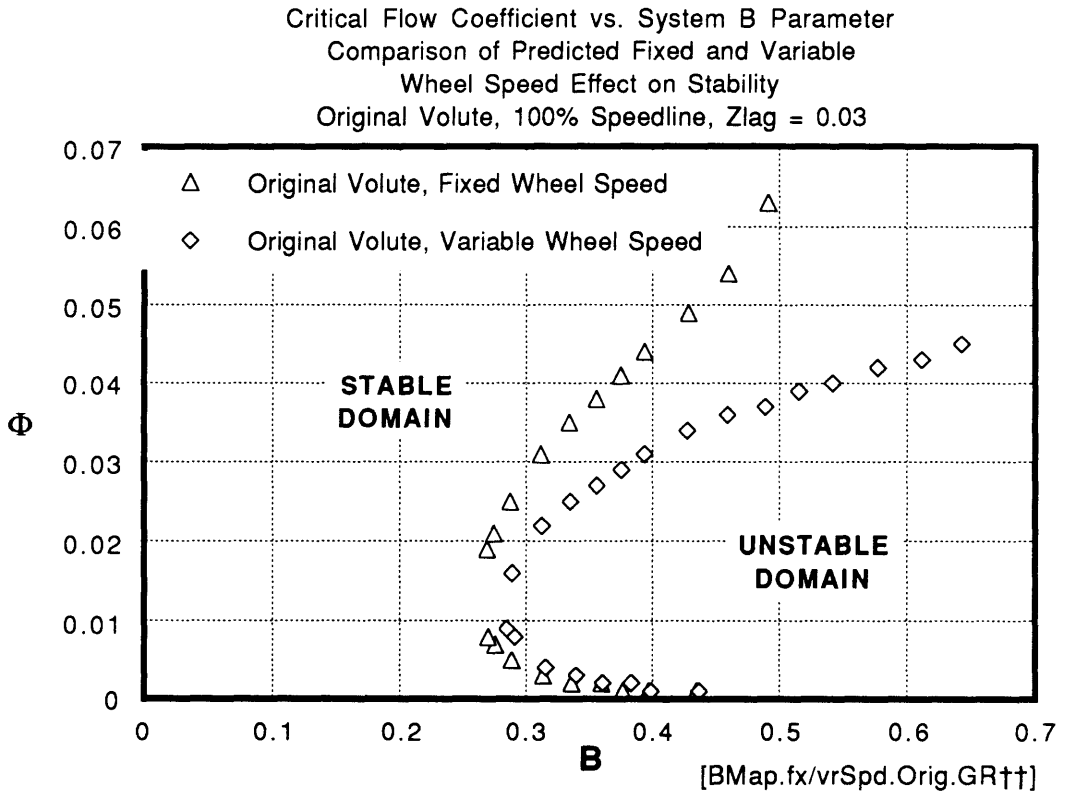
Critical Flow Coefficient vs. System B Parameter
Comparison of Predicted Fixed and Variable
Wheel Speed Effect on Stability
Original Volute, 100% Speedline, Zlag = 0.03
Original Volute, Fixed Wheel Speed
Original Volute, Variable Wheel Speed
STABLE DOMAIN
UNSTABLE DOMAIN
Φ
B
0.07
0.06
0.05
0.04
0.03
0.02
0.01
0
0
0.1
0.2
0.3
0.4
0.5
0.6
0.7
[BMap.fx/vrSpd.Orig.GR††]

Fig.5.1.2

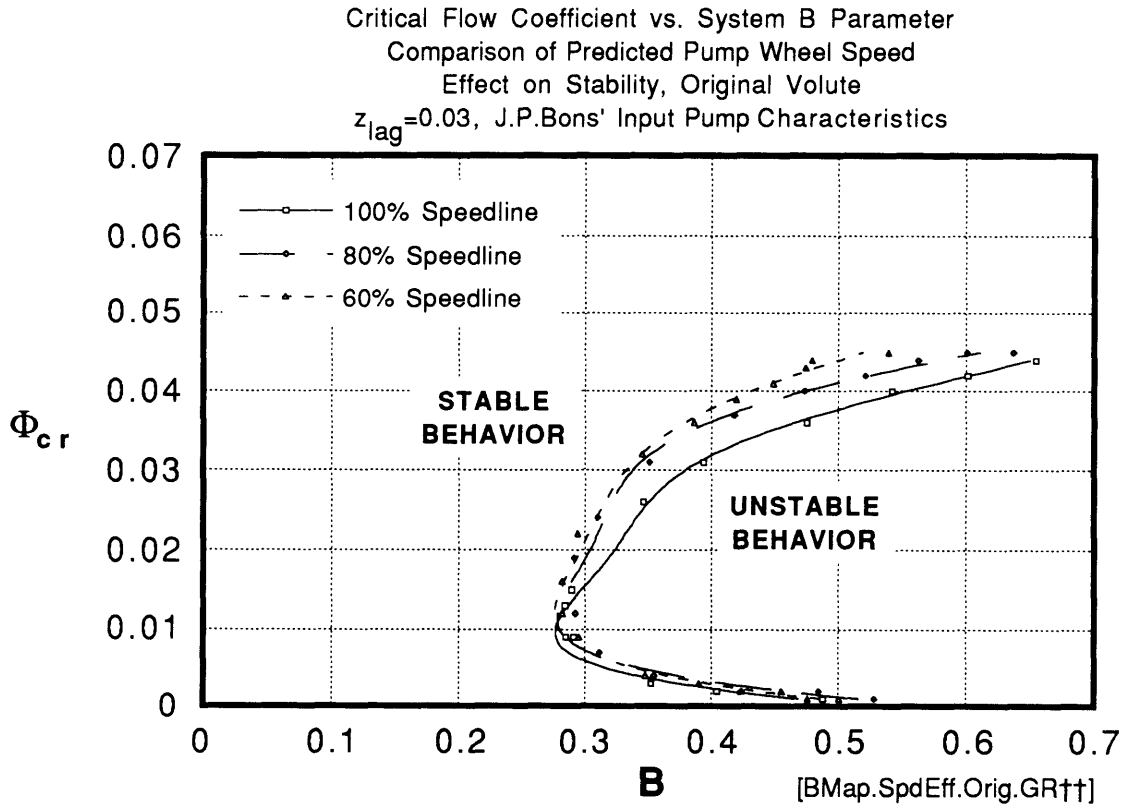
Critical Flow Coefficient vs. System B Parameter
Comparison of Predicted Pump Wheel Speed
Effect on Stability, Original Volute
z_{lag}=0.03, J.P.Bons' Input Pump Characteristics
100% Speedline
80% Speedline
60% Speedline
STABLE BEHAVIOR
UNSTABLE BEHAVIOR
Φ_{cr}
0.07
0.06
0.05
0.04
0.03
0.02
0.01
0
0
0.1
0.2
0.3
0.4
0.5
0.6
0.7
B
[BMap.SpdEff.Orig.GR†††]

Fig.5.1.3

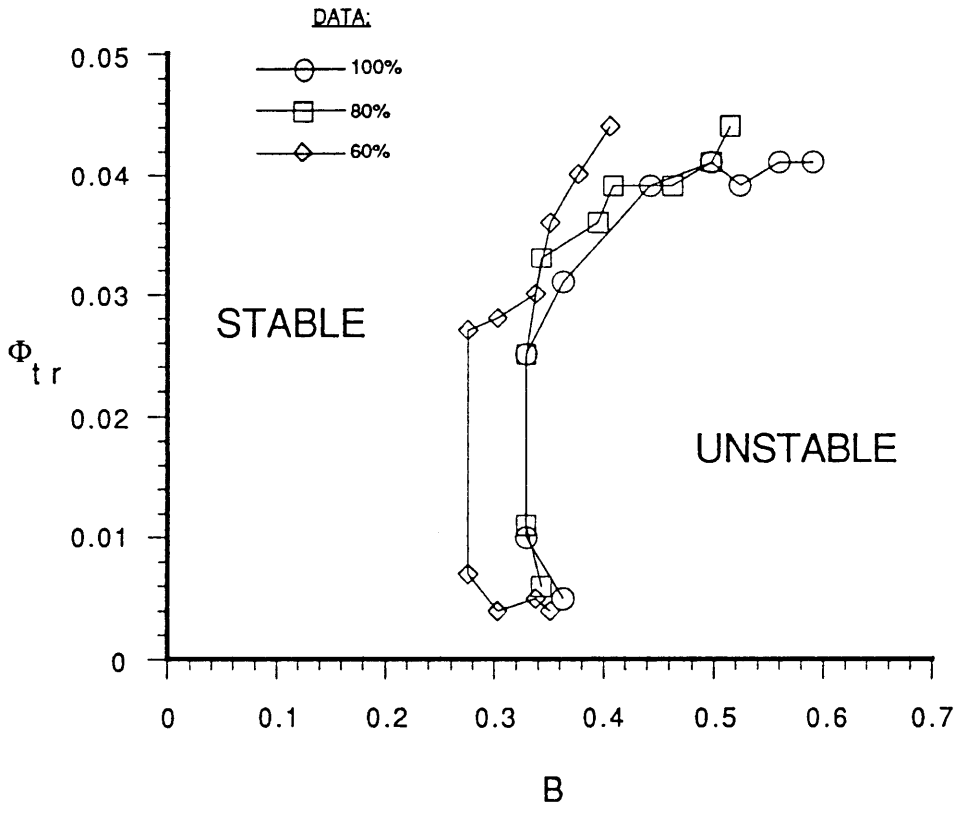

Fig.5.1.4

Critical Flow Coefficient vs. System B Parameter - Comparison of Measured Pump Wheel Speed Effect on Stability
(from Bons)

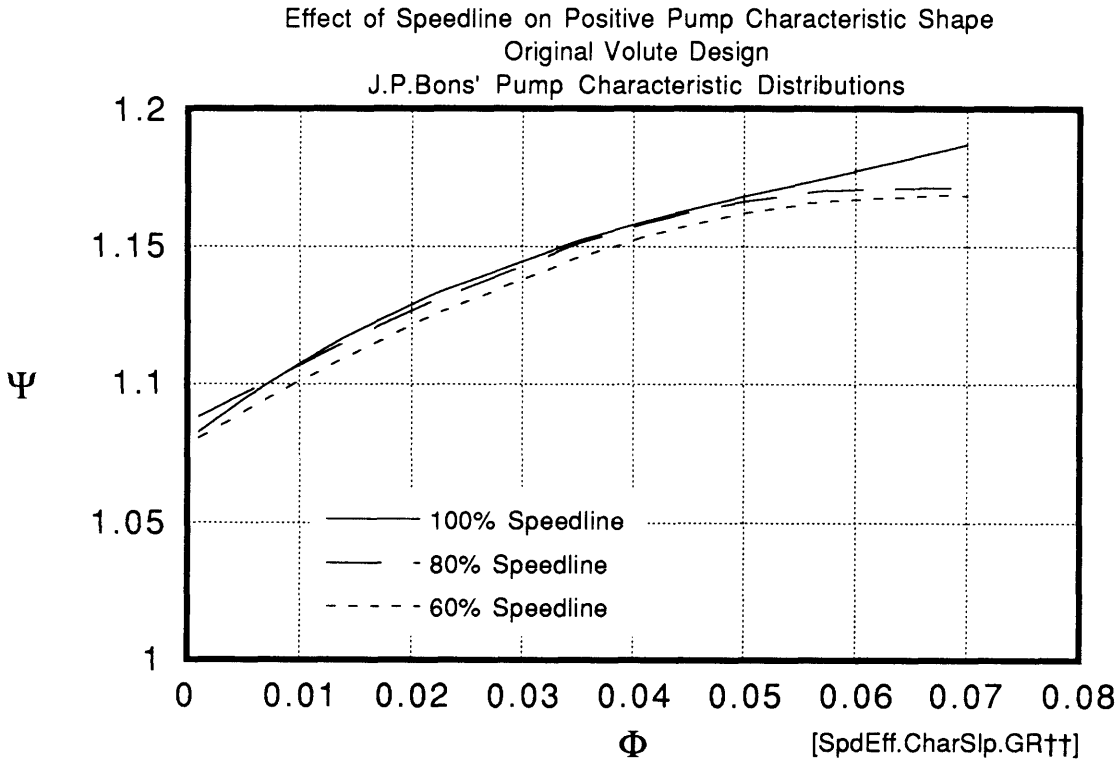
Effect of Speedline on Positive Pump Characteristic Shape
Original Volute Design
J.P.Bons' Pump Characteristic Distributions
1.2
1.15
1.1
1.05
1
Ψ
0
0.01
0.02
0.03
0.04
0.05
0.06
0.07
0.08
Φ
[SpdEff.CharSlp.GR††]
100% Speedline
80% Speedline
60% Speedline

Fig.5.1.5

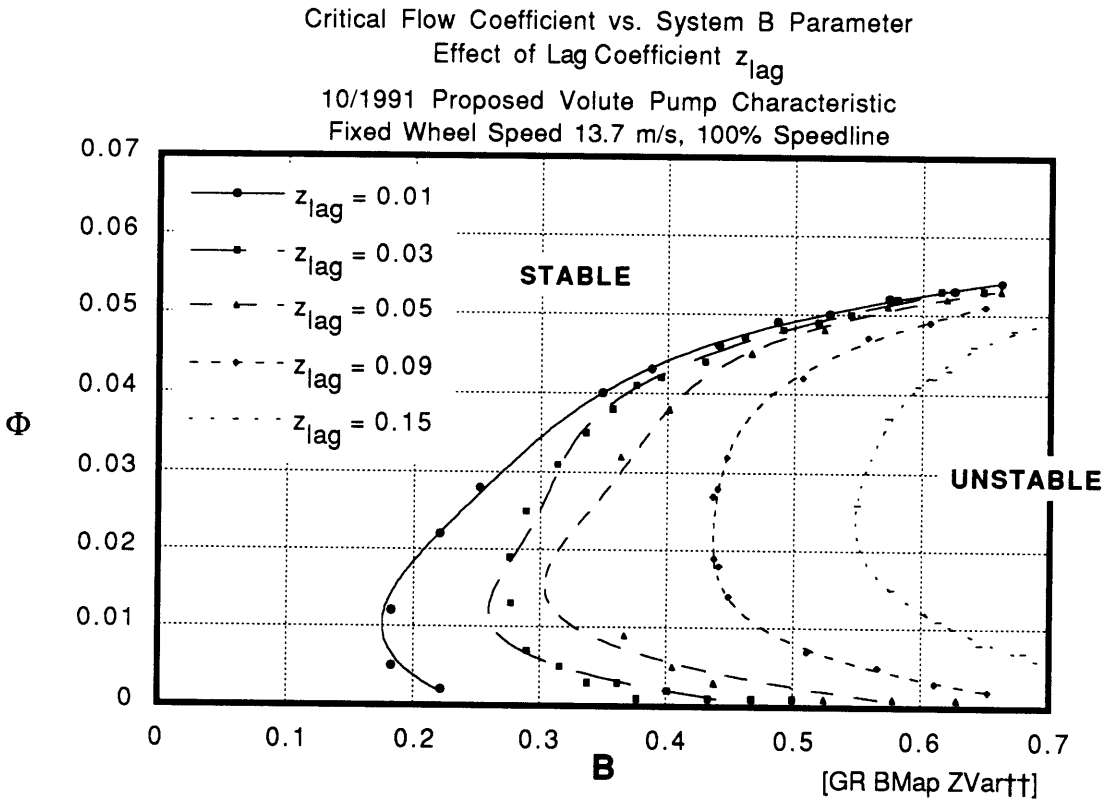
Critical Flow Coefficient vs. System B Parameter
Effect of Lag Coefficient z_{lag}
10/1991 Proposed Volute Pump Characteristic
Fixed Wheel Speed 13.7 m/s, 100% Speedline
z_{lag} = 0.01
z_{lag} = 0.03
z_{lag} = 0.05
z_{lag} = 0.09
z_{lag} = 0.15
STABLE
UNSTABLE
Φ
0.07
0.06
0.05
0.04
0.03
0.02
0.01
0
0
0.1
0.2
0.3
0.4
0.5
0.6
0.7
B
[GR BMap ZVar††]

Fig.5.1.6

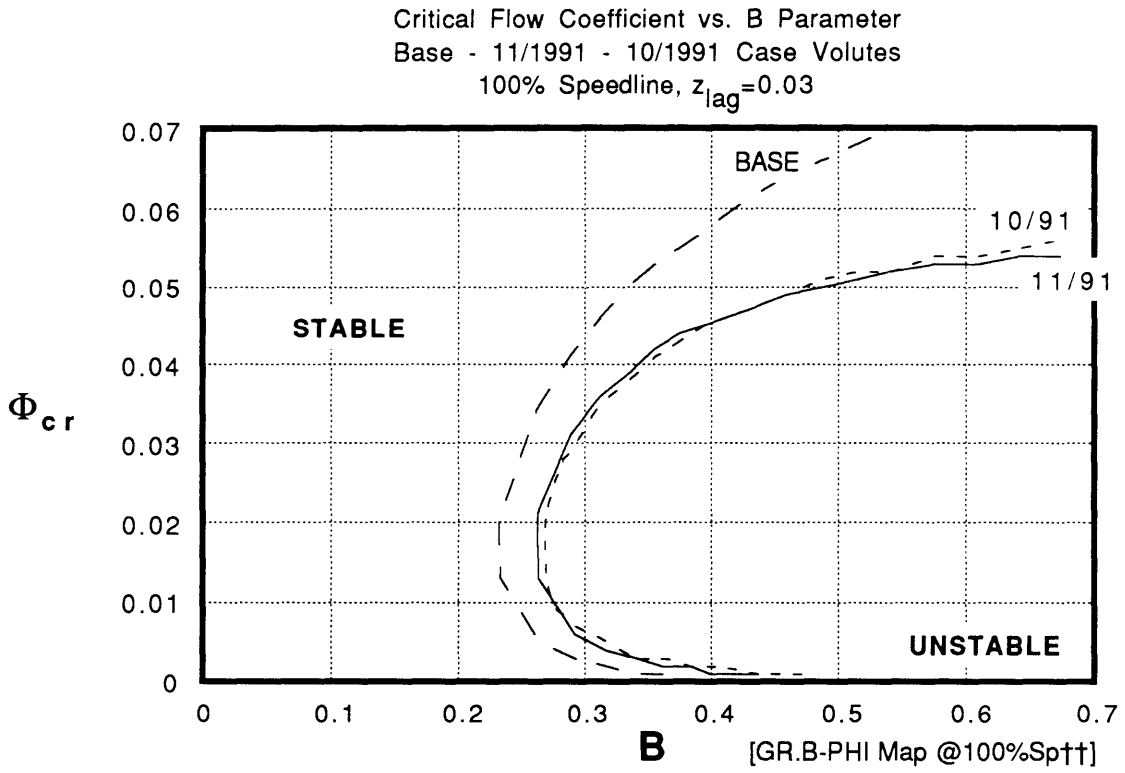
Critical Flow Coefficient vs. B Parameter
Base - 11/1991 - 10/1991 Case Volutes
100% Speedline, z_{lag}=0.03
BASE
10/91
11/91
STABLE
UNSTABLE
Φ_{cr}
0.07
0.06
0.05
0.04
0.03
0.02
0.01
0
0
0.1
0.2
0.3
0.4
0.5
0.6
0.7
B
[GR.B-PHI Map @100%Sp††]

Fig.5.3.1.i

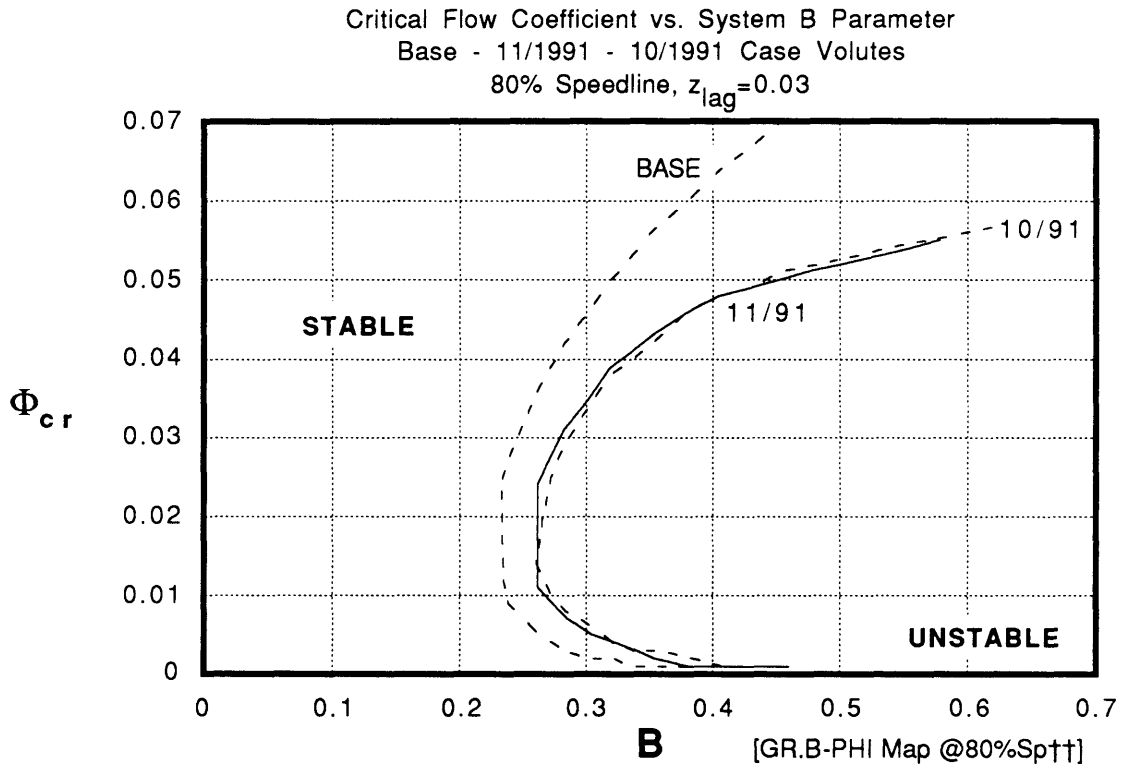
Critical Flow Coefficient vs. System B Parameter
Base - 11/1991 - 10/1991 Case Volutes
80% Speedline, z_{lag}=0.03
Φ_{cr}
0.07
0.06
0.05
0.04
0.03
0.02
0.01
0
BASE
10/91
11/91
STABLE
UNSTABLE
0
0.1
0.2
0.3
0.4
0.5
0.6
0.7
B
[GR.B-PHI Map @80%Sp††]

Fig.5.3.1.ii

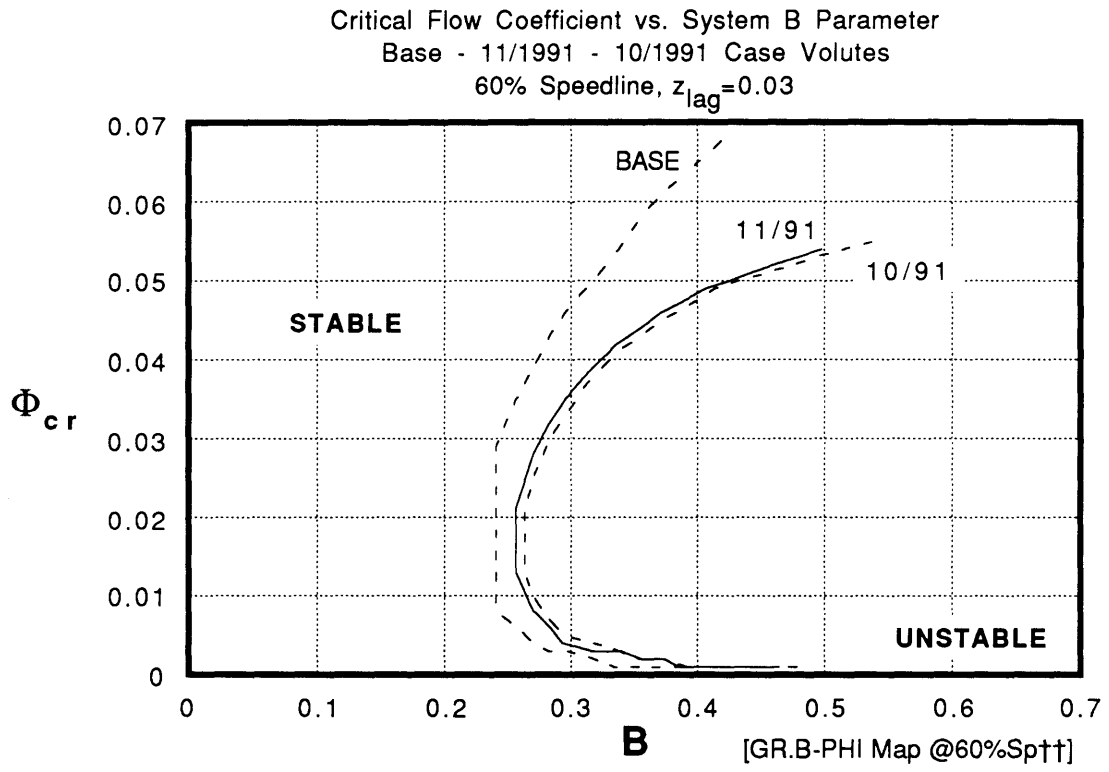
Critical Flow Coefficient vs. System B Parameter
Base - 11/1991 - 10/1991 Case Volutes
60% Speedline, z_{lag}=0.03
BASE
11/91
10/91
STABLE
UNSTABLE
Φ_{cr}
0.07
0.06
0.05
0.04
0.03
0.02
0.01
0
0
0.1
0.2
0.3
0.4
0.5
0.6
0.7
B
[GR.B-PHI Map @60%Sp††]

Fig.5.3.1.iii

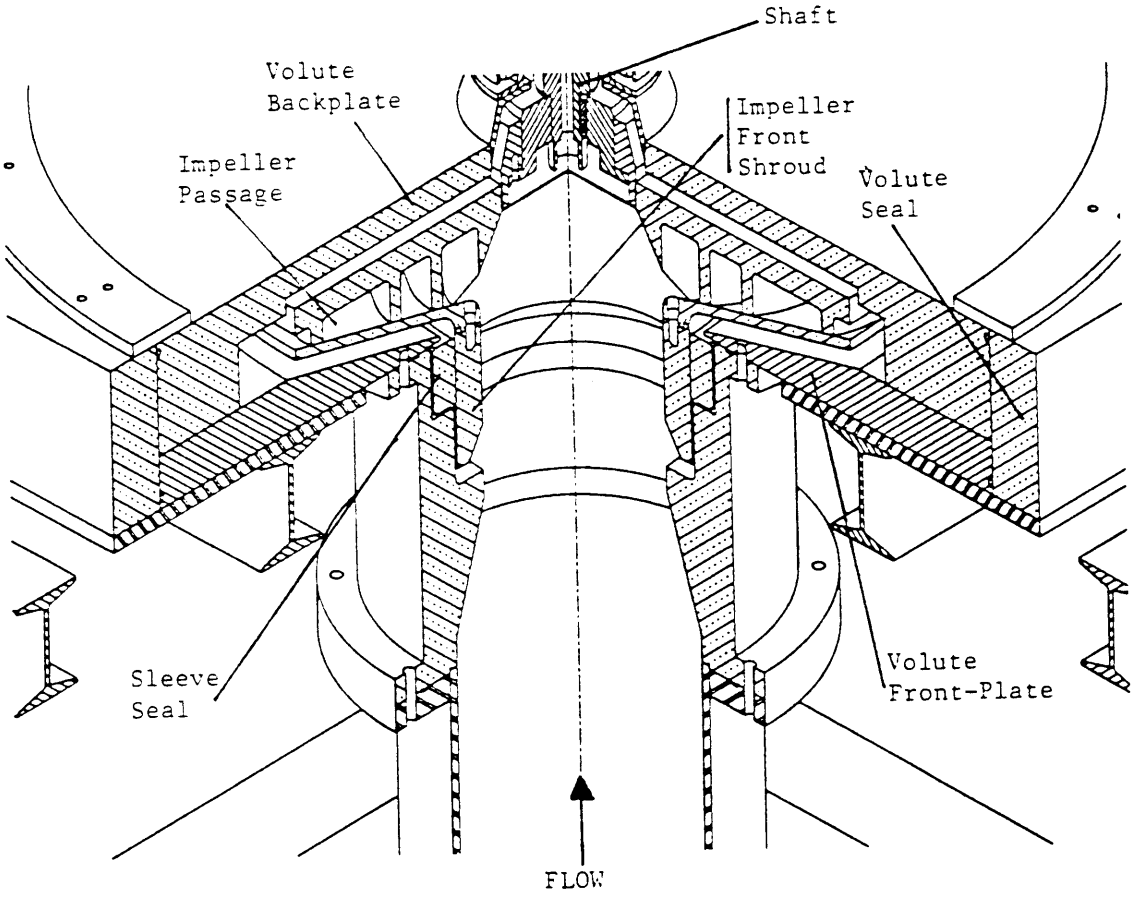

Fig.6.1.1 Volute Backplate, Front Plate and Seal Arrangement (from Goulet)

Modified Volute Pressure Tap Locations

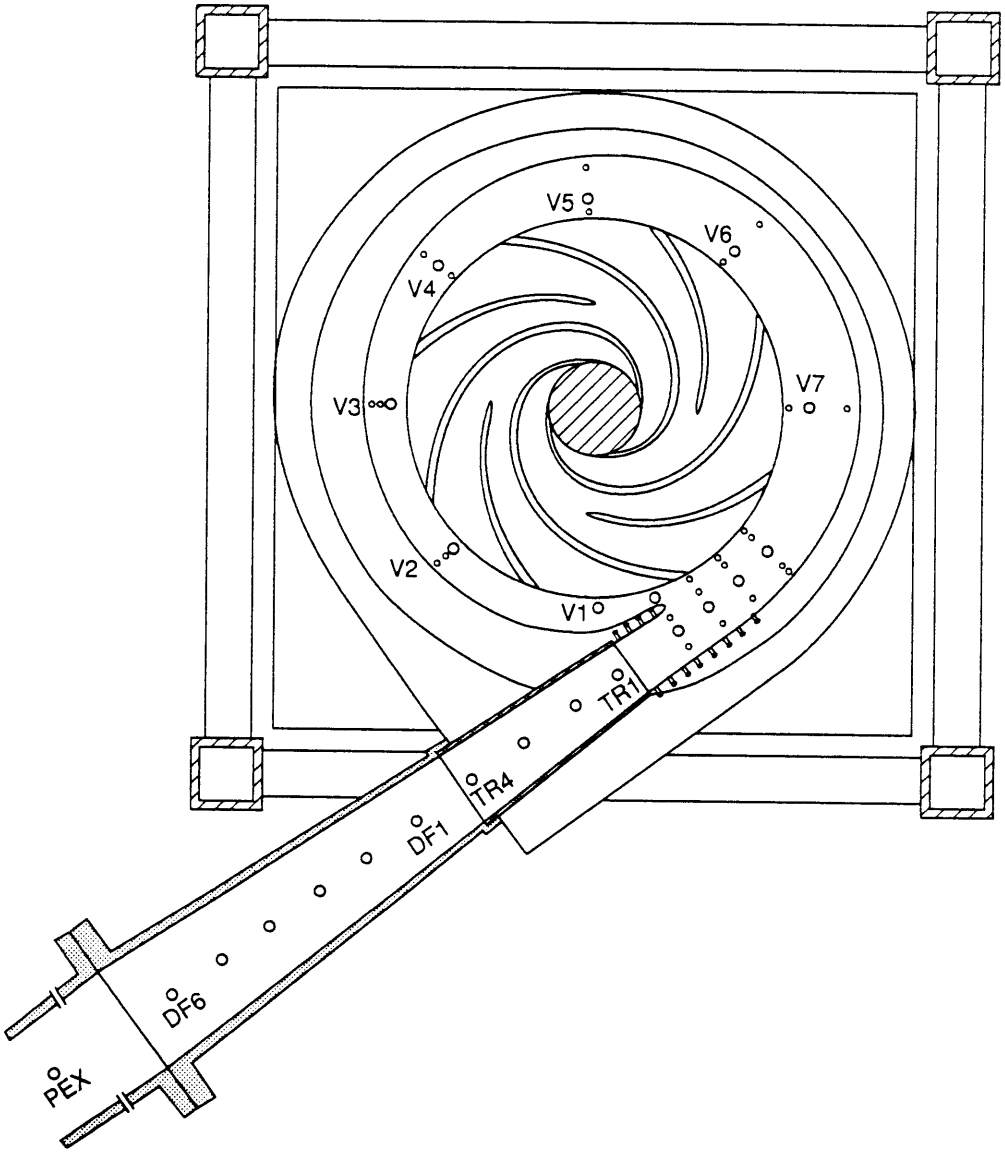

Fig.6.1.2

FIG. 6.1.B

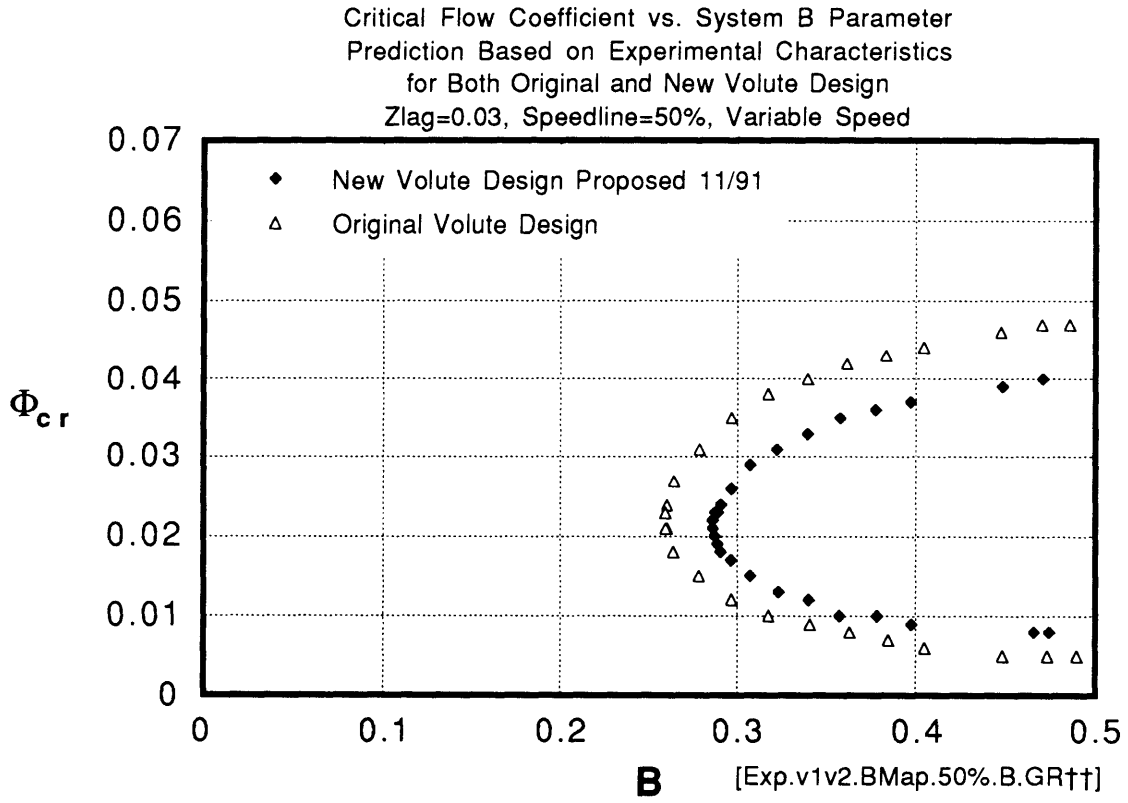
Critical Flow Coefficient vs. System B Parameter
Prediction Based on Experimental Characteristics
for Both Original and New Volute Design
Zlag=0.03, Speedline=50%, Variable Speed
New Volute Design Proposed 11/91
Original Volute Design
Φ_{cr}
0.07
0.06
0.05
0.04
0.03
0.02
0.01
0
0
0.1
0.2
0.3
0.4
0.5
B
[Exp.v1v2.BMap.50%.B.GR††]

Fig.6.3.1

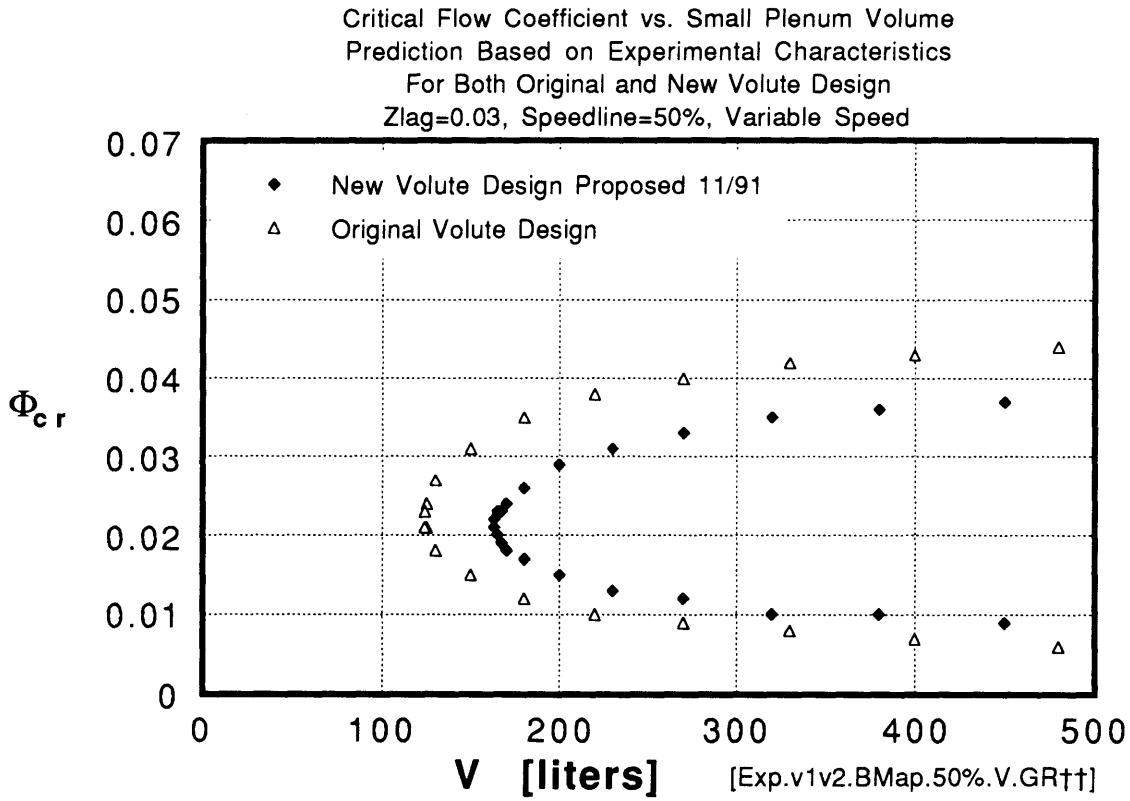
Critical Flow Coefficient vs. Small Plenum Volume
Prediction Based on Experimental Characteristics
For Both Original and New Volute Design
Zlag=0.03, Speedline=50%, Variable Speed
New Volute Design Proposed 11/91
Original Volute Design
Φcr
0.07
0.06
0.05
0.04
0.03
0.02
0.01
0
0
100
200
300
400
500
V [liters]
[Exp.v1v2.BMap.50%.V.GR††]

Fig.6.3.2

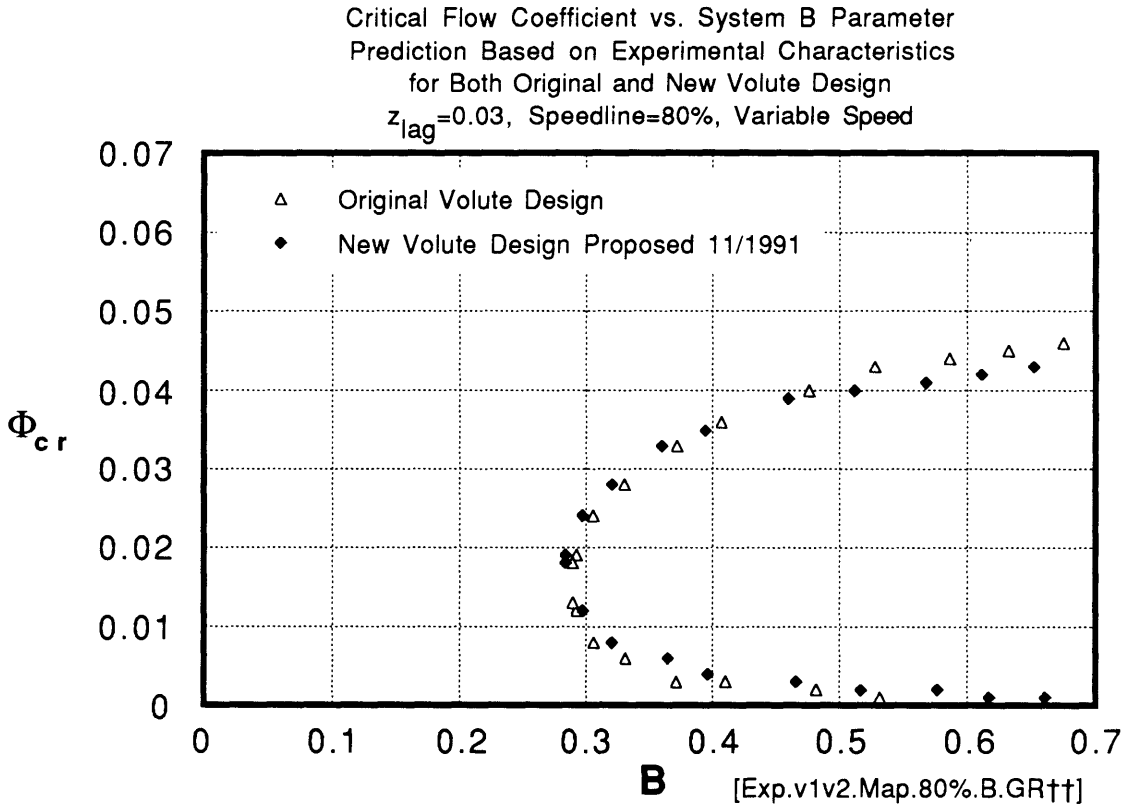
Critical Flow Coefficient vs. System B Parameter
Prediction Based on Experimental Characteristics
for Both Original and New Volute Design
z_{lag}=0.03, Speedline=80%, Variable Speed
Original Volute Design
New Volute Design Proposed 11/1991
Φ_{cr}
0.07
0.06
0.05
0.04
0.03
0.02
0.01
0
0
0.1
0.2
0.3
0.4
0.5
0.6
0.7
B
[Exp.v1v2.Map.80%.B.GR††]

Fig.6.3.3

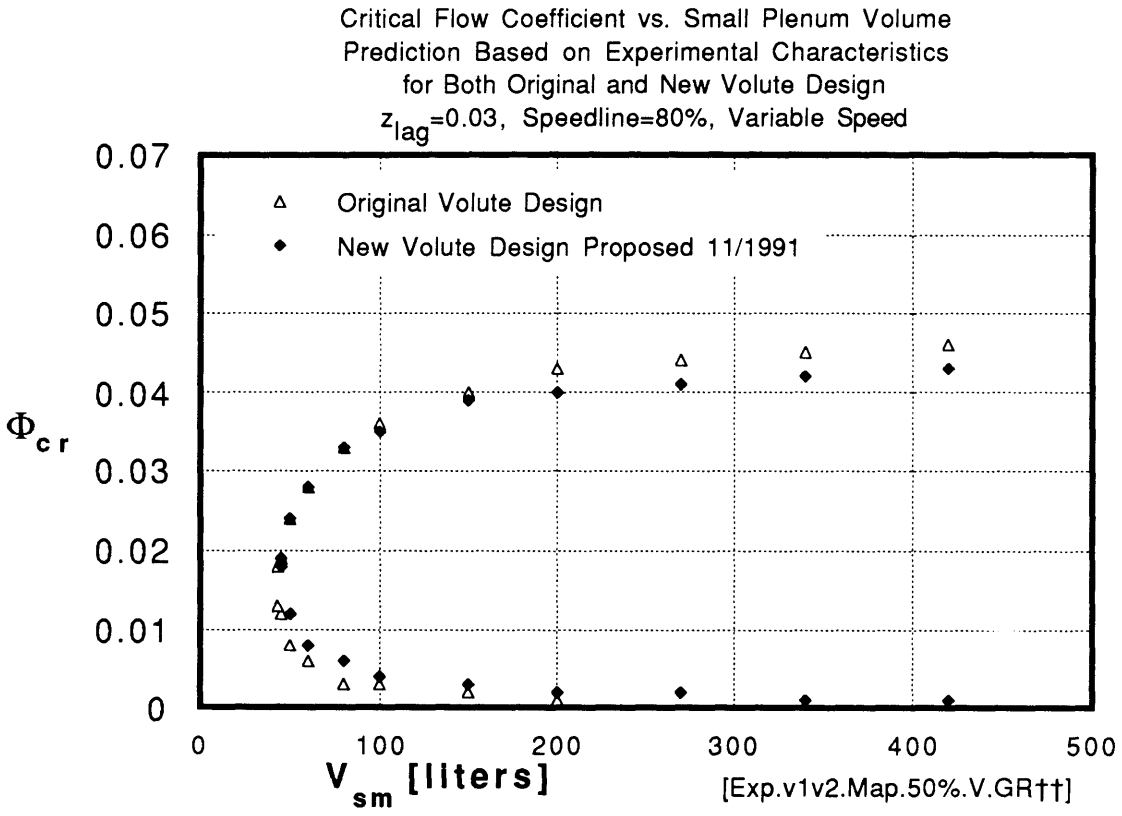
Critical Flow Coefficient vs. Small Plenum Volume
Prediction Based on Experimental Characteristics
for Both Original and New Volute Design
z_{lag}=0.03, Speedline=80%, Variable Speed
Original Volute Design
New Volute Design Proposed 11/1991
Φ_{cr}
0.07
0.06
0.05
0.04
0.03
0.02
0.01
0
0
100
200
300
400
500
V_{sm} [liters]
[Exp.v1v2.Map.50%.V.GR††]

Fig.6.3.4

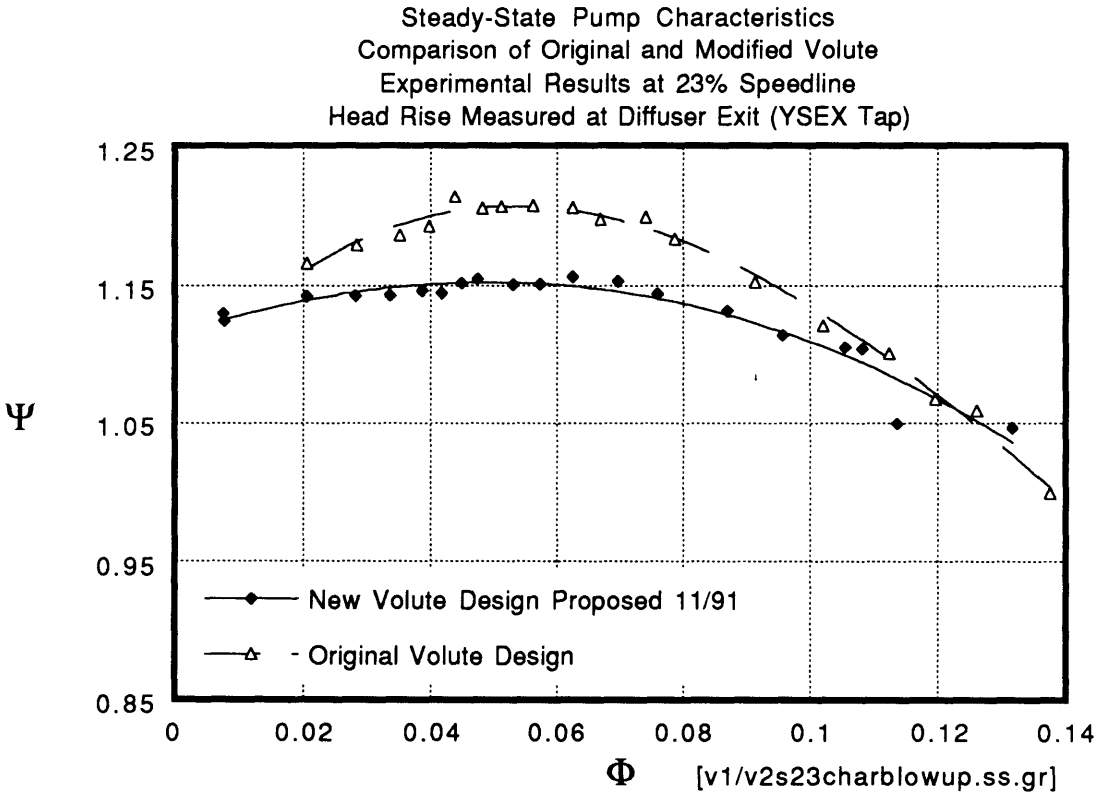
Steady-State Pump Characteristics
Comparison of Original and Modified Volute
Experimental Results at 23% Speedline
Head Rise Measured at Diffuser Exit (YSEX Tap)
Ψ
1.25
1.15
1.05
0.95
0.85
0
0.02
0.04
0.06
0.08
0.1
0.12
0.14
Φ
New Volute Design Proposed 11/91
- Original Volute Design
[v1/v2s23charblowup.ss.gr]

Fig.6.3.5.i

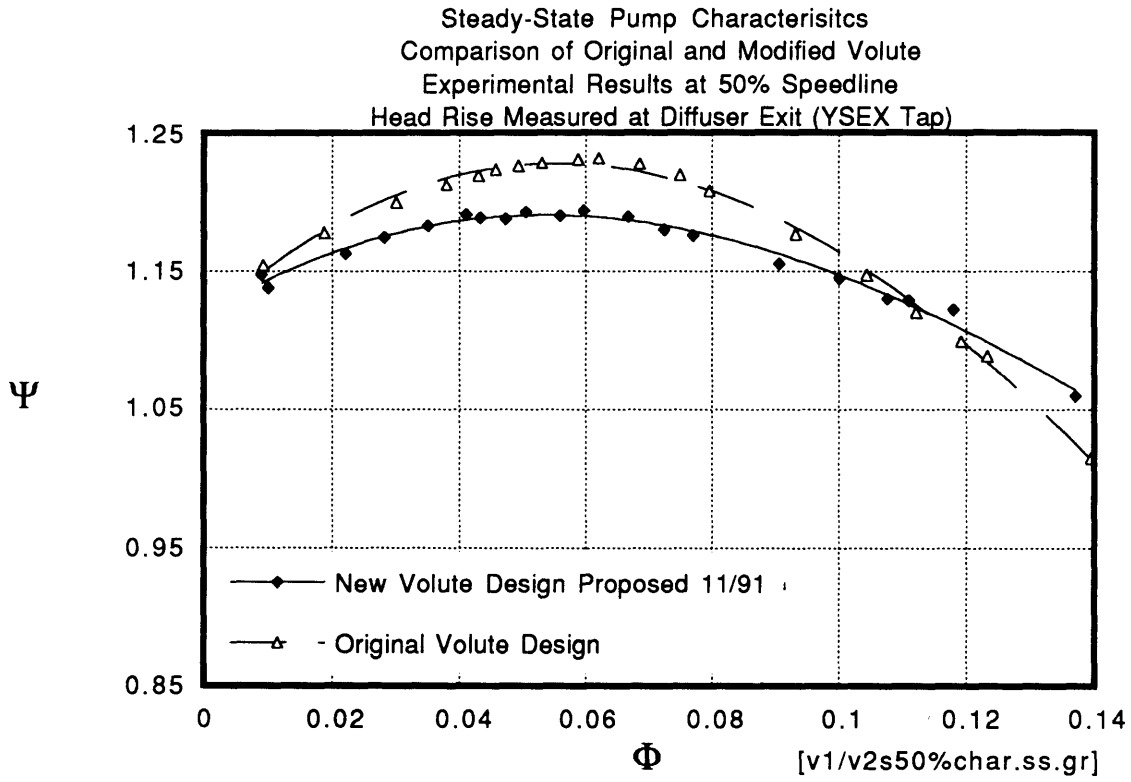
Steady-State Pump Characterisitcs
Comparison of Original and Modified Volute
Experimental Results at 50% Speedline
Head Rise Measured at Diffuser Exit (YSEX Tap)
Ψ
1.25
1.15
1.05
0.95
0.85
0
0.02
0.04
0.06
0.08
0.1
0.12
0.14
Φ
New Volute Design Proposed 11/91
- Original Volute Design
[v1/v2s50%char.ss.gr]

Fig.6.3.5.ii

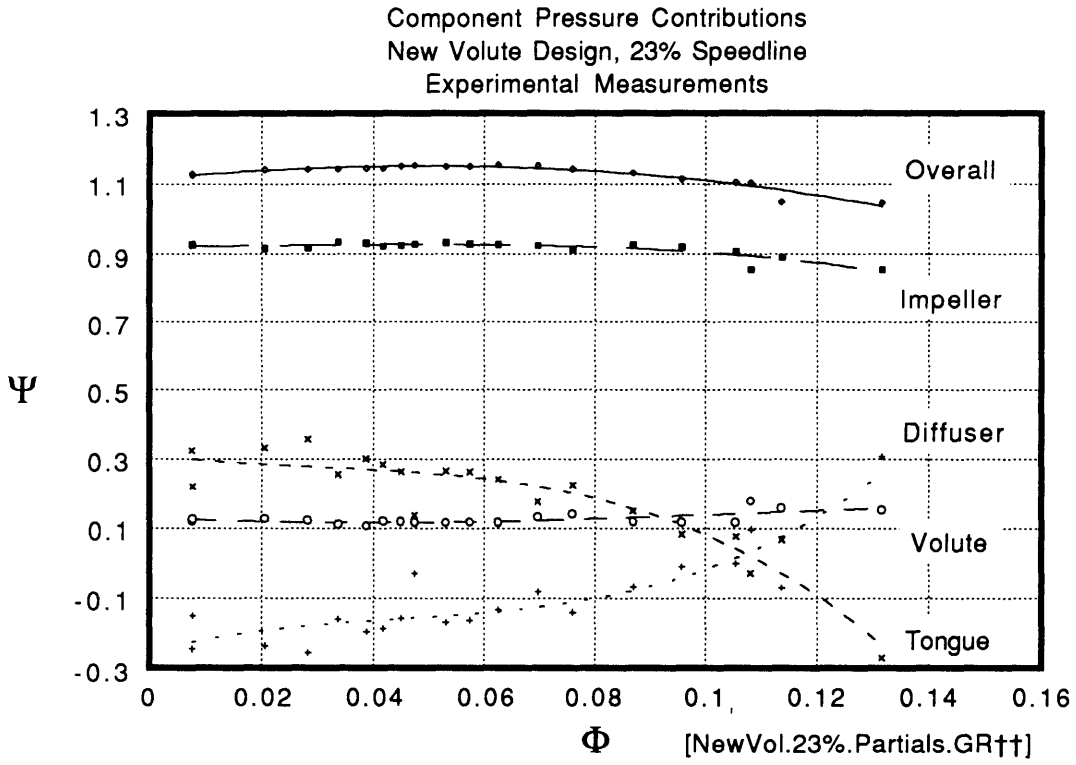
Component Pressure Contributions
New Volute Design, 23% Speedline
Experimental Measurements
1.3
1.1
0.9
0.7
0.5
0.3
0.1
-0.1
-0.3
Ψ
Overall
Impeller
Diffuser
Volute
Tongue
0
0.02
0.04
0.06
0.08
0.1
0.12
0.14
0.16
Φ
[NewVol.23%.Partials.GR††]

Fig.6.3.6

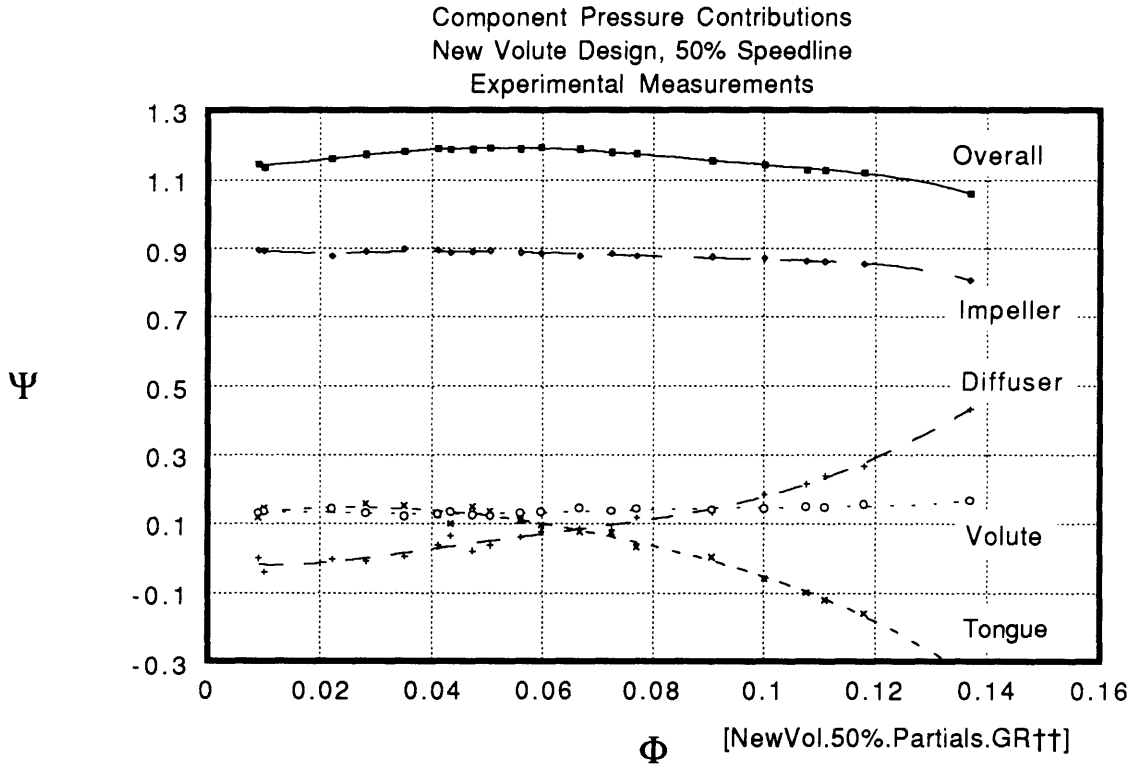
Component Pressure Contributions
New Volute Design, 50% Speedline
Experimental Measurements
1.3
1.1
0.9
0.7
0.5
0.3
0.1
-0.1
-0.3
Ψ
Overall
Impeller
Diffuser
Volute
Tongue
0
0.02
0.04
0.06
0.08
0.1
0.12
0.14
0.16
Φ
[NewVol.50%.Partials.GR†††]

Fig.6.3.7

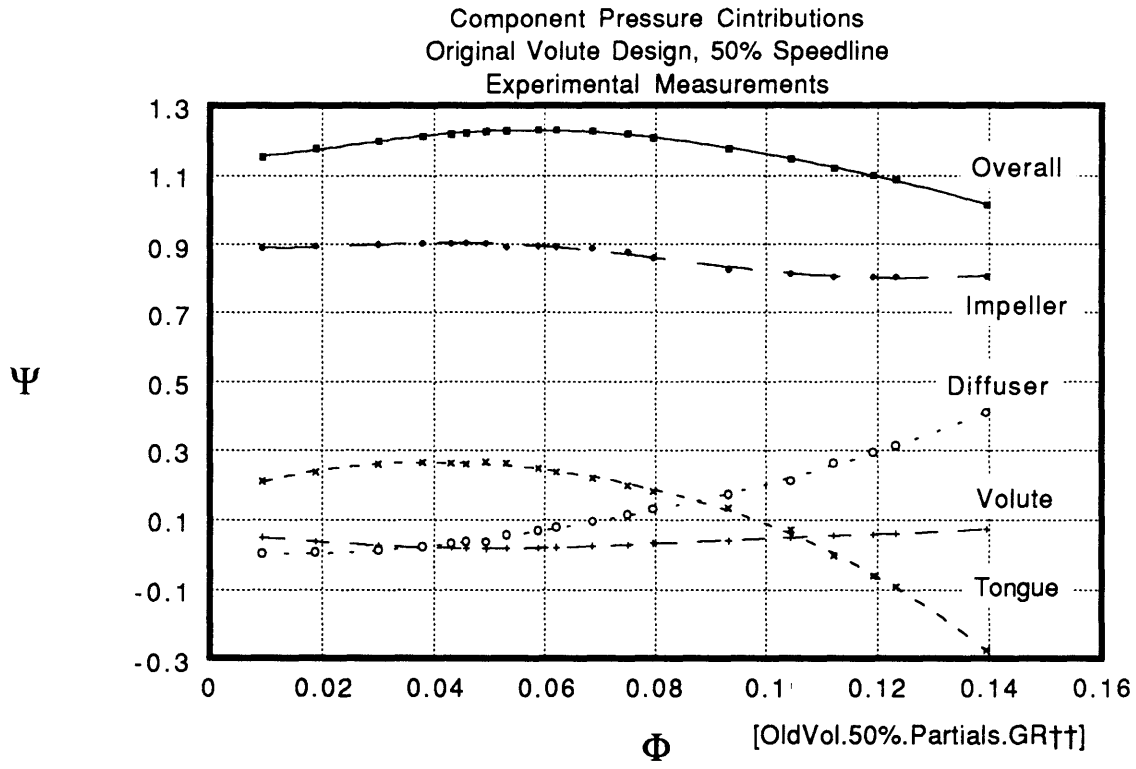
Component Pressure Cintributions
Original Volute Design, 50% Speedline
Experimental Measurements
1.3
1.1
0.9
0.7
0.5
0.3
0.1
-0.1
-0.3
Ψ
Overall
Impeller
Diffuser
Volute
Tongue
0
0.02
0.04
0.06
0.08
0.1
0.12
0.14
0.16
Φ
[OldVol.50%.Partials.GR††]

Fig.6.3.8

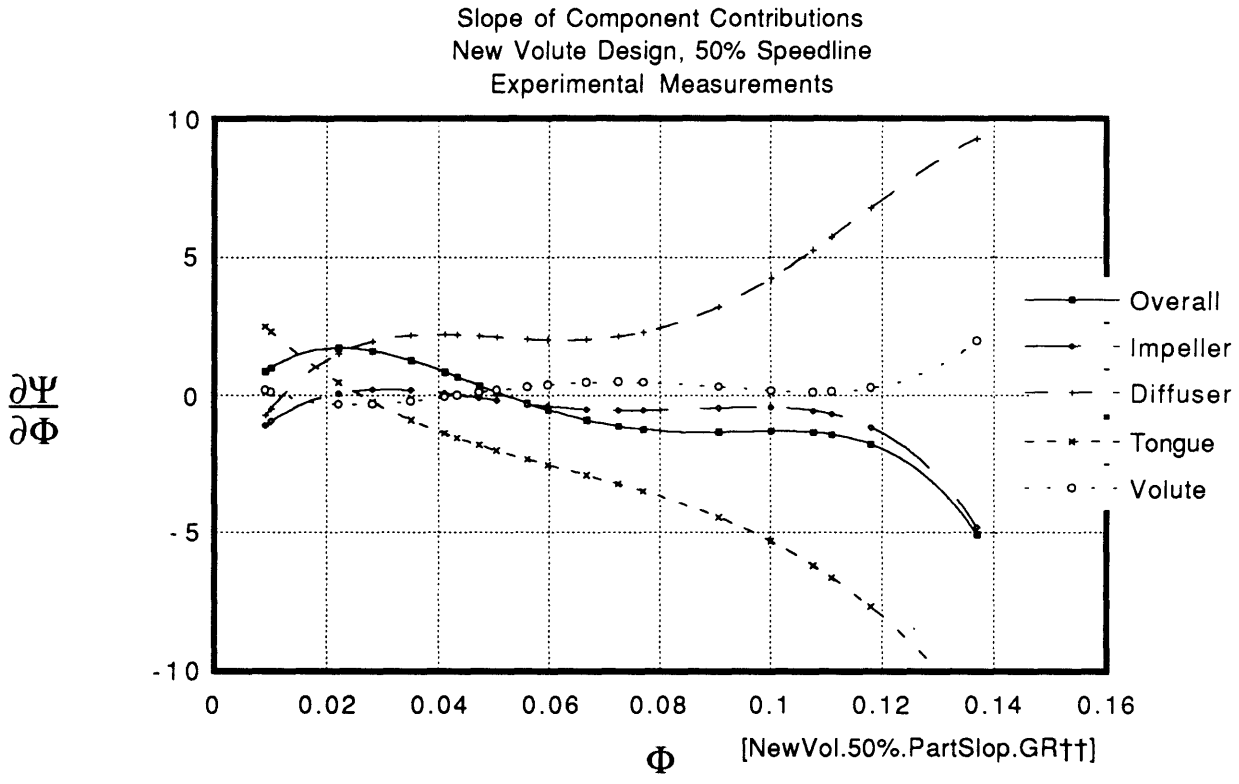
Slope of Component Contributions
New Volute Design, 50% Speedline
Experimental Measurements
10
5
0
-5
-10
0
0.02
0.04
0.06
0.08
0.1
0.12
0.14
0.16
Φ
[NewVol.50%.PartSlop.GR††]
∂Ψ/∂Φ
Overall
Impeller
Diffuser
Tongue
Volute

Fig.6.3.9

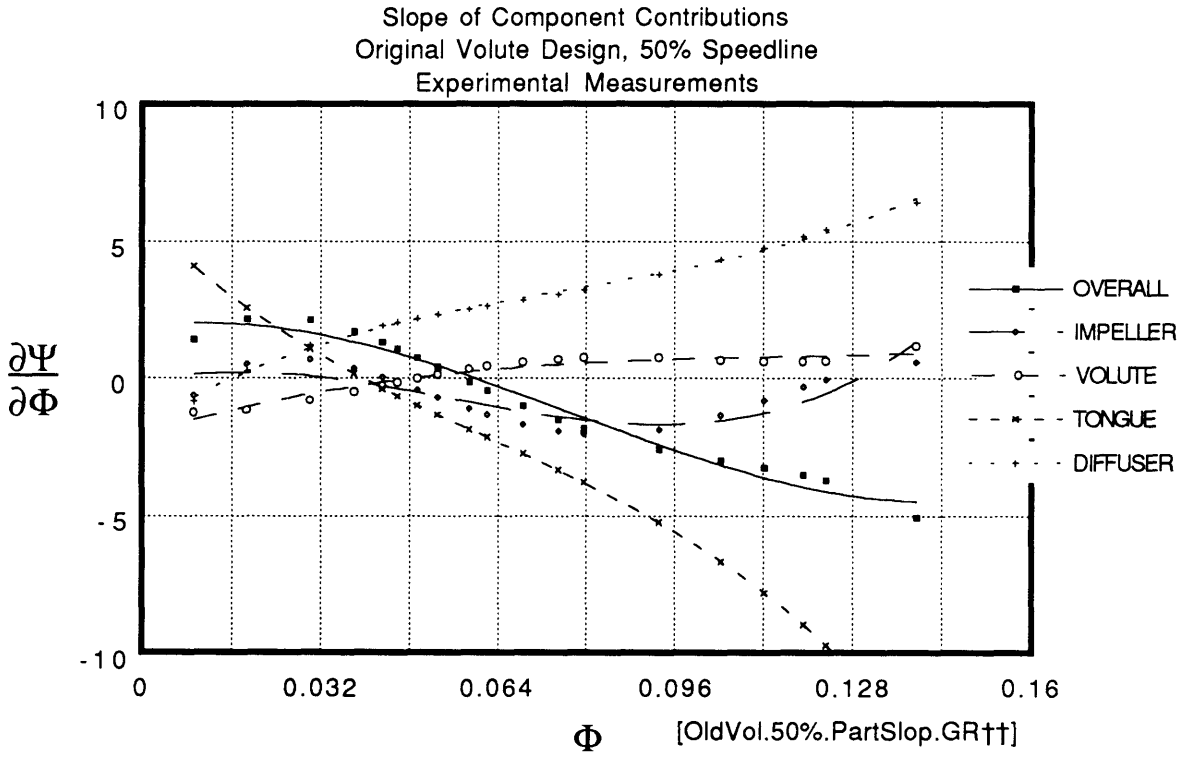
Slope of Component Contributions
Original Volute Design, 50% Speedline
Experimental Measurements
10
5
0
-5
-10
0
0.032
0.064
0.096
0.128
0.16
∂Ψ/∂Φ
Φ
[OldVol.50%.PartSlop.GR††]
OVERALL
IMPELLER
VOLUTE
TONGUE
DIFFUSER

Fig.6.3.10

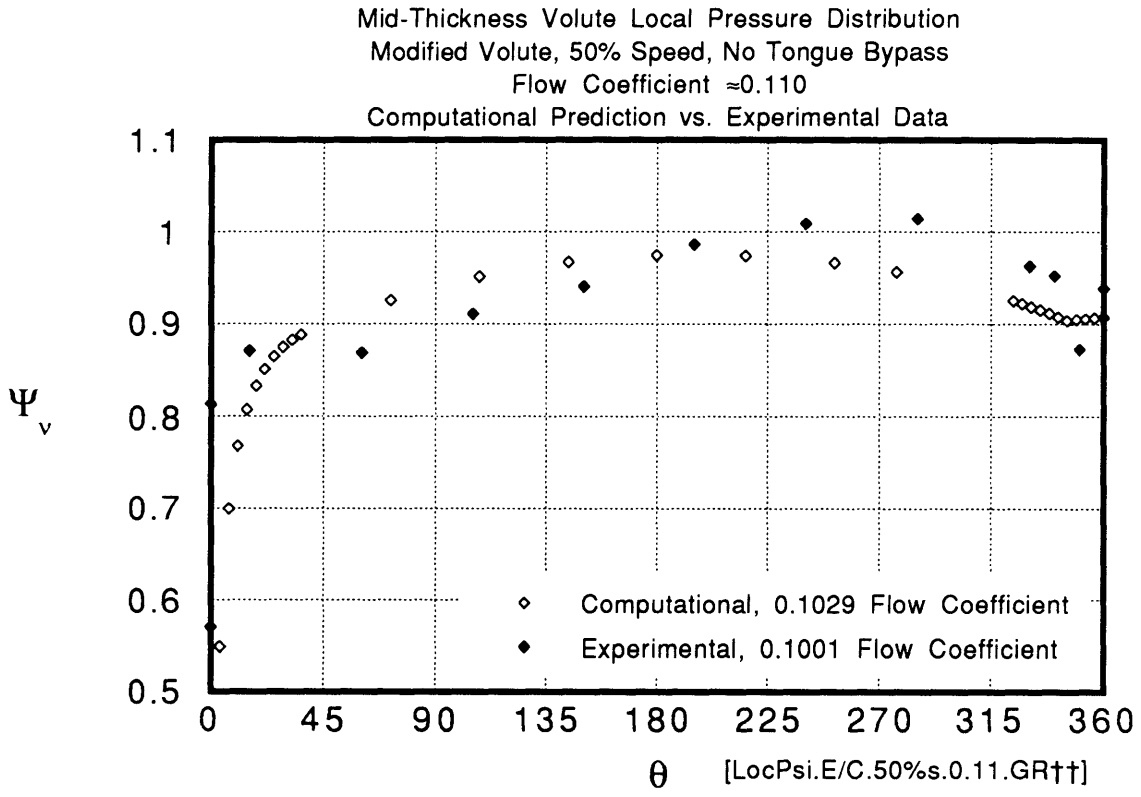
Mid-Thickness Volute Local Pressure Distribution
Modified Volute, 50% Speed, No Tongue Bypass
Flow Coefficient ≈0.110
Computational Prediction vs. Experimental Data
1.1
1
0.9
0.8
0.7
0.6
0.5
Ψν
0
45
90
135
180
225
270
315
360
θ
[LocPsi.E/C.50%s.0.11.GR††]
Computational, 0.1029 Flow Coefficient
Experimental, 0.1001 Flow Coefficient

Fig.6.3.11

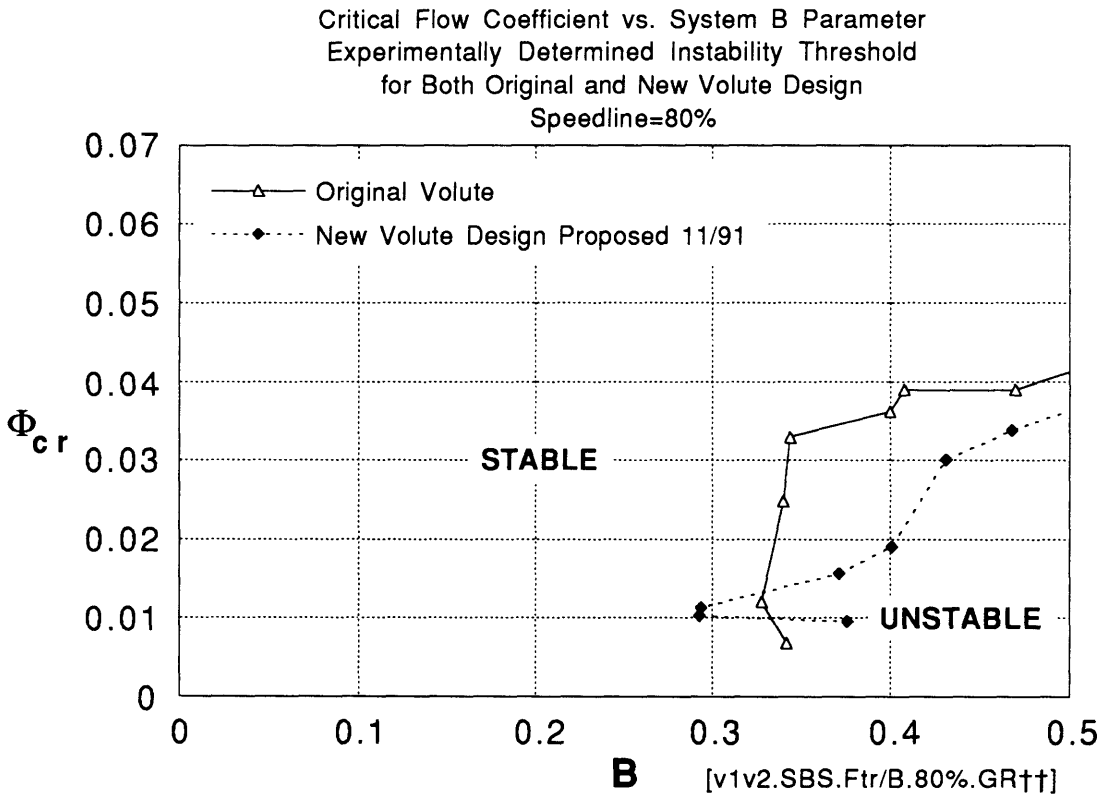
Critical Flow Coefficient vs. System B Parameter
Experimentally Determined Instability Threshold
for Both Original and New Volute Design
Speedline=80%
Original Volute
New Volute Design Proposed 11/91
STABLE
UNSTABLE
Φcr
0.07
0.06
0.05
0.04
0.03
0.02
0.01
0
0
0.1
0.2
0.3
0.4
0.5
B
[v1v2.SBS.Ftr/B.80%.GR††]

Fig.6.3.12

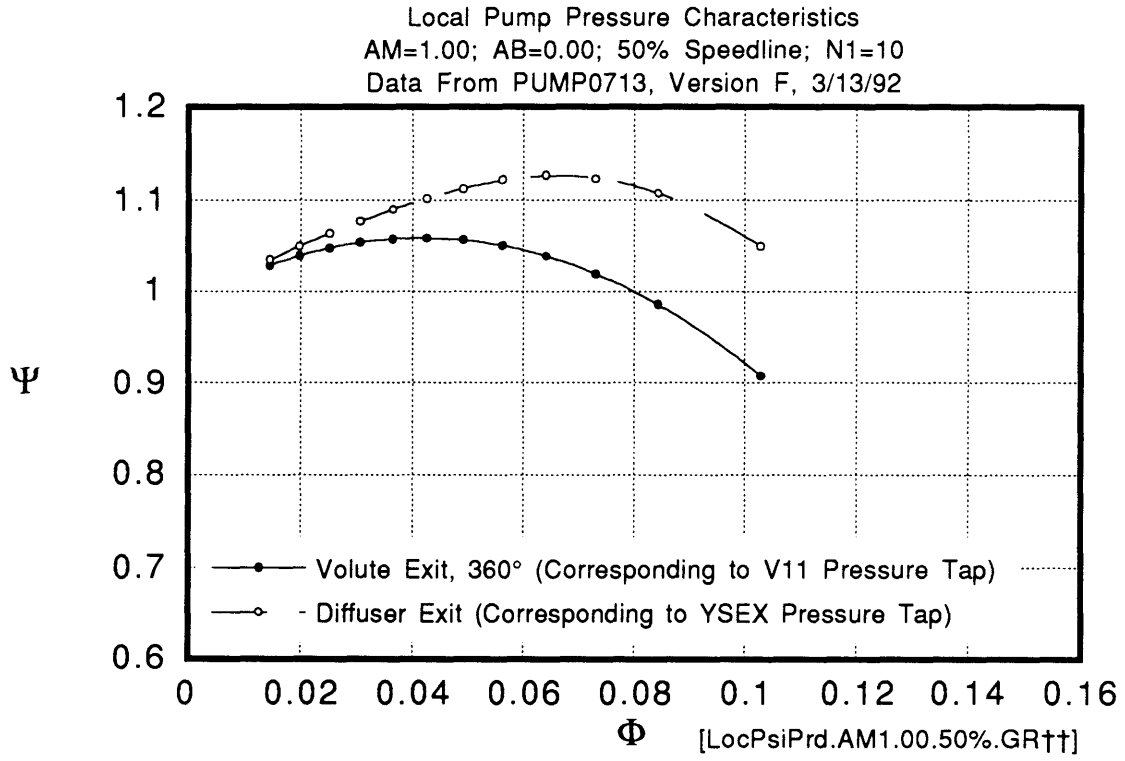
Local Pump Pressure Characteristics
AM=1.00; AB=0.00; 50% Speedline; N1=10
Data From PUMP0713, Version F, 3/13/92
Ψ
1.2
1.1
1
0.9
0.8
0.7
0.6
0
0.02
0.04
0.06
0.08
0.1
0.12
0.14
0.16
Φ
[LocPsiPrd.AM1.00.50%.GR††]
Volute Exit, 360° (Corresponding to V11 Pressure Tap)
Diffuser Exit (Corresponding to YSEX Pressure Tap)

Fig.7.3.1

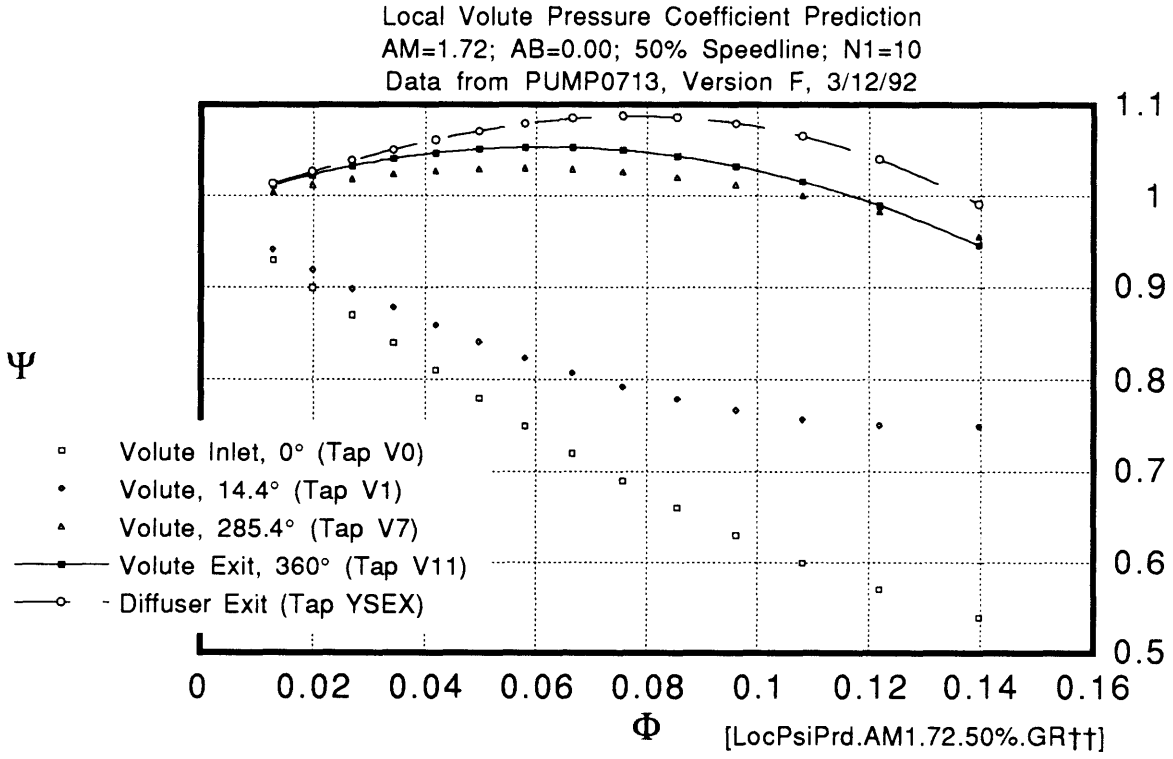
Local Volute Pressure Coefficient Prediction
AM=1.72; AB=0.00; 50% Speedline; N1=10
Data from PUMP0713, Version F, 3/12/92
Ψ
1.1
1
0.9
0.8
0.7
0.6
0.5
Volute Inlet, 0° (Tap V0)
Volute, 14.4° (Tap V1)
Volute, 285.4° (Tap V7)
Volute Exit, 360° (Tap V11)
Diffuser Exit (Tap YSEX)
0
0.02
0.04
0.06
0.08
0.1
0.12
0.14
0.16
Φ
[LocPsiPrd.AM1.72.50%.GR††]

Fig.7.3.2

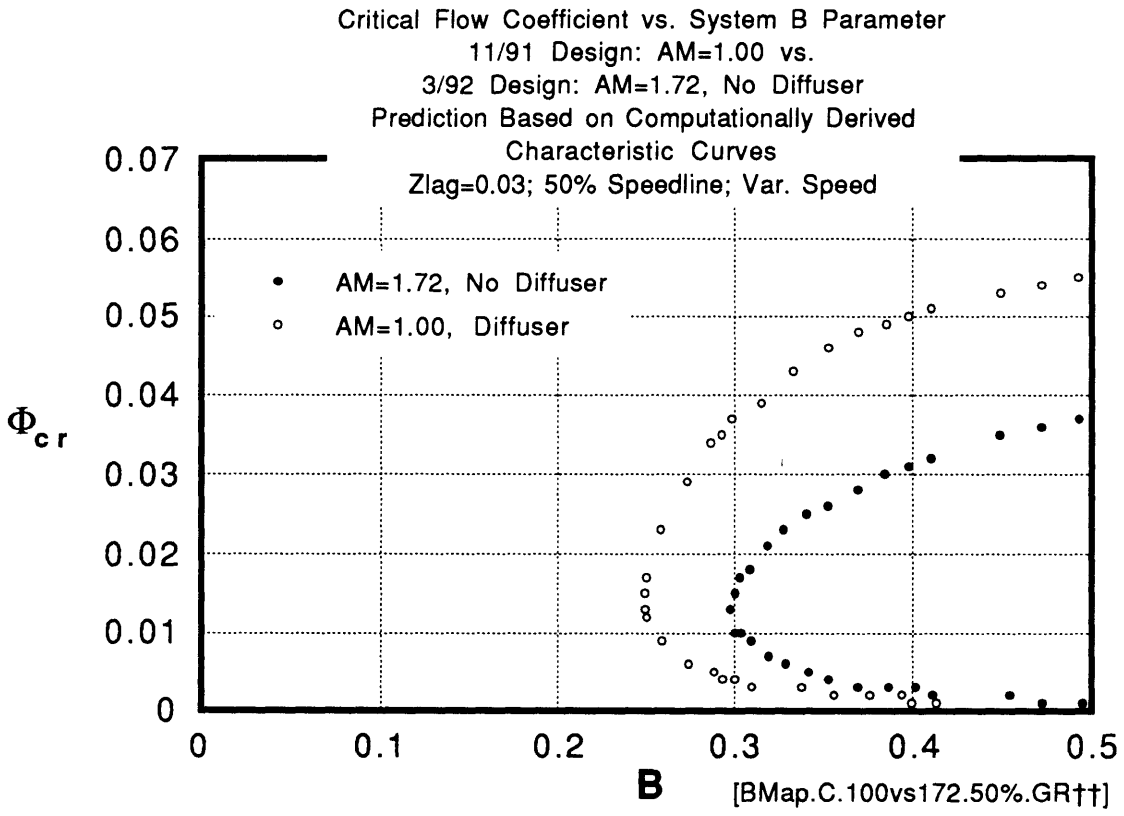
Critical Flow Coefficient vs. System B Parameter
11/91 Design: AM=1.00 vs.
3/92 Design: AM=1.72, No Diffuser
Prediction Based on Computationally Derived
Characteristic Curves
Zlag=0.03; 50% Speedline; Var. Speed
AM=1.72, No Diffuser
AM=1.00, Diffuser
Φ_{cr}
0.07
0.06
0.05
0.04
0.03
0.02
0.01
0
0
0.1
0.2
0.3
0.4
0.5
B
[BMap.C.100vs172.50%.GR††]

Fig.7.3.3

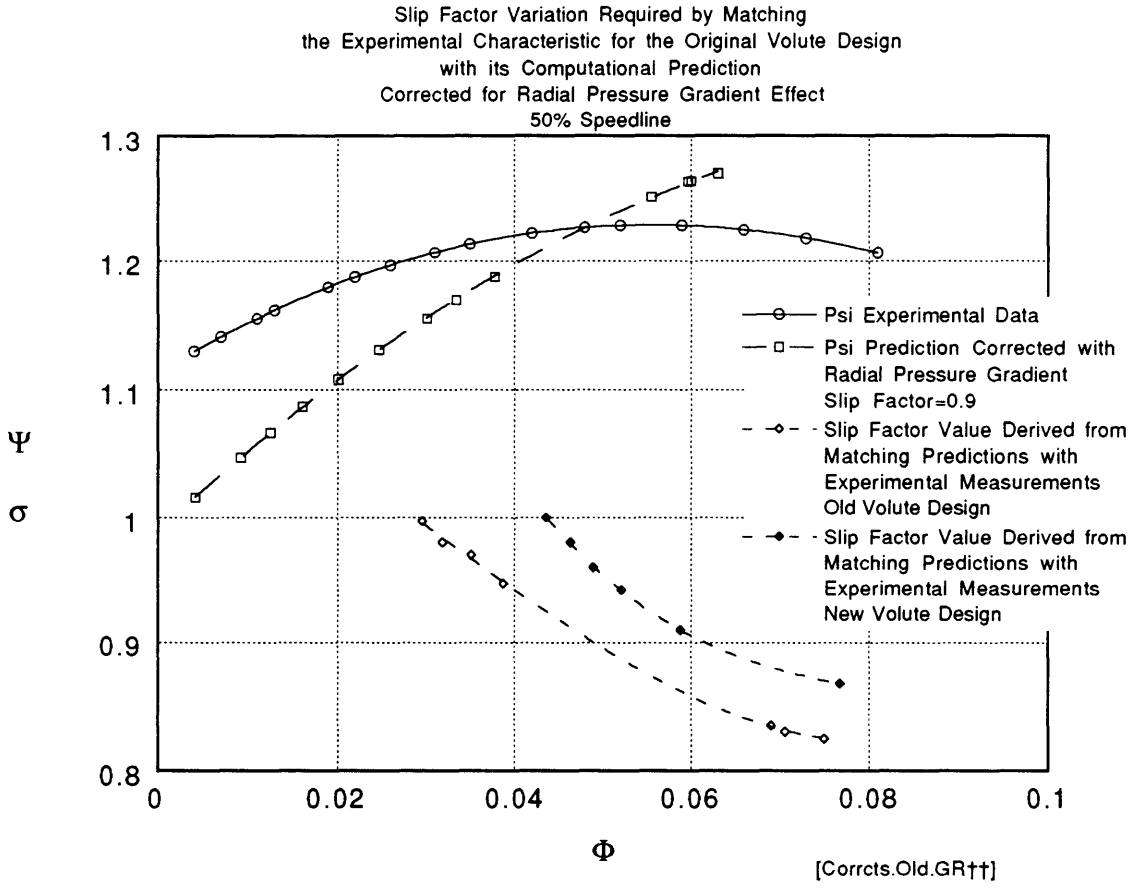
Slip Factor Variation Required by Matching
the Experimental Characteristic for the Original Volute Design
with its Computational Prediction
Corrected for Radial Pressure Gradient Effect
50% Speedline
1.3
1.2
1.1
1
0.9
0.8
Ψ
σ
0
0.02
0.04
0.06
0.08
0.1
Φ
Psi Experimental Data
Psi Prediction Corrected with Radial Pressure Gradient Slip Factor=0.9
Slip Factor Value Derived from Matching Predictions with Experimental Measurements Old Volute Design
Slip Factor Value Derived from Matching Predictions with Experimental Measurements New Volute Design
[Corrcts.Old.GR††]

Fig.7.3.4

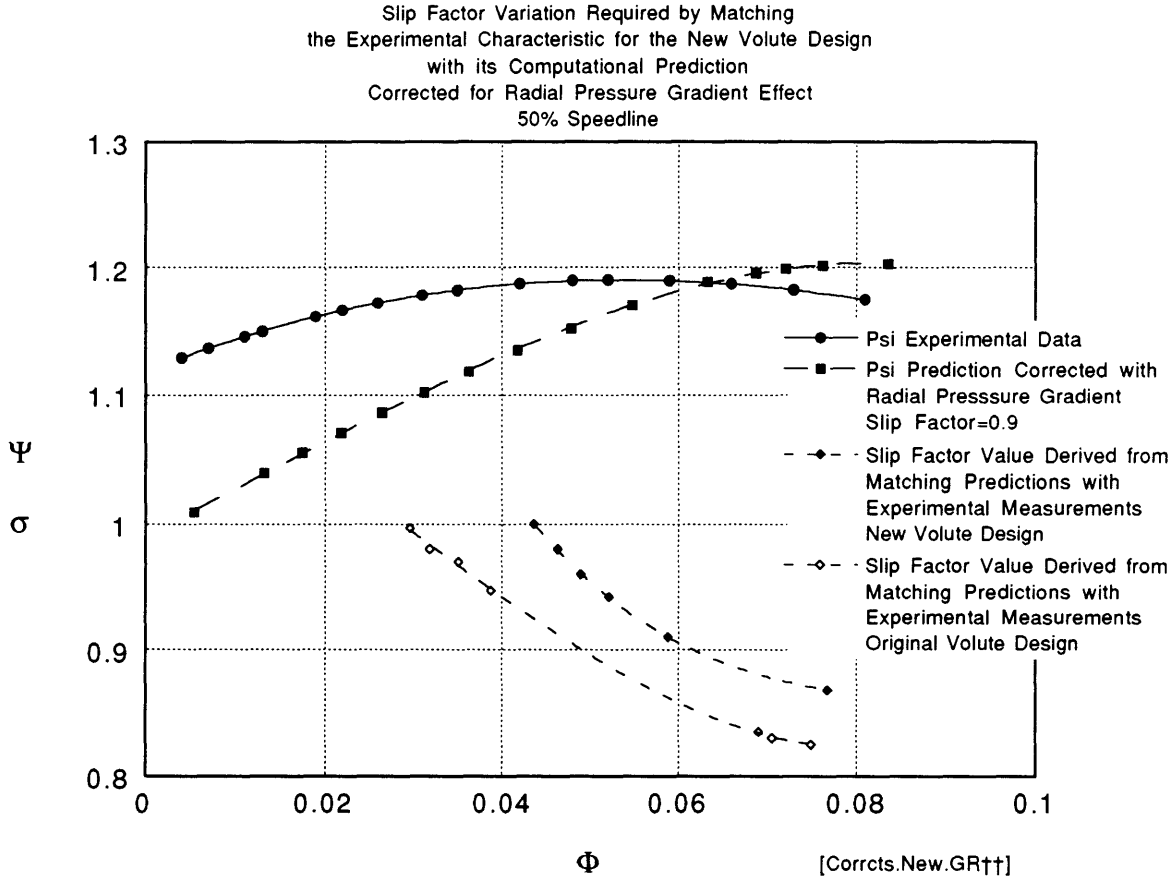
Slip Factor Variation Required by Matching
the Experimental Characteristic for the New Volute Design
with its Computational Prediction
Corrected for Radial Pressure Gradient Effect
50% Speedline
1.3
1.2
1.1
1
0.9
0.8
Ψ
σ
0
0.02
0.04
0.06
0.08
0.1
Φ
[Corrcts.New.GR††]
Psi Experimental Data
Psi Prediction Corrected with
Radial Presssure Gradient
Slip Factor=0.9
Slip Factor Value Derived from
Matching Predictions with
Experimental Measurements
New Volute Design
Slip Factor Value Derived from
Matching Predictions with
Experimental Measurements
Original Volute Design

Fig.7.3.5

APPENDIX A:
PERFORMANCE PREDICTION CODE

A.1. Code

The version shown on the following pages was denominated PUMP0713.F. This version was developed in order to test the predicted effect on pump performance of adopting a volute with exit area equivalent to that of the transition outlet in the original design and of eliminating the diffuser.

```
************************************************************************
*       INTERACT VAX VERSION 7.13F - MARCH 12, 1992
************************************************************************
*       THIS VERSION IS DESIGNED TO DO A NUMBER OF THINGS:
*       0)      INCORPORATE SCOTT'S EQUAL AREA AT 343 DEGREES REQUIREMENT
*       1)      INCORPORATE A.WOO AND P.WESTHOFF SUGGESTIONS
*               ABOUT CORRECTIONS TO SLIP FACTOR DEFINITION AND
*               IMPELLER EXIT VELOCITY TRIANGLES
*       2):NO   INCORPORATE RADIAL VARIATIONS OF VOLUTE PRESSURE FOR THE
*               PURPOSE OF COMPUTING CORRECTED IMPELLER EXIT VELOCITY:
*               DETERMINE AND USE THE PRESSURE COEFFICIENT AT IMPELLER
*               EXIT IN ORDER TO IMPROVE IMPELLER-VOLUTE INTERACTION
*               MODELING
*       3)      PLOT LOCAL VOLUTE PRESSURE AND AREA DISTRIBUTIONS
*               AT USER'S REQUEST
*       4)      FIND BEST TRANSITION POINT BETWEEN TWO VOLUTE AREA SLOPES
*               WHILE EXIT AREA IS MAINTAINED AT ORIGINAL VALUE
*       5)      FIND SECOND-ORDER CURVE FITS FOR THAT TRANSITION POINT:
*               y = AA1 n↑2 + BB1 n + CC1; y(N)=F, y(N1)=F/2, y'(N)=0
*               z = AA2 n↑2 + BB2 n;       z(0)=0, z(N1)=F/2, z'(N1)=y'(N1)
*               N1 IS NO. OF CELLS W/ HI AREA GROWTH (INPUT)
*               N2 IS NO. OF CELLS W/ LO AREA GROWTH (N-N1)
*       6)      DISPLAY CURVE FIT COEFFICIENTS
*       7)      DISPLAY VARIABLES MORE RATIONALLY IN OUTPUT
************************************************************************
*       THE FOLLOWING ARE USER-SPECIFIED THROUGHOUT EXECUTION TIME:
*               MULTIPLE BYPASS CELL DUCT AREA,AREA MULTIPLIER,VOLUTE AREA
*               SLOPE TRANSITION CELL,% OF SPEED,LOCAL PSIV DISPLAY OPTION
************************************************************************
*       AUTOMATIC C(0), Cm2(0) GUESSING
*       OVERALL PHI,OVERALL PSI,C(0),Cm2(0),EFFICIENCY SCREEN DISPLAY
*       OUTPUT HEADER LISTS INPUT VALUES
************************************************************************

        REAL*8 LOSSF,F,FD,W,D2,B2,BETAB,BLB2,LP,PI,RIMPEX
        REAL*8 LOSSFV,SIGMA,D1,REL,PHIDES,BETA
        REAL*8 PHIT,PSIT,DELC,DELCM2,CTR,DT,U,ALPHA,PDELCM2,SGCM2
        REAL*8 PHILT,PDELC,SGC,LAMBDA,DL,PSIS,COT,ONE,CP,EFF
        REAL*8 AB,AM,UCOEF,CGUESS,CM2GUESS
        REAL*8 AA1,BB1,CC1,AA2,BB2
        REAL*8 BYGAMMA

        INTEGER N,N1,N2,ND,LEAKCO,Z
        INTEGER TEST,LEAKF,PLOCAL,ALOCAL,INDEX,COUNT
        INTEGER BYPLOC,BYPCO

        PARAMETER (D2=0.6096,B2=0.015,BLB2=1.6933,D1=0.2032,F=0.0054805413)
        PARAMETER (LP=0.372872,PI=3.141592654,N=100,Z=8,BETAB=0.5759586532)
        PARAMETER (RIMPEX=12.0,BYGAMMA=0.785,BYPCO=1,FD=0.0052548282,ND=96)
        PARAMETER (LOSSFV=0.9,SIGMA=0.9,PHIDES=0.134,LEAKF=1,REL=0.004)
        PARAMETER (LOSSF=0.5,LEAKCO=17000,W=0.0635)

        REAL*8 A(0:1001),AREF(0:1001),DH(0:1001),C(0:1001),CM2(0:1000)
        REAL*8 CU(0:1000),VR(0:1000),CLM(0:1000),CLU(0:1000),PHIV(0:1001)
        REAL*8 PSIM(0:1000),PSIV(0:1001),DCM2(0:1000),DELPSIV(0:1000)
        REAL*8 C2(0:1000),FLOW(1:15),VELD(0:1000,15),PRESD(0:1000,15)
        REAL*8 CD(0:1000,15),CL(0:1000,1:15),PSIE(0:1001),RMIDW(0:1001)
        REAL*8 CB(0:1001),CBM(0:1001),CBU(0:1001)

************************************************************************
*       ENTER USER-DEFINED PARAMETERS
************************************************************************

50      WRITE(*,*)'DO YOU WANT LOCAL PRESSURE PLOTS? (YES: 0)'
        READ(*,*) PLOCAL
        WRITE(*,*)'DO YOU WANT LOCAL VOLUTE AREA PLOTS? (YES: 0)'
        READ(*,*) ALOCAL
        WRITE(*,*)'BYPASS AREA VALUE:'
        READ(*,*) AB
        WRITE(*,*)'VOLUTE AREA MULTIPLIER:'
        READ(*,*) AM
        WRITE(*,*)'VOLUTE AREA TRANSITION CELL:'
        READ(*,*) N1
        WRITE(*,*)'FRACTION OF DESIGN SPEED:'
```

```
        READ(*,*) UCOEF
        WRITE(*,*)'FIRST C(0) GUESS:'
        READ(*,*) CGUESS
        WRITE(*,*)'FIRST Cm2(0) GUESS:'
        READ(*,*) CMB2GUESS

*******************************************************************************
*       WRITE OUTPUT HEADER
*******************************************************************************

        WRITE(15,*)' OUTPUT FROM PUMP VERSION 7.13F - 3/12/1992'
        WRITE(15,*)'  '
        WRITE(15,4060) AM,AB
        WRITE(15,4061) UCOEF,N1
        WRITE(15,*)' N1: CELL NUMBER WHERE A-A(0)=F/2'
        WRITE(15,4062) N
        WRITE(15,*) '  '

*******************************************************************************
*       INITIALIZE VARIABLES AND CURVE FIT COEFFICIENTS
*       AT BEGINNING OF EXECUTION
*******************************************************************************

        AA1=FD/(2*(2*ND*N1-(ND**2)-(N1**2)))
        BB1=-2*ND*AA1
        CC1=FD+(ND**2)*AA1
        AA2=(2*ND*N1*AA1+N1*BB1-FD/2)/(N1**2)
        BB2=2*ND*AA1+BB1-2*N1*AA2

        WRITE(15,*)' CURVE FIT FUNCTIONS:'
        WRITE (15,4070) AA2,BB2
        WRITE (15,4080) AA1,BB1,CC1
        WRITE(15,*)'  '

        DELCM2=2
        PDELCM2=0.1
        PDELC=0.1
        SGCM2=1
        SGC=1
        U=13.5*UCOEF

*******************************************************************************
*       INITIALIZE VARIABLES AT BEGINNING OF VOLUTE LOOP
*******************************************************************************

100     WRITE(*,*)'ENTER TONGUE PRESSURE COEFFICIENT (0 TO QUIT).'
        READ(*,*) PSIV(0)
        IF(PSIV(0).LE.0) THEN
                GOTO 5000
        ENDIF

        C(0)=CGUESS
        CM2(0)=CM2GUESS
        A(0)=0.00138

        RMIDW(0)=628.04*A(0)
        AREF(0)=A(0)/(PI*D2*B2)
        DH(0)=4*W*A(0)/(2*(A(0)+W**2))
        DL=1.91511/N
        DT=DL/U
        COUNT=0
        ONE=1.0
        BETA=BETAB
        N2=N-N1

500     PHIV(0)=C(0)*AREF(0)/U
        CLM(0)=LEAKF*(U*DSQRT(PSIV(0)/LEAKCO))
        CLU(0)=CU(0)

*******************************************************************************
*       MARCH THROUGH THE VOLUTE LOOP
*******************************************************************************

        DO 1000 I=0,N
```

```
                IF (I.LT.N1) THEN
                        A(I+1)=A(0)+AM*((I**2)*AA2+I*BB2)
                ELSE IF (I.LT.ND) THEN
                        A(I+1)=A(0)+AM*((I**2)*AA1+I*BB1+CC1)
                ELSE
                        A(I+1)=A(I)+AM*((F-FD)/(N-ND))
                ENDIF

                RMIDW(I+1)=628.04*A(I+1)
                AREF(I+1)=A(I+1)/(PI*D2*B2)
                DH(I+1)=4*W*A(I+1)/(2*(A(I+1)+W**2))

                C2(I)=DSQRT(CM2(I)**2+(SIGMA*(U-(CM2(I)/DTAN(BETA))))**2)
                CU(I)=SIGMA*(U-CM2(I)/DTAN(BETA))
                VR(I)=CM2(I)/DSIN(BETA)
                PSIM(I)=(2*CU(I)/U)-((C2(I)/U)**2)+((BLB2*CM2(I)/U)**2)-
     /  (LOSSF*(VR(I)/U)**2)
                CLM(I)=DSIGN(ONE,PSIV(I))*LEAKF*
     /  (U*DSQRT(DABS(PSIV(I))/LEAKCO))
                CLU(I)=CU(I)

                CBM(I)=CB(I)*DSIN(BYGAMMA)
                CBU(I)=CB(I)*DCOS(BYGAMMA)
                PHIV(I+1)=PHIV(I)+(CM2(I)/(N*U))-(CLM(I)/(N*U))*BLB2+
     /  (CB(I)/U)*(AB/(PI*D2*B2))
* * * * * * * * * * * * * * * * * * * * * * * * * * * * * * * * * * * * * * *
*       Contribution of bypass to flow coefficient bypass exit
* * * * * * * * * * * * * * * * * * * * * * * * * * * * * * * * * * * * * * *
                C(I+1)=U*(PHIV(I+1)/AREF(I+1))

                DELPSIV(I)=PHIV(I)*C(I)/U
                DELPSIV(I)=DELPSIV(I)-(PHIV(I+1)*C(I+1)/U)
                DELPSIV(I)=DELPSIV(I)+(CM2(I)*CU(I)/(N*U**2))
                DELPSIV(I)=DELPSIV(I)-(BLB2*CLM(I)*CLU(I)/(N*U**2))
                DELPSIV(I)=DELPSIV(I)+(AB*CBM(I)*CBU(I)/(PI*D2*B2*U**2))
* * * * * * * * * * * * * * * * * * * * * * * * * * * * * * * * * * * * * * *
*       Contribution of bypass to pressure coefficient at bypass exit
* * * * * * * * * * * * * * * * * * * * * * * * * * * * * * * * * * * * * * *
                DELPSIV(I)=DELPSIV(I)*(4/(AREF(I)+AREF(I+1)))
                DELPSIV(I)=DELPSIV(I)-((LAMBDA(C(I),DH(I))*DL/DH(I))*
     /  ((C(I)/U)**2))
                PSIV(I+1)=PSIV(I)+DELPSIV(I)
* * * * * * * * * * * * * * * * * * * * * * * * * * * * * * * * * * * * * * *
*       Correction of PSIV to find PSIE at impeller exit
* * * * * * * * * * * * * * * * * * * * * * * * * * * * * * * * * * * * * * *
                PSIE(I+1)=PSIV(I+1)-
     /  ((C(I+1)/U)**2)*DLOG10(RMIDW(I+1)/RIMPEX)
                ALPHA=(DT*DSIN(BETA)*U**2)/(2*LP)
* * * * * * * * * * * * * * * * * * * * * * * * * * * * * * * * * * * * * * *
*       Here the correction is not included in the impeller response
* * * * * * * * * * * * * * * * * * * * * * * * * * * * * * * * * * * * * * *
                DCM2(I)=ALPHA*(PSIM(I)-PSIV(I+1))
                CM2(I+1)=CM2(I)+DCM2(I)
1000    CONTINUE

*************************************************************************
*       CALCULATE EFFECT OF BYPASS ON SPEED
*************************************************************************

        PHIB=0
        DO 1050 I=1,51,2
                CB(I)=PSIV(N)-PSIV(I)
                IF (CB(I).LT.0) THEN
                        CB(I)=0
                ENDIF
                CB(I)=DSIGN(PSIV(I),PSIV(N))*U*DSQRT(CB(I)/BYPCO)
                PHIB=PHIB+(CB(I)/U)*AB/(PI*D2*B2)
1050    CONTINUE

*************************************************************************
*       CALCULATE ERROR IN CLOSURE EQUATIONS
*************************************************************************

        COT=C(0)
```

```
        CTR=DABS(PSIV(N)-PSIV(0))
        CTR=(C(N)/U)**2+DSIGN(ONE,COT)*CTR*(1-LOSSFV)
        CTR=DSQRT(CTR)
        CTR=CTR*U*DSIGN(ONE,COT)
        DELC=CTR-C(0)

        DELCM2=CM2(N)-CM2(0)

*******************************************************************************
*       CONVERGENCE CRITERION AND ITERATION SETUP
*******************************************************************************

        IF (DABS(DELC).LT.9E-3 .AND. DABS(DELCM2).LT.9E-3) THEN
                GOTO 2000
        ELSE
                C(0)=C(0)+5*REL*(DSIGN(ONE,(ABS(PDELC)-ABS(DELC)))*
     /  SGC*DABS(DELC))
                CM2(0)=CM2(0)+REL*(DSIGN(ONE,(ABS(PDELCM2)-ABS(DELCM2)))*
     /  SGCM2*DABS(DELCM2))

                SGCM2=DSIGN(ONE,(ABS(PDELCM2)-ABS(DELCM2)))*SGCM2
                SGC=DSIGN(ONE,(ABS(PDELC)-ABS(DELC)))*SGC
                PDELCM2=DELCM2
                PDELC=DELC

                IF((DELC.GT.10) .OR. (DELCM2.GT.10)) THEN
                        GOTO 3000
                ELSE
                        COUNT=COUNT+1
                        WRITE (*,4040) COUNT,DELC,DELCM2,C(0),CM2(0)
                        GOTO 500
                ENDIF
        ENDIF

*******************************************************************************
*       CALCULATE RELEVANT OPERATING PARAMETERS
*******************************************************************************

2000    PHIT=PHIV(N)-PHIV(0)-PHIB
        PSIT=PSIV(N)+(C(N)/U)**2
        PSIS=PSIV(N)+CP(PHIT)*(PSIT-PSIV(N))
        PHILT=CLM(0)
        EFF=0
        DO 2005 I=1,N
                EFF=EFF+(CM2(I)*CU(I))
2005    CONTINUE
        EFF=(N*PHIT*PSIS*(U**2))/(2*EFF)
        EFF=EFF*100
        DO 2010 I=1,N
                PHILT=PHILT+CLM(I)
2010    CONTINUE
        PHILT=PHILT*(BLB2/(N*U))

*******************************************************************************
*       SCREEN DISPLAY OF RESULTS
*******************************************************************************

        WRITE (*,4090) PHIT,PSIS,C(0),CM2(0),PSIV(0),EFF
        WRITE (15,4090) PHIT,PSIS,C(0),CM2(0),PSIV(0),EFF

        IF (PLOCAL.EQ.0) THEN
                WRITE (15,4100) PSIV(0),PSIV(1),PSIV(2),PSIV(3),
     /          PSIV(4),PSIV(5),PSIV(6),PSIV(7),PSIV(8),PSIV(9)
                WRITE (15,4100) PSIV(0),PSIV(10),PSIV(20),PSIV(30),
     /          PSIV(40),PSIV(50),PSIV(60),PSIV(70),PSIV(79),PSIV(90)
                WRITE (15,4100) PSIV(N-9),PSIV(N-8),PSIV(N-7),PSIV(N-6),
     /          PSIV(N-5),PSIV(N-4),PSIV(N-3),PSIV(N-2),PSIV(N-1),PSIV(N)
                WRITE(15,*) ' '
        ENDIF

        CGUESS=C(0)
        CM2GUESS=CM2(0)
        GOTO 100
```

```
3000    WRITE (*,*)' DIVERGENCE!'
        GOTO 100

*************************************************************************
*       DEFINE FORMATS
*************************************************************************

4040    FORMAT('   ',I4,2X,E11.5,2X,E11.5,2X,F9.5,2X,F9.5)
4060    FORMAT(' VOLUTE AREA MULTIPLE (AM):',F4.2,'- BYPASS AREA:',F8.5)
4061    FORMAT(' SPEEDLINE:',F4.2,'PERCENT - SLOPE BREAKPOINT CELL:',I3)
4062    FORMAT(' CELL NUMBER WHERE A-A(0)=F (N):',I3)
4070    FORMAT(' FIRST CURVE FIT: a=',F12.10,'  b=',F12.10)
4080    FORMAT(' SECOND CURVE FIT: a=',F12.10,'  b=',F12.10,'  c=',F12.10)
4090    FORMAT(' PHI:',F8.5,'  PSI:',F8.5,'  C(0):',F5.2,'  Cm2(0):',F5.2,
     /  '  PSI(0):',F4.2,'  ETA:',F6.2)
4100    FORMAT(10F9.5)
5000    IF (ALOCAL.EQ.0) THEN
                WRITE (15,*) '  AREA VALUES: A(1,9); A(0,90,10); A(91,100)'
                WRITE (15,4100) A(0),A(1),A(2),A(3),
     /          A(4),A(5),A(6),A(7),A(8),A(9)
                WRITE (15,4100) A(0),A(10),A(20),A(30),
     /          A(40),A(50),A(60),A(70),A(80),A(90)
                WRITE (15,4100) A(91),A(92),A(93),A(94),
     /          A(95),A(96),A(97),A(98),A(99),A(100)
                WRITE(15,*) '  '
        ENDIF
        PAUSE
        END

*************************************************************************
*       DEFINITION FUNCTION OF Cp(FLOW)
*************************************************************************

        FUNCTION CP(PHIT)
        REAL*8 CP,PHIT

        IF (PHIT.LE.0.06) THEN
                CP=0.75
        ELSE
                CP=0.75-6.4*(PHIT-0.06)
        ENDIF
        IF (CP.LE.0) THEN
                CP=0
        ENDIF
        RETURN
        END

*************************************************************************
*       DEFINITION FUNCTION OF LAMBDA(Re)
*************************************************************************

        FUNCTION LAMBDA(C,DH)
        REAL*8 LAMBDA,C,DH

        LAMBDA=DABS((C*DH)/1E-6)
        LAMBDA=0.02-0.005*(DLOG10(LAMBDA)-5)

        RETURN
        END
```

A.2. Output

The output shown on the following page was produced by PUMP0713.F, shown and described in the previous section of this Appendix. The major working parameters of the simulation are presented in the header. The curve-fitted volute cross-section area distibution is determined by specifying the slope break point location. The area distribution at each cell is then shown once for that design choice. The volute static pressure is shown at each cell for each operating point considered.

```
 OUTPUT FROM PUMP VERSION 7.13F - 3/12/1992

VOLUTE AREA MULTIPLE (AM):1.00- BYPASS AREA: 0.00000
SPEEDLINE:0.50PERCENT - SLOPE BREAKPOINT CELL: 10
 N1: CELL NUMBER WHERE A-A(0)=F/2
CELL NUMBER WHERE A-A(0)=F (N):100

 CURVE FIT FUNCTIONS:
FIRST CURVE FIT: a=-.0000262741  b=0.0005254828
SECOND CURVE FIT: a=-.0000003552  b=0.0000682076  c=0.0019808628

PHI: 0.02881  PSI: 1.07265  C(0): 1.52  Cm2(0): 0.11  PSI(0):0.82  ETA: 44.32
 0.82000  0.82012  0.84379  0.85449  0.86075  0.86508  0.86845  0.87128  0.87379  0.87611
 0.82000  0.87829  0.90362  0.93265  0.96123  0.98710  1.00906  1.02653  1.03819  1.04710
 1.04762  1.04809  1.04850  1.04887  1.04919  1.04946  1.05017  1.05083  1.05143  1.05198

PHI: 0.03263  PSI: 1.08134  C(0): 1.65  Cm2(0): 0.12  PSI(0):0.80  ETA: 46.66
 0.80000  0.80030  0.82849  0.84131  0.84883  0.85404  0.85807  0.86144  0.86440  0.86711
 0.80000  0.86963  0.89799  0.92949  0.95992  0.98711  1.00999  1.02814  1.04028  1.04967
 1.05023  1.05073  1.05119  1.05160  1.05196  1.05226  1.05313  1.05395  1.05471  1.05542

PHI: 0.03654  PSI: 1.08960  C(0): 1.79  Cm2(0): 0.14  PSI(0):0.78  ETA: 48.81
 0.78000  0.78044  0.81366  0.82884  0.83776  0.84392  0.84867  0.85262  0.85606  0.85917
 0.78000  0.86204  0.89329  0.92697  0.95888  0.98702  1.01051  1.02903  1.04143  1.05110
 1.05168  1.05221  1.05269  1.05313  1.05351  1.05385  1.05488  1.05586  1.05679  1.05767

PHI: 0.04058  PSI: 1.09748  C(0): 1.93  Cm2(0): 0.16  PSI(0):0.76  ETA: 50.82
 0.76000  0.76052  0.79924  0.81699  0.82744  0.83465  0.84018  0.84473  0.84868  0.85221
 0.76000  0.85543  0.88946  0.92504  0.95811  0.98686  1.01062  1.02924  1.04166  1.05138
 1.05197  1.05251  1.05301  1.05345  1.05385  1.05419  1.05540  1.05655  1.05766  1.05871

PHI: 0.04478  PSI: 1.10496  C(0): 2.07  Cm2(0): 0.18  PSI(0):0.74  ETA: 52.72
 0.74000  0.74050  0.78524  0.80581  0.81792  0.82625  0.83262  0.83783  0.84230  0.84626
 0.74000  0.84983  0.88650  0.92369  0.95757  0.98658  1.01029  1.02872  1.04093  1.05044
 1.05102  1.05154  1.05202  1.05245  1.05284  1.05318  1.05455  1.05588  1.05716  1.05840

PHI: 0.04919  PSI: 1.11201  C(0): 2.21  Cm2(0): 0.21  PSI(0):0.72  ETA: 54.54
 0.72000  0.72035  0.77169  0.79534  0.80927  0.81883  0.82609  0.83200  0.83702  0.84143
 0.72000  0.84535  0.88447  0.92296  0.95728  0.98620  1.00952  1.02744  1.03917  1.04815
 1.04868  1.04916  1.04960  1.04999  1.05034  1.05064  1.05218  1.05368  1.05514  1.05655

PHI: 0.05383  PSI: 1.11859  C(0): 2.37  Cm2(0): 0.24  PSI(0):0.70  ETA: 56.29
 0.70000  0.70002  0.75864  0.78569  0.80160  0.81249  0.82072  0.82736  0.83296  0.83782
 0.70000  0.84209  0.88343  0.92287  0.95724  0.98568  1.00826  1.02531  1.03626  1.04432
 1.04478  1.04518  1.04554  1.04585  1.04612  1.04634  1.04804  1.04971  1.05133  1.05292

PHI: 0.05877  PSI: 1.12460  C(0): 2.52  Cm2(0): 0.28  PSI(0):0.68  ETA: 58.00
 0.68000  0.67944  0.74615  0.77695  0.79505  0.80739  0.81666  0.82409  0.83029  0.83561
 0.68000  0.84021  0.88349  0.92346  0.95745  0.98501  1.00644  1.02225  1.03205  1.03872
 1.03905  1.03932  1.03956  1.03974  1.03988  1.03998  1.04182  1.04363  1.04541  1.04715

  AREA VALUES: A(1,9); A(0,90,10); A(91,100)
 0.00138  0.00138  0.00188  0.00233  0.00272  0.00306  0.00335  0.00359  0.00377  0.00390
 0.00138  0.00398  0.00453  0.00504  0.00548  0.00585  0.00615  0.00638  0.00653  0.00662
 0.00662  0.00663  0.00663  0.00663  0.00663  0.00663  0.00669  0.00675  0.00680  0.00686
```

APPENDIX B:
LINEAR SYSTEM STABILITY PREDICTION CODE

B.1. Code

The code shown on the following pages is the modified Version #8 of the code used by Bons in order to assess the predictive capabilities of the linearized system stability theory applied to the system under study. This and the previous version were introduced to incorporate the effect of different pump designs and resulting performance.

```
**********************************************************************
*       DYNAMIC SIMULATION OF THE MIT PUMP LOOP
*       The MIT test facility is a closed loop consisting of 2 legs, one inlet plenum (#2,
*       lg), and one discharge plenum (#1, sm).
*       The four equations which define this system are: conservation of momentum in the
*       pump and throttle legs, and conservation of mass in the two tanks (plenums).
*       A fifth equation representing a time lag in pump pressure rise has been used as
*       well. All five equations have been linearized by assuming only small perturbations
*       about a known operating point.
*       This program determines the instability point and frequency of unstable oscillations
*       by calculating the system eigenvalues. It uses inputs corresponding to
*       predetermined experimental conditions. The operating range from Phi = 0.001 to
*       0.07 is scanned.
*       The original code was developed by N. Goulet for his Master's thesis. His
*       program allowed for the use of multiple plenums. Subsequently, the code was
*       modified by J.P.Bons to assume only two plenums, and to account for variations in
*       impeller wheelspeed with mass flow and the pressure and volume adjustments of
*       the air bags which occurred when the pump was turned on.
**********************************************************************
**********************************************************************
*       VERSION #8 - 3/13/1992
*       This updated version is the EIGHTH in a series by F.Ciacci. These versions
*       were produced in order to test the effect on the whole system of changes in the
*       structure and performance of the pump.
*
*       Version #8 allowed one to compare:
*       1) eigenvalues for the original volute case AFTER THE APPROPRIATE
*          CHANGES TO THE CODE AND THE DISTRIBUTION OF THE VOLUTE
*          AREA WERE MADE
*       2) eigenvalues for the case of a pump with 11/1991 modified volute design:
*            • DUAL PARABOLIC CURVE FIT of original inlet and exit areas
*            • SLOPE BREAK POINT AT CELL NUMBER 10
*            • NO TONGUE BYPASS system around tongue (ZERO AREA)
*            • Configuration parameters: AB=0.0 AM=1.00 N1=10:
*       3) FOR THE 50% SPEEDLINE, eigenvalues for the following cases:
*            • OLD: same as the 11/1991 modified volute design, AM=1.00
*            • NEW: AM=1.72. The volute exit area is now about equal to the transition
*              exit area. The diffuser has been elininated.
*       All characteristic shapes for Cases (1) and (2) were determined experimentally.
*       Those for Case (3) were both predicted computationally.
*
*       The speedlines tested on the new volutewere not always the same as those tested on
*       the old volute. These were 80%, 50% and 23%. Of these, only 80% could be
*       compared including the effect of the actual plenum pressure characteristics
*       measured by Bons. The remaining two, 50% and 23% could be compared only to
*       the old volute data measured by Sandler and Wo, with the newly measured volute
*       pressure characteristics, which are strictly valid only for the new volute design.
*       Note that THE 50% CHARACTERISTIC WAS PREDICTED
*       COMPUTATIONALLY, AND THE AM=1.0 SPEED AND PLENUM
*       PRESSURE CHARACTERISTICS WERE USED WITH IT, so the accuracy of
*       the prediction is doubly limited.
```

```
*       For the same reason, IMPELLER WHEEL SPEED CHARACTERISTICS for
*       those speedlines WERE OBTAINED FROM EXPERIMENTAL DATA both in the
*       new and old design cases.  Please refer to the comments in the SLOPE
*       subroutine.
*
*       New variables are labeled with the prefix NW- RN-
*       Speed variation with flow ARE accounted for in THIS version.
*       A note: due to the choice of the normalizing factor for pressure coefficient, psi
*       values in this code are 1/2 of those used in the volute/impeller interaction code and
*       other applications.
**********************************************************************

      PARAMETER (NMAX=2,NMAX2=5,GAMMA=1.4)
      PARAMETER (RO=1000,PI=3.14159,D2=.6096)
      INTEGER N,Z,NSPDLN,NFILE,NWCHAR
      REAL PSLOPE,TSLOPE,SPEED,PHI,PSI,INC,CSPD,ZLAG,DLAG
      REAL
AREA(NMAX),VCOM(NMAX),PCOM(NMAX),LEN(NMAX),DYN(NMAX)
      REAL
MATRIX(NMAX2,NMAX2),WR(NMAX2),WI(NMAX2),PDAMP(NMAX)
      REAL
B(NMAX2),FREQ(NMAX2),UPAR(NMAX2),ZAPR(NMAX2),ZAPI(NMAX2)
      REAL REDFREQ(NMAX2),SHFREQ,PSMI,PLGI,VSMI,VLGI
      CHARACTER*1 CONF
      CHARACTER*8 DATFIL
      COMMON  LEN(NMAX),AREA(NMAX),VCOM(NMAX),
     /    PCOM(NMAX),MATRIX(NMAX2,NMAX2),
     /    DYN(NMAX),PDAMP(NMAX),PSMI,PLGI,VSMI,VLGI

**********************************************************************
*       DATA  ACQUISITON
*       The number of legs is set to N = 2, and the following parameters
*       are defined:
*       -DYN(), this is the dynamic head loss coefficient for each leg.
*       -ZLAG, this is the correction term to the pressure lag time constant.
*       -VCOM(), this is the air volume in each plenum [m3].
*       -PCOM(), this is the pressure of the air volumes in each plenum  [Pa].
*       -AREA(), this is the reference area used for each leg [m].
*       -LEN(), this is the lumped inertial length of each leg [m].
**********************************************************************

 2    N = 2
      DYN(1) = 6
      DYN(2) = 1.5
      ZLAG = 0.03
      AREA(2) = .0290
      LEN(2) = 3.277
      AREA(1) = .0572
      LEN(1) = 41.92
```

```
**********************************************************************
*       These air volumes and pressures are as measured with the pump off. They will be
*       adjusted later for the operating point of interest. #1 is the small plenum and #2 is
*       the large.
**********************************************************************

3       VCOM(2) = .300
        PCOM(1) = 1.427E5
        PCOM(2) = 1.389E5
        VCOM(2) = VCOM(2)*1000

**********************************************************************
*       The program can be run without accounting for variations in impeller wheelspeed.
*       If the constant speed value (CSPD) is set to zero, then the program assumes the
*       speed does vary with massflow (for a given speedline). This is prompted for.
**********************************************************************

        CSPD = 0.0

**********************************************************************
*       If a data file is desired, set NFILE = 1. Important data is spooled to the screen so
*       this is not always necessary. NFILE = 0 will bypass the datafile creation.
**********************************************************************

        NFILE = 1

**********************************************************************
*       Experimental curve fits for three different speedlines are available in the present
*       version.
**********************************************************************

        WRITE(9,*) 'ENTER THE TYPE OF SPEEDLINE BEING TESTED'
        WRITE(9,*) '100% = 1, 80%=2, 60%=3, 50% = 4, 23% = 5'
        READ(9,*) NSPDLN
        WRITE(9,*) 'ENTER THE PUMP CONFIGURATION TESTED'
        WRITE(9,*) 'BASE CASE: 0, NEW VOLUTE/BYPASS: 1'
        READ(9,*) NWCHAR
        WRITE(9,*) 'VOLUMES AS MEASURED WITH PUMP OFF'
        WRITE(9,*) 'AIR VOLUME OF LARGE PLENUM (liters): ',VCOM(2)
        WRITE(9,*) 'WHEEL SPEED IS A VARIABLE'
        WRITE(9,*) 'ZLAG = ',ZLAG
        WRITE(9,*) 'DO YOU WISH TO CHANGE ANY OF THESE (Y/N)?'
        READ (9,1011) CONF
        IF (CONF='N') GO TO 7
        WRITE (9,*) 'ENTER PHASE LAG FACTOR, ZLAG'
        READ (9,*)ZLAG
        WRITE (9,*) 'ENTER CONSTANT WHEEL SPEED VALUE (m/s),
0=VARIABLE'
        READ(9,*) CSPD
        WRITE(9,*) 'ANY FURTHER CHANGES?'
        READ (9,1011) CONF
```

```
      IF (CONF='N') GO TO 7
      WRITE (9,*) 'ENTER LG PLENUM VOLUME (liters):'
      READ (9,*)VCOM(2)
      WRITE (9,*) 'ENTER SMALL PLENUM PRESSURE W PUMP OFF (Pa)'
      READ(9,*)PCOM(1)
      WRITE (9,*) 'ENTER LARGE PLENUM PRESSURE W PUMP OFF (Pa)'
      READ(9,*)PCOM(2)

*****************************************************************
*     Enter volume for pump leg (measured with pump off). Experimentally, this is one
*     of the primary loop variables (wheelspeed being the other).
*****************************************************************

 7    WRITE (9,*) 'ENTER SM PLENUM VOLUME (liters):'
      READ (9,*) VCOM(1)
      VCOM(1) = VCOM(1)/1000.0
      VCOM(2) = VCOM(2)/1000.0

*****************************************************************
*     The pump leg (NP) is #1 and the throttle leg is #2.
*****************************************************************

      NP = 1
      NT = 2

*****************************************************************
*     A datafile can be generated containing the important program output for each run.
*****************************************************************

      WRITE(9,*) 'DO YOU WANT A DATA FILE CREATED? (Y/N)'
      READ (9,1011) CONF
      IF (CONF='N') THEN
            NFILE = 0
            GOTO 10
      ENDIF
      WRITE(9,*)'ENTER FILE NAME FOR RESULTS'
      READ(9,'(A8)') DATFIL
      OPEN(UNIT=6,FILE=DATFIL,STATUS='NEW')
      CALL HEADER (N,NSPDLN,NP,NT,ZLAG)
      WRITE (6,*) ' '
      WRITE (6,1028)

*****************************************************************
*     TREATMENT
*     The loop, #600, determines the system eigenvalues over the interval 0.001 to 0.07,
*     stepping by 0.001. At each new operating point, the subroutine SLOPE is called to
*     calculate the necessary phi-dependent parameters: Utip, psi, and dpsi/dphi. Then
*     the subroutine STIFMATRIX assembles the 5x5 matrix elements.
*****************************************************************

 10   WRITE(9,*) 'COMPUTING EIGENVALUES'
```

```
      DO 600 PHI=0.001,0.07,0.001
      CALL
SLOPE(PHI,PSI,PSLOPE,TSLOPE,SPEED,NSPDLN,NWCHAR,CSPD,DLAG)
      CALL
STIFMATRIX(N,NSPDLN,PSLOPE,TSLOPE,SPEED,PHI,DLAG,ZLAG)

*****************************************************************
*     The matrix is reduced to upper Hessenberg form using the subroutine ELMHES.
*     Then the system eigenvalues are extracted by employing a QR algorithm
*     (subroutine HQR).
*****************************************************************

      N=NMAX2
      CALL ELMHES(MATRIX,N,NMAX2)
      CALL HQR(MATRIX,N,NMAX2,WR,WI)
      N=2

*****************************************************************
*     Now the program calculates the frequency of oscillation and the associated B
*     parameter and spools the results to the screen (and to a datafile, if so requested).
*     REDFREQ is the reduced frequency of the oscillation (normalized by the shaft
*     frequency).
*****************************************************************

      DO 12 I=1,NMAX2
            IF (WI(I).NE.0) THEN
                  SHFREQ = SPEED/(PI*D2)
                  FREQ(I)=ABS(WI(I)/(2*PI))
                  REDFREQ(I) = (FREQ(I)/SHFREQ)*100.0
                  B(I)=SPEED/(2*FREQ(I)*LEN(1))
                  UPAR(I)=(B(I)**2)*PSLOPE*TSLOPE
            ELSE
                  B(I)=0
                  REDFREQ(I) =0
                  FREQ(I)=0
                  UPAR(I)=0
            ENDIF
12    CONTINUE

      DO 15 Z=1,NMAX2
            ZAPI(Z)=0
            ZAPR(Z)=0
15    CONTINUE
      Z=1

*****************************************************************
*     The program ignores the following eigenvalues:
*     1)    Those which have very small ( <1E-8 ) real parts.
*     2)    Those which are equal to other eigenvalues.
*     3)    Those which have imaginary parts = 0.
*     4)    Those with negative real parts.
```

```
*       The others are spooled to the screen, along with the air volumes,
*       pressures, and wheelspeed at each operating point.
**********************************************************************

        DO 13 I=1,NMAX2
              IF (((WI(I).EQ.0).AND.(WR(I).EQ.0)).OR.
     /          (ABS(WR(I)).LE.1E-8)) GOTO 13
              DO 16 J=1,Z
                    IF ((ABS(WI(I)).EQ.ABS(ZAPI(J)))
     /               .AND.(WR(I).EQ.ZAPR(J))) GOTO 13
16            CONTINUE
              IF (WI(I).EQ.0) GOTO13
              IF (WR(I).GT.0) THEN
                    WRITE (9,1026)PHI,PSI,WI(I),WR(I)
     /              ,REDFREQ(I),B(I),UPAR(I)
                    WRITE(9,1040) VCOM(1),PCOM(1),VCOM(2)
     /                    ,PCOM(2),SPEED
              ENDIF
              IF (NFILE.EQ.1) THEN
                    WRITE (6,1026)PHI,PSI,WI(I),WR(I),REDFREQ(I)
     /              ,B(I),UPAR(I)
              ENDIF
              Z=Z+1
              ZAPI(Z)=WI(I)
              ZAPR(Z)=WR(I)
13      CONTINUE

600     CONTINUE

**********************************************************************
*     The program can now be terminated or continued with new initial values.
**********************************************************************

        WRITE (9,1023)
        READ (9,1011) CONF
        IF (CONF='N') GO TO 3

**********************************************************************
*               FORMAT statements and END
**********************************************************************

1011    FORMAT (A1)
1022    FORMAT  (I2,5X,1PE10.3,4X,1PE10.3,5X,1PE10.3,5X
     /          ,1PE10.3,5X,1PE10.3)
1023    FORMAT (/,'DO YOU WANT TO END (Y/N)?:')
1026    FORMAT  (F4.3,X,F4.3,X,1PE10.3,X,1PE10.3,X,1PE10.3
     /       ,X,1PE10.3,X,1PE10.3)
1028    FORMAT (' PHI  PSI    WI       WR
     /  REDFREQ     B PAR     UPAR ')
1040    FORMAT  (2X,F5.3,1X,F8.1,1X,F5.3,1X,F8.1,1X,F5.2)
200     END
```

```
*****************************************************************************
*****************************************************************************
*       SUBROUTINES
*****************************************************************************
*****************************************************************************

*****************************************************************************
*       The first subroutine, HEADER, writes the header for the present configuration in a
*       datafile.
*****************************************************************************

      SUBROUTINE HEADER (N,NSPDLN,NP,NT,ZLAG)
      PARAMETER (NMAX=2,NMAX2=5)
      REAL AREA(NMAX),VCOM(NMAX),PCOM(NMAX),ZLAG
      REAL MATRIX(NMAX,NMAX),DYN(NMAX)
      COMMON LEN(NMAX),AREA(NMAX),VCOM(NMAX),
     /  PCOM(NMAX),MATRIX(NMAX2,NMAX2),
     /  DYN(NMAX),PDAMP(NMAX)

      WRITE (6,2003)
      WRITE (6,3002)VCOM(2),PCOM(2),ZLAG
      WRITE (6,2005)

      WRITE(6,3004) 1,LEN(1),AREA(1),DYN(1),
     /          VCOM(1),PCOM(1)
      WRITE (6,3005) 2,LEN(2),AREA(2),DYN(2)
      WRITE (6,2006)
      IF (NSPDLN.EQ.1) THEN
            NSPD = 100
      ELSEIF (NSPDLN.EQ.2) THEN
            NSPD = 80
      ELSEIF (NSPDLN.EQ.3) THEN
            NSPD = 60
      ELSEIF (NSPDLN.EQ.4) THEN
            NSPD = 50
      ELSE
            NSPD = 23
      ENDIF
      WRITE (6,3006) NSPD,NP,NT

2003  FORMAT (' PLENUM  VOLUME (l) PLENUM PRESSURE(Pa)
     /        PHASE LAG FACTOR')
2005  FORMAT (' N    LENGTH (m)  REF. AREA (m2)  LOSS
     /   COMPL.VOL. (l)   COMPL.PR. (Pa)')
2006  FORMAT ('  SPEED(%)  PUMP LEG    THROTTLE LEG')
3001  FORMAT (6X,I2)
3002  FORMAT (1X,1PE10.3,3X,1PE10.3,3X,1PE5.3)
3003  FORMAT (4X,1PE10.3)
3004  FORMAT (I2,3X,1PE10.3,4X,1PE10.3,4X,1PE10.3,
     /        6X,1PE10.3,8X,1PE10.3)
```

```
3005   FORMAT (I2,3X,1PE10.3,4X,1PE10.3,4X,1PE10.3)
3006   FORMAT (1PE10.3,4X,I2,14X,I2)
       RETURN
       END

*****************************************************************************
*      The subroutine SLOPE calculates the steady state operating point and the various
*      damping coefficients. The pump and throttle slopes are also computed.
*****************************************************************************

       SUBROUTINE
SLOPE(PHI,PSI,PSLOPE,TSLOPE,SPEED,NSPDLN,NWCHAR,CSPD,
  /                  DLAG)
       INTEGER NSPDLN,NWCHAR
       REAL PHI,PSI,PSLOPE,TSLOPE,SPEED,DUDM,CSPD
       PARAMETER (NMAX=2,NMAX2=5,RO=1000,PI=3.1415926)
       PARAMETER (D2=0.6096,B2=1.189E-2)
       REAL LEN(NMAX),AREA(NMAX),DYN(NMAX),PDAMP(NMAX),DLAG
       COMMON  LEN(NMAX),AREA(NMAX),VCOM(NMAX),
  /      PCOM(NMAX),MATRIX(NMAX2,NMAX2),
  /      DYN(NMAX),PDAMP(NMAX)

*****************************************************************************
*      Each speedline has a corresponding equation for the pump performance
*      characteristic. The pump wheelspeed and speed variation slope with mass flow
*      (dU/dm), as well as the local pump characteristic slope (dpsi/dphi) are also
*      determined.
*      NOTE: OLD 100%SPDLN PSI IS GIVEN BY NRG CODE @ OLD VOLUTE
*      PROFILE
*****************************************************************************

*      100% Speedline, OLD design
*      MEASURED
       IF (NSPDLN.EQ.1 .AND. NWCHAR.EQ.0) THEN
         PSI=PSI=0.5*(1.0794+3.1670*PHI-39.430*PHI**2+231.06*PHI**3)
        IF (CSPD.EQ.0) THEN
          SPEED = 13.812-3.4823*PHI+1.2017*PHI**2
          DUDM = -1.116E-2
        ELSE
          SPEED = CSPD
          DUDM = 0.0
        ENDIF
         PSLOPE=0.5*(3.1670-2*39.430*PHI+3*231.06*PHI**2)

*      100% Speedline, NEW design
*      PREDICTED
       ELSEIF (NSPDLN.EQ.1 .AND. NWCHAR.EQ.1) THEN
         PSI=0.5*(0.98474+2.9702*PHI-2.8656*PHI**2-168.73*PHI**3)
        IF (CSPD.EQ.0) THEN
        SPEED = 13.812-3.4823*PHI+1.2017*PHI**2
       DUDM = -1.116E-2
```

```
          ELSE
            SPEED = CSPD
            DUDM = 0.0
          ENDIF
           PSLOPE=0.5*(2.9702-2*2.8656*PHI-3*168.73*PHI**2)

*         80% Speedline, OLD design
*         MEASURED
          ELSEIF (NSPDLN.EQ.2 .AND. NWCHAR.EQ.0) THEN
           PSI=0.54291+1.0539*PHI+1.2051*PHI**2-169.4*PHI**3
     /     +1021.2*PHI**4-2056.4*PHI**5
            IF (CSPD.EQ.0) THEN
              SPEED = 10.876-0.80951*PHI-6.6898*PHI**2
              DUDM = -8.037E-3
            ELSE
              SPEED = CSPD
              DUDM = 0.0
            ENDIF
          PSLOPE=1.0539+2*1.2051*PHI-3*169.4*PHI**2
     / +4*1021.2*PHI**3-5*2056.4*PHI**4

*         80% Speedline, NEW design
*         MEASURED
          ELSEIF (NSPDLN.EQ.2 .AND. NWCHAR.EQ.1) THEN
           PSI=0.5594+0.5469*PHI+29.074*PHI**2-766.10*PHI**3
     /     +5996.7*PHI**4-16548*PHI**5
            IF (CSPD.EQ.0) THEN
              SPEED = 10.5792-2.73749*PHI+0.34407*PHI**2
              DUDM = -7.6399E-3
            ELSE
              SPEED = CSPD
              DUDM = 0.0
            ENDIF
          PSLOPE=0.5469 + 2*29.074*PHI - 3*766.10*PHI**2
     /     + 4*5996.7*PHI**3 - 5*16548*PHI**4

*         60% Speedline, OLD design
*         MEASURED
          ELSEIF (NSPDLN.EQ.3 .AND. NWCHAR.EQ.0) THEN
           PSI=0.5*(1.0781+2.4180*PHI-11.458*PHI**2-66.302*PHI**3)
            IF (CSPD.EQ.0) THEN
              SPEED = 8.1296-0.45335*PHI-4.3236*PHI**2
              DUDM = -6.38E-3
            ELSE
              SPEED = CSPD
              DUDM = 0.0
            ENDIF
          PSLOPE=0.5*(2.4180-2*11.458*PHI-3*66.302*PHI**2)

*         60% Speedline, NEW design
*         MEASURED
```

```
      ELSEIF (NSPDLN.EQ.3 .AND. NWCHAR.EQ.1) THEN
     PSI=0.5*(1.1428 - 1.0562*PHI + 145.33*PHI**2 - 3187.2*PHI**3
     /          + 25743*PHI**4 - 73319*PHI**5)
        IF (CSPD.EQ.0) THEN
          SPEED = 7.97210-1.56522*PHI-0.03456*PHI**2
          DUDM = -5.8692E-3
        ELSE
          SPEED = CSPD
          DUDM = 0.0
        ENDIF
      PSLOPE=0.5*(-1.0562 + 2*145.33*PHI - 3*3187.2*PHI**2
     /          + 4*25743*PHI**3 - 5*73319*PHI**4)

*     50% Speedline, AM=1.00, with diffuser
*     PREDICTED
      ELSEIF (NSPDLN.EQ.4 .AND. NWCHAR.EQ.0) THEN
        PSI=0.5*(0.9778 + 5.0955*PHI - 108.99*PHI**2 + 2246.5*PHI**3
     /          - 24874*PHI**4 + 90406*PHI**5)
        IF (CSPD.EQ.0) THEN
*     Approximated to 50% Speedline, NEW Design
          SPEED = 6.17681-1.01700*PHI+1.82500*PHI**2
          DUDM = -3.6288E-3
        ELSE
          SPEED = CSPD
          DUDM = 0.0
        ENDIF
        PSLOPE=0.5*(5.0955 - 2*108.99*PHI + 3*2246.5*PHI**2
     /          - 4*24874*PHI**3 + 5*90406*PHI**4)

*     50% Speedline, AM=1.72 w/o diffuser
*     PREDICTED
      ELSEIF (NSPDLN.EQ.4 .AND. NWCHAR.EQ.1) THEN
        PSI=0.5*(0.9859 + 2.2741*PHI - 20.373*PHI**2 + 31.423*PHI**3
     /          - 168.773*PHI**4 - 347.29*PHI**5)
        IF (CSPD.EQ.0) THEN
          SPEED = 6.17681-1.01700*PHI+1.82500*PHI**2
          DUDM = -3.6288E-3
        ELSE
          SPEED = CSPD
          DUDM = 0.0
        ENDIF
        PSLOPE=0.5*(2.2741 - 2*20.373*PHI + 3*31.423*PHI**2
     /          - 4*168.77*PHI**3 + 5*347.29*PHI**4)

*     23% Speedline, OLD design
*     MEASURED
      ELSEIF (NSPDLN.EQ.5 .AND. NWCHAR.EQ.0) THEN
        PSI=0.5*(1.1153+3.2417*PHI-29.913*PHI**2)
        IF (CSPD.EQ.0) THEN
*     Approximated to 23% Speedline, NEW Design
          SPEED = 3.00832-0.19771*PHI-0.66512*PHI**2
```

```
            DUDM = -2.7958E-3
          ELSE
            SPEED = CSPD
            DUDM = 0.0
          ENDIF
          PSLOPE=0.5*(3.2417-2*29.913*PHI)

*       23% Speedline, NEW design
*       MEASURED
        ELSE
          PSI=0.5*(1.1132+1.6287*PHI-16.743*PHI**2)
          IF (CSPD.EQ.0) THEN
            SPEED = 3.00832-0.19771*PHI-0.66512*PHI**2
            DUDM = -2.7958E-3
          ELSE
            SPEED = CSPD
            DUDM = 0.0
          ENDIF
          PSLOPE=0.5*(1.6287-2*16.743*PHI)

        ENDIF

*****************************************************************************
*       The pump exit and inlet areas are used to convert from the total pressure rise of the
*       pump characteristic to the static pressure rise required by the linearized equations.
*       Also the local throttle characteristic slope is calculated by equating the pressure loss
*       in the throttle and the piping legs to the pressure rise in the pump. Differentiating
*       this with respect to mass flow, gives the local throttle curve slope, PDAMP(2),
*       which is derived in two steps:  first TSLOPE then PDAMP(1).
*****************************************************************************

        AEX = AREA(2)
        AIN = AREA(1)
        TSLOPE = 2*SPEED*PSI/(PI*D2*B2*PHI)-PHI*PI*D2*B2*SPEED*
     /                  (1/AEX**2-1/AIN**2)
        PDAMP(1) = DYN(1)*(PHI/AREA(1)**2)*SPEED*PI*D2*B2
        PDAMP(2) = PDAMP(1)-TSLOPE

*****************************************************************************
*       The nondimensional steady state pump slope is first dimensionalized and then
*       corrected for wheelspeed variations (DUDM). The dynamic pressure rise is also
*       subracted, the result being DLAG.
*****************************************************************************

        DLAG = (PSLOPE*SPEED/(PI*D2*B2)+PSI*2*RO
     /          *SPEED*DUDM-PI*D2*B2*SPEED*PHI*(1/AEX**2-
     /            1/AIN**2))
        RETURN
        END
```

```
************************************************************************
*       The subroutine, STIFMATRIX, calculates the system matrix for the subsequent
*       eigenvalue extraction.
************************************************************************

      SUBROUTINE
STIFMATRIX(N,NSPDLN,PSLOPE,TSLOPE,SPEED,PHI,DLAG
     /    ,ZLAG)
      PARAMETER (NMAX=2,NMAX2=5,GAMMA=1.4,RO=1000,PI=3.14159,
     /           EPS=0.001)
      INTEGER NSPDLN
      REAL PSMI,PLGI,VLGI,GM,LENLG,RLG,HIN
      REAL NUMB,VGSS,DVOL,VSMF,PSMF,VLGF,PLGF
      REAL NUMER,DEN1,DEN2,DENTOT,VRES,DVRES,DPEX,DPIN
      REAL VSMI,ALGF,LSMT,RISM,ASMF
      REAL AREA(NMAX),VCOM(NMAX),PCOM(NMAX),LEN(NMAX)
      REAL MATRIX(NMAX2,NMAX2),PDAMP(NMAX),PHI,DLAG,ZLAG
      COMMON  LEN(NMAX),AREA(NMAX),VCOM(NMAX),
     /    PCOM(NMAX),MATRIX(NMAX2,NMAX2),
     /    DYN(NMAX),PDAMP(NMAX),PSMI,PLGI,VSMI,VLGI

      DO 6 I=1,NMAX2
            DO 7 J=1,NMAX2
                  MATRIX(I,J)=0
6           CONTINUE
7     CONTINUE

************************************************************************
*       The plenum air volumes and pressures (as input earlier) are measured with the
*       pump off.  At the operating point of interest, the air volumes adjust to equalize the
*       pressure drops across each air-water interface.  So the equilibrium values of air
*       pressure and volume are calculated at each new operating point in the manner
*       outlined below (see J. Bons thesis).
************************************************************************

      IF (PHI.EQ.0.001) THEN
        PSMI = PCOM(1)
        PLGI = PCOM(2)
        VSMI = VCOM(1)
        VLGI = VCOM(2)
      ENDIF

************************************************************************
*       The added pressure of the water in each plenum (from pump off to current
*       operating point) is determined from epirical fits to experimental data (as a function
*       of speedline, of course).
************************************************************************

*       100% Speedline, OLD Design
*       MEASURED
      IF (NSPDLN.EQ.1 .AND. NWCHAR.EQ.0) THEN
```

```
        DPEX = 90631 + 2.3286E5*PHI - 2410700*PHI**2 + 2872200*PHI**3
        DPIN = -11408 - 18329*PHI + 2.1705E5*PHI**2 - 1.5318E5*PHI**3

*       100% Speedline, NEW Design
*       PREDICTED
        ELSEIF (NSPDLN.EQ.1 .AND. NWCHAR.EQ.1) THEN
          DPEX = 90631 + 2.3286E5*PHI - 2410700*PHI**2 + 2872200*PHI**3
          DPIN = -11408 - 18329*PHI + 2.1705E5*PHI**2 - 1.5318E5*PHI**3

*       80% Speedline, OLD Design
*       MEASURED
        ELSEIF (NSPDLN.EQ.2 .AND. NWCHAR.EQ.0) THEN
          DPEX = 62190 + 1.6366E5*PHI - 1649700*PHI**2 + 1961000*PHI**3
          DPIN = -1072.9 - 3309.8*PHI + 24825*PHI**2 - 4568.8*PHI**3

*       80% Speedline, NEW Design
*       MEASURED
        ELSEIF (NSPDLN.EQ.2 .AND. NWCHAR.EQ.1) THEN
          DPEX = 62915 + 733.14*PHI + 1.2176E6*PHI**2 - 1.6000E7*PHI**3
          DPIN = -431.17 - 74.473*PHI + 28534*PHI**2 - 1.9033E5*PHI**3

*       60% Speedline, OLD Design
*       MEASURED
        ELSEIF (NSPDLN.EQ.3 .AND. NWCHAR.EQ.0) THEN
          DPEX = 34494 + 89893*PHI - 8.5243E5*PHI**2 + 7.7986E5*PHI**3
          DPIN = -588.01 - 2099.9*PHI + 22133*PHI**2 - 36778*PHI**3

*       60% Speedline, NEW Design
*       MEASURED
        ELSEIF (NSPDLN.EQ.3 .AND. NWCHAR.EQ.1) THEN
          DPEX = 52727 + 64675*PHI - 8.2036E5*PHI**2 - 2.7266E5*PHI**3
          DPIN = -230.15 + 294.45*PHI - 9721.0*PHI**2 + 1.0939E5*PHI**3

*       50% Speedline, OLD Design
*       Approximated to 60% Speedline, OLD Design
        ELSEIF (NSPDLN.EQ.4 .AND. NWCHAR.EQ.0) THEN
          DPEX = 34494 + 89893*PHI - 8.5243E5*PHI**2 + 7.7986E5*PHI**3
          DPIN = -588.01 - 2099.9*PHI + 22133*PHI**2 - 36778*PHI**3

*       50% Speedline, NEW Design
*       MEASURED
        ELSEIF (NSPDLN.EQ.4 .AND. NWCHAR.EQ.1) THEN
          DPEX = 23898 + 51122*PHI - 6.4812E5*PHI**2 + 3.8840E5*PHI**3
          DPIN = -148.15 + 8316.7*PHI - 63243*PHI**2 + 1.5442E5*PHI**3

*       23% Speedline, NEW Design
*       MEASURED
        ELSE
          DPEX = 21050 + 5012.0*PHI - 42359*PHI**2 - 5.1253E5*PHI**3
          DPIN = 194.05 + 995.24*PHI - 29343*PHI**2 + 1.7864E5*PHI**3
        ENDIF
```

```
**********************************************************************
*       When the large plenum air volume is 300 liters, the surface area of the air water
*       interface has been computed to be 1.460 square meters. The small plenum air
*       volume interface area is computed for the initial volume specified (see J. Bons'
*       thesis for complete derivation). RISM and LSMT are relevant length scales for the
*       small plenum air volume.
**********************************************************************

      ALGF = 1.460
      RISM = 0.20
      LSMT = 1.016
      ASMF = 4*PI*LSMT*0.5*(RISM + SQRT(RISM**2+VSMI/(LSMT*PI)))

**********************************************************************
*       If VLGI is not 300 liters, we need to calculate the new corresponding surface area
*       of the air water interface in the inlet plenum. This is done with the following
*       iteration.
**********************************************************************

      IF (VLGI.EQ.0.300) GOTO 35
      LENLG = 1.27
      RLG = 0.71
      HIN = 0.4166
30    NUMB = SQRT(RLG**2-HIN**2)
      VGSS = LENLG*(RLG**2*ASIN(NUMB/RLG)-HIN*NUMB)
      DVOL = ABS(VGSS-VLGI)
      IF (DVOL.LT.EPS) GOTO 32
      HIN = HIN*(VGSS/VLGI)**2
      GOTO 30
32    ALGF = 2*LENLG*NUMB

**********************************************************************
*       The program now iterates to find the final volumes in both the small and large
*       plenums at the new operating point (first the small then the large). To simplify the
*       iteration, the surface areas are assumed constant (at their value with the pump  off).
*       The initial guess for the large plenum air volume at the  operating point in question
*       is the initial volume.
**********************************************************************

35    VGSS = VLGI
40    NUMB = VSMI/(((DPEX+PSMI)/PSMI)-ALGF*(DPIN+PLGI-
     /            PLGI*(VLGI/VGSS)**GAMMA)/(ASMF*PSMI))**(1/GAMMA)
      VRES = VLGI + VSMI - NUMB
      DVRES = ABS(VRES-VGSS)
      IF (DVRES.LT.EPS) GOTO 50
      VGSS = VGSS - 0.5*(VGSS-VRES)
      GOTO 40
50    VCOM(2) = VRES
      VCOM(1) = VLGI + VSMI - VCOM(2)
      PCOM(1) = PSMI*(VSMI/VCOM(1))**GAMMA
```

```
      PCOM(2) = PLGI*(VLGI/VCOM(2))**GAMMA

**********************************************************************
*     These volumes and pressures, along with information from the other parts of the
*     program, are now used to construct the system matrix.  The non-zero entries are
*     filled below.
**********************************************************************

      MATRIX(1,1) = -PDAMP(1)*AREA(1)/LEN(1)
      MATRIX(1,3) = AREA(1)/LEN(1)
      MATRIX(1,4) = -AREA(1)/LEN(1)
      MATRIX(1,5) = AREA(1)/LEN(1)

      MATRIX(2,2) = PDAMP(2)*AREA(2)/LEN(2)
      MATRIX(2,3) = -AREA(2)/LEN(2)
      MATRIX(2,4) = AREA(2)/LEN(2)

      MATRIX(3,1) = -(GAMMA*PCOM(1))/(RO*VCOM(1))
    MATRIX(3,2) = -MATRIX(3,1)

      MATRIX(4,1) = (GAMMA*PCOM(2))/(RO*VCOM(2))
      MATRIX(4,2) = -MATRIX(4,1)

      MATRIX(5,1) = DLAG*PHI*SPEED/(ZLAG*2.3)
      MATRIX(5,5) = -PHI*SPEED/(ZLAG*2.3)

      RETURN
      END

**********************************************************************
*     This subroutine, ELMHES, reduces the system matrix to Upper Hessenberg form.
*     The algorithm shown was taken from a standard numerical recipes text.
**********************************************************************

      SUBROUTINE ELMHES(A,N,NP)
      DIMENSION A(NP,NP)
      IF (N.GT.2) THEN
            DO 17 M=2,N-1
                  X=0
                  I=M
                  DO 11 J=M,N
                        IF (ABS(A(J,M-1)).GT.ABS(X)) THEN
                              X=A(J,M-1)
                              I=J
                        ENDIF
11                CONTINUE
                  IF (I.NE.M) THEN
                        DO 12 J=M-1,N
                              Y=A(I,J)
                              A(I,J)=A(M,J)
                              A(M,J)=Y
```

```
12                      CONTINUE
                        DO 13 J=1,N
                              Y=A(J,I)
                              A(J,I)=A(J,M)
                              A(J,M)=Y
13                      CONTINUE
                  ENDIF
                  IF (X.NE.0) THEN
                        DO 16 I=M+1,N
                          Y=A(I,M-1)
                          IF (Y.NE.0) THEN
                              Y=Y/X
                              A(I,M-1)=Y
                              DO 14 J=M,N
                                A(I,J)=A(I,J)-Y*A(M,J)
14                            CONTINUE
                              DO 15 J=1,N
                                A(J,M)=A(J,M)+Y*A(J,I)
15                            CONTINUE
                          ENDIF
16                      CONTINUE
                  ENDIF
17          CONTINUE
      ENDIF
      RETURN
      END

*************************************************************************
*     This subroutine, HQR, extracts the system eigenvalues from the upper hessenberg
*     matrix created above. This algorithm is also from a standard numerical recipes text.
*************************************************************************

      SUBROUTINE HQR(A,N,NP,WR,WI)
      DIMENSION A(NP,NP),WR(NP),WI(NP)
      ANORM=ABS(A(1,1))
      DO 12 I=2,N
            DO 11 J=I-1,N
                  ANORM=ANORM+ABS(A(I,J))
11          CONTINUE
12    CONTINUE
      NN=N
      T=0
1     IF (NN.GE.1) THEN
            ITS=0
2           DO 13 L=NN,2,-1
                  S=ABS(A(L-1,L-1))+ABS(A(L,L))
                  IF (S.EQ.0.) S=ANORM
                  IF (ABS(A(L,L-1))+S.EQ.S) GO TO 3
13          CONTINUE
            L=1
3           X=A(NN,NN)
```

```
      IF (L.EQ.NN) THEN
            WR(NN)=X+T
            WI(NN)=0
            NN=NN-1
      ELSE
            Y=A(NN-1,NN-1)
            W=A(NN,NN-1)*A(NN-1,NN)
            IF (L.EQ.NN-1) THEN
                  P=0.5*(Y-X)
                  Q=P**2+W
                  Z=SQRT(ABS(Q))
                  X=X+T
                  IF (Q.GE.0.) THEN
                        Z=P+SIGN(Z,P)
                        WR(NN)=X+Z
                        WR(NN-1)=WR(NN)
                        IF (Z.NE.0.) WR(NN)=X-W/Z
                        WI(NN)=0
                        WI(NN-1)=0
                  ELSE
                        WR(NN)=X+P
                        WR(NN-1)=WR(NN)
                        WI(NN)=Z
                        WI(NN-1)=-Z
                  ENDIF
                  NN=NN-2
            ELSE
                  IF(ITS.EQ.30)PAUSE 'Too many its.'
                  IF(ITS.EQ.10.OR.ITS.EQ.20)THEN
                    T=T+X
                    DO 14 I=1,NN
                          A(I,I)=A(I,I)-X
14                  CONTINUE
                    S=ABS(A(NN,NN-1))+ABS(A(NN-1,NN-2))
                    X=0.75*S
                    Y=X
                    W=-0.4375*S**2
                  ENDIF
                  ITS=ITS+1
                  DO 15 M=NN-2,L,-1
                    Z=A(M,M)
                    R=X-Z
                    S=Y-Z
                    P=(R*S-W)/A(M+1,M)+A(M,M+1)
                    Q=A(M+1,M+1)-Z-R-S
                    R=A(M+2,M+1)
                    S=ABS(P)+ABS(Q)+ABS(R)
                    P=P/S
                    Q=Q/S
                    R=R/S
                    IF(M.EQ.L)GO TO 4
```

```
                U=ABS(A(M,M-1))*(ABS(Q)+ABS(R))
                V=ABS(P)*(ABS(A(M-1,M-1))+ABS(Z)
     /                +ABS(A(M+1,M+1)))
                IF (U+V.EQ.V)GO TO 4
15              CONTINUE
 4              DO 16 I=M+2,NN
                A(I,I-2)=0
                IF (I.NE.M+2) A(I,I-3)=0
16              CONTINUE
                DO 19 K=M,NN-1
                IF(K.NE.M)THEN
                      P=A(K,K-1)
                      Q=A(K+1,K-1)
                      R=0
                      IF(K.NE.NN-1)R=A(K+2,K-1)
                      X=ABS(P)+ABS(Q)+ABS(R)
                      IF(X.NE.0.)THEN
                        P=P/X
                        Q=Q/X
                        R=R/X
                      ENDIF
                ENDIF
                S=SIGN(SQRT(P**2+Q**2+R**2),P)
                IF(S.NE.0)THEN
                      IF(K.EQ.M)THEN
                        IF(L.NE.M)A(K,K-1)=
     /                 -A(K,K-1)
                      ELSE
                        A(K,K-1)=-S*X
                      ENDIF
                      P=P+S
                      X=P/S
                      Y=Q/S
                      Z=R/S
                      Q=Q/P
                      R=R/P
                      DO 17 J=K,NN
                        P=A(K,J)+Q*A(K+1,J)
                        IF(K.NE.NN-1)THEN
                          P=P+R*A(K+2,J)
                          A(K+2,J)=A(K+2,J)-P*Z
                        ENDIF
                        A(K+1,J)=A(K+1,J)-P*Y
                        A(K,J)=A(K,J)-P*X
17                    CONTINUE
                      DO 18 I=L,MIN(NN,K+3)
                        P=X*A(I,K)+Y*A(I,K+1)
                        IF(K.NE.NN-1)THEN
                          P=P+Z*A(I,K+2)
                          A(I,K+2)=A(I,K+2)-P*R
                        ENDIF
```

```
                                    A(I,K+1)=A(I,K+1)-P*Q
                                    A(I,K)=A(I,K)-P
18                                CONTINUE
                                ENDIF
19                              CONTINUE
                                GO TO 2
                            ENDIF
                        ENDIF
                    GO TO 1
                    ENDIF
                    RETURN
                    END
```

B.2. Output

The output shown on the following pages was directed by the code on a specified memory file. Only the unstable flow coefficients, whose eigenvalue has positive real part (WR), are spooled to the screen. Bold-face characters and underlining have been added ho highlight certain features.

LARGE PLENUM VOLUME (l)	LARGE PLENUM PRESSURE (Pa)	PHASE LAG FACTOR
3.000E-01	1.389E+05	3.000E-2

N	LENGTH (m)	AREA (m2)	LOSS	VOLUME (l)	PRESSURE (Pa)
1	4.192E+01	5.720E-02	6.000E+00	1.000E-01	1.427E+05
2	3.277E+00	2.900E-02	1.500E+00		

SPEED(%)	PUMP LEG	THROTTLE LEG
5.878E-39	1	2

PHI	PSI	WI	WR	REDFREQ	B PAR	UPAR	
.001	.496	-2.333E+00	-2.739E-03	6.539E+00	3.493E-01	9.407E+04	**STABLE**
.002	.498	-2.304E+00	-6.027E-04	6.457E+00	3.537E-01	4.816E+04	**BEHAVIOR**
.003	.499	-2.276E+00	4.276E-03	6.380E+00	3.581E-01	3.284E+04	**UNSTABLE**
.004	.501	-2.251E+00	1.217E-02	6.310E+00	3.620E-01	2.512E+04	**BEHAVIOR**
.005	.502	-2.230E+00	2.476E-02	6.251E+00	3.654E-01	2.042E+04	$\Phi_{cr1} \approx 0.002$
.006	.504	-2.212E+00	3.732E-02	6.201E+00	3.684E-01	1.724E+04	
.007	.506	-2.198E+00	5.200E-02	6.163E+00	3.706E-01	1.491E+04	
.008	.507	-2.188E+00	6.659E-02	6.136E+00	3.723E-01	1.312E+04	
.009	.509	-2.180E+00	7.958E-02	6.114E+00	3.736E-01	1.169E+04	
.010	.510	-2.176E+00	9.261E-02	6.103E+00	3.743E-01	1.052E+04	
.011	.512	-2.173E+00	1.029E-01	6.095E+00	3.748E-01	9.539E+03	
.012	.513	-2.173E+00	1.130E-01	6.095E+00	3.748E-01	8.698E+03	
.013	.515	-2.173E+00	1.213E-01	6.096E+00	3.747E-01	7.979E+03	
.014	.516	-2.175E+00	1.281E-01	6.101E+00	3.744E-01	7.351E+03	
.015	.518	-2.177E+00	1.331E-01	6.108E+00	3.740E-01	6.801E+03	
.016	.519	-2.179E+00	1.369E-01	6.116E+00	3.735E-01	6.315E+03	
.017	.521	-2.183E+00	1.405E-01	6.127E+00	3.728E-01	5.877E+03	
.018	.522	-2.187E+00	1.425E-01	6.139E+00	3.721E-01	5.484E+03	
.019	.524	-2.191E+00	1.435E-01	6.151E+00	3.714E-01	5.133E+03	
.020	.525	-2.196E+00	1.440E-01	6.164E+00	3.706E-01	4.812E+03	
.021	.526	-2.200E+00	1.434E-01	6.176E+00	3.698E-01	4.520E+03	
.022	.528	-2.205E+00	1.420E-01	6.192E+00	3.689E-01	4.250E+03	
.023	.529	-2.210E+00	1.396E-01	6.206E+00	3.681E-01	4.005E+03	
.024	.530	-2.214E+00	1.373E-01	6.219E+00	3.673E-01	3.778E+03	
.025	.532	-2.220E+00	1.342E-01	6.235E+00	3.664E-01	3.567E+03	
.026	.533	-2.224E+00	1.297E-01	6.249E+00	3.656E-01	3.372E+03	
.027	.534	-2.231E+00	1.259E-01	6.267E+00	3.645E-01	3.186E+03	
.028	.536	-2.236E+00	1.209E-01	6.281E+00	3.637E-01	3.016E+03	
.029	.537	-2.240E+00	1.150E-01	6.295E+00	3.629E-01	2.858E+03	
.030	.538	-2.245E+00	1.093E-01	6.310E+00	3.620E-01	2.708E+03	
.031	.539	-2.250E+00	1.031E-01	6.325E+00	3.612E-01	2.567E+03	
.032	.540	-2.256E+00	9.646E-02	6.341E+00	3.602E-01	2.433E+03	
.033	.542	-2.260E+00	8.888E-02	6.354E+00	3.595E-01	2.308E+03	
.034	.543	-2.265E+00	8.126E-02	6.370E+00	3.586E-01	2.189E+03	
.035	.544	-2.270E+00	7.384E-02	6.384E+00	3.578E-01	2.076E+03	
.036	.545	-2.275E+00	6.526E-02	6.397E+00	3.571E-01	1.970E+03	
.037	.546	-2.279E+00	5.623E-02	6.410E+00	3.563E-01	1.868E+03	
.038	.547	-2.284E+00	4.748E-02	6.426E+00	3.555E-01	1.770E+03	
.039	.548	-2.289E+00	3.792E-02	6.441E+00	3.546E-01	1.677E+03	
.040	.549	-2.295E+00	2.884E-02	6.457E+00	3.538E-01	1.587E+03	
.041	.550	-2.298E+00	1.838E-02	6.468E+00	3.532E-01	1.503E+03	

.042	.551	-2.303E+00	8.392E-03	6.483E+00	3.524E-01	1.421E+03	
.043	.552	-2.308E+00	-2.326E-03	6.498E+00	3.516E-01	1.342E+03	**STABLE**
.044	.553	-2.314E+00	-1.265E-02	6.514E+00	3.507E-01	1.266E+03	**BEHAVIOR**
.045	.554	-2.317E+00	-2.422E-02	6.524E+00	3.501E-01	1.195E+03	$\Phi_{cr2} \approx 0.043$
.046	.554	-2.322E+00	-3.561E-02	6.537E+00	3.494E-01	1.126E+03	
.047	.555	-2.327E+00	-4.749E-02	6.553E+00	3.486E-01	1.058E+03	
.048	.556	-2.330E+00	-5.886E-02	6.563E+00	3.480E-01	9.936E+02	
.049	.557	-2.336E+00	-7.143E-02	6.581E+00	3.471E-01	9.297E+02	
.050	.557	-2.340E+00	-8.396E-02	6.592E+00	3.465E-01	8.700E+02	
.051	.558	-2.344E+00	-9.677E-02	6.606E+00	3.458E-01	8.113E+02	
.052	.559	-2.349E+00	-1.098E-01	6.619E+00	3.451E-01	7.547E+02	
.053	.559	-2.354E+00	-1.229E-01	6.634E+00	3.443E-01	6.993E+02	
.054	.560	-2.358E+00	-1.366E-01	6.646E+00	3.437E-01	6.463E+02	
.055	.560	-2.362E+00	-1.503E-01	6.659E+00	3.430E-01	5.949E+02	
.056	.561	-2.365E+00	-1.640E-01	6.670E+00	3.425E-01	5.451E+02	
.057	.561	-2.369E+00	-1.786E-01	6.681E+00	3.419E-01	4.968E+02	
.058	.562	-2.373E+00	-1.933E-01	6.694E+00	3.412E-01	4.494E+02	
.059	.562	-2.378E+00	-2.072E-01	6.708E+00	3.405E-01	4.033E+02	
.060	.563	-2.382E+00	-2.228E-01	6.720E+00	3.399E-01	3.587E+02	
.061	.563	-2.385E+00	-2.379E-01	6.729E+00	3.394E-01	3.155E+02	
.062	.563	-2.389E+00	-2.534E-01	6.743E+00	3.388E-01	2.731E+02	
.063	.563	-2.394E+00	-2.693E-01	6.757E+00	3.380E-01	2.317E+02	
.064	.564	-2.397E+00	-2.849E-01	6.768E+00	3.375E-01	1.917E+02	
.065	.564	-2.401E+00	-3.011E-01	6.781E+00	3.369E-01	1.525E+02	
.066	.564	-2.405E+00	-3.175E-01	6.792E+00	3.363E-01	1.144E+02	
.067	.564	-2.408E+00	-3.345E-01	6.802E+00	3.358E-01	7.725E+01	
.068	.564	-2.412E+00	-3.514E-01	6.815E+00	3.352E-01	4.092E+01	
.069	.564	-2.416E+00	-3.687E-01	6.827E+00	3.346E-01	5.501E+00	
.070	.564	-2.418E+00	-3.858E-01	6.834E+00	3.343E-01	-2.911E+01	